AD-A077 551 COLORADO RESEARCH AND PREDICTION LAB INC BOULDER F/G 17/7
LORAN-C PULSE TRANSIENT PROPAGATION. PART I. GEOPHYSICAL AND GE--ETC(U)
MAY 79 J R JOHLER , R H DOHERTY , A R COOK DOT-CG-842923-A
UNCLASSIFIED CRPLI-78-9 USCG-D-52-79 NL

1 OF 3
ADA 077551

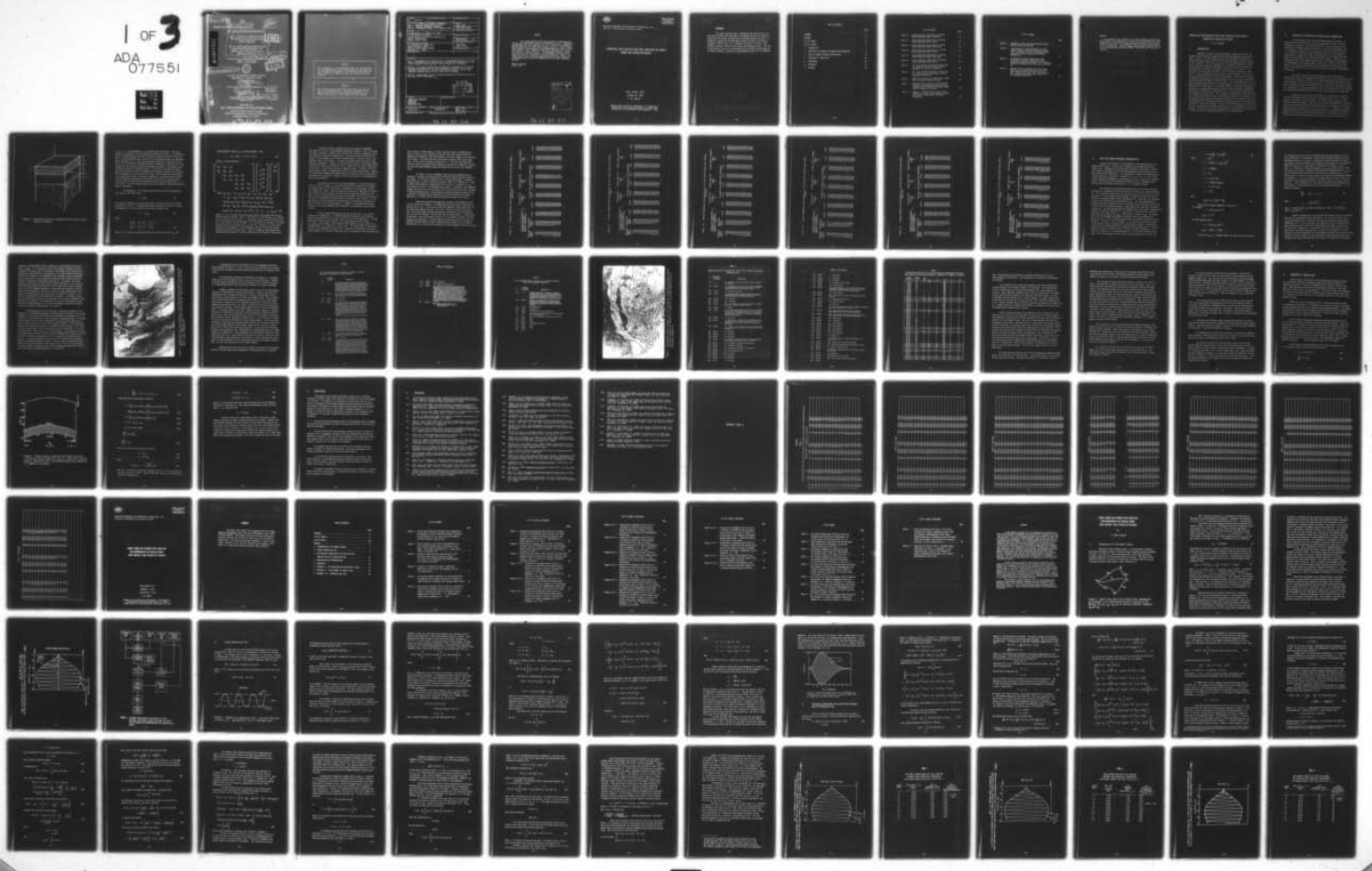

(14) CRPLI-78-9

(18) USCG-D-52-79

(19)

(12)

REPORT NO. DOT-

LORAN-C PULSE TRANSIENT PROPAGATION.

PART I. GEOPHYSICAL AND GEOLOGICAL DATA BASE EVALUATION FOR LORAN-C GROUND WAVE PROPAGATION MEDIUM.

LEVEL II

PART II. LORAN-C GROUND WAVE SECONDARY PHASE CORRECTIONS OVER NONHOMOGENEOUS AND IRREGULAR GROUND USING TRANSIENT SIGNAL PROPAGATION TECHNIQUES. Part III, (With Addendum)

J. Ralph Johler
Colorado Research and Prediction Laboratory, Inc.
1898 So. Flatiron Court
Boulder, Colorado 80301

(15) DOT-CG-842923-A

PART III. AN EXPERIMENTAL PROGRAM TO MEASURE ECD AND TEST THE TRANSIENT SOLUTION (WITH ADDENDUM).

(16) J. Ralph Johler
R. H. Doherty
A. R. Cook
Colorado Research and Prediction Laboratory, Inc.

(11) 1 MAY 1979

(12) 91

CRPL FINAL REPORT

(9) 1 Sep 78 - 1 May 79

PREPARED FOR

U.S. DEPARTMENT OF TRANPORTATION

UNITED STATES COAST GUARD

OFFICE OF RESEARCH AND DEVELOPMENT

WASHINGTON, D.C. 20590

1. Report No.	2. Government Accession No.	3. Recipient's Catalog No.
DOT - CG-D-52-79		

4. Title and Subtitle	5. Report Date
LORAN-C PULSE TRANSIENT PROPAGATION PART I: GEOPHYSICAL AND GEOLOGICAL DATA BASE PART II: TRANSIENT PROPAGATION TECHNIQUES PART III: EXPERIMENTAL PROGRAM TO TEST TRANSIENT THEORY	May 1, 1979
	6. Performing Organization Code 78-9, 78-10, 78-12
7. Author(s) J. Ralph Johler, R. H. Doherty, A. R. Cook	8. Performing Organization Report No.
9. Performing Organization Name and Address Colorado Research and Prediction Laboratory, Inc. 1898 So. Flatiron Court Boulder, Colorado 80301	10. Work Unit No. (TRAIS)
	11. Contract or Grant No. DOT-CG-842923-A
12. Sponsoring Agency Name and Address U.S. Department of Transportation United States Coast Guard Office of Research and Development Washington, D.C. 20590	13. Type of Report and Period Covered FINAL REPORT 9/1/78 - 5/1/79
	14. Sponsoring Agency Code

15. Supplementary Notes

16. Abstract

Part I: The geophysical data available for a select propagation path for use in the study of the propagation of a Loran-C pulse is evaluated and recommendations for the initial estimates of ground geoelectric section resistivities is presented.

Part II: A new rigorous technique for the computation and prediction of loran time difference coordinates from loran receiver geographic coordinates and visa versa is introduced by application to a specific loran overland situation. The full wave theoretical transient solution for the Loran-C pulse is employed.

Part III: An experimental program to validate the theoretical transient solution for the Loran-C pulse is presented.

17. Key Words	18. Distribution Statement
LORAN-C PULSE TRANSIENTS PROPAGATION NAVIGATION GROUND WAVE PULSE	

19. Security Classif. (of this report)	20. Security Classif. (of this page)	21. No. of Pages	22. Price
UNCLASSIFIED	UNCLASSIFIED	Total: 215 Part I: 51 Part II: 78 Part III: 86	

Form DOT F 1700.7 (8-72) Reproduction of completed page authorized

PREFACE

This volume comprises three papers written in compliance with the U.S. Coast Guard-CRPL; contract DOT-CG-842923-A. Part I: "Geophysical and Geological Data Base Evaluation for Loran-C Ground Wave Propagation Medium" comprises Task 1 under this contract. Part II: "Loran-C Ground Wave Secondary Phase Corrections Over Nonhomogeneous and Irregular Ground Using Transient Signal Propagation Techniques" represents Task 3 under this contract. Finally, Part III: "An Experimental Program to Measure ECD and Test the Transient Solution (With Addendum)" comprises Task 2 under this contract. Each paper is designed separately. However, the common topic of Loran-C Pulse Propagation engulfs all three papers and are presented here as the final documentation on the above referenced contract.

Boulder, Colorado
June 1, 1979

1888 SOUTH FLATIRON COURT
BOULDER, COLORADO 80301
P.O. BOX 1056
BOULDER, COLORADO 80306
TELEPHONE: 303/444-1530

COLORADO RESEARCH AND PREDICTION LABORATORY, INC.
SPECIALISTS IN ELECTROMAGNETICS AND COMPUTER SIMULATION

GEOPHYSICAL AND GEOLOGICAL DATA BASE EVALUATION FOR LORAN-C GROUND WAVE PROPAGATION MEDIUM

CRPL$_I$ REPORT 78-9

OCTOBER 15, 1978

J. R. JOHLER

Report on work sponsored by Department of Transportation, United States Coast Guard, Washington, D.C. 20590 under Contract No. DOT-C-CG-842923A, dated September 1, 1978

FOREWORD

This paper comprises Task 1: Geophysical Data Evaluation of U.S. Coast Guard Contract #DOT-CG-842923-A. The geophysical data provided GFE or obtained by this company through various government agencies as public information is applied to the Searchlight, Nevada (latitude: 35°19'18.18"; longitude: 114°48'17.43") to Ft. Cronkhite, California (latitude: 37°50' 29.464"; longitude: 122°52'41.170") ground wave propagation path. This work is preliminary to its use in the evaluation of the Loran-C pulse dispersion for which a computer simulation of the groundwave pulse will be configured.

TABLE OF CONTENTS

LIST OF TABLES

LIST OF FIGURES

ABSTRACT

The geophysical data available for a select propagation path for use in the study of the propagation of a Loran-C pulse is evaluated and recommendations for the initial estimates of ground geoelectric section resistivities is presented. Soil, geological data and terrain are considered in the impedance data. Coupling between ground surface impedance and terrain is postulated through the soil depth. The continuity of the data is stressed.

GEOPHYSICAL AND GEOLOGICAL DATA BASE EVALUATION FOR LORAN-C GROUND WAVE PROPAGATION MEDIUM

J. R. JOHLER

1. INTRODUCTION

Operation of Loran-C overland introduces a need for using the full elegance of the ground wave theory that has been developed during the past 70 years. Loran-C is a pulse transmission but the development of special techniques for pulses permits the use of this ground wave theory by Loran-C engineers and scientists. The full exploitation of the ground wave theory of propagation requires a data base independent of the Loran-C coordinate data base--the geophysical data base for the ground, References 12, 13, and 14. It is fortuitous that the ground wave theory, after 70 years of development, Reference 14, can use geophysical data to predict loran coordinates. This leads us to the interesting situation in which we have found a link between the sciences of geophysics and geography on the one hand with that of radio wave propagation about the terrestrial sphere on the other hand. It is recognized that this link really already existed, but not in any great detail. Thus, since publication of NBS Circular 573, Reference 15, it has been possible to represent the geophysical condition of a ground wave propagation path for Loran-C as smooth, homogeneous with electrical constants, σ, the conductivity, ε_2, the dielectric constant and μ_2 the permeability of the ground. Thus, starting with Sommerfeld (1909), Reference 37, it took almost 30 years to get a satisfactory solution to this problem. But the advent of large scale and now smaller but more efficient computers has led to a representation of the boundary condition for the ground wave at the surface of the earth in a more precise manner. Thus, we are now interested in the nature of the soil, the geological structure under the soil and the topography of the earth's surface. All of this can be used to refine Loran-C prediction and we believe such is quite necessary if nanosecond predictability is to be obtained.

2. GEOPHYSICAL STRUCTURES FOR GROUND WAVE PROPAGATION

The land masses of the earth are nonhomogeneous and irregular in varying degrees, depending upon a particular geographic location. In fact, one wonders in general if the complicated earth's surface can indeed be represented by a suitable boundary condition for ground wave propagation. One of the reasons for going to a low frequency such as 100 kHz used by Loran-C, is to reduce to a negligible value the scatter fields from such objects as large mountian ranges and to reduce the attenuation of the signal over land masses, expecially those that contain mountainous regions. The ground wave propagation problem then becomes primarily one of diffraction in the presence of nonhomogeneous and irregular ground. While such a problem is still formidable, it is tractable and we believe can be reduced to an operational pragmatism in the case of Loran-C chains that are now operated over the land masses of the earth.

This paper reviews the specific geographical data that could be obtained for an area of the Western United States in which a considerable diversity of such data is possible. A geodetic line between the Searchlight, Nevada transmitter (latitude: 35°19'18.18" north; longitude: 114°48'17.43" west) and Ft. Cronkhite, California (latitude: 37°50'29.464" north and longitude: 122°52'41.170" west) was researched for available geographical data. This work describes this research and pertinent philosophy applicable to duo-disciplinary enterprise of this type.

Consider first the nature of the ground in any particular locality as it changes with depth below the surface of the topmost layer of soil. Figure 1 depicts a geoelectric section of ground. The Loran-C signal propagates in the half space above such ground. Thus, the waves entering the ground are exponentially attenuated with depth or distance through the material that comprises the ground, depending upon the conductivity, σ, or the resistivity, ρ. Although the ground is layered geologically, such layering does not necessarily represent an electrical boundary like the much clearer air-ground boundary at the surface of the ground. But the ground does vary in electrical resistivity, ρ_i, dielectric constant, ϵ_i

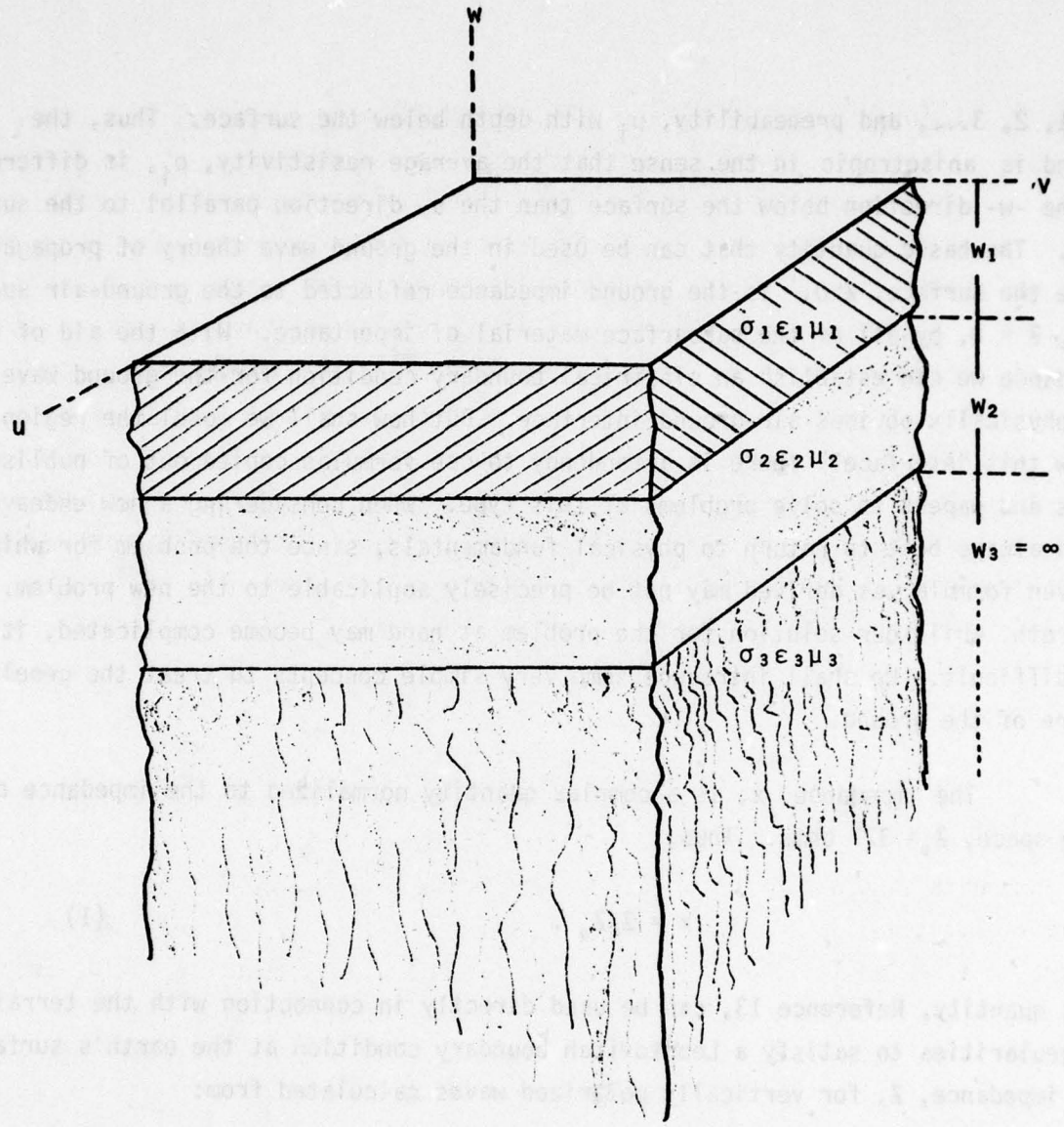

FIGURE 1. GEOELECTRIC SECTION OF GROUND DEPICTING THREE DISTINCT LAYERS OF MATERIAL.

$i = 1, 2, 3...$, and premeability, μ_i with depth below the surface. Thus, the ground is anisotropic in the sense that the average resistivity, ρ_i, is different in the -w- direction below the surface than the u- direction parallel to the surface. The basic quantity that can be used in the ground wave theory of propagation above the surface, $Z>0$, is the ground impedance reflected to the ground-air surface, $Z = 0$, by all of the subsurface material of importance. With the aid of this impedance we can establish an electrical boundary condition for the ground wave at the physically obvious air-ground interface. But how shall we model the region below this interface? There is a tendency to use formulas copied out of published books and papers to solve problems of this type. When considering a new endeavor, it is always best to return to physical fundamentals, since the problem for which a given formula was derived may not be precisely applicable to the new problem. In truth, while our solution for the problem at hand may become complicated, it is not difficult. We shall introduce some very simple concepts to treat the geoelectric nature of the ground.

The impedance, x, is a complex quantity normalized to the impedance of free space, $Z_0 = 377$ ohms. Thus,

$$x = Z/Z_0 \ . \tag{1}$$

This quantity, Reference 13, can be used directly in connection with the terrain irrgeularities to satisfy a Leontovitch boundary condition at the earth's surface. The impedance, Z, for vertically polarized waves calculated from:

$$Z = \xi_v/H_u, \tag{2}$$

where,

$$\begin{bmatrix} \xi_v \\ \xi_u \end{bmatrix} = \begin{bmatrix} 0 & Z_{12} \\ Z_{21} & 0 \end{bmatrix} \cdot \begin{bmatrix} H_v \\ H_u \end{bmatrix} \tag{3}$$

where a u, v, w Cortesian coordinate system for the electric fields, $\xi_{u,v}$ and

and the magnetic fields, $H_{u,v}$, has been employed. Then,

$$xC_i = Z/Z_0 = (1 - T)(1 + T)^{-1} C_i \qquad (4)$$

where T is calculated from:

$$\begin{bmatrix} a_{11} & a_{12} & a_{13} & & & \\ a_{21} & a_{22} & a_{23} & & & \\ & a_{32} & a_{33} & a_{34} & a_{35} & \\ & a_{42} & a_{43} & a_{44} & a_{45} & \\ & & & a_{54} & a_{55} & a_{56} \\ & & & a_{64} & a_{65} & a_{66} \end{bmatrix} \cdot \begin{bmatrix} T \\ U_i^{(1)} \\ U_r^{(1)} \\ U_i^{(2)} \\ U_r^{(2)} \\ U_i^{(3)} \end{bmatrix} = \begin{bmatrix} a_{10} \\ a_{20} \\ \\ \\ \\ \\ \end{bmatrix} \qquad (5)$$

where $a_{10} = a_{11} = -C_i$; $a_{20} = a_{12} = a_{13} = -a_{21} = a_{34} = a_{35} = -a_{56} = -1$; $a_{23} = -a_{22} = S_i^2/\delta_1 + \delta_1^2$; $a_{32} = \exp(-jk, w_1\delta_1)$; $a_{33} = \exp(jk_1 w_1\delta_1)$; $a_{42} = a_{22} a_{32}$; $a_{43} = a_{23} a_{33}$; $a_{44} = S_i^2/\delta_2 + \delta_2^2$; $a_{45} = -a_{44}$; $a_{54} = \exp(-jk_1 w_2\delta_2)$; $a_{55} = \exp(jk_1 w_2\delta_2)$; $a_{64} = a_{44} a_{54}$; $a_{65} = a_{45} a_{55}$; $a_{66} = S_i^2/\delta_3 + \delta_3^2$; $\delta_q = \varepsilon_q - i\sigma_q(\varepsilon_o\omega)^{-1} S_i^2$,

where q = 1, 2, 3, refers to the three layer model of the ground starting with the top electrical horizon. Here, $\omega = 2\pi f$, where f is the frequency, σ_q = conductivity of qth electrical horizon; ε_q = electrical horizon dielectric constant, and w_q is the electrical horizon thickness. C_i is the cosine of the angle of incidence of the wave on the u-v surface, and S_i is the sine. Reference 13, gives the relationship of the impedance to the propagation simulator of both the integral equation type and the classical type. $U_{i,r}^{(1,2)}$ are upgoing and downgoing waves (subscript) respectively in the first and second layer (subscript) respectively.

Of course, the matrix equation (5) can be enlarged to accomodate any number of horizons of ground material depicted in Figure 1. This is a trivial but tedious extension. However, there seems to exist in most circumstances a top soil layer and a geological basement rock. The soil may vary in thickness from exposure of the basement rock to several hundred meters. A typical value of soil thickness seems to be 20 meters. In regions of heavy rainfall, the soil is comparatively homogeneous. However, in arid regions and desert or semi-desert regions during the dry season the top part of the soil seems to dry out and a double horizon may exist. This process reflects an impedance change. Of course, in special areas, multiple layers of comparatively precise distinction may be noted. However, it is anticipated that the three horizon model will serve for initial estimation of the impedance of the ground. Indeed, it may be very difficult to find geophysical data in greater detail.

The effect of the soil on the ground impedance is illustrated theoretically in Tables 1 through 3. Here we have postulated a 20 meter soil thickness. The topmost layer of soil conductivity is parametric in values between 5 mhos/m and .02 mhos/m in Tables 1 and 2 and between .01 mhos/m and .0001 mhos/m in Table 3. The thickness of the top horizon has been varied in each case between 0 and 20 meters, whilst the second horizon has been varied between 10 and 0 meters such that the total soil thickness has been constant at 20 meters. Thus, Figure 1, if the top layer of soil were 5 mhos/m (the conductivity of seawater) at a thickness of only 1.6 meters, the surface impedance, $x = 0.00105 \exp(j0.79699)$ would obtain, Tables 1A, 1B, and the impedance would thereafter be controlled by the top layer of soil.

If such a highly conducting top horizon did not exist, i.e., the top horizon was of conductivity, $\sigma = 0.0001$ mhos/m and the bedrock, of infinite extent and located 20 meters below the top of the soil with a conductivity, $\sigma = 0.005$ mhos/m the combination would reflect a very high impedance to the surface, $x = 0.06911 \exp(j1.16066)$. Now the phase of the impedance can vary about 45° or 0.79699 radians (for seawater) to $\pm \pi/2$ or $\pm$ 90°. It is more common in the natural ground for the impedance to approach + 90°. Under such circumstances, we say the ground impedance is inductive. Less than 45° we call capacitive. The case just cited

with a value of 1.16066 radians is highly inductive ground, corresponding perhaps to a desert or arid condition of the soil with a more highly conducting basement rock underneath. Most arid regions of the world, however, do on occasion have rainfall. One would then expect considerable change in the surface impedance. If the wet soil obtained a conductivity, σ = .02 under such conditions, one would expect the ground surface impedance to decrease to 0.01639 exp (j0.79117) such that the ground impedance phase also reduced to a very much less inductive value.

The effect of such an impedance change upon the propagated wave is profoundly a function of the proportion of the total propagation path involved in the change. If the entire propagation path is involved the change in secondary phase correction is given in our previous report, $CRPL_i$ 77-9, Reference 13. Thus, at 1000 km there would be a change from 10 μs to 2.5 μs or a change of 7.5 μs. This example of course, is an extremely great change. In general, ground impedance changes, when they occur are much smaller and not of such an extent as to influence a 1000 km propagation path. The application of detailed impedance changes to the calculation of secondary phase correction and time difference has been given in Reference 13, and hence will be considered beyond the scope of this report.

Tables 2A and 2B give the amplitude and phase of the impedance with a very low conductivity bedrock, σ = 0.00001 mhos/m and more highly conducting and variable soil on top. In this case we note the impedance is more capacitive, i.e., the phase angle becomes less than $\pi/4$ or 45°. Finally in Tables 3A and 3B we have illustrated a poorly conducting bedrock with moderate to poorly conducting soil on top of this bedrock. Here we note that the conductivity σ = 0.0001 mhos/m on top tends to make the impedance inductive as its thickness increases, and then abruptly turns capacitive. If such a species of electrical horizon occured, considerable secondary phase correction changes would be evident as can be deduced from Reference 13, provided a great proportion of the propagation path were involved.

Table 1A. Ground Impedance Calculations at 100 kHz Using Three-Layer Model, Amplitude

	Top Layer Soil	Second Layer Soil	Bottom Layer or Bedrock
Conductivity (MHOS/Meter) =	Variable	.0001	.005
Dielectric Constant =	15.	15.	15.
Magnetic Permeability =	1.	1.	1.

Top Layer Depth, Meters	Second Layer Depth, Meters	Top Layer Soil Conductivity, MHOS/Meter							
		5.00000	2.00000	1.00000	.50000	.20000	.10000	.05000	.02000
0.000	20.000	.06911	.06911	.06911	.06911	.06911	.06911	.06911	.06911
.200	19.800	.00263	.00639	.01220	.02207	.04054	.05327	.06123	.06610
.400	19.600	.00137	.00329	.00642	.01225	.02625	.04061	.05332	.06290
.600	19.400	.00102	.00226	.00438	.00847	.01915	.03214	.04644	.05967
.800	19.200	.00093	.00179	.00337	.00649	.01504	.02640	.04076	.05650
1.000	19.000	.00094	.00157	.00279	.00530	.01239	.02234	.03614	.05348
1.200	18.800	.00099	.00148	.00244	.00451	.01056	.01935	.03237	.05064
1.400	18.600	.00103	.00147	.00224	.00398	.00922	.01707	.02927	.04799
1.600	18.400	.00105	.00150	.00213	.00360	.00821	.01529	.02670	.04554
1.800	18.200	.00106	.00154	.00209	.00334	.00742	.01385	.02453	.04329
2.000	18.000	.00106	.00159	.00209	.00317	.00681	.01269	.02270	.04121
4.000	16.000	.00105	.00167	.00237	.00318	.00475	.00761	.01344	.02771
6.000	14.000	.00105	.00167	.00236	.00335	.00498	.00677	.01055	.02139
8.000	12.000	.00105	.00167	.00236	.00334	.00525	.00700	.00977	.01819
10.000	10.000	.00105	.00167	.00236	.00333	.00530	.00731	.00981	.01662
12.000	8.000	.00105	.00167	.00236	.00334	.00528	.00746	.01010	.01597
14.000	6.000	.00105	.00167	.00236	.00334	.00527	.00749	.01036	.01584
16.000	4.000	.00105	.00167	.00236	.00334	.00527	.00748	.01051	.01596
18.000	2.000	.00105	.00167	.00236	.00334	.00527	.00746	.01057	.01618
20.000	.000	.00105	.00167	.00236	.00334	.00527	.00746	.01058	.01639

Table 1B. Ground Impedance Calculations at 100 kHz Using Three-Layer Model, Phase

		Top Layer Soil	Second Layer Soil	Bottom Layer or Bedrock
Conductivity (MHOS/Meter)	=	Variable	.0001	.005
Dielectric Constant	=	15.	15.	15.
Magnetic Permeability	=	1.	1.	1.

Top Layer Depth, Meters	Second Layer Depth, Meters	Top Layer Soil Conductivity, MHOS/Meter							
		5.00000	2.00000	1.00000	.50000	.20000	.10000	.05000	.02000
0.000	20.000	1.16066	1.16066	1.16066	1.16066	1.16066	1.16066	1.16066	1.16066
.200	19.800	.08862	.10739	.17462	.30387	.57131	.78699	.94957	1.07045
.400	19.600	.22384	.12967	.12994	.18703	.36687	.57569	.78997	.98956
.600	19.400	.43116	.21672	.15530	.16358	.27988	.45376	.67186	.91775
.800	19.200	.62393	.33806	.21230	.17415	.23967	.37969	.58438	.85441
1.000	19.000	.74607	.47074	.28946	.20413	.22354	.33337	.51936	.79881
1.200	18.800	.79992	.59194	.37827	.24749	.22220	.30459	.46989	.75014
1.400	18.600	.81211	.68664	.47006	.30045	.23108	.28778	.43277	.70761
1.600	18.400	.80643	.75090	.55671	.35974	.24762	.27963	.40483	.67049
1.800	18.200	.79699	.78853	.63216	.42218	.27014	.27809	.38407	.63813
2.000	18.000	.78973	.80640	.69320	.48469	.29740	.28176	.36903	.60995
4.000	16.000	.78538	.78425	.79703	.80435	.63900	.46406	.38685	.47613
6.000	14.000	.78535	.78542	.78443	.79252	.79519	.67784	.52484	.47880
8.000	12.000	.78535	.78537	.78540	.78423	.80297	.78233	.66207	.53541
10.000	10.000	.78535	.78538	.78535	.78518	.78905	.80430	.75034	.60845
12.000	8.000	.78535	.78538	.78535	.78535	.78442	.79735	.79015	.67636
14.000	6.000	.78535	.78538	.78535	.78531	.78458	.78878	.80003	.72872
16.000	4.000	.78535	.78538	.78535	.78531	.78509	.78488	.79701	.76336
18.000	2.000	.78535	.78538	.78535	.78531	.78521	.78418	.79121	.76276
20.000	.000	.78535	.78538	.78535	.78531	.78519	.78451	.78680	.79117

Table 2A. Ground Impedance Calculations at 100 kHz Using Three-Layer Model, Amplitude

		Top Layer Soil	Second Layer Soil	Bottom Layer or Bedrock
Conductivity (MHOS/Meter)	=	Variable	.00500	.00001
Dielectric Constant	=	15.	15.	15.
Magnetic Permeability	=	1.	1.	1.

Top Layer Depth, Meters	Second Layer Depth, Meters	Top Layer Soil Conductivity, MHOS/Meter							
		5.00000	2.00000	1.00000	.50000	.20000	.10000	.05000	.02000
0.000	20.000	.02996	.02996	.02996	.02996	.02996	.02996	.02996	.02996
.200	19.800	.00248	.00557	.00952	.01466	.02142	.02516	.02758	.02910
.400	19.600	.00133	.00307	.00561	.00958	.01652	.02159	.02538	.02828
.600	19.400	.00101	.00217	.00401	.00713	.01342	.01888	.02354	.02751
.800	19.200	.00093	.00175	.00316	.00573	.01131	.01676	.02195	.02677
1.000	19.000	.00095	.00155	.00267	.00479	.00979	.01508	.02055	.02607
1.200	18.800	.00099	.00148	.00237	.00417	.00865	.01371	.01932	.02541
1.400	18.600	.00103	.00148	.00220	.00374	.00778	.01259	.01824	.02478
1.600	18.400	.00105	.00151	.00212	.00344	.00709	.01165	.01728	.02418
1.800	18.200	.00106	.00155	.00209	.00323	.00654	.01086	.01643	.02361
2.000	18.000	.00106	.00159	.00210	.00310	.00611	.01019	.01566	.02308
4.000	16.000	.00105	.00167	.00237	.00322	.00471	.00707	.01119	.01903
6.000	14.000	.00105	.00167	.00236	.00335	.00502	.00670	.00969	.01669
8.000	12.000	.00105	.00167	.00236	.00334	.00527	.00704	.00945	.01543
10.000	10.000	.00105	.00167	.00236	.00333	.00530	.00735	.00972	.01489
12.000	8.000	.00105	.00167	.00236	.00334	.00528	.00748	.01009	.01479
14.000	6.000	.00105	.00167	.00236	.00334	.00527	.00750	.01038	.01497
16.000	4.000	.00105	.00167	.00236	.00334	.00527	.00748	.01054	.01527
18.000	2.000	.00105	.00167	.00236	.00334	.00527	.00746	.01060	.01561
20.000	.000	.00105	.00167	.00236	.00334	.00527	.00746	.01061	.01594

Table 2B. Ground Impedance Calculations at 100 kHz Using Three-Layer Model, Phase

		Top Layer Soil	Second Layer Soil	Bottom Layer or Bedrock
Conductivity (MHOS/Meter)	=	Variable	.00500	.00001
Dielectric Constant	=	15.	15.	15.
Magnetic Permeability	=	1.	1.	1.

Top Layer Depth, Meters	Second Layer Depth, Meters	Top Layer Soil Conductivity, MHOS/Meter							
		5.00000	2.00000	1.00000	.50000	.20000	.10000	.05000	.02000
0.000	20.000	.51873	.51873	.51873	.51873	.51873	.51873	.51873	.51873
.200	19.800	.10054	.11994	.17443	.25468	.36704	.43198	.47381	.50289
.400	19.600	.23827	.14757	.14758	.19128	.29301	.37459	.43835	.48084
.600	19.400	.44530	.23791	.17878	.18288	.25635	.33662	.41055	.47645
.800	19.200	.63374	.36144	.23959	.20112	.24112	.31222	.38903	.46563
1.000	19.000	.75069	.49140	.31899	.23628	.23987	.29778	.37274	.45618
1.200	18.800	.80140	.60849	.40807	.28334	.24862	.29394	.36286	.44810
1.400	18.600	.81200	.69824	.49805	.33863	.26498	.29614	.35273	.44124
1.600	18.400	.80564	.75801	.58119	.39881	.28730	.29422	.34783	.43554
1.800	18.200	.79645	.79223	.65218	.46066	.31434	.30236	.34573	.43091
2.000	18.000	.78940	.80780	.70858	.52122	.34505	.31390	.34610	.42727
4.000	16.000	.78538	.78424	.79605	.80781	.67633	.52395	.43567	.43336
6.000	14.000	.78535	.78542	.78444	.79152	.80420	.71769	.58450	.46780
8.000	12.000	.78535	.78537	.78540	.78419	.80284	.79921	.70852	.56191
10.000	10.000	.78535	.78538	.78535	.78520	.78818	.80943	.78200	.63651
12.000	8.000	.78535	.78538	.78535	.78535	.78406	.79819	.80775	.70013
14.000	6.000	.78535	.78538	.78535	.78531	.78450	.78843	.81043	.74806
16.000	4.000	.78535	.78538	.78535	.78531	.78510	.78436	.80315	.78032
18.000	2.000	.78535	.78538	.78535	.78531	.78523	.78378	.79462	.79940
20.000	.000	.78535	.78538	.78535	.78531	.78520	.78428	.78837	.80861

Table 3A. Ground Impedance Calculations at 100 kHz Using Three-Layer Model, Amplitude

	Top Layer Soil	Second Layer Soil	Bottom Layer or Bedrock
Conductivity (MHOS/Meter) =	Variable	.05	.00001
Dielectric Constant =	15.	15.	15.
Magnetic Permeability =	1.	1.	1.

Top Layer Depth, Meters	Second Layer Depth, Meters	Top Layer Soil Conductivity, MHOS/Meter						
		.01000	.00500	.00200	.00100	.00050	.00020	.00010
0.000	20.000	.01061	.01061	.01061	.01061	.01061	.01061	.01061
.200	19.800	.01095	.01088	.01090	.01091	.01091	.01091	.01091
.400	19.600	.01110	.01116	.01120	.01121	.01122	.01123	.01122
.600	19.400	.01135	.01144	.01150	.01152	.01154	.01154	.01154
.800	19.200	.01160	.01173	.01181	.01184	.01186	.01187	.01186
1.000	19.000	.01196	.01203	.01213	.01216	.01219	.01220	.01219
1.200	18.800	.01212	.01232	.01245	.01249	.01252	.01253	.01252
1.400	18.600	.01238	.01262	.01277	.01283	.01286	.01287	.01285
1.600	18.400	.01264	.01293	.01310	.01316	.01320	.01322	.01319
1.800	18.200	.01291	.01323	.01343	.01350	.01354	.01357	.01354
2.000	18.000	.01317	.01354	.01377	.01385	.01389	.01392	.01388
4.000	16.000	.01581	.01668	.01722	.01741	.01750	.01754	.01746
6.000	14.000	.01823	.01976	.02070	.02102	.02118	.02123	.02110
8.000	12.000	.02027	.02260	.02404	.02451	.02474	.02481	.02463
10.000	10.000	.02179	.02505	.02711	.02778	.02810	.02820	.02795
12.000	8.000	.02274	.02700	.02987	.03081	.03126	.03141	.03114
14.000	6.000	.02313	.02837	.03232	.03369	.03437	.03464	.03437
16.000	4.000	.02296	.02905	.03451	.03667	.03780	.03838	.03818
18.000	2.000	.02218	.02890	.03699	.04116	.04370	.04535	.04557
20.000	.000	.02081	.02996	.05628	.08991	.13197	.18546	.21475

Table 3B. Ground Impedance Calculations at 100 kHz Using Three-Layer Model, Phase

	Top Layer Soil	Second Layer Soil	Bottom Layer or Bedrock
Conductivity (MHOS/Meter) =	Variable	.05	.00001
Dielectric Constant =	15.	15.	15.
Magnetic Permeability =	1.	1.	1.

Top Layer Depth, Meters	Second Layer Depth, Meters	Top Layer Soil Conductivity, MHOS/Meter						
		.01000	.00500	.00200	.00100	.00050	.00020	.00010
0.000	20.000	.78837	.78837	.78837	.78837	.78837	.78837	.78837
.200	19.800	.81029	.81309	.81474	.81522	.81533	.81494	.81431
.400	19.600	.83079	.83635	.83964	.84061	.84083	.84008	.83886
.600	19.400	.84993	.85822	.86315	.86461	.86494	.86387	.86211
.800	19.200	.86778	.87877	.88535	.88730	.88777	.88639	.88413
1.000	19.000	.88441	.89809	.90632	.90878	.90937	.90772	.90501
1.200	18.800	.89988	.91624	.92613	.92910	.92984	.92794	.92482
1.400	18.600	.91426	.93329	.94486	.94835	.94925	.94712	.94363
1.600	18.400	.92762	.94930	.96257	.96659	.96766	.96533	.96151
1.800	18.200	.94000	.96434	.97932	.98389	.98514	.98264	.97851
2.000	18.000	.95145	.97846	.99518	1.00031	1.00175	.99910	.99469
4.000	16.000	1.02516	1.07921	1.11481	1.12635	1.13037	1.12733	1.12135
6.000	14.000	1.04717	1.12857	1.18577	1.20521	1.21289	1.21095	1.20471
8.000	12.000	1.03839	1.14497	1.22516	1.25354	1.26564	1.26565	1.25974
10.000	10.000	1.01132	1.13700	1.23909	1.27671	1.29357	1.29591	1.29049
12.000	8.000	.97405	1.10844	1.22803	1.27421	1.29569	1.30041	1.29540
14.000	6.000	.93170	1.05990	1.18793	1.24069	1.26618	1.27303	1.26814
16.000	4.000	.88594	.98604	1.10401	1.15817	1.18578	1.19398	1.18864
18.000	2.000	.82956	.85785	.91483	.95140	.97297	.97903	.97194
20.000	.000	.71375	.51873	.29351	.19422	.13675	.09496	.07640

3. DATA FOR GROUND IMPEDANCE DETERMINATION

Figures 2 and 3 depict soil and geological information available for western United States. The particular propagation path between Searchlight, Nevada and Ft. Cronkhite, California has been indicated on these maps. Tables 4 and 5 summarize the types of soil along this propagation path based upon information obtained from Reference 1, (U.S. Department of Interior) and Reference 10, (Soviet Geography), respectively. References 2, 3, 4, 5, 6, 7, 8, and 9, give further supporting information on the nature of the soil. Table 6 gives the geological information for the basement rock pertinent to this propagation path. This data can be obtained from Reference 1, (U.S. Geological Survey).

The correlation of the spatial perturbations in the Loran-C phase (or LF phase) with geology was noticed some time ago by Pressy et al (1953), Reference 22. For continental United States an extensive radio survey of ground wave field strengths in the low frequency band (broadcast frequencies 540-1640 kHz) was conducted and published as NBS Circular 546, Reference 21. These data were expressed in terms of an effective ground conductivity, σ_{eff}. This was accomplished by matching ground wave attenuation versus distance curves with those observed in the vicinity of various broadcast stations. These observations have been interpreted in many ways. One such interpretation was accomplished by the Federal Communications Commission scientists, Reference 23, in the form of a map delineating areas of effective ground conductivity, σ_{eff}. What exactly is meant by σ_{eff}? The ground wave theory of propagation, References 13 and 24, does not use conductivity, mhos/m, directly. Thus, the quantity that enters into Maxwell's equations is the ground-air interface surface impedance. If the ground is of infinite extent in the negative vertical direction and a conductivity σ, mhos/m is specified as constant for this entire half space, we have the type of ground used in classical ground wave theory for deducing σ_{eff} in Kirby et al,(1958), Reference 21. The dielectric constant, "ε_2", and the permeability, "μ_2" are also specified as constant. Then, the impedance, relative to free space, equation (1), is given by:

$$x = k_1/k_2 \left[1 - (k_1/k_2)^2\right]^{\frac{1}{2}}, \qquad (6)$$

where, $\omega = 2\pi f$,

$$k_1 = (\omega/c)\left[\varepsilon_2 - j\,\sigma_{eff}/\varepsilon_0\omega\right]^{\frac{1}{2}}$$

$\eta_1 = 1.000338$,

$\varepsilon_2 \sim 15$,

$\varepsilon_0 = (c^2\mu_0)^{-1}$ F/m,

$c = 2.997925\ (10^8)$m/S,

$\mu_0 = 4\pi\ (10^{-7})$ H/m,

$j = \sqrt{-1.}$

then,

$$\sigma_{eff} \approx j\omega\varepsilon_0 \left[\eta_1^2/x^2 - \varepsilon_2\right]. \qquad (7)$$

Some values of ground impedance of interest are:

for seawater,

$x = 0.0011 \exp(j0.79)$

$\sigma_{eff} = 5 - j0$

for high impedance land,

$x = 0.040 \exp(j0.81)$

$\sigma_{eff} = 0.0034 - j\,0.0003.$

In general, σ_{eff}, is a complex number, but other uncertainties about

its precise value usually do not justify worrying about the imaginary part, as far as Reference 21, is concerned. However, when we change frequency, the non-homogeneous nature of the ground in the negative vertical direction can affect σ_{eff} because x changes profoundly with frequency and the nature of the subsurface electrical layers as discussed above in connection with Tables 1, 2 and 3. Thus, as a consequence a frequency dependence in σ_{eff} was indeed noticed. Then the term σ_{dc} was coined to represent the extremely low frequency limit of $\sigma_{eff}(\omega)$. Thus, since the ground is made up of a multiplicity of conductivities, σ, or resistivities, ρ, ohm-m, it is more logical to work with the more general quantity, the impedance, x. It is of interest to note that even the classical theory, Reference 15, has an impedance calculator installed to convert σ or σ_{eff} into impedance, x. Thus, References 15, in the case of vertical electric polarization, the residues, s, of the residue series are calculated from the roots $\tau = \tau_s$ of Riccati's equation,

$$\frac{\partial \delta_e}{\partial \tau} - 2\,\delta_e^2\,\tau + 1 = 0, \tag{8}$$

where,

$$\delta_e = -j\left[(k_1 a)^{\frac{1}{3}}\,x\right]^{-1}. \tag{9}$$

where $a = 6.36739\ (10^6)$m, the radius of the earth. Here x is calculated as shown in equation (6).

Another interpretation of NBS Circular 546, Reference 21, was instituted by Keller and Frischknecht (1966), Reference 20. In this work we find a very interesting correlation of the conductivity (resistivity) with geologic age of sedimentary rocks. Also, at extremely low frequencies (60 Hz) a correlation between geologic age and resistivity was published by Card (1935), Reference 18, and Löwy (1911), Reference 16. The absolute values for the resistivity of the bedrock for a particular geological age in these cases is different. At such drastically different frequencies one could expect a difference in the resistivities deduced for various reasons, the most important of which may be the depth of penetration of the longer wavelength into the ground. One would expect the medium

frequencies of the broadcast band to penetrate to a considerably shorter distance. However, it is interesting to note that broadcast frequencies exhibit attenuation rate changes with the geological underlayment that correlates with geologic age, notwithstanding the overburden or soil which tends to decorrelate with the age of bedrock in its formation. More important is the corresponding strong correlation of Loran-C frequency attenuation rates and phase lags with the age of the geologic underlayment, Reference 22. In contrast, the higher frequencies seem to be correlated with soil types, References 17 and 19, and indeed, Smith-Rose (1934) gives conductivities of various soil types in England. He also noted the frequency dependence of the ground wave attenuation rates between 1 kHz and 10,000 kHz. We are, as a result of such considerations led to consider the multiple electrical horizon type soil depicted in Figure 1 as at least a triple electrical horizon geoelectric structure. If necessary, we can use more sophistication later, but the availability of pertinent geophysical data does limit us at present. The improvement to be gained in this model over the classical half space concept is in our opinion enormous, and may be sufficient to achieve our initial prediction goals for Loran-C.

The description to follow is designed to illustrate procedure or the beginning of an evolutionary technique for making initial estimates of the surface impedance of the ground from the rather vast information on geology and soil. It is important to note that most of the information on geology and soil is irrelevant to the problem at hand, but this information in any particular problem must be sifted to obtain the very few "bits" of information required. In our estimation model we shall look for three values of conductivity and two values of soil depth. It is anticipated that all of this information may not be available. It is also anticipated that in some cases it may not be necessary. The procedure will be one of development of an expertise that will require judgement and intuition; that will be improved by further experience and will, of course, be as quantitative as is possible. Our initial estimates for the soils will consider only the dominant orders and suborders depicted in Figure 2. There are detailed delinations available of various kinds of special soils that do exist in any of the great orders. The amount of detail we require for our initial impedance estimates will thus be quite restricted, so that the approach will be practical.

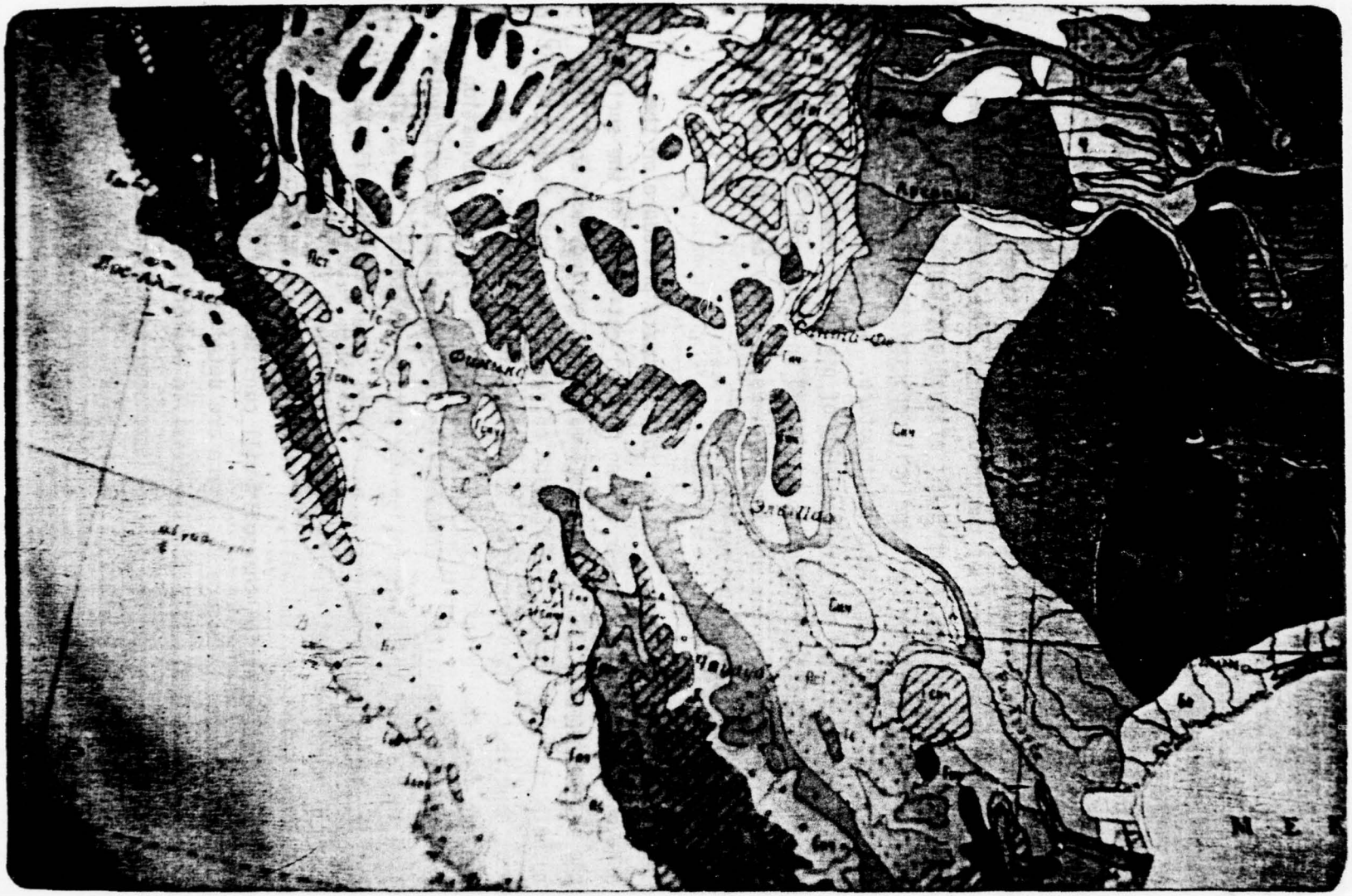

FIGURE 2. ILLUSTRATING SOIL TYPE DELINEATION IN SOUTH WESTERN UNITED STATES WITH SEARCHLIGHT, NEVADA TO FT. CRONKHITE, CALIFORNIA PROPAGATION PATH INDICATED IN UPPER LEFTHAND PART OF CHART, REFERENCE 10.

The geological and soil characteristics of the propagation path have been delineated in Tables 4, 5, and 6. Table 7 gives the estimated soil resistivities along the propagation path from Searchlight, Nevada and Ft. Cronkhite, California.

Soil depths were estimated from References 29 through 35. The hardpan below the soil was included with soil in most of the cases considered. However, the actual depth of the bedrock was quite uncertain for the literature surveyed. It is expected that many of the values given in Table 7 may require adjustment.

Between a distance of 0 and 30 km, we find an area of thick Quarternary (Q) deposits characteristic of western United States. Reference 20, gives Gila conglomerate with a lithology description as alluvium, enclosed debris filled basins known as bolson deposits, lake beds, and windblown sands. The corresponding soil description (D2-8) of the general order extends over this area between 0 and 148 km is a warm, dry soil of the ARGID classification with a mean annual temperature greater than 47°F. The region is quite arid for periods much greater than 3 months of the year. Alkali (sodium) deposits exist; clay has accumulated; there is low organic content in the soil. Indeed, the region comprises a subtropical desert soil that may be intersperced with both mountain serozems and typical desert soils. These are brownish gray near the surface and lighter colored below and are underlain with a carbonate or hardpan layer. We set thickness at 6 meters for the dry top soil and 10 meters for the moist underlayment. The dry top layer estimated at 2,000 ohm-m and the underlayment at 100 ohm-m, including the Quarternary alluvium type deposits of great depth. References 18, 20, 25, 26, and 27, may be used to assist with resistivity estimations. At 30 km we note Precambrian orthogneiss and paragneiss (Xm), 2,500,000,000 to 1,600,000,000 years old as underlayment to the ARGID soils. Such underlayment in western United States has varied composition and origin. Such Precambrian gneisses may exhibit a resistivity range 4,000 ohm-meters to 250 ohm-meters on the average. In fact, Reference 18, gives a range of 1,000-14,000 ohm-m for the intersperced Cambrian and Precambrian geologic ages. We shall use 2,000 ohm-m for our initial estimate.

Between 30 and 47 km, we find the Precambrian orthogneiss and paragneiss basement rocks that range from 2,500,000,000 to 1,600,000,000 years in geologic

TABLE 4

SOIL TYPES BETWEEN SEARCHLIGHT, NEVADA AND FT. CRONKHITE, CALIFORNIA BASED UPON U.S. DEPARTMENT OF INTERIOR, REFERENCE 1.

%	DISTANCE KILOMETERS	DESCRIPTION
19.9	0	D2-8: Warm, dry* soil of ARGID type with mean annual temperature greater than 47°F. Haplargids plus Paleorthids, Torripsamments, Paleargids, and Calciorthids, gently sloping to steep. This soil is an ARIDISOL that includes soils that have pedogenic horizons and are low in organic matter and are never moist as long as 3 consecutive months. AGRIDS are a subgroup of ARIDISOLS that have a horizon in which clay has accumulated with or without alkali (sodium); these soils can be used mostly for range and some irrigated crops.
3.32	148.953	D2-7: Warm, dry soil of ARGID type with mean annual temperature greater than 47°F. Haplargids plus Paleorthids, Torriorthents, and Rock land, gently or moderately sloping.
4.15	173.743	D2-8: (see above).
16.58	204.731	D2-7: (see above).
8.29	328.533	U7-2: Warm, dry soil of XERULT type with mean annual temperature greater than 47°F. Haploxerulfs plus Xerumbrepts and Xerorthents, steep. This soil if an ULTISOL that includes soils that are low in bases and have subsurface horizons of clay accumulation; usually moist, but during the warm season of the year, some are dry par' of the time. XERULTS are a subgroup of ULTISOLS that are relatively low in organic matter in the subsurface horizons. They exist in climates with rainy winters but dry summers; during the warm season of the year, these soils are continually dry for a long period; these soils can be of use as range or woodland. * Dry soils lack moisture for plant growth for long periods.
19.9	390.434	A12-2: Warm, dry soil of XERALF type with mean annual temperature greater than 47°F. Haplozeralfs plus Palexeralfs and Xerorthants (shallow), moderately sloping to steep. This soil is an ALFISOL that includes soils that are medium to high in bases (base saturation at pH 8.2) and have gray to brown surface horizon and subsurface horizons of clay accumulation; usually moist but during the warm season of the year some are dry part of the time. XERALFS are a subgroup of ALFISOLS that exist in climates with rainy winters but dry summers; during the warm season of the year these soils are continually dry for a long period; these soils can be used for range, small grain and irrigated crops.
4.15	539.027	D3-3: Warm, dry soil of ARGID type with mean annual temperature greater than 47°F. Natrargids plus Nadurargids, Haplaquolls, and Torriorthents, gently sloping.
2.99	570.015	A12-2: (see above).
4.64	592.341	E7-2: Warm soils of ORTHENT type with mean annual temperature greater than 47°F. Xerorthents plus Durixeralfs, Haploxeralfs, Xerofluvents, and Palexeralfs, gently sloping. This soil is an ENTISOL that includes soils that have no pedogenic horizon. ORTHENTS are a subgroup of ENTISOLS comprising loamy or clayey ENTISOLS that have a regular decrease in organic-matter content with depth; these soils may be used for range or irrigated crops in dry regions and for general farming in humid regions. The E7-2 belongs to the subspecies XERORTHENTS (formerly Regosols, Brown, or Alluvial soils) and comprise ORTHENTS that are in climates with rainy winters but dry summers and during the warm season of the year, they are continually dry for a long period.

TABLE 4 (continued)

13.6	626.988	A12-2: (see above).
1.66	728.539	H2O: Saltwater San Francisco Harbor.
0.83	740.934	M16-1: Warm soil of XEROLL type with mean annual temperature greater than 47°F. Haploxerolls plus Argixerolls, Chromoxererts, and Xerothants (shallow), steep. This soil is a MOLLISOL that includes soils that have nearly black, friable, organic-rich, surface horizons high in bases; formed mostly in subhumid and semiarid warm to cold climates. XEROLLS are MOLLISOLS that are in climates with rainy winters but dry summers; during the warm season of the year, these soils are continually dry for a long period; they may be used for wheat, range and irrigated crops. Under the XEROLLS, this soil is classified under the great group (or phase) of HAPLOXEROLLS (formerly Chestnut and Brown soils) that are XEROLLS that have a subsurface horizon high in bases but without large accumulations of clay, calcium carbonate, or gypsum.
END	746.697	

Note: Gently sloping--slope mainly <10%
Moderately sloping--10% ≤ slope <25%
Steep--slope >25%

TABLE 5.

Soil types Between Searchlight, Nevada and Ft. Cronkhite, California Based on Soviet Geography, Reference 10.

%	DISTANCES, KILOMETERS	DESCRIPTION
19.9	0	Subtropical Desert Soils: intersperced with mountain Serozems and desert soils. The Serozems (sierozems) comprise any of a group of zonal soils that are brownish gray at the surface and lighter colored below, based in a carbonate layer or a hardpan layer, and characteristic of temperate to cool arid regions with mixed shrub vegitation.
3.32	148.953	Solonchak: Salt marsh; any of an intrazonal group of stongly saline soils; usually light colored and without characteristic structural form and typically developed in poorly drained arid and semiarid areas vegitated mostly by halophytes.
4.15	173.743	Brown mountain soils.
16.58	204.731	Semidesert soils.
8.29	328.533	Brown mountian soils. Mountain meadow soils.
19.9	390.434	Brown forest soils (largely neutral) and gray forest mountain soils. Brown mountian soils.
4.15	539.027	Brown soils of Xerographytic Subtropical forest and shrub.
2.99	570.015	(same)
4.64	592.341	(same)
13.6	626.988	Turf-carbonate mountain soils.
1.66	728.539	(same)
0.83	740.934	(same)
END	746.697	

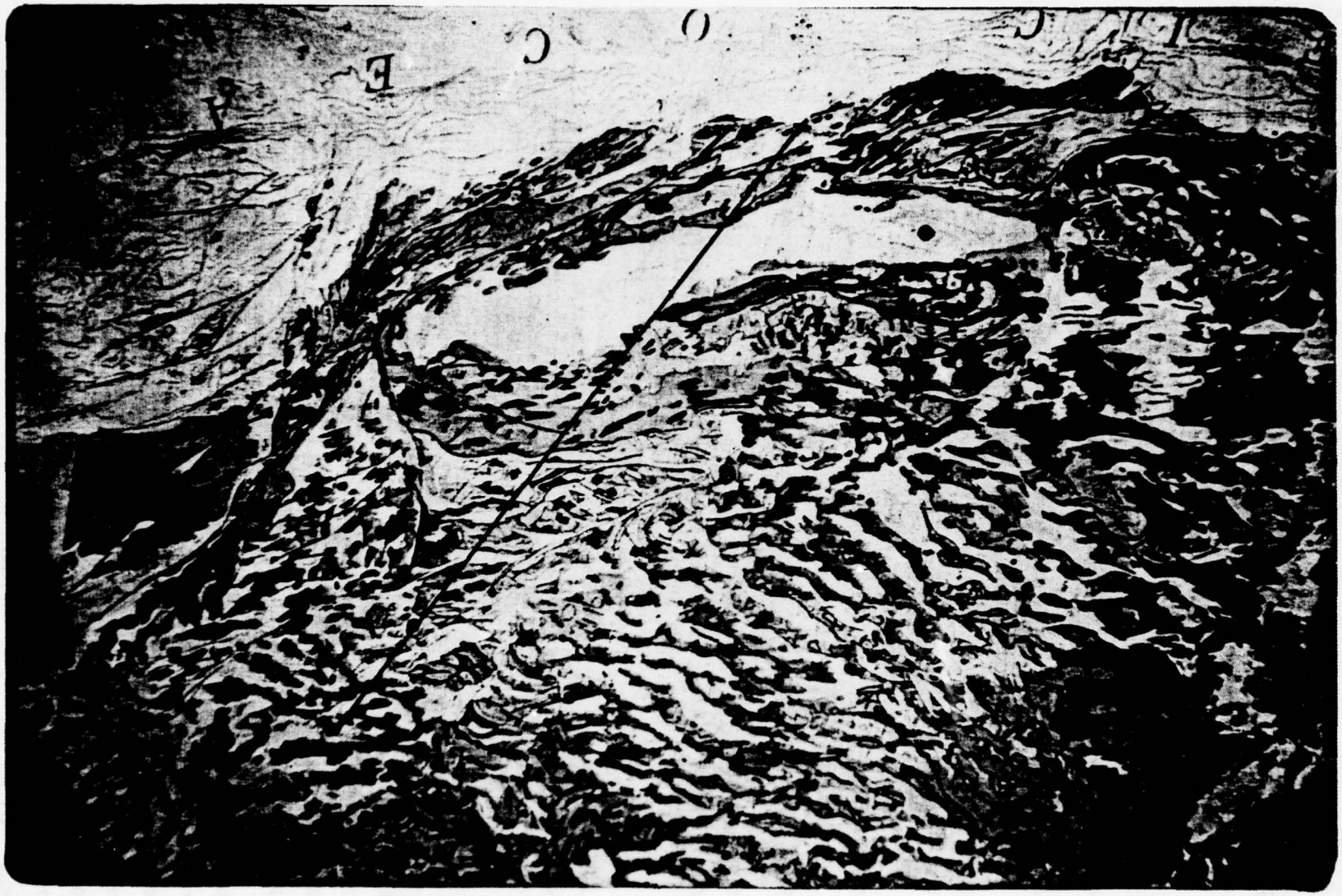

FIGURE 3. ILLUSTRATING GEOLOGIC BASEMENT ROCK TYPE DELINEATION IN WESTERN CONTINENTAL UNITED STATES WITH SEARCHLIGHT, NEVADA TO FT. CRONKHITE, CALIFORNIA PROPAGATION PATH INDICATED, REFERENCE 11.

TABLE 6.

GEOLOGICAL FORMATIONS ON SEARCHLIGHT, NEVADA TO FT. CRONKHITE, CALIFORNIA PROPAGATION PATH

%	DISTANCE KILOMETERS	DESCRIPTION
4.07	0	Q: Quanternary; large areas of thick deposits of Western United States.
2.32	30.391	Xm: Orthogneiss and paragneiss; Precambrian, 2,500,000,000 to 1,600,000,000 years old: extensive in Western United States and of varied composition and origins.
4.07	47.714	Q: Quanternary (see above)
0.58	78.105	uPz: Upper Paleozoic; Permean separated in part, P; UPzc clastic wedge facies in Nevada and Idaho, Diamond Peak, Wood River, Milligen and asscciated formations.
0.58	82.436	Xm: (see above)
0.58	86.767	uPz: (see above)
0.58	91.098	lPz: Lower Paleozoic; Western United States and Piedmont Province; €, Cambrian separated in parts.
0.58	95.429	€: Cambrian
0.87	99.760	Z: Pre Cambrian; 800,000,000 years to Cambrian; Z-Sedimentary rocks, include (among other unites): in Northwestern United States: Windermere Group; in Great Basin: Noonday, Johnnie and other formations; in Grand Canyon, Chuar Group of Grand Canyon subgroup.
1.16	106.256	Q: (see above)
0.58	114.918	Y: Pre Cambrain: 1,600,000,000 to 800,000,000 to Cambrian: Y-sedimentary rocks: Includes (among other units): in Southwestern Untied States: Pahrump Group, UnKan Group of Grand Canyon.
2.32	119.249	Ti: Tertiary intrusive rocks: Plugs, stocks, and lacoliths of all tertiary ages; some granite plutons of early middle tertiary age.
0.58	136.572	Q: (see above)
1.16	140.903	Y: (see above)
3.48	149.565	Q: (see above)
1.16	175.550	lTv: Lower tertiary volcanic rocks; Oligocene and Cocene; some Cretaceous included in Arizona and elsewhere.
0.58	184.212	Xm: Pre Cambrian: Orthogneiss and Paragneiss.
0.58	188.543	Z: Pre Cambrian: Sedimentary.
0.29	192.874	Xm: Pre Cambrian: Orthogneiss and Paragreiss.
0.70	195.039	Xm: Tertiary intrusive rocks.
0.58	200.266	Xm: (see above)
2.32	204.597	Q: (see above)
0.73	221.920	€: (see above)
0.87	227.371	Z: (see above)

TABLE 6 (continued)

0.46	233.867	Ti: (see above)
2.32	237.302	Y: (see above)
1.74	254.625	Q: (see above)
0.35	267.618	Qv: Quarternary volcanic rocks.
1.45	270.231	uPz: Upper paleozoic.
0.70	281.058	uK,b: Upper Cretaceous, Taylor Group (= Montana Group); in Montana plains, separated into UK,a and b at base of Judith River formation, Western interior region.
0.58	286.285	uPz: Upper Paleozoic
0.58	290.616	lPz: Lower Paleozoic; Western United States and Piedmont Province.
1.74	294.947	Qv: Quanternary volcanic rocks.
2.32	307.940	uK,b: Upper Cretaceous.
1.16	235.263	Q: Quarternary.
5.23	333.925	Kg_2: Upper Cretaceous granite rocks; 80,000,000 to 90,000,000 years old,--Sierra Nevada, California.
4.07	372.977	Kg_1: Lower Cretaceous granite rocks; 105,000,000 to 120,000,000 years old; Sierra Nevada, California.
3.48	403.368	lMze: Lower Mesozoic, eugeogynclinal deposits, Middle and Lower Jurassic and Triassic, Western United States.
1.74	429.353	uPz: Upper Paleozoic.
0.58	442.346	lMze: (see above)
0.58	446.677	Kg_1: Lower Cretaceous.
0.29	451.000	lMze: Lower Mesazoic.
1.16	453.173	Kg_1: Lower Cretaceous.
1.16	461.837	lMze: Lower Mesazoic.
2.90	470.497	Kg_1: Lower Cretaceous.
16.26	492.142	Q: Quanternary.
0.87	613.555	Tx: Tertiary; Paleocene; includes Midway Group of Gulf Coastal Plain.
7.55	620.051	uMze: Upper Mesozoic engeosynclinal deposits.
1.16	676.426	Tpc: Tertiary; Pliocene continental deposits of Tertiary.
2.90	685.088	uK: Mesazoic; Upper Cretaceous.
0.58	706.742	um: Mesazoic; Ultramafic rock of Mesozoic Age in Western United States
2.32	711.073	Q: Quarternary.
1.74	728.396	H2O: Seawater: San Francisco Bay.
0.70	741.389	lMze: Lower Mesozoic eugeosgnclinal deposits.
END	746.697	

TABLE 7

ESTIMATED SOIL RESISTIVITY, SOIL DEPTH AND GEOLOGICAL UNDERLAYMENT RESISTIVITY ALONG PROPAGATION PATH BETWEEN SEARCHLIGHT, NEVADA AND FT. CRONKHITE, CALIFORNIA

DISTANCE, KILOMETERS	GEOLOGICAL TYPE	SOIL TYPE	ρ_1	ρ_2	ρ_3	W_1	W_2
0	Q	D2-8	2000	100	100	6	10
30.391	Xm				2000		
47.714	Q				100		
78.105	uPz				280		
82.436	Xm				2000		
86.767	uPz				280		
91.098	lPz				300		
95.429	Є				400		
99.760	Ż				1000		
106.256	Q				100		
114.918	Y				2000		
119.249	Ti				20		
136.572	Q				100		
140.903	Y				2000		
148.953*	Y	D2-7	1000	100	2000	6	10
149.565	Q				100		
173.743*	Q	D2-8	2000	100	100	6	10
175.550	lTv				12		
184.212	Xm				2000		
188.543	Ż				1000		
192.874	Xm				2000		
195.039	Ti				20		
200.266	Xm				2000		
204.597	Q				100		
204.731*	Q	D2-7	2000	100	100	6	10
221.920	Є				400		
227.371	Ż				170		
233.867	Ti				20		
237.302	Y				2000		
254.625	Q				100		
267.618	Qv				90		
270.231	uPz				280		
281.058	uK_3b				25		
286.285	uPz				280		
290.616	lPz				300		
294.947	Qv				200		
307.940	uK_3b				10		
325.263	Q				100		
328.533*	Q	U7-2	500	200	100	2	10
333.925	Kg_2				1850		
312.977	Kg_1				1850		
390.434*	Kg_1	A12-2	500	200	1850	1.5	10
403.368	lMze				140		
429.353	uPz				280		
442.346	lMze				140		
446.677	Kg_1				1850		
451.000	lMze				140		
453.173	Kg_1				1850		
461.837	lMze				140		
470.497	Kg_1				1850		
492.142	Q				100		
539.027*	Q	D3-3	2000	100	100	6	10
570.015*	Q	A12-2	500	200	100	1.5	10
592.341*	Q	E7-2	100	100	100	1	2
613.555	Tx				25		
620.051	uMze				15		
626.980*	uMze	A12-2	15	15	15	1.5	10
676.426	TPc				150		
685.088	uK				15		
706.742	um				15		
728.386	Q				75		
728.539*	H_2Os	H_2Os	0.2	0.2	0.2	10	10
741.389*	lMze	M16-1	15	15	40	2	10
747.697	END	END			END		

age. These rocks are quite extensive in western United States and are of varied composition and origins. From Reference 18, an estimate of 2,000 ohm-m was selected.

At a distance of 78 km along the propagation path under consideration an upper Paleozoic (uPz) geologic basement is encountered. From Reference 26, values of 300-400 ohm-m are noted and from Reference 18, values between 8 and 44 ohm-m. These limestone, bituminous shale, clays and sandstones of the Permean ages are quite variable, perhaps due to the water and saline content. A value of 280 ohm-m has been employed in our initial estimate. A slightly higher value of 300 ohm-m was selected for the lower Paleozoic (lPz) formations encountered at 91 km. The more ancient Cambrian formations according to Reference 18, exhibit values between 6-605 ohm-m, typified by the Cambrian, Eocambrian, Arzberger series or Saxothuringien formation found in Europe.

At 95 km, the most ancient of the Paleozoic rocks are found, i.e., the Cambrian (€) for which a value of 400 ohm-m was selected as an initial estimate. This formation is followed by Precambrian sedimentary (Ƶ) rocks separated from the Cambrian (€) by 800,000,000 years. Such rocks include (amongst other units) in northwestern United States: Windermere group; in Great Basin; the Noonday, Johnnie and other formations; in the Grand Canyon, Chuar group of the Grand Canyon subgroup. In general the unarticulated Precambrian range between 100 and 5,000 ohm-m. From Reference 18, we find that Precambrian and combinations of Precambrian and Cambrian exhibit resistivities between 1,000 and 14,000 ohm-m. Also, the Cambrian and Ordivician exhibit resistivities between 100 and 1,000 ohm-m. One may then estimate the upper Precambrian between 450 and 6,500 ohm-m. Similarily, at 114 km we find Precambrian rocks 1,600,000,000 to 800,000,000 years old as sedimentary rocks (Y) in southwestern United States belonging to the Paheump group, Unkan group of the Grand Canyon subgroup. For this lower group we ascribe a value of 2,000 ohm-m.

At 119 km Tertiary intrusive rocks (Ti) are encountered, comprising plugs, stocks, and laccoliths of all Tertiary ages. Some granite plutons of early middle Tertiary age are also found. According to Reference 18, Cretaceous, Tertiary,

Quaternary and combinations of these periods of geologic time exhibit resistivities between 2 and 30 ohm-m. Quarternary-Tertiary-Pleistocene deposits are quoted at a range of 7 to 19 ohm-m. A value of 20 ohm-m was selected.

At a distance of 148 km from the transmitter a change in soil order is noted. The order D2-7 is similar to the D2-8 noted to this point. Thus, it is a warm dry soil of the ARGID type over gently or moderately sloping rock land, Table 4. The difference between this soil and previous soils is more evident in Table 5 in which we note the soil is classified as Salonchak, comprising salt marsh; belonging to a group of strongly saline soils, usually light colored and without characteristic structural form and typically developed in poorly drained arid and semi-arid areas vegitated mostly by halophytes. Thus, only salt resistant plants can survive in such soil. Notwithstanding the high saline content of the soil we assign a surface value of 1,000 ohm-m because of the existent desert conditions. As we go to greater depths a resistivity of 100 ohm-m was selected. It should be noted, however, that rapid conductivity changes can occur if and when it does rain on the desert. During the dry season, the water table, or the level at which the soil becomes saturated with water, occurs at depths of 2 to 5 meters. This level is quite unclear as a geoelectric boundary. It is rather a gradual increase in water content.

At a distance of 175 km from the Searchlight, Nevada transmitter, Lower Tertiary volvanic rocks ($_{l}Tv$) are found with specific identities of Oligocene and Eocene and some Cretaceous. These rocks range in value between 4 and 31 ohm-m, Reference 18. A value of 12 ohm-m was selected as the initial estimate. Beyond this point the geologic formation and soil repeat the various species already discussed, to a distance of 267 km. Here Quarternary volcanic rocks (Qv) are noted. These structures range between 10 and 200 ohm-m, Reference 36. For these rocks a value of 90 ohm-m was selected.

At a distance of 281 km from the transmitter we note Upper Cretaceous ($_{u}K_{3b}$) rocks of the Taylor group characteristic of the Montanna plains. For these rocks a range in Reference 18, between 8 and 17 ohm-m was noted. A value of 10 ohm-m was selected.

A soil order change at 328 km from the transmitter is noted (U7-2). As noted in Tables 4 and 5, these are characterized as brown mountain soils or mountain meadow soils. This area, 328 km to 390 km ranges in elevation between 3,300 and 2,300 meters above sea level, Table 8, and slopes downhill in a westward direction. The desert conditions continue to prevail, but the rainfall and moisture conditions in the soil are greater. A value of 500 ohm-m was selected for the top 1.5 to 2 meters of soil and a value of 200 ohm-m was selected for the lower layers of soil. An order (A12-2) soil with similar electric properties was noted at 390 km from the transmitter. These are semidesert soils as described in Tables 4 and 5.

At distances between 333 and 390 km we note Upper Cretaceous granite rocks (Kg_2), 80,000,000 to 90,000,000 years old and Lower Cretaceous granite rocks (Kg_1), 105,000,000 to 120,000,000 years of a type that are characteristic of the Sierra Nevada range of mountains in California. Granite rocks tend to exhibit high resistivity, Reference (36), and range in value between 500 and 2,000 ohm-m in the Mesozoic geologic age. A value of 1,850 ohm-m has been selected for these granite rocks.

At 403 km, Lower Mesozoic (lMze) eugeosynclinal deposits (a syncline with volcanic materials mixed with sediments) including Middle and Lower Triasso-Jurassic. Reference 18, gives a range of values for the Triasso-Jurassic between 4 and 350 ohm-m. A value of 140 ohm-m was selected.

At a distance of 613 km from the transmitter, Tertiary (Tx), Paleocene rocks were noted. Reference 18 gives values 4 to 31 ohm-m for this geologic age. A value of 25 ohm-m was selected for the initial estimate.

At a distance of 676 km from the transmitter Lower Tertiary (Tpc) Pliocene deposits were delineated. These rocks are sedimentary and volcanic in nature, Reference 36 and 37, gives a resistivity range of 10-200 ohm-m. A value of 150 ohm-m was selected. Also at 685 and 706 Mesozoic rocks, Upper and Middle, (uK, um) ultramafic (extremely basic, very low in silica, an insulator, and rich in iron, a conductor). A value of 15 ohm-m was selected for these rocks. Also the Quarternary deposits as we approach the California coast were lowered to a resistivity of 75 ohm-m

4. TREATMENT OF TERRAIN DATA

Figue 4 depicts the terrain as the elevation above sea level, meters, as a function of distance in kilometers between Searchlight, Nevada and Ft. Cronkhite, California. Table 8 (in APPENDIX) gives a computer listing of the data. These data are also required by the propagation simulator of the type described in CRPL$_i$ Report 77-9, Reference 13. The curve in Figure 4 of elevation as a function of distance from the transmitter does contain discrete points, but it is necessary to treat these data as a continuous curve for use in such a propagation simulator.

Similarily, the soil and geologic data is taken at discrete intervals as discussed in this report. It is important to note that this also is not meant to imply sudden discontinuities in the ground wave propagation medium. Such sudden discontinuities require special treatment available from other CRPL$_i$ techniques. But the natural ground is rarely discontinuous. In fact, the various soils and geological rocks seem to blend into a continuum.

There is another fundamental observation regarding the inter-relationship of the ground boundary condition at the surface and the terrain. Thus, the soil thickness, W1 + W2, does not form a discontinuous step function as might be implied from the tabulations of data given in this report. Indeed, the soil is usually studied and sampled in the fertile valleys where the soil is quite deep and suitable for agricultural purposes. As we climb the slopes of mountains, the soil slides back into the valleys or at least tends to do same. Thus, on steep mountain slopes we may find very little soil. This immediately suggests the smoothing technique and a coupling technique between soil and terrain.

In the previous report, Reference 13, we noted at a distance point, X_i, the elevation point Z_i and the terrain derivatives:

$$Z_i = A + BX_i + CX_i^2 , \tag{10}$$

$$\frac{\partial Z_i}{\partial X_i} = B + 2CX_i , \tag{11}$$

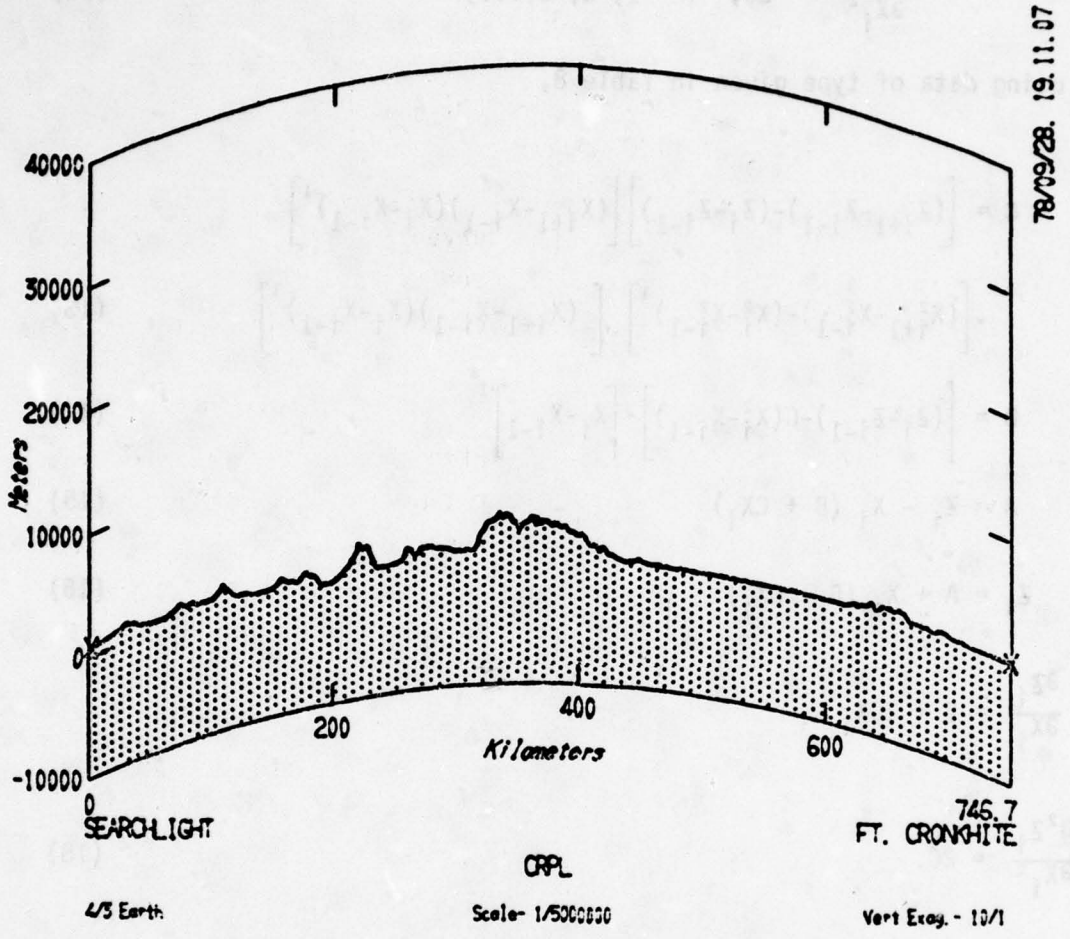

FIGURE 4. GEODESIC PROFILE FROM DIGITIZED TERRAIN DATA BASE ILLUSTRATING ELEVATION ABOVE SEA LEVEL AS A FUNCTION OF DISTANCE FROM THE TRANSMITTER OVER A PATH BETWEEN SEARCHLIGHT, NEVADA AND FT. CRONKHITE, CALIFORNIA.

$$\frac{\partial^2 Z_i}{\partial X_i^2} = 2C, \quad i = 1, 2, 3...., \tag{12}$$

where using data of type given in Table 8,

$$C = \left[(Z_{i+1}-Z_{i-1})-(Z_i-Z_{i-1})\right]\left[(X_{i+1}-X_{i-1})(X_i-X_{i-1})^{-1}\right]$$

$$\cdot\left[(X_{i+1}^2-X_{i-1}^2)-(X_i^2-X_{i-1}^2)^{1}\right]\cdot\left[(X_{i+1}-X_{i-1})(X_i-X_{i-1})^{-1}\right] \tag{13}$$

$$B = \left[(Z_i-Z_{i-1})-C(X_i^2-X_{i-1})\right]\cdot\left[X_i-X_{i-1}\right]^{-1} \tag{14}$$

$$A = Z_i - X_i\,(B + CX_i) \tag{15}$$

$$Z_i = A + X_i\,(B + CX_i) \tag{16}$$

$$\frac{\partial Z_i}{\partial X_i} = B + 2CX_i$$

$$\frac{\partial^2 Z_i}{\partial X_i^2} = 2C. \tag{18}$$

Now, let W_1 and W_2 be our soil data base and,

$$R = W_1/S \tag{19}$$

$$s = W_1 + W_2 . \tag{20}$$

then

$$S\,(X_i,Z_i) = s - \left| s\,\frac{\partial Z_i}{\partial X_i} \right| \beta_i, \tag{21}$$

where β_i is a function of the sheer strength of the soil and the end points of the step of the data interval. Then for each small step X_i in the propagation simulator of Reference 13,

$$W_1 (X_i, Z_i) = R\,S, \tag{22}$$

$$W_2 (X_i, Z_i) = S - W_1, \tag{23}$$

where W is the precise geoelectric section thickness used in the impedance calculation at each point X_i. Then, the surface impedance relative to free space, $x = x_i$, equations (4,5)

$$x_i = f (Z_i, X_i) \tag{24}$$

A detailed discussion of these matters rests in the domain of $CRPL_i$ computer technology and hence is beyond the scope of this paper. However, this brief summary indicated the notion of both soil and terrain continuum and the notion that these continuum are coupled to each other and to the impedance which in turn must also be continuous. If the geology, soil or terrain data are not continuous, as might well be the case in certain very anomalous regions of the earth, special treatment of the problem is required and $CRPL_i$ will in these cases employ other appropriate techniques. This also is beyond the scope of this paper.

5. CONCLUSIONS

The propagation path between Searchlight, Nevada and Ft. Cronkhite, California is indeed a "Worst Case" type path if diversity of terrain and geology is a criterion. It certainly is not necessarily a "Worst Case" path as far as effects on propagation are concerned, because we have found that such diversity often tends to "average out" in some strange fortuitous manner leaving one disappointed as to the observation of the dramatic propagation phenomenon. It is, however, an excellent choice for demonstration purposes and we recommend its use to demonstrate the transient propagation and "envelope to cycle difference" phenomenon.

We conclude that the dominant feature of the propagation path is probably the terrain and the geological structure, but we are also of the opinion that soil should be considered.

We would like to stress the continuous nature of the soil, terrain and geological data if propagation simulators like the referenced integral equation technique are employed. Thus, the soil order boundaries and the geological structure boundary should not be treated as sharp discontinuities unless special appropriate techniques for such matters are introduced.

We recommend that geological resistivity initial estimates should be based on extremely low frequency observations, since radio measurements show a frequency dependence caused by soil and rock stratification.

We note that the ground wave does not propagate in the ground. Thus, sharp boundaries in the ground are permissible because the waves entering the ground are highly damped. The lower stratum of ground do reflect a surface impedance locally that is significant.

The number of geoelectric horizons of ground can be increased to a greater number than three for more accuracy in the initial estimates, if geophysical data can be obtained for this purpose.

6. REFERENCES

(1) U.S. Department of Interior (1969), Distribution of principal kinds of soils: orders, suborders and great groups; National Cooperative Soil Survey Classification of 1967 (U.S. Geological Survey, Washington, D.C. 20242).

(2) Soil Survey Staff (1960), Soil classification, a comprehensive system, 7th approximation (U.S. Dept. Agriculture Soil Conserv. Service, Washington, D.C. 20242); see also: Supplement to soil classification system (7th Approximation).

(3) Thorp, J. and G.O. Smith (1949), Higher categories of soil classification--order, suborder, and great soil groups; Soil Sci., 67, No. 2, 117-126.

(4) U.S. Dept. of Agriculture (1938), Soilds and men, yearbook of agriculture (U.S. Dept. of Agriculture, Washington, D.C. 20402).

(5) Oakes, H., and J. Thorp (1951), Dark-clay soils of warm regions variously called Rendzina, black cotton soils, regur, and tirs, (Soil Sci. Soc. America Proc., 15, 347-354. (definition of Grumusols).

(6) Tavernier, R., and G.O. Smith (1957), The concept of braumerde (Brown forest soil) in Europe and the United States; Advances in agronomy, 9; 217-281(New York, N.Y., Academic Press Inc.) (definition of Sols Brans Acides).

(7) Harper, W.G. (1957), Morphology and genesis of calcisols, Soil Sci. Soc. America Proc., 21, No. 4, 420-424. (definition of calcisols).

(8) Cline, M.G. (1955), Relationships among soils of Hawaii, U.S. Dept. of Agriculture Soil Conserv. Service Soil Survey, Territory of Hawaii, ser 1939, No.25, 67-88 (definition of Hzdrol Humic and Humic Gerruginous Latosols).

(9) McClelland, J.E., C.A. Mogen, W.M. Johnson, F.W. Schroer, and J.S. Allen (1959), Chernozems and associated soils of eastern North Dakota--Some properties and topographic relationships, Soil Sci. Soc. America Proc., 23, No.1, 51-56.

(10) Soviet Geography (1965), Physical-Geographic atlas of the world, 1964 (Review and translation, American Geographical Society, Broadway at 156th Street, New York, N.Y.)

(11) King, P.B., H.M. Beikman, G.J. Edmonston (1974), Geologic map of the United States, scale : :2,500,000 (U.S. Geological Survey, Washington, D.C.).

(12) Burch, L.B., R.H. Doherty and J.R. Johler (1976), Loran calibration by prediction, NAVIGATION, JOurn. of Instit. of Navigation, 23, No. 3, Fall, 195-200.

(13) Johler, J.R. (1977), Loran-C propagation error corrections over nonhomogeneous, irregualr ground using the integral equation technique, CRPL, Report 77-9, U.S.C.G. Contract DOT-CG-74629-A, (Colorado Research and Prediction Laboratory, Inc., 1898 South Flatiron Court, Boulder, CO 80301).

(14) Samaddar, S.N., The theory of Loran-C ground wave propagation--a review (U.S. Coast Guard, G-DOE-4.TP54; Washington, D.C. 20590; presented at Helsinki Conference of URSI; to be published).

(15) Johler, J.R., W.J. Kellar, and L.C. Walters (1956), Phase of low radio frequency ground wave, NBS Circular 573 (Supt. of Doc., U.S. Gov. Print. Off., Washington, D.C. 20402).

(16) Löwy, H. (1911), Dielektrizitätskonstante und Leitfähigkeit der Gesteine; Annualen der Physik, 36, 125-133.

(17) Smith-Rose, R.L. (1934), Electrical measurements on soil with alternating currents; J. Inst. Elec. Engrs., 75, 221-237.

(18) Card, R.H. (1935), Correlation of earth resistivity with geologic structure and age. Trans. Amer. Inst. Elec. Engrs., 54, 1153-1161,(See Figure 1,p 387).

(19) Barfield, R.H. (1934), Some measurements of the electrical constants of the ground at short wave lengths by the wave-tilt method; J. Inst. of Elec. Engrs., 75, 214-220.

(20) Keller, W.J. and F.C. Frischknecht (1966), Electrical Methods in Geophysical Prospecting (Pergamon Press, New York, N.Y., see Table 10, p. 40).

(21) Kirby, R.S., J.G. Harman, J.G. Capps, and R.N. Jones (1954), Effective radio ground conductivity measurements in the United States, NBS Circular 546 (Suptd. of Doc., U.S. Gov. Print. Off., Washington, D.C. 20402).

(22) Pressey, B.G., G.E. Ashwell, and C.S. Fowler (1953), The measurement of the phase velocity of ground wave propagation at low frequencies over a land path, Proc. Inst. Elec. Engrs., 100, pt. III, 73-84.

(23) Fine, H. (1954), An effective ground conductivity map for continental United States, Proc. IRE, 42, No. 9, 1405-1408.

(24) Johler, J.R. (1971), Loran radio navigation over irregular, inhomogeneous ground with effective ground impedance maps, Telecommunications Research and Engineering Report 22 (Suptd. of Doc., U.S. Gov. Print. Off., Washington, D.C. 20402).

(25) Parkhomenko, E.I. (1967), Electrical Properties of Rocks, (Plenim Press, See Table 19, p. 111).

(26) Heiland, C.A. (1946), Geophysical Exploration, (Prentice-Hall, see Tables 65-67, pp. 660-664)

(27) Wait, J.R. (1959), Overvoltage Research and Geophysical Applications (Pergamon Press, see Table 2, p. 106).

(28) Soil Survey Staff (1951), Soil Survey Manual, U.S. Dept. of Agriculture, Soil Survey Staff, Handbook No. 18 (Suptd. of Doc., U.S. Gov. Print. Off., Washington, D.C. 20402).

(29) Cosby, S.W. and E.B. Watson (1928), Soil Survey The Gilroy Area California, U.S. Dept. Agr. Series 1923, No. 19 (Suptd. of Doc., U.S. Gov. Print. Off., Washington, D.C. 20402).

(30) Carpenter, E.J. and Cosby, S.W. (1939), Soil Survey of Contra Costa County, California, U.S. Dept. of Agr. Series 1933, No. 26 (Suptd. of Doc., U.S. Gov Print. Off., Washington, D.C. 20402).

(31) Carpenter, E.J. and Cosby, S.W. (1934), Soil Survey of the Svisum Area, California, U.S. Dept. of Agr. Series 1930, No. 18 (Suptd. of Doc., U.S. Print. Off., Washington, D.C. 20402).

(32) Watson, E.B. and Storie, R.E. (1928), Soil Survey of the Bishop Area, California, U.S. Dept. of Agr. Series 1924, No. 3 (Suptd. of Doc., U.D. Dept. Print. Off, Washington, D.C. 20402).

(33) Storie, R.E. and Owen, B.C. (1940), Soil Survey of the Visalia Area, California, U.S. Dept. of Agr. Series 1935, No. 16 (Suptd. of Doc., U.S. Gov. Print. Off., Washington, D.C. 20402).

(34) Storie, R.E. and Trussell, D.F. (1937), Soil Survey of the Barstow Area, California, U.S. Dept. of Agr. Series 1933, No. 8 (Suptd. of Doc., U.S. Gov. Print. Off., Washington, D.C. 20402)

(35) Carpenter, E.J. and Youngs, F.O. (1928), Soil Survey of the Las Vegas Area, Nevada, U.S. Dept. Agr. Series 1923, No. 8 (Suptd. of Doc., U.S. Gov. Print. Off., Washington, D.C. 20402).

(36) Keller, G.V. (1966), Electrical properties of rocks and minerals, Section 26, Handbook of Physical Constnats, p. 562.

(37) Sommerfeld, A. (1909), "Über Die Ausbreitung der Wellen in der Drahtlosen Telegraphie," Ann. Phys., vol. 28. pp/ 665-736: March.

APPENDIX: TABLE 8

APPENDIX

TABLE 8

Elevation Above Sea Level As A Function Of Distance Along Geodesic Between Searchlight, Nevada and Ft. Cronkhite, California.

i	$X_{i,km}$	$Z_{i,m}$						
1	0.00	911.1	2	1.24	874.1	3	2.49	850.3
4	3.73	840.4	5	4.98	834.4	6	6.22	839.7
7	7.47	846.4	8	8.71	857.0	9	9.96	870.5
10	11.20	887.5	11	12.45	909.3	12	13.69	930.8
13	14.93	974.6	14	16.18	1010.4	15	17.42	1035.4
16	18.67	1042.0	17	19.91	1081.2	18	21.16	1108.4
19	22.41	1148.7	20	23.65	1188.7	21	24.89	1234.0
22	26.13	1289.7	23	27.38	1344.5	24	28.62	1416.7
25	29.87	1527.8	26	31.11	1593.2	27	32.36	1488.4
28	33.60	1406.0	29	34.85	1374.9	30	36.09	1368.5
31	37.34	1355.9	32	38.58	1270.1	33	39.82	1138.4
34	41.07	1064.6	35	42.31	1013.5	36	43.56	988.9
37	44.80	957.0	38	46.05	939.6	39	47.29	911.2
40	48.54	873.0	41	49.78	849.8	42	51.03	841.1
43	52.27	837.0	44	53.51	835.2	45	54.76	838.1
46	56.00	841.2	47	57.25	845.3	48	58.49	853.4
49	59.74	853.4	50	60.98	853.4	51	62.23	853.4
52	63.47	856.5	53	64.71	900.3	54	65.96	946.8
55	67.20	1011.8	56	68.45	1036.2	57	69.69	1178.1
58	70.94	1268.8	59	72.18	1374.0	60	73.43	1446.8
61	74.67	1555.0	62	75.92	1465.9	63	77.16	1350.6
64	78.40	1268.6	65	79.65	1214.3	66	80.89	1196.2
67	82.14	1213.0	68	83.38	1334.7	69	84.63	1376.0
70	85.87	1228.7	71	87.12	1093.5	72	88.36	1067.1
73	89.61	1058.3	74	90.85	1107.6	75	92.09	1117.0
76	93.34	1094.5	77	94.58	1055.0	78	95.83	1033.1
79	97.07	1066.8	80	98.32	1064.5	81	99.56	1036.6
82	100.81	1065.9	83	102.05	1101.4	84	103.29	1225.6
85	104.54	1310.6	86	105.78	1479.2	87	107.03	1635.4
88	108.27	1821.8	89	109.52	1951.2	90	110.76	1750.5
91	112.01	1605.5	92	113.25	1423.0	93	114.50	1369.1
94	115.74	1157.5	95	116.98	997.4	96	118.23	954.1
97	119.47	845.9	98	120.72	791.7	99	121.96	750.6
100	123.21	740.4	101	124.45	731.3	102	125.70	733.7
103	126.94	761.7	104	128.19	689.2	105	129.43	647.4
106	130.67	621.5	107	131.92	580.3	108	133.16	534.0
109	134.41	509.4	110	135.65	498.3	111	136.90	472.5
112	138.14	423.6	113	139.39	466.5	114	140.63	486.1
115	141.87	491.5	116	143.12	500.8	117	144.36	477.3
118	145.61	466.2	119	146.85	473.0	120	148.10	491.9
121	149.34	529.3	122	150.59	586.0	123	151.83	664.0
124	153.08	750.6	125	154.32	850.3	126	155.56	967.6
127	156.81	1164.3	128	158.05	1070.8	129	159.30	973.5
130	160.54	894.9	131	161.79	826.1	132	163.03	778.2
133	164.28	729.0	134	165.52	792.6	135	166.77	631.1
136	168.01	534.8	137	169.25	620.7	138	170.50	609.1
139	171.74	718.7	140	172.99	747.1	141	174.23	800.8
142	175.48	1060.3	143	176.72	1127.0	144	177.97	1186.6
145	179.21	958.0	146	180.45	813.7	147	181.70	935.6

TABLE 8 CONTINUED

148	182.94	853.3	149	184.19	797.7	150	185.43	601.6
151	186.68	441.7	152	187.92	115.2	153	189.17	-49.2
154	190.41	-69.1	155	191.66	-73.6	156	192.90	-71.9
157	194.14	-61.0	158	195.39	-61.0	159	196.63	-61.8
160	197.89	-64.1	161	199.12	-41.4	162	200.37	30.9
163	201.61	123.5	164	202.86	193.0	165	204.10	262.9
166	205.35	331.5	167	206.59	447.5	168	207.83	598.8
169	209.08	784.7	170	210.32	837.1	171	211.57	994.7
172	212.81	1168.5	173	214.06	1430.2	174	215.30	1446.4
175	216.55	1666.1	176	217.79	1927.1	177	219.03	2221.9
178	220.28	2651.3	179	221.52	2351.7	180	222.77	2142.6
181	224.01	2255.2	182	225.26	2276.2	183	226.50	2443.6
184	227.75	2292.3	185	228.99	1813.1	186	230.24	1590.6
187	231.48	1150.6	188	232.72	841.3	189	233.97	562.6
190	235.21	516.3	191	236.46	523.8	192	237.70	522.7
193	238.95	515.1	194	240.19	508.9	195	241.44	500.7
196	242.68	500.9	197	243.92	495.0	198	245.17	404.8
199	246.41	492.2	200	247.66	531.9	201	248.90	552.8
202	250.15	581.7	203	251.39	632.5	204	252.64	702.2
205	253.88	731.5	206	255.13	858.7	207	256.37	1059.3
208	257.61	1112.0	209	258.86	1609.5	210	260.10	1746.9
211	261.35	1625.7	212	262.59	1595.8	213	263.84	1366.1
214	265.08	1224.3	215	266.33	1139.9	216	267.57	1174.5
217	268.82	1276.7	218	270.06	1412.0	219	271.30	1642.1
220	272.55	1689.8	221	273.79	1561.1	222	275.04	1591.2
223	276.28	1667.0	224	277.53	1632.8	225	278.77	1629.9
226	280.02	1625.5	227	281.26	1549.2	228	282.50	1491.1
229	283.75	1463.8	230	284.99	1463.0	231	286.24	1463.0
232	287.48	1431.8	233	288.73	1402.1	234	289.97	1395.1
235	291.22	1361.5	236	292.46	1372.6	237	293.71	1322.4
238	294.95	1237.8	239	296.19	1204.9	240	297.44	1157.7
241	298.68	1122.6	242	299.93	1095.9	243	301.17	1091.2
244	302.42	1091.2	245	303.66	1091.2	246	304.91	1091.2
247	306.15	1091.2	248	307.40	1091.2	249	308.64	1091.2
250	309.88	1087.4	251	311.13	1068.2	252	312.37	1083.6
253	313.62	1103.2	254	314.86	1148.6	255	316.11	1365.6
256	317.35	1626.9	257	318.60	2063.3	258	319.84	2327.4
259	321.08	2531.2	260	322.33	2611.0	261	323.57	2967.4
262	324.82	3132.6	263	326.06	3175.5	264	327.31	3304.1
265	328.55	327.4.4	266	329.80	3370.8	267	331.04	3436.4
268	332.29	3469.3	269	333.53	3569.8	270	334.77	3910.8
271	336.02	3730.4	272	337.26	3485.2	273	338.51	3746.2
274	339.75	3779.1	275	341.00	3810.5	276	342.24	3604.5
277	343.49	3696.7	278	344.73	3334.6	279	345.98	3157.8
280	347.22	3134.5	281	348.46	3131.8	282	349.71	2708.0
283	351.95	2534.4	284	352.20	2884.4	285	353.44	2942.3
286	354.69	3013.6	287	355.93	3085.5	288	357.18	3167.4
289	358.42	3166.6	290	359.66	3391.6	291	360.91	3589.0
292	362.15	3474.3	293	363.40	3170.1	294	364.64	3504.3
295	365.89	3321.9	296	367.13	2949.5	297	368.38	2982.4
298	369.62	3222.1	299	370.87	3049.4	300	372.11	3249.5
301	373.35	3207.6	302	374.60	3088.3	303	375.84	3070.3
304	377.09	2766.5	305	378.33	2857.1	306	379.58	3039.3
307	380.82	2881.3	308	382.07	2952.1	309	383.31	2847.2
310	384.56	2720.2	311	385.80	2723.3	312	387.04	2764.6
313	388.29	2783.3	314	389.53	2561.2	315	390.78	2467.3
316	392.02	2353.8	317	393.27	2321.6	318	394.51	2363.3
319	395.76	2306.2	320	397.00	2054.3	321	398.24	2027.6
322	399.49	2141.6	323	400.73	2049.3	324	401.98	2225.6
325	403.22	2112.6	326	404.47	2010.8	327	405.71	1845.2
328	406.96	1657.1	329	408.20	1433.6	330	409.45	1349.0
331	410.69	1457.5	332	411.93	1557.8	333	413.18	1426.9
334	414.42	1295.4	335	415.67	980.2	336	416.91	1058.0
337	418.16	1358.5	338	419.40	1362.0	339	420.65	1146.5

TABLE 8 CONTINUED

340	421.84	882.4	341	423.14	753.9	342	424.38	727.0
343	425.62	804.3	344	426.87	798.6	345	428.11	629.5
346	429.36	505.6	347	430.60	510.0	348	431.85	458.9
349	433.09	503.2	350	434.34	353.3	351	435.58	317.0
352	436.82	281.4	353	438.07	299.6	354	439.31	368.5
355	440.56	361.4	356	441.80	432.3	357	443.05	371.2
358	444.29	354.1	359	445.54	509.0	360	446.78	573.2
361	448.03	563.5	362	449.27	456.2	363	450.51	450.7
364	451.76	377.6	365	453.00	339.6	366	454.25	313.1
367	455.49	291.5	368	456.74	237.9	369	457.98	206.6
370	459.23	233.2	371	460.47	239.3	372	461.72	285.3
373	462.96	290.2	374	464.20	272.9	375	465.45	200.7
376	466.69	182.9	377	467.94	190.1	378	469.18	223.3
379	470.43	241.6	380	471.67	192.7	381	472.92	167.6
382	474.16	179.4	383	475.40	135.5	384	476.65	110.1
385	477.89	144.0	386	479.14	160.9	387	480.38	173.2
388	481.63	208.2	389	482.87	167.6	390	484.12	165.9
391	485.36	165.7	392	486.61	154.8	393	487.85	165.7
394	489.09	143.7	395	490.34	139.2	396	491.58	135.9
397	492.83	121.9	398	494.07	121.9	399	495.32	119.7
400	496.56	118.9	401	497.81	115.8	402	499.05	118.6
403	500.30	115.8	404	501.54	115.8	405	502.78	115.8
406	504.03	111.6	407	505.27	109.3	408	506.52	103.7
409	507.76	92.2	410	509.01	91.4	411	510.25	91.4
412	511.50	91.4	413	512.74	91.4	414	513.98	91.4
415	515.23	91.4	416	516.47	91.4	417	517.72	91.4
418	518.96	91.4	419	520.21	88.3	420	521.45	84.9
421	522.70	79.2	422	523.94	79.5	423	525.19	84.8
424	526.43	85.3	425	527.67	74.8	426	528.92	73.2
427	530.16	73.2	428	531.41	73.2	429	532.65	72.2
430	533.90	63.0	431	535.14	61.0	432	536.39	61.0
433	537.63	61.0	434	538.88	61.0	435	540.12	61.0
436	541.36	61.0	437	542.61	56.3	438	543.85	54.9
439	545.11	54.9	440	546.34	54.9	441	547.59	54.9
442	548.83	54.5	443	550.08	50.9	444	551.32	47.5
445	552.56	48.4	446	553.81	42.7	447	555.05	42.7
448	556.30	42.7	449	557.54	42.7	450	558.79	40.9
451	560.03	36.6	452	561.28	36.6	453	562.52	36.6
454	563.77	36.6	455	565.01	36.6	456	566.25	33.0
457	567.50	30.5	458	568.74	30.5	459	569.99	30.5
460	571.23	30.5	461	572.48	30.5	462	573.72	30.5
463	574.97	30.5	464	576.21	30.5	465	577.46	30.5
466	578.70	30.5	467	579.94	30.5	468	581.19	30.5
469	582.43	30.5	470	583.68	30.5	471	584.92	26.5
472	586.17	30.5	473	587.41	30.5	474	588.66	24.8
475	589.91	24.4	476	591.14	24.4	477	592.39	24.3
478	593.63	18.4	479	594.98	20.8	480	596.12	18.3
481	597.37	18.3	482	598.61	18.3	483	599.86	17.6
484	601.10	19.2	485	602.35	24.4	486	603.59	25.0
487	604.83	28.8	488	606.08	30.8	489	607.32	34.2
490	608.57	40.0	491	609.81	42.6	492	611.06	51.7
493	612.30	55.4	494	613.55	66.7	495	614.79	114.8
496	616.04	126.4	497	617.28	166.1	498	618.52	236.0
499	619.77	279.4	500	621.01	395.7	501	622.26	382.2
502	623.50	191.6	503	624.75	264.3	504	625.99	350.3
505	627.24	424.7	506	628.48	436.7	507	629.72	424.3
508	630.97	467.9	509	632.21	523.8	510	633.46	714.2
511	634.70	866.1	512	635.95	746.3	513	637.19	564.3
514	638.44	397.6	515	639.68	459.4	516	640.93	439.7
517	642.17	582.8	518	643.41	787.3	519	644.66	823.1
520	645.90	803.4	521	647.15	797.4	522	648.39	791.9
523	649.64	860.1	524	650.88	706.4	525	652.13	685.5
526	653.37	682.7	527	654.62	677.6	528	655.86	758.5
529	657.11	936.1	530	658.35	700.9	531	659.59	772.8

TABLE 8 CONTINUED

532	660.84	846.8	533	662.00	684.6	534	663.33	477.0
535	664.57	302.3	536	665.82	304.5	537	667.06	240.2
538	668.30	248.5	539	669.55	254.8	540	670.79	324.2
541	672.04	331.1	542	673.28	304.9	543	674.53	244.9
544	675.77	229.0	545	677.02	250.7	546	678.26	279.6
547	679.51	206.3	548	680.75	223.9	549	681.99	153.8
550	683.24	121.9	551	684.48	121.9	552	685.73	126.1
553	686.97	197.6	554	688.22	347.7	555	689.46	374.9
556	690.71	409.5	557	691.95	331.2	558	693.19	374.8
559	694.44	314.5	560	695.68	192.6	561	696.93	181.8
562	698.17	163.7	563	699.42	96.5	564	700.66	68.5
565	701.91	80.7	566	703.15	94.2	567	704.40	121.7
568	705.64	136.1	569	706.88	102.3	570	708.13	53.6
571	709.37	43.2	572	710.62	41.4	573	711.86	33.3
574	713.11	27.0	575	714.35	9.5	576	715.60	0.0
577	716.84	0.0	578	718.09	0.0	579	719.33	0.0
580	720.57	0.0	581	721.82	0.0	582	723.06	0.0
583	724.31	0.0	584	725.55	0.0	585	726.80	0.0
586	728.04	0.0	587	729.29	0.0	588	730.53	0.0
589	731.77	2.9	590	733.02	27.6	591	734.26	40.7
592	735.51	10.4	593	736.75	.8	594	738.00	0.0
595	739.24	0.0	596	740.49	0.0	597	741.73	41.2
598	742.98	89.0	599	744.22	62.2	600	745.46	136.2

i	$X_{i,mi.}$	$Z_{i,ft.}$						
1	0.00	2989.3	2	.77	2867.8	3	1.55	2789.7
4	2.32	2757.1	5	3.09	2737.6	6	3.87	2754.8
7	4.64	2776.1	8	5.41	2811.7	9	6.19	2856.1
10	6.95	2911.9	11	7.73	2963.2	12	8.51	3080.1
13	9.28	3197.4	14	10.05	3314.8	15	10.83	3397.0
16	11.60	3418.7	17	12.37	3547.2	18	13.15	3636.4
19	13.92	3768.8	20	14.69	3900.1	21	15.47	4048.4
22	16.24	4231.3	23	17.01	4411.0	24	17.79	4647.9
25	18.56	5012.5	26	19.33	5227.0	27	20.11	4883.1
28	20.88	4612.8	29	21.65	4510.7	30	22.43	4490.0
31	23.20	4448.5	32	23.97	4167.0	33	24.75	3734.8
34	25.52	3492.7	35	26.29	3325.0	36	27.07	3244.5
37	27.84	3172.5	38	28.61	3083.4	39	29.39	2989.6
40	30.16	2854.2	41	30.93	2788.0	42	31.71	2759.5
43	32.48	2746.2	44	33.25	2740.0	45	34.03	2749.7
46	34.80	2760.0	47	35.57	2773.2	48	36.35	2800.0
49	37.12	2800.0	50	37.89	2800.0	51	38.67	2800.0
52	39.44	2810.3	53	40.21	2953.7	54	40.99	3106.4
55	41.76	3319.6	56	42.53	3596.6	57	43.31	3865.1
58	44.08	4162.6	59	44.85	4507.9	60	45.63	4746.6
61	46.40	5101.8	62	47.17	4809.5	63	47.94	4431.2
64	48.72	4162.2	65	49.49	3983.9	66	50.26	3924.6
67	51.04	3979.5	68	51.81	4378.9	69	52.58	4514.5
70	53.36	4031.0	71	54.13	3587.5	72	54.90	3500.9
73	55.68	3472.1	74	56.45	3633.8	75	57.22	3664.6
76	58.00	3590.7	77	58.77	3461.3	78	59.54	3389.5
79	60.32	3502.1	80	61.09	3492.4	81	61.86	3400.9
82	62.64	3496.3	83	63.41	3876.1	84	64.18	4021.1
85	64.96	4239.8	86	65.73	4852.9	87	66.50	5365.4
88	67.26	5976.3	89	68.05	6401.7	90	68.82	5743.1

TABLE 8 CONTINUED

91	69.64	5267.2	92	70.37	4658.7	93	71.14	4491.7
94	71.92	3797.5	95	72.69	3272.3	96	73.46	3130.4
97	74.24	2772.3	98	75.01	2597.5	99	75.78	2488.7
100	76.56	2429.0	101	77.33	2399.2	102	78.10	2407.3
103	78.88	2498.9	104	79.65	2261.0	105	80.42	2123.9
106	81.20	2039.1	107	81.97	1903.9	108	82.74	1752.1
109	83.52	1671.4	110	84.29	1635.0	111	85.06	1550.2
112	85.84	1389.7	113	86.61	1537.0	114	87.38	1594.8
115	88.16	1612.4	116	88.93	1643.1	117	89.70	1566.0
118	90.48	1529.5	119	91.25	1551.9	120	92.02	1613.8
121	92.80	1736.6	122	93.57	1922.4	123	94.34	2178.5
124	95.12	2462.6	125	95.89	2789.8	126	96.66	3174.6
127	97.46	3826.6	128	98.21	3513.1	129	98.98	3194.0
130	99.76	2933.1	131	100.53	2710.4	132	101.30	2553.0
133	102.08	2391.6	134	102.85	2600.3	135	103.62	2070.7
136	104.40	1951.3	137	105.17	2036.4	138	105.94	1998.2
139	106.72	2357.9	140	107.49	2451.0	141	108.26	2653.6
142	109.04	3544.4	143	109.81	3697.3	144	110.58	3899.7
145	111.36	3143.2	146	112.13	2669.5	147	112.90	3069.6
148	113.68	2799.5	149	114.45	2617.0	150	115.22	1973.8
151	116.00	1449.1	152	116.77	378.0	153	117.54	-161.3
154	118.32	-226.8	155	119.09	-241.4	156	119.86	-235.7
157	120.64	-200.0	158	121.41	-200.0	159	122.18	-202.9
160	122.96	-210.2	161	123.73	-135.8	162	124.50	101.4
163	125.23	405.2	164	126.05	633.1	165	126.82	862.5
166	127.60	1087.7	167	128.37	1468.2	168	129.14	1964.4
169	129.92	2574.5	170	130.69	2746.3	171	131.46	3263.5
172	132.24	3833.6	173	133.01	4692.1	174	133.78	4752.1
175	134.56	5466.2	176	135.33	6322.6	177	136.10	7289.9
178	136.88	8698.6	179	137.65	7715.6	180	138.42	7029.4
181	139.23	7398.9	182	139.97	7467.8	183	140.74	8017.0
184	141.51	7520.6	185	142.29	5948.6	186	143.06	5218.5
187	143.83	3775.0	188	144.61	2760.3	189	145.38	1845.8
190	146.15	1693.8	191	146.93	1718.4	192	147.70	1714.8
193	148.47	1696.0	194	149.25	1669.7	195	150.02	1642.7
196	150.79	1643.2	197	151.57	1623.9	198	152.34	1590.6
199	153.11	1614.8	200	153.89	1745.0	201	154.66	1813.7
202	155.43	1908.4	203	156.21	2075.3	204	156.98	2303.9
205	157.75	2400.0	206	158.53	2817.1	207	159.30	3475.5
208	160.07	3645.1	209	160.85	5280.5	210	161.62	5731.2
211	162.39	5333.8	212	163.17	5235.5	213	163.94	4481.9
214	164.71	4016.8	215	165.49	3739.9	216	166.26	3853.5
217	167.03	4188.7	218	167.81	4632.6	219	168.58	5387.5
220	169.35	5544.0	221	170.13	5187.4	222	170.90	5220.6
223	171.67	5469.1	224	172.45	5357.1	225	173.22	5347.3
226	173.99	5333.0	227	174.77	5082.5	228	175.54	4892.1
229	176.31	4802.4	230	177.09	4600.0	231	177.86	4600.0
232	178.63	4697.6	233	179.41	4600.0	234	180.18	4577.1
235	180.95	4466.7	236	181.73	4503.3	237	182.50	4338.6
238	183.27	4061.0	239	184.05	3953.2	240	184.82	3798.2
241	185.59	3683.2	242	186.37	3595.4	243	187.14	3580.0
244	187.91	3580.0	245	188.69	3580.0	246	189.46	3580.0
247	190.23	3580.0	248	191.01	3580.0	249	191.78	3580.0
250	192.55	3567.4	251	193.33	3504.5	252	194.10	3555.3
253	194.87	3619.6	254	195.65	3768.3	255	196.42	4480.5
256	197.19	5344.1	257	197.97	6769.3	258	198.74	7635.9
259	199.51	8304.3	260	200.29	8566.2	261	201.06	9735.5
262	201.83	10277.5	263	202.61	10418.3	264	203.38	10840.2
265	204.15	10742.9	266	204.93	11059.2	267	205.70	11200.9
268	206.47	11382.3	269	207.25	11777.7	270	208.02	12830.6
271	208.79	12238.7	272	209.57	11434.4	273	210.34	12290.7
274	211.11	12398.7	275	211.89	12501.8	276	212.66	11825.9
277	213.43	12128.2	278	214.21	10940.2	279	214.98	10360.3
280	215.75	10480.3	281	216.53	10275.0	282	217.30	6884.5

TABLE 8 CONTINUED

283	214.87	8315.1	284	216.85	9463.4	285	218.82	9653.1
286	220.34	9867.0	287	221.17	10123.2	288	221.94	10391.6
289	222.71	10389.2	290	223.49	11127.5	291	224.26	11775.0
292	225.03	11398.5	293	225.81	10408.7	294	226.58	11496.9
295	227.35	10894.7	296	228.13	9676.9	297	228.90	9784.8
298	229.67	10571.1	299	230.45	10004.6	300	231.22	10661.0
301	231.99	10523.5	302	232.77	10132.1	303	233.54	10073.1
304	234.31	9076.4	305	235.08	9373.8	306	235.86	9971.5
307	236.63	9453.1	308	237.40	9685.3	309	238.18	9341.3
310	238.95	8924.6	311	239.72	8934.6	312	240.50	9070.3
313	241.27	9131.6	314	242.04	8402.7	315	242.82	8094.8
316	243.59	7722.6	317	244.36	7616.7	318	245.14	7753.6
319	245.91	7566.4	320	246.68	6739.8	321	247.46	6652.1
322	248.23	7026.1	323	249.00	6723.5	324	249.78	7301.8
325	250.55	6931.2	326	251.32	6597.3	327	252.10	6053.9
328	252.87	5436.8	329	253.64	4703.4	330	254.42	4426.0
331	255.19	4781.7	332	255.96	5111.0	333	256.74	4681.4
334	257.51	4256.1	335	258.28	3215.7	336	259.06	3471.0
337	259.83	4457.2	338	260.60	4460.4	339	261.38	3761.4
340	262.15	2896.7	341	262.92	2473.3	342	263.70	2385.3
343	264.47	2638.6	344	265.24	2619.9	345	266.02	2065.2
346	266.79	1658.7	347	267.56	1673.1	348	268.34	1505.7
349	269.11	1651.0	350	269.88	1159.1	351	270.66	1040.0
352	271.43	923.2	353	272.20	982.9	354	272.98	1209.0
355	273.75	1185.7	356	274.52	1418.5	357	275.30	1217.8
358	276.07	1161.9	359	276.84	1669.8	360	277.62	1880.5
361	278.39	1848.7	362	279.16	1496.7	363	279.94	1478.6
364	280.71	1238.8	365	281.48	1114.3	366	282.26	1027.2
367	283.03	956.2	368	283.80	780.4	369	284.58	678.0
370	285.35	765.2	371	286.12	785.2	372	286.90	936.2
373	287.67	952.2	374	288.44	895.2	375	289.22	658.4
376	289.99	600.0	377	290.76	623.6	378	291.54	732.6
379	292.31	792.5	380	293.08	632.1	381	293.86	549.7
382	294.63	588.5	383	295.40	444.5	384	296.18	387.3
385	296.95	472.3	386	297.72	527.8	387	298.50	568.2
388	299.27	683.0	389	300.04	549.9	390	300.82	544.4
391	301.59	543.6	392	302.36	507.9	393	303.14	543.6
394	303.91	471.3	395	304.68	456.6	396	305.46	446.0
397	306.23	406.0	398	307.00	400.0	399	307.78	392.8
400	308.55	389.9	401	309.32	380.0	402	310.10	389.1
403	310.87	380.0	404	311.64	380.0	405	312.42	380.0
406	313.19	366.2	407	313.96	358.5	408	314.74	340.3
409	315.51	302.4	410	316.28	300.0	411	317.06	300.0
412	317.83	300.0	413	318.60	300.0	414	319.38	300.0
415	320.15	300.0	416	320.92	300.0	417	321.70	300.0
418	322.47	300.0	419	323.24	289.7	420	324.02	278.5
421	324.79	260.0	422	325.56	260.7	423	326.34	278.3
424	327.11	280.0	425	327.88	245.3	426	328.66	240.0
427	328.43	240.0	428	330.20	240.0	429	330.97	237.0
430	331.75	206.7	431	332.52	200.0	432	333.29	200.0
433	334.07	200.0	434	334.84	200.0	435	335.61	200.0
436	336.39	200.0	437	337.16	184.8	438	337.93	180.0
439	338.71	180.0	440	339.48	180.0	441	340.25	180.0
442	341.03	178.7	443	341.80	167.0	444	342.57	155.8
445	343.35	158.8	446	344.12	140.0	447	344.89	140.0
448	345.67	140.3	449	346.44	140.0	450	347.21	134.3
451	347.99	120.0	452	348.76	120.0	453	349.53	120.0
454	350.31	120.0	455	351.08	120.0	456	351.85	108.3
457	352.63	100.1	458	353.40	100.0	459	354.17	100.0
460	354.95	100.0	461	355.72	100.0	462	356.49	100.0
463	357.27	100.0	464	358.04	100.0	465	358.81	100.0
466	359.59	100.0	467	360.36	100.0	468	361.13	100.0
469	361.91	100.0	470	362.68	100.0	471	363.45	86.9
472	364.23	101.0	473	365.00	100.0	474	365.77	81.5

TARIF 8 CONTINUED

475	366.55	80.0	476	367.32	80.0	477	368.09	79.7
478	368.87	60.2	479	369.64	60.2	480	370.41	60.0
481	371.19	60.0	482	371.96	60.0	483	372.73	57.7
484	373.51	62.9	485	374.28	89.0	486	375.05	81.9
487	375.83	94.6	488	376.60	101.1	489	377.37	112.4
490	378.15	131.1	491	378.92	139.7	492	379.69	169.6
493	380.47	181.6	494	381.24	210.8	495	382.01	376.6
496	382.79	414.7	497	383.56	545.0	498	384.33	774.2
499	385.11	916.5	500	385.88	1298.3	501	386.65	1253.9
502	387.43	628.7	503	388.20	932.6	504	388.97	1149.2
505	389.75	1393.5	506	390.52	1432.7	507	391.29	1392.0
508	392.07	1535.1	509	392.84	1718.4	510	393.61	2343.3
511	394.39	2841.4	512	395.16	2440.3	513	395.93	1851.3
514	396.71	1271.7	515	397.48	1507.3	516	398.25	1442.6
517	399.03	1912.1	518	399.80	2533.0	519	400.57	2700.4
520	401.35	2635.8	521	402.12	2616.2	522	402.89	2598.1
523	403.67	2846.1	524	404.44	2317.6	525	405.21	2249.1
526	405.99	2239.7	527	406.76	2223.2	528	407.53	2488.6
529	408.31	3471.1	530	409.08	2562.0	531	409.85	2535.4
532	410.63	2627.2	533	411.40	2246.2	534	412.17	1564.9
535	412.95	990.9	536	413.72	998.9	537	414.49	814.3
538	415.27	815.4	539	416.04	835.9	540	416.81	1063.8
541	417.59	1086.3	542	418.36	1000.4	543	419.13	803.6
544	419.91	751.2	545	420.68	822.6	546	421.45	917.3
547	422.23	939.1	548	423.00	734.5	549	423.77	504.5
550	424.54	400.0	551	425.32	400.0	552	426.09	413.8
553	426.86	648.3	554	427.64	1140.8	555	428.41	1229.9
556	429.18	1343.4	557	429.96	1086.5	558	430.73	1229.8
559	431.50	1032.0	560	432.28	631.7	561	433.05	596.5
562	433.82	537.1	563	434.60	316.5	564	435.37	224.6
565	436.14	264.6	566	436.92	308.9	567	437.69	399.3
568	438.46	446.5	569	439.24	335.8	570	440.01	175.8
571	440.78	141.7	572	441.56	135.9	573	442.33	109.3
574	443.10	88.6	575	443.88	31.2	576	444.65	0.0
577	445.42	0.0	578	446.20	0.0	579	446.97	0.0
580	447.74	0.0	581	448.52	0.0	582	449.29	0.0
583	450.06	0.0	584	450.84	0.0	585	451.61	0.0
586	452.38	0.0	587	453.16	0.0	588	453.93	0.0
589	454.70	9.4	590	455.48	90.7	591	456.25	133.4
592	457.02	34.2	593	457.80	2.5	594	458.57	0.0
595	459.34	0.0	596	460.12	0.0	597	460.89	135.1
598	461.66	292.0	599	462.44	203.9	600	463.21	446.9
601	463.98	443.3						

1698 SOUTH FLATIRON COURT
BOULDER, COLORADO 80301
P.O. BOX 1056
BOULDER, COLORADO 80306
TELEPHONE: 303/444-1530

COLORADO RESEARCH AND PREDICTION LABORATORY, INC.
SPECIALISTS IN ELECTROMAGNETICS AND COMPUTER SIMULATION

LORAN-C GROUND WAVE SECONDARY PHASE CORRECTIONS OVER NONHOMOGENEOUS AND IRREGULAR GROUND USING TRANSIENT SIGNAL PROPAGATION TECHNIQUES

CRPL$_I$ REPORT 78-12

FEBRUARY 1, 1979

REVISED MAY 1, 1979

J. R. Johler

Report on work sponsored by Department of Transportation,
United States Coast Guard, Washington, D.C. 20590
Under Contract No. DOT-CG-842923A, dated August 15, 1978

FOREWORD

This paper, $CRPL_i$ Report 78-12, comprises Task 3B or Final Report of Deliberables, under Contract DOT-CG-842923A, Loran-C Pulse Transient Analysis. $CRPL_i$ Reports 78-9 and 78-10 have already been submitted (10/15/78 and 12/1/78) for Tasks 1 and 2 of this contract respectively. Task 3A has already been submitted as a draft of this report. Approval of this draft was received by this company in the form of U. S. Coast Guard letter of 23 April 1979, G-FCP-2/71.

TABLE OF CONTENTS

LIST OF FIGURES

LIST OF FIGURES (CONTINUED)

LIST OF FIGURES (CONTINUED)

LIST OF FIGURES (CONTINUED)

LIST OF TABLES

LIST OF TABLES (CONTINUED)

ABSTRACT

A new rigorous technique for the computation and prediction of loran time difference coordinates from loran receiver geographic coordinates and visa versa is introduced by application to a specific loran overland situation. The Loran-C standard antenna current pulse has been used to describe the propagation of the transient signal over ground that is nonhomogeneous and irregular. It is demonstrated that the less sophisticated and traditional continuous wave approach to the calculation of secondary phase correction (or the propagation time correction relative to the speed of light) may be in error over nonhomogeneous and irregular land masses due to the dispersion of the pulse. In this paper we employ this technology to the problem of resolving the relationship between the antenna current pulse, the near field pulse and the far field pulse. Whilst a topographic data base has been incorporated into the technique for the Continental United States, there exists a need to introduce geologic, soil and hydrology data bases (in addition to topographic data bases for other parts of the world) if this technology is to be used in a prediction scheme.

We have found as a result of the analysis presented in this paper that the rigorous definition of the envelope to cycle difference requires the introduction of a concept of a tagged point in time on the leading edge of the pulse envelope in addition to the conventional tagged point in time on the cycle. The behavior of the difference between these tagged points in time is a function of the propagation mechanism. It is suggested by the results obtained that spatial propagation error compensation in the receiver may be possible over very irregular ground. However, it is recommended that any such compensation be implemented in the context of the theory presented to guarantee uniqueness.

The envelope to cycle difference (ECD) of the standard pulse manifests a near field phenomenon because its value decreases with increasing distance from 0.42 μs at 100 and 135 km to a value of 0.39 at 200 km and a value of 0.19 at 500 km in the presence of average ground electrical constants. Severe terrain features impose local perturbations in the ECD.

LORAN-C GROUND WAVE SECONDARY PHASE CORRECTIONS OVER NONHOMOGENEOUS AND IRREGULAR GROUND USING TRANSIENT SIGNAL PROPAGATION TECHNIQUES

BY

J. RALPH JOHLER

1. INTRODUCTION TO THE LORAN-C SIGNAL

The Loran-C radio navigation chain is a configuration of three or more pulse transmitters located at precisely known geographic positions depicted in Figure 1 as M, SW, SX. These transmitters emit a radio pulse that has a frequency composition cresting between 90 kHz and 110 kHz. The time of transmission of each pulse is precisely synchronized in Universal Time with the aid of cesium oscillator clocks (Hefley, 1972), Reference (1).

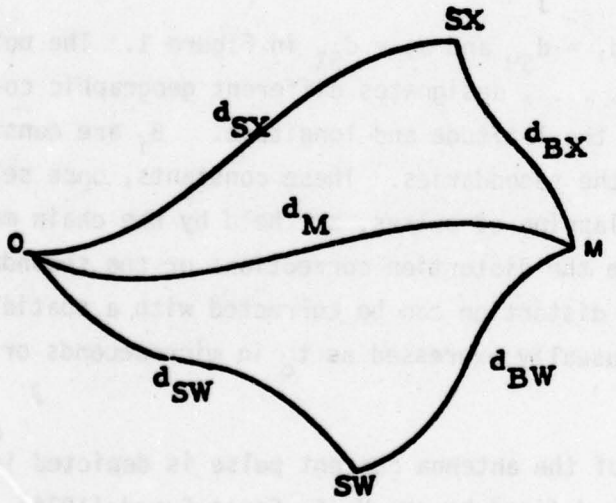

FIGURE 1. LORAN-C CHAIN DEPICTING THE MASTER (M), SECONDARY-W, AND SECONDARY-X WITH CORRESPONDING GEODESIC DISTANCES TO THE OBSERVER (O), d_M, d_{SW}, d_{SX} AND THE BASELINE (CONSTANT) GEODESICS d_{BW} AND d_{BX}.

One of the pulse transmitters is designated the Master (M) and the others are called Secondary-W, Secondary-X, Secondary-Y and Secondary-Z, SW, SX, SY, SZ. In the past the notation SM, S1, S2, ... has been used.

The minimal chain for navigation requires only two secondaries as shown in Figure 1, as SW and SX. A navigator using such a system can locate his position at O, Figure 1, by making a time difference measurement y, with a loran receiver. Thus, he may use the Master--Secondary-W and the Master--Secondary-X time differences, y_i, i = 1, 2 respectively. If the loran signals transmitted over the various propagation paths, d_{SW}, d_{SX}, and d_M, traveled at the speed of light, c = 2.997925(10^8) m/s, the equation,

$$y_i = \text{a constant}, \tag{1}$$

would describe a spatial arrangement of hyperbolas over the surface of the earth, for each i = 1, 2. Any two hyperbolas comprising one from each set, i = 1 and 2, would intersect almost uniquely at the observer's position, O. In general, equation (1) is not precisely true. The hyperbolas are ever so slightly distorted by propagation times that vary from the speed of light propagation time,

$$y_{i,k} = \beta_i + \frac{\eta_1}{c}\left[d_{i,k} - d_{o,k}\right] + t_c\,(d_{i,k}) - t_c\,(d_{o,k}) \tag{2}$$

where i = 1, 2, and $d_0 = d_M$, $d_1 = d_{SW}$ and $d_2 = d_{SX}$ in Figure 1. The points for the observer, k = 1, 2, 3, ... , designates different geographic coordinates such as ϕ_k, λ_k, for the latitude and longitude. β_i are constants called the emission delay of the secondaries. These constants, once selected for convenience to avoid overlapping of pulses, are held by the chain management. The quantities, t_c, are the distortion corrections or the secondary phase corrections. Thus, the distortion can be corrected with a spatially dependent correction that is usually expressed as t_c in microseconds or ϕ_c in radians.

The precise nature of the antenna current pulse is depicted in Figure 2. This pulse has been defined by the U. S. Coast Guard (1974) Reference (2). The time of arrival measurement at the receiver, O, is usually accomplished on the zero crossing of the third cycle. Each transmitter emits pulse groups of eight pulses except the Master which emits a ninth pulse for identification. Each group is spaced in time so that overlap does not occur and after some time has elapsed another sequential group

of pulses is transmitted at the Loran-C chain group repetition rate. This repetition rate varies such that there exists 40,000 to 99,990 microseconds between Loran-C chain pulse groups and gives the interesting illusion of line spectra in frequency domain of the pulse. The position of the various spectra in frequency is dependent upon the repetition rate. If we consider only a single pulse as depicted in Figure 2, our repetition rates become zero and the line spectra merge into a continuum in the frequency domain. Thus, the very powerful analysis tool of the Fourier Transform Integral becomes applicable because one can then integrate over the complex (amplitude and phase are used) spectrum. This approach will be employed in this paper. Finite repetition rates can be introduced if required using discrete frequencies under the amplitude and phase envelopes for a particular pulse repetition rate. Thus, the analysis to follow is completely general.

We perform the analysis with a recently conceived theoretical propagation analysis scheme. This analysis scheme has been programmed on a large scale computer for use in a proposed experimental program to measure ECD and test the transient solution described in this paper, Reference (21), (CRPL$_i$ Report 78-10). This scheme uses a modular construction shown in Figure 3. Thus, for example, the propagation transform simulator can be the more advanced integral equation technique modified for transient analysis and originally reported in Reference (9). Also, new and more advanced techniques under study can be inserted at this point in the analysis as a result of the modular arrangement of the analysis scheme.

Whilst the development of such advanced computer technology is important, it cannot be used for precision general Loran-C coordinate prediction without the basic geophysical data bases shown in Figure 3. The soil, hydrology and geologic data bases require considerable development as digital data bases at this point in time. Thus, geophysical data base development in a form suitable for Loran-C has not at all kept pace with the geophysical data requirements of ground wave theoretical development. The soil, hydrology and geologic data base modules have been improvised as discussed in Reference (20). This specially improvised data base will be used in this paper to exercise the analysis scheme.

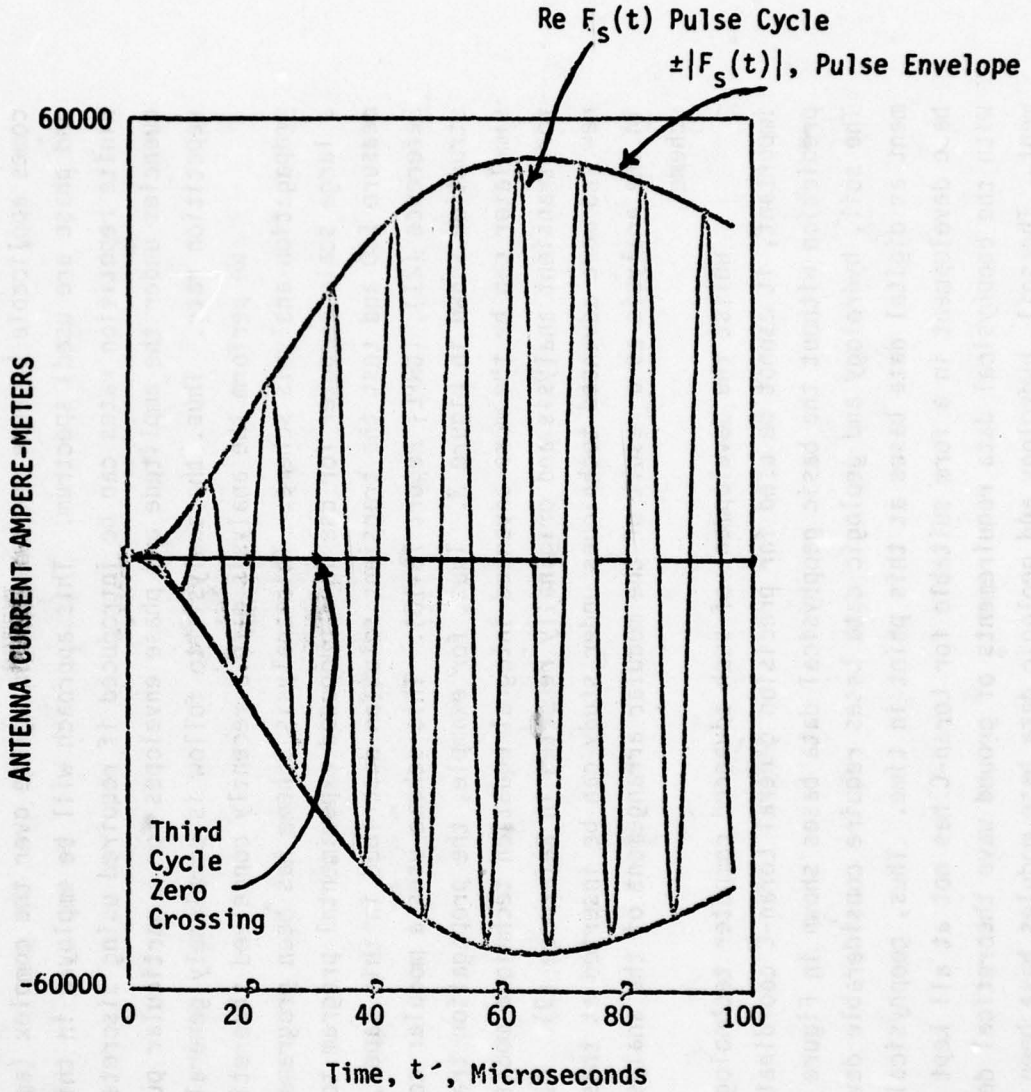

FIGURE 2. LORAN-C ANTENNA CURRENT PULSE IN AMPERE-METERS FOR 500 KILOWATTS RADIATED POWER AT THE CREST OF THE PULSE. PULSE SHAPE IS DEFINED BY U.S. COAST GUARD (1974), OR EQUATION (19).

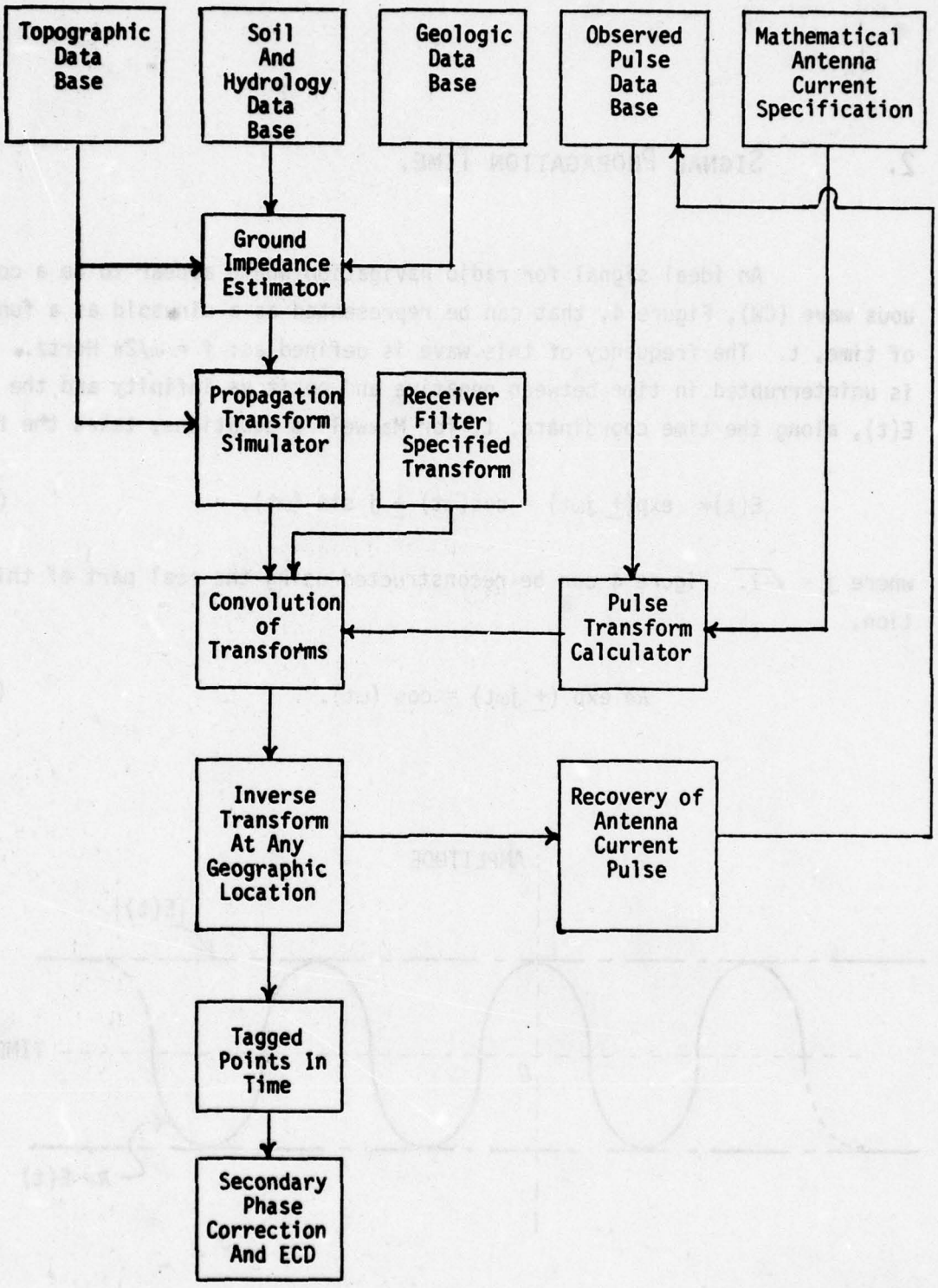

FIGURE 3. SECONDARY PHASE CORRECTION AND ENVELOPE TO CYCLE DIFFERENCE (ECD) MODULAR SIMULATION SCHEME FOR LORAN-C PULSE PROPAGATION OVER NONHOMOGENEOUS AND IRREGULAR LAND MASSES.

2. Signal Propagation Time.

An ideal signal for radio navigation would appear to be a continuous wave (CW), Figure 4, that can be represented as a sinusoid as a function of time, t. The frequency of this wave is defined as: $f = \omega/2\pi$ Hertz. The wave is uninterrupted in time between negative and positive infinity and the solution, E(t), along the time coordinate, t, for Maxwell's equations, takes the form,

$$E(t) \propto \exp(\pm j\omega t) = \cos(\omega t) \pm j \sin(\omega t), \qquad (3),$$

where $j = \sqrt{-1}$. Figure 4 can be reconstructed using the real part of this solution,

$$Re \exp(\pm j\omega t) = \cos(\omega t). \qquad (4)$$

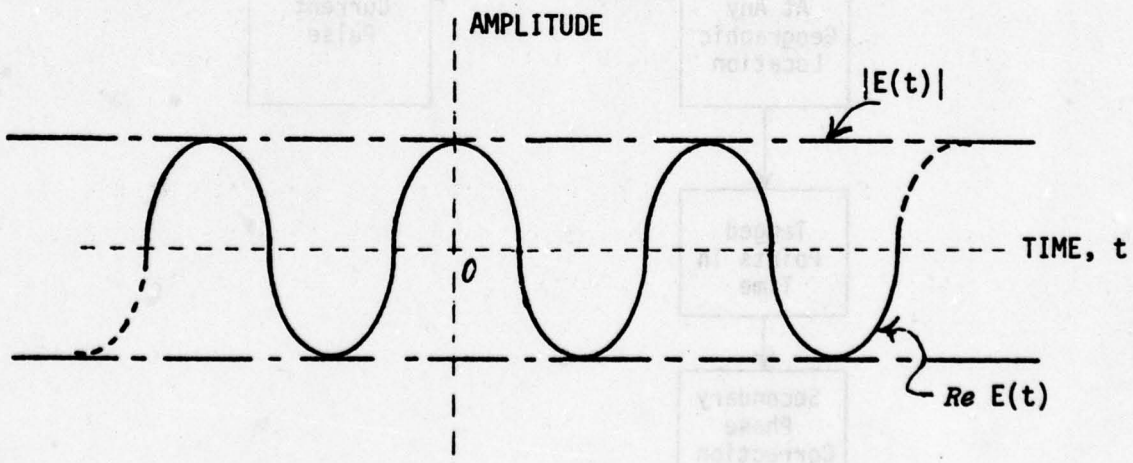

FIGURE 4. SINUSOID AS A FUNCTION OF TIME, t, DEPICTING AMPLITUDE OF CYCLE *Re* E(t) AND ENVELOPE |E (t)| OF A CONTINUOUS WAVE.

The imaginary part does not exist per se physically, but may be used to synthesize the signal envelope, $|E(t)|$,

$$|E(t)| \propto \sqrt{\cos^2(\omega t) + \sin^2(\omega t)} = 1. \qquad (5)$$

We then say the signal amplitude is unmodulated, because its envelope is constant with all time.

Such a signal can be propagated via the ground wave propagation medium over the distances, Figure 1, d_{SW}, d_{SX} and d_M and from the zero crossing of the cycles, phase information can be obtained so that the propagation time, equation (2),

$$(n_1 d_{i,k})/c + t_c (d_{i,k}), \qquad (6)$$

can be deduced. Since this wave train has infinite length, it has an infinite number of zero crossings, so without further knowledge we could not decide which cycle to use in our calculation of position. This basic problem in radio navigation is often called "lane ambiguity" and at 100 kHz the lane widths are 10 microseconds, (1 cycle).

This problem is resolved by interrupting the wave train at precise times such that the signal becomes the pulse specified in Figure 2. Mathematically, the pulse is specified as a source function, $F_s(t)$, such that its Fourier transform, $f_s(\omega)$, is given by:

$$f_s(\omega) = \int_{-\infty}^{\infty} \exp(-j\omega t)\, F_s(t)\, dt. \qquad (7)$$

This mathematical approach to pulse synthesis (1) permits introduction of propagation media involving complicated boundary conditions; (2) permits

synthesis of most any pulse shape from continuous wave solutions; and (3) permits ready adaptation to large scale computer analysis of signals. Such approaches have been exploited in the past by the author, References (3, 4, 5, 6, 7, 8, and 9) using a considerable number of pulse shapes, including pulses from nuclear detonations (EM-pulses). Thus, inversion of the source transform, $f_s(\omega)$, with the propagated electric field for a time harmonic source transform $\xi(\omega,d)$, allows one to reconstruct the transient field, $E(t',d)$,

$$E(t',d) = \frac{1}{2\pi}\int_{-\infty}^{\infty} \exp(j\omega t')\, \xi(\omega,d)\left\{\int_{0}^{\infty} F_s(t)\exp(-j\omega t)dt\right\} d\omega\ , \qquad (8)$$

where,

$$t' = t - \eta_1 d/c \qquad (9)$$

and $\eta_1 = 1.000338$ for air at the surface of the ground. Here we have recognized the spatial parameter, d, representing distance from the transmitter. Equation (8) is valid for all linear amplitude analysis schemes. Thus, it clearly applies to the propagation of the Loran-C ground wave pulse. Indeed, we can employ this analysis to calculate the propagation time corrections (secondary phase corrections) for most any condition of the ground over which the signal propagates.

The selection of the source function, $F_s(t)$, is quite arbitrary. Pulses like the Loran-C pulse can be constructed from sinusoides. This technique uses complex source functions, Reference (3). Suppose a carrier frequency, ω_c, modulated by a frequency, ω_p, has the form,

$$\begin{aligned} Re\ F_s(t) &= Re\ \exp(-\nu_k t) \\ &= \exp(-c_k t)\cos(\omega_k t),\ (0 \leq t < \infty) \\ &= 0,\ (t < 0)\ . \end{aligned} \qquad (10)$$

Thus, a complex frequency, ν_k, has been employed such that,

$$\nu_k = c_k + j\omega_k \quad . \qquad (11)$$

$$k = 1, 2, 3, \ldots .$$

where

$$\nu_1 = c_1 + j\omega_1 \qquad \omega_1 = \omega_c$$

$$\nu_2 = c_2 + j\omega_2 \qquad \omega_2 = \omega_c + 2\omega_p$$

$$\nu_3 = c_3 + j\omega_3 \ldots . \qquad \omega_3 = \omega_c - 2\omega_p \quad .$$

Here, c_k, is a damping constant. Application of equation (10) to equation (8) leads to:

$$E(t',d) = \frac{1}{2\pi} \int_{-\infty}^{\infty} \left[c_k + j(\omega_k + \omega)\right]^{-1} \xi(\omega,d) \exp(j\omega t') \, d\omega. \qquad (12)$$

The field of a continuous wave, $\xi(\omega,d)$ is defined:

$$\xi(\omega,d) = |\xi(\omega,d)| \exp\left[j\omega t' - j(\phi_c - \frac{\pi}{2})\right]$$

or

$$\xi(\omega,d) = j\,|\xi(\omega,d)| \exp\left[j\omega t' - j\phi_c\right]$$

where ϕ_c is the secondary phase correction in radians. The use of t' in the transformation of equation (9) eliminates the factor $\exp\left[-jk_1 d\right]$ in subsequent formulations (see for example, equation (39) et. seq.). The factor j arises from the assumed transmitter model, i.e., the Hertzian dipole, equation (6 AI), and is not regarded as part of the secondary phase correction.

Upon separation of real and imaginary parts and introducing:

$$\phi'_c = \phi_c - \frac{\pi}{2}$$

we find:

$$E(t',d) = \frac{1}{2\pi} \int_{0}^{\infty} |\xi(\omega,d)|$$

$$\cdot \left[\left\{ \left[c_k^2 + (\omega_k + \omega)^2 \right]^{-\frac{1}{2}} \cos \{\omega t' - \phi'_c + \tan^{-1} \left[-(\omega_k + \omega)/c_k \right] \} \right. \right.$$

$$\left. + \left[c_k^2 + (\omega_k - \omega)^2 \right]^{-\frac{1}{2}} \cos\{-\omega t' + \phi'_c + \tan^{-1}\left[-(\omega_k - \omega)/c_k \right]\} \right\}$$

$$+j \left\{ \left[c_k^2 + (\omega_k + \omega)^2 \right]^{-\frac{1}{2}} \sin\{ \omega t' - \phi'_c + \tan^{-1} \left[-(\omega_k + \omega)/c_k \right] \} \right.$$

$$\left. \left. + \left[c_k^2 + (\omega_k - \omega)^2 \right]^{-\frac{1}{2}} \sin \{-\omega t' + \phi'_c + \tan^{-1} \left[-(\omega_k - \omega)/c_k \right]\} \right\} \right] d\omega. \quad (14)$$

Using this quite general form of a damped sinusoid, we can now introduce the modulation frequency, ω_p, as, for example, a sine squared type of modulation:

$$Re\ F_s(t) = \exp(-c_1 t) \sin^2(\omega_p t) \sin(\omega_c t)$$

$$Re\ F_s(t) = \tfrac{1}{2} \exp(-c_1 t) \sin(\omega_c t)$$

$$- \tfrac{1}{4} \exp(-c_1 t) \sin(\omega_c + 2\omega_p)t$$

$$- \tfrac{1}{4} \exp(-c_1 t) \sin(\omega_c - 2\omega_p)t. \quad (15)$$

Therefore,

$$F_s(t) = (j/2) \exp(-\nu_1 t) - (j/4) \exp(-\nu_2 t)$$

$$- (j/4) \exp(-\nu_3 t), \quad (16)$$

where

$$\nu_1 = c_1 + j\omega_c = c_1 + j\omega_1$$

$$\nu_2 = c_1 + j(\omega_c + 2\,\omega_p) = c_2 + j\omega_2$$

$$\nu_3 = c_1 + j(\omega_c - 2\,\omega_p). = c_3 + j\omega_3 \qquad (17)$$

Then,

$$E(t',d) = (j/2)\,E(t',d,\nu_1) - (j/4)\,E(t',d,\nu_2) - (j/4)\,E(t',d,\nu_3) \qquad (18)$$

Figure 5 depicts a ground wave pulse propagated to a distance of 1000 km from the source over average ground with a surface impedance, $x = 0.33 \exp(j0.777)$ using the equations (14) and (15) and the constants,

$$c_1 = 2500$$

$$f_p = 2500 \text{ Hz} = \omega_p/2\pi$$

$$f_c = 100 \text{ kHz} = (\omega_c/2\pi)/10^3 \ .$$

Both the envelope $\pm\,|E(t',d)|$ and the cycles under the envelope, $Re\,E(t',d)$ are depicted as a function of local time, t'. The amplitude is in volts per meter for a one ampere-meter source current dipole. This pulse is similar to the Loran-C pulse depicted in Figure 2. Whilst we have shown the entire pulse, it is necessary to magnify detail of the pulse to study the effects of propagation via the ground wave. Ionospheric waves distort this pulse in practice and the reader is referred to Reference (8) for the ionospheric wave pulse. This latter pulse is of no consequence to Loran-C under normal conditions, since the pulse is measured for navigation timing purposes at the last zero crossing of the third cycle. This occurs before the arrival of the ionospheric wave.

It can be concluded from equation (16) that the sine squared pulse modulation is merely the sum of three sinusoids with the complex frequencies ν_1, ν_2, and ν_3 (the carrier, the upper and the lower sidebands). It is interesting to note that this is perhaps the purest form of amplitude

modulation. Thus, any reduction in the upper or lower sideband relative to each other or to the carrier can result in a concommittant phase modulation. Since the sidebands are not propagated with equal vigor, some phase modulation can be imposed by the time harmonic transform of the field, $\xi(\omega,d)$. Computer simulation studies of such modulation has been accomplished depicting both ground waves and ionospheric waves, Reference (5, 8, 9).

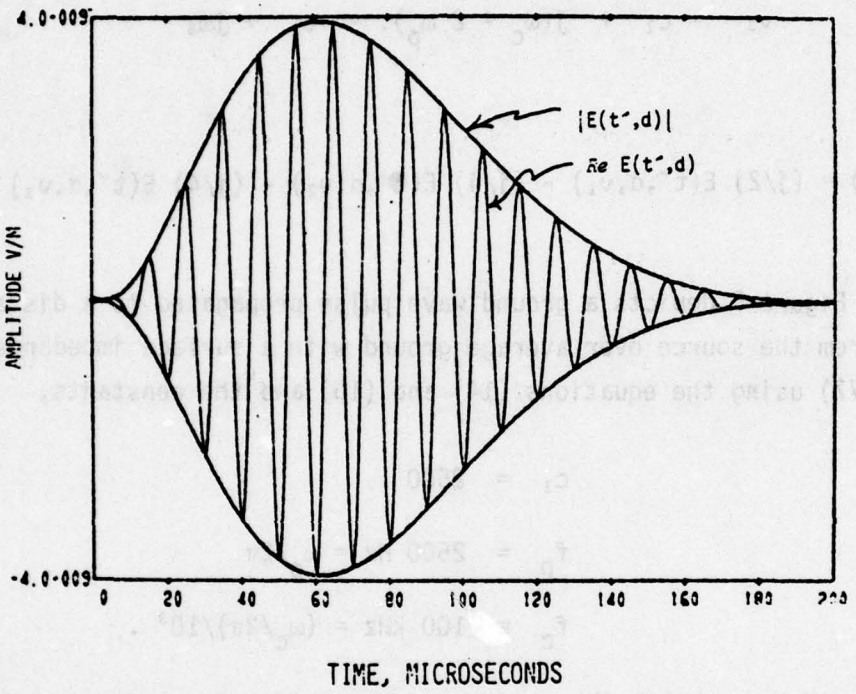

FIGURE 5. ILLUSTRATING COMPUTER SYNTHESIS OF A GROUND WAVE PULSE BY SUPERPOSITION OF DAMPED SINUSOIDS AT A DISTANCE OF 1000 KM FROM THE TRANSMITTER OVER AVERAGE, SMOOTH GROUND.

3. RELATIONSHIP BETWEEN NEAR FIELD AND FAR FIELD ENVELOPE AND CYCLE PROPAGATION TIME.

The U.S. Coast Guard (1974), Reference (2), has given a standard form of pulse, Figure 2, such that the Loran-C modulation can be written:

$$Re\ F_s(t) = b_1 t^2 \exp(-c_1 t)\sin(\omega_c t),\ (t>0), \qquad (19)$$
$$= 0\ (t<0)$$

where $c_1 = (2/65)(10^6)$ and $b_1 = 1.753(10^9)$ for 1 ampere-meter current pulse crest. For 500 kilowatts radiated power at the pulse crest, $b_1 = 9.576(10^{13})$. This leads to a complex source function,

$$F_s(t) = jb_1t^2 \exp(-\nu_1 t) \tag{20}$$

$$= b_1t^2 \exp(-c_1t) \left[\sin(\omega_c t) + j\cos(\omega_c t)\right] \quad (t \geq 0),$$

$$f_s(\omega) = 2jb_1(\nu_1 + j\omega)^{-3} = 2jb_1\left[c_1 + j(\omega_c + \omega)\right]^{-3}. \tag{21}$$

This modulation can be completely represented by a slight modification of equation (14) as follows:

$$E(t', d) = \frac{j}{\pi} b_1 \int_0^{\infty} \left|\xi(\omega,d)\right| \left[\left\{\left[c_1^2 + (\omega_c + \omega)^2\right]^{-\frac{3}{2}} \cos\{\omega t' - \phi_c' + 3\tan^{-1}\left[-(\omega_c + \omega)/c_1\right]\}\right.\right.$$

$$\left.\left. + \left[c_1^2 + (\omega_c - \omega)^2\right]^{-\frac{3}{2}} \cos\{-\omega t' + \phi_c' + 3\tan^{-1}\left[-(\omega_c - \omega)/c_1\right]\}\right\}\right.$$

$$\left. + j\left\{\left[c_1^2 + (\omega_c + \omega)^2\right]^{-\frac{3}{2}} \sin\{\omega t' - \phi_c' + 3\tan^{-1}\left[-(\omega_c + \omega)/c_1\right]\}\right.\right.$$

$$\left.\left. + \left[c_1^2 + (\omega_c - \omega)^2\right]^{-\frac{3}{2}} \sin\{-\omega t' + \phi_c' + 3\tan^{-1}\left[-(\omega_c - \omega)/c_1\right]\}\right\}\right] d\omega. \tag{22}$$

In this specific case a single damped sinusoid is all that is required to represent the modulation.

In general, given the arbitrary modulation, $F_s(t)$, that we have described above, equation (8) can be written,

$$E(t', d) = \frac{1}{2\pi} \int_{-\infty}^{\infty} \xi(\omega,d) \exp(j\omega t') f_s(\omega) d\omega, \tag{23}$$

and a periodic modulation envelope has a transform,

$$f_s(\omega) = \int_0^T F_s(t) \exp(-j\omega t) dt, \tag{24}$$

where T, is the period of the envelope. The Loran-C receiver can tag points in time on both the pulse cycle and the pulse envelope. This can be simulated mathematically. The equations for amplitude independent tagged points in time are:

$$|E(t',d)| - C_e \frac{d}{dt'} |E(t',d)| = 0, \text{ and} \tag{25 a}$$

$$\frac{d^2}{dt'^2}|E(t',d)| = 0, \tag{25 b}$$

where C_e is the constant that determines a particular tagged point in time on the envelope. The inflection point can be determined by the 2nd derivative. The cycle zero crossings are of course the roots of:

$$Re\ E(t',d) = 0. \tag{26}$$

Such quantities can be calculated from the above described theory. Thus, the roots of equation (25)

$$t' = T_c\ , \tag{27}$$

and the roots of equation (26),

$$t' = t_c \tag{28}$$

give the envelope and cycle propagation time corrections respectively. The envelope to cycle discrepancy or the envelope to cycle difference, Γ, (ECD) is then the difference between envelope and cycle propagation corrections, T_c and t_c respectively,*

$$\Gamma = T_c - t_c\ . \tag{29}$$

We select in our loran receivers a zero cycle crossing that is closest to T_c, the envelope propagation time correction. Thus, C_e in equation (25) is set so that T_c is close to the last zero crossing of the third cycle. This quantity, when derived at various geographic positions for constant C_e, is a measure of the pulse dispersion by the propagation medium. The propagation time of the envelope, u_e, and the cycle, u, are given by:

$$u_e = T_c + n_1 d/c, \tag{29 a}$$

$$u = t_c + n_1 d/c\ . \tag{29 b}$$

The envelope derivatives can be calculated from:

$$\frac{d}{dt'}\left| E(t',d)\right| = \left|\frac{d}{dt'}\ E(t',d)\ \right| \cos\{\arg \frac{d}{dt'} E(t',d) - \arg E(t',d)\}\ . \tag{30}$$

* *Equations (25 a, 26, 27, 28 and 29) comprise a rigorous definition of envelope to cycle difference (ECD).*

Also, it follows that:

$$\frac{d^2}{dt'^2}\left|E(t',d)\right| = \left|\frac{d^2}{dt'^2}E(t',d)\right| \cos\left\{\arg\frac{d^2}{dt'^2}E(t',d) - \arg E(t',d)\right\} .$$

$$+ \{|E(t',d)|\}^{-1}\left\{\left|\frac{d}{dt'}E(t',d)\right|^2\right\} \sin^2\left\{\arg\frac{d}{dt'}E(t',d) - \arg E(t',d)\right\} . \quad (31)$$

The derivatives indicated by (30) and (31) are calculated from the analytic function for the transient field, equation (14), for example,

$$\frac{d}{dt'}E(t',d) = \frac{1}{2\pi}\int_0^\infty |\xi(\omega_1 d)|$$

$$\cdot \left\{\left[-\left[c_k^2 + (\omega_k + \omega)^2\right]^{-\frac{1}{2}} \sin\left\{\omega t' - \phi_c'(\omega_1 d) + \tan^{-1}\left[-(\omega_k + \omega)/c_k\right]\right\}\right.\right.$$

$$+\left[c_k^2 + (\omega_k - \omega)^2\right]^{-\frac{1}{2}} \sin\left\{-\omega t' + \phi_c'(\omega_1 d) + \tan^{-1}\left[-(\omega_k - \omega)/c_k\right]\right.$$

$$+ j\left[c_k^2 + (\omega_k + \omega)^2\right]^{-\frac{1}{2}} \cos\left\{\omega t' - \phi_c'(\omega_1 d) + \tan^{-1}\left[-(\omega_k + \omega)/c_k\right]\right\}$$

$$\left.\left. - \left[c_k^2 + (\omega_k - \omega)^2\right]^{-\frac{1}{2}} \cos\left\{-\omega t' + \phi_c'(\omega_1 d) + \tan^{-1}\left[-(\omega_k - \omega)/c_k\right]\right\}\right]\right\} \omega d\omega, \quad (32)$$

and,

$$\frac{d^2}{dt'^2}E(t',d) = \frac{1}{2\pi}\int_0^\infty |\xi(\omega,d)|$$

$$\left\{\left[-\left[c_k^2 + (\omega_k + \omega)^2\right]^{-\frac{1}{2}} \cos\left\{\omega t' - \phi_c'(\omega,d) + \tan^{-1}\left[-(\omega_k + \omega)/c_k\right]\right\}\right.\right.$$

$$\left. - \left[c_k^2 + (\omega_k - \omega)^2\right]^{-\frac{1}{2}} \cos\left\{-\omega t' + \phi_c'(\omega,d) + \tan^{-1}\left[-(\omega_k - \omega)/c_k\right]\right\}\right]$$

$$+j\left[-\left[c_k^2 + (\omega_k + \omega)^2\right]^{-\frac{1}{2}} \sin\left\{\omega t' - \phi_c'(\omega,d) + \tan^{-1}\left[-(\omega_k + \omega)/c_k\right]\right\}\right.$$

$$\left.\left. - \left[c_k^2 + (\omega_k - \omega)^2\right]^{-\frac{1}{2}} \sin\left\{-\omega t' + \phi_c'(\omega,d) + \tan^{-1}\left[-(\omega_k - \omega)/c_k\right]\right\}\right]\right\}$$

$$\omega^2 d\omega . \quad (33)$$

The effect of the finite bandwidth of the Loran-C receiver is ordinarily negligible. However, filters of various types are often employed. These filters distort the pulse and affect the measured propagation times, u, u_e. The effect of a filter can be readily assessed with the aid of this analysis by introducing into equations (22) or (23), the transform of the filter, $f_r(\omega)$:

$$E(t',d) = \frac{1}{2\pi} \int_{-\infty}^{\infty} \xi(\omega,d) \exp(j\omega t') f_r(\omega) f_s(\omega) d\omega. \qquad (34)$$

A filter typically has the form:

$$f_r(\omega) = \{j\omega\alpha_1 [-\omega^2 + j\omega\alpha_1 + \alpha_2]^{-1}\}^n, \qquad (35)$$

where, $\omega = 2\pi (10^5)$, $\alpha_1 = 2.5 (10^5)$, $\alpha_2 = 4.1 (10^7)$.

The quantity $n = 1,2,3...$ can be increased to reduce the bandwidth of the filter and assess the effect of bandwidth upon the pulse dispersion.*

In equation (28) we have rigorously deduced the secondary phase correction, t_c. This quantity plus the propagation time at the speed of light in air, $\eta_1 d/c$, is u, the true propagation time of the cycle. It is this quantity that the Loran-C receiver measures with precision (usually nanosecond precision). It is important to note that t_c is a function of distance from the transmitter, d, and time, t',

$$t_c = t_c(d,t'). \qquad (36)$$

It has been standard engineering practice to use the last zero crossing of the third cycle under the pulse envelope as depicted in Figure 4. Thus, this point in time is approximately 30 microseconds from the beginning of the pulse. It can never be precisely this amount because the pulse is subject to dispersion by the propagation medium. The dependence of t_c upon t' is curious. Thus, in the past it has been common practice to derive the secondary phase correction from the continuous wave carrier frequency, $f = 100$ kHz, Figure 3. This is not an exact secondary phase correction. However, various numerical studies

* *An extensive study of loran pulse dispersion due to a receiver filter that in turn was convolved with the ground wave propagation medium as shown in equation (34) is given in Reference 15.*

References (3, 5) have validated the approximation of equation (31):

$$t_c \tilde{=} t_c(d). \tag{37}$$

at least for the cases of smooth homogeneous ground and nanosecond precision. In the case of irregular and nonhomogeneous ground this approximation may require further scrutiny.

Indeed, whilst in previous works, References (3, 5, 9) we found very weak dependence of the envelope to cycle difference, i.e., the response of the dispersion measure Γ to changes in the secondary phase correction,

$$\Gamma = \Gamma\,(t_c); \tag{38}$$

a strong dependence was noted locally in the presence of perturbations due to mountains (ridges) and ground impedance nonhomogenities. Under such conditions one wonders about the validity of the approximation in equation (37). These matters will be expounded using the full transient solution developed for this project. Thus, our secondary phase corrections are the rigorous equation (36) and we shall use the third cycle of the pulse like Loran-C receivers ordinarily do.

The field representation close to the transmitter for a damped sinusoid, Reference (3), can be written as a transform for the Sommerfeld-Norton surface wave, References (11, 12):

$$\xi(s,d).\ f_s(s) = C\left\{\left[\frac{s}{s+\nu} - \frac{s^2}{s+\nu}\ \sqrt{\pi\alpha}\ \exp(s^2\alpha)\operatorname{erfc}(s\sqrt{\alpha})\right.\right.$$
$$\left.\left. + \frac{1}{t_0(s+\nu)} + \frac{1}{t_0^2 s(s+\nu)}\right]\right\} \tag{39}$$

where $s = j\omega$. Let $I_0\ell = \pm$ 1 ampere-meter*, the dipole current moment corresponding to a 1 ampere current in a 1 meter antenna, then,

$$C = 2I_0\ell t_0^2/(4\pi\,\varepsilon d^3) = 2(10^{-7})/d,$$

$$\varepsilon = \varepsilon_0\varepsilon_1 = \varepsilon_0 n_1^2,$$

and neglecting the dielectric constant ε_2, of the ground, the numerical distance factor, α, is:

* *The sign reversal on the antenna current on successive pulses is known as phase coding in Loran-C navigation parlance.*

$$\alpha \tilde{=} \eta_1^3 d/(2\sigma\mu_0 c^3),$$

and the propagation time in air at the surface of the ground, t_0, is:

$$t_0 = \eta_1 d/c.$$

Now, a complex inversion integral,

$$E(t',d) = \mathcal{L}^{-1}\xi(s,d), \tag{40}$$

is implied where,

$$f(s) = \mathcal{L}F(t') = \int_0^\infty \exp(-st')\,F(t')dt'. \tag{41}$$

Thus, after considerable ado,

$$\begin{aligned} E(t',d) = \nu C \exp(-\nu t') \Bigg\{ & -1 - \nu\sqrt{\pi\alpha}\ \exp(\nu^2\alpha) \\ & \cdot \left[\operatorname{erfc}(-\nu\sqrt{\alpha}) - \operatorname{erfc}\left(\frac{t'}{2\sqrt{\alpha}} - \nu\sqrt{\alpha} \right) \right] + \frac{1}{t_0\nu} - \frac{1}{t_0^2\nu^2} \Bigg\} \\ & + \nu C \left(\frac{1}{t_0^2\nu^2} \right) + C\left[\frac{t'}{2\alpha} + \nu \right] \exp\left(\frac{-t'^2}{4\alpha} \right). \end{aligned} \tag{42}$$

At very short distances, d, the field can be written:

$$\xi(s,d).\quad f_s(s) = C\left\{ \frac{s}{s+\nu} + \frac{1}{t_0(s+\nu)} + \frac{1}{t_0^2 s(s+\nu)} \right\}. \tag{43}$$

Whereupon the transform inversion gives:

$$\begin{aligned} E(t',d) = \nu\, C \exp(-\nu t') & \left\{ -1 + \frac{1}{t_0\nu} - \frac{1}{t_0^2\nu^2} \right\} \\ & + \nu C \left\{ \frac{1}{t_0^2\nu^2} \right\} + C u_1(t'); \end{aligned} \tag{44}$$

where

$$u_0(t) = 1 \quad t>0,$$

$$= 0 \quad t<0,$$

and

$$u_0(t) = \int_0^t u_1(\tau)\, d\tau.$$

Thus, $u_1(t)$, is the Dirac function, which can be written:

$$u_1(t') = \lim_{\alpha \to o} \left[\frac{t'}{2\alpha} + \nu \right] \quad \exp\left(\frac{-t'^2}{4\alpha}\right) .$$

Independently, equation (42) reduces to equation (44) for $\alpha = o$ and equation (44) becomes independent of the electrical constants of the ground. This implies $\sigma \to \infty$ or $d \to 0$. Thus, equation (39) can be calculated from the rigorous expression, Reference (10):

$$\rho_1 = -j\omega\eta_1 x^2 d/2c$$

$$\rho_1 = (-jk_1^3/2k_2^2)) \left[1 - k_1^2/k_2^2 \right] d \simeq \omega^2\alpha , \qquad (45)$$

As d grows small the first two terms of equation (39) approach

$$\frac{s}{s+\nu} = 1 - \frac{\nu}{s+\nu} ,$$

and it reduces ultimately to equation (43). In equation (42),

$$\operatorname{erfc}(x) = \frac{2}{\sqrt{\pi}} \int_x^\infty \exp(-y^2)dy.$$

Alternatively, using the U.S. Coast Guard Loran-C pulse specified in equation (19), equation (39) can be rewritten:

$$\xi(s,d). \quad f_s(s) = b_1 C \left\{ \frac{s}{(s+\nu)^3} - \frac{s^2}{(s+\nu)^3} \sqrt{\pi\alpha} \exp(s^2\alpha) \operatorname{erfc}(s\sqrt{\alpha}) + \frac{1}{t_0(s+\nu)^3} + \frac{1}{t_0^2 s(s+\nu)^3} \right\} , \qquad (46)$$

or equation (43) becomes

$$\xi(s,d). \quad f_s(s) = b_1 C \left\{ \frac{s}{(s+\nu)^3} + \frac{1}{t_0(s+\nu)^3} + \frac{1}{t_0^2 s(s+\nu)^3} \right\} . \qquad (47)$$

The inverse transform of equation (47) then is:

$$E(t',d) = b_1 \nu C \exp(-\nu t') \left\{ \left(-\frac{1}{2} + \frac{1}{2t_0\nu} - \frac{1}{2t_0^2\nu^2} \right) t'^2 + \left(\frac{1}{\nu} - \frac{1}{t_0^2\nu^3} \right) t' + \left(\frac{-1}{t_0^2\nu^4} \right) \right\} + b_1\nu C \left\{ \frac{1}{t_0^2\nu^4} \right\} . \qquad (48)$$

This equation (48) comprises the near field representation of the U.S. Coast Guard Loran-C current pulse specified by equation (19). There exists an electrostatic or non-sinusoidal component to this pulse. Here, $\nu = c_1 + j\omega_c$ where,

$$c_1 = (2/65)(10^6),$$

$$\omega_c = 2\pi(10^5).$$

The modulus, $\pm |E(t',d)|$, would give the pulse envelope as a function of time. The "real part of" the analytic function, $Re E(t',d)$ would give the cycles under the pulse envelope as a function of time. Here it should be emphasized that time is local time, t', equation (9). Thus, causality specifies that: $t' > 0$. This fundamental attribute of electromagnetic theory was investigated by Sommerfeld and Brillouin (1914), References (13 and 14).

The finite conductivity of the ground in the vicinity of the transmitter can be introduced into equation (48) through the factor, α, and we find the inverse transform of equation (46) is,

$$E(t',d) = b_1\nu\, C \exp(-\nu t') \left\{ \left[-\frac{1}{2} + \frac{1}{2t_0\nu} - \frac{1}{2t_0^2\nu^2} \right] t'^{-2} + \left[\frac{1}{\nu} + 4\alpha\nu\sqrt{\alpha} - \frac{1}{t_0^2\nu^3} \right] t' \right.$$

$$+ \left[-2\alpha\,(1+2\sqrt{\alpha}+ 4\alpha^2\,\nu^2) - \frac{1}{t_0^2\nu^4} \right]$$

$$+ \left[(-2\alpha\nu\sqrt{\alpha})t' + 2\alpha(1 + 4\alpha^2\nu^2 + 2\sqrt{\alpha}) \right] \exp(\nu^2\alpha) \exp\left[\left(\frac{t'}{2\sqrt{\alpha}} - \nu\sqrt{\alpha}\right)^2 \right]$$

$$+ \left[(-\nu\sqrt{\alpha})t'^2 + (1 + 8\alpha^2\nu^2 + 2\sqrt{\alpha})t' - (8\alpha^2\nu + \frac{1}{\nu} + 6\alpha\nu\sqrt{\alpha} + 16\alpha^3\nu^2\sqrt{\alpha}) \right]$$

$$\left. \cdot \sqrt{\pi\alpha} \exp(\nu^2\alpha) \left[\operatorname{erfc}(-\nu\sqrt{\alpha}) - \operatorname{erfc}\left(\frac{t'}{2\sqrt{\alpha}} - \nu\sqrt{\alpha}\right) \right] \right\}$$

$$+ b_1\nu C \left\{ \frac{1}{t_0^2\nu^4} \right\}. \qquad (49)$$

A more exact expression for equation (49) is derived in Appendix I.

Finally, the rigorous solution of the U.S. Coast Guard pulse for all distances from the transmitter in the presence of nonhomogeneous and irregular ground is given by equation (22). A solution is obtained using special numerical techniques on the computer. The rigorous solution can,

of course, be checked numerically at short distances against computations on equation (49) to give confidence in the numerical mastery of the problem. The rigorous solution to the problem currently uses in the transform $\xi(\omega,d)$ calculation, a Volterra integral equation of a type discussed in our previous CRPL$_i$ Report 77-9, Reference (17). This rigorous approach to the calculation of the transform has been greatly improved recently and is more efficient numerically than the classical Sommerfeld-Norton formula, equation (46).

Equation (25) establishes a tagged point-in-time, t', rigorously on the pulse envelope, at either an arbitrary point for which a value of C_e is selected or at the special inflection point prescribed by the second derivative with respect to time. Whilst such tagged points in time have been implemented in the past, modern loran receivers do not attempt an exact envelope tag. In fact, it is probably not necessary under most practical circumstances. The AN/BRN-5 Loran receiver serves as an example of modern receiver envelope detection, Reference (16). In this receiver, $\Gamma \sim \hat{T}$ such that,

$$\hat{T} = f\left\langle \left[\text{Re } E(t_2',d)/\text{Re } E(t_1',d) \right] \right\rangle$$

or

$$\hat{T} = -16 \left[\text{Re } E(t_2',d)/\text{Re } E(t_1',d) + 0.7 \right]^{-1} + 20. \qquad (50)$$

where, $\hat{T}$ is expressed in microseconds and, using the last zero crossing of the 4th cycle,

$$t_2' = t_c + 37.5$$

$$t_1' = t_2' - 5 = t_c + 32.5$$

$\hat{T}$ is measured using the last zero crossing of the 4th cycle as the value of $t'_2 + 2.5$. As a consequence of the secondary phase correction and pulse cycle dispersion $t'_2 + 2.5$ will not be precisely 40 microseconds. Then the envelope to cycle difference, Γ, is thus,

$$\Gamma \propto \hat{T} \qquad (51)$$

If Re $E(t'_2,d)$/Re $E(t'_1,d)$ is $\sim$ 1.33, then $\hat{T}$ = 12.12 μs and changes in $\hat{T}$ will be proportional to Γ. This is not exact because, the root, $t' = T_0$, of,

$$\frac{\partial}{\partial t'} \text{ Re } E(t',d) = 0 ,$$

or the crest of the half cycles $t' = t_1$ and t_2 are not exact at t_c + 37.5 and t_c + 32.5 respectively because the pulse may be stretched in time due to dispersion. Thus, strictly speaking, t_c is not constant along the leading edge of the pulse due to the propagation mechanism. However, this procedure is accurate enough to resolve cycle or lane ambiguity.

The various techniques used by receiver manufacturers to asertain envelope time, T_c or $\hat{T}$, would enter into any experiment to validate the pulse dispersion theory presented in this paper. Therefore, the theory should be validated using cycle zero crossings and crests along the leading edge of the pulse. From such measurements the rigorous, T_c, or the other envelope tags like $\hat{T}$ can be synthesized.

It is possible to observe the Loran-C pulse at an area monitor and adjust the antenna current pulse for the ideal pulse at this point in the service area. Suppose the distance to the monitor is d_1. Then, the antenna current pulse can be deduced:

$$F_s(t) = \frac{1}{2\pi} \int_{-\infty}^{\infty} f(\omega,d_1) \left[\xi(\omega,d_1)\right]^{-1} \exp(j\omega t)\, d\omega \qquad (52)$$

where the current pulse is,

$$\text{Re } F_s(t),$$

and the envelope is,

$$|F_s(t)| .$$

Thus,

$$f(\omega,d_1) = \int_0^T F(t',d_1) \exp(-j\omega t')\, dt' \qquad (53)$$

where F (t´,d) is the observed pulse at a distance, d_1, from the transmitter. If F (t´,d) looks like an ideal pulse, the transform must have a spectrum like equation (21),

$$f(\omega, d_1) \simeq b_2 \left[c_1 + j(\omega_c + w) \right]^{-3} ,$$

and, according to equation (20),

$$E(t´,d_1) \simeq jb_2 t´^2 \exp(-\nu_1 t´) . \qquad (54)$$

where b_2 is the amplitude constant.

Furthermore, the transient field at some other distance, say $d = d_2$, can also be predicted:

$$E(t´,d_2) = \frac{1}{2\pi} \int_{-\infty}^{\infty} f(\omega,d_1) \; \xi(\omega,d_2) \left[\xi(\omega,d_1) \right]^{-1} \exp(j\omega t´) \, d\omega . \qquad (55)$$

Thus, from an observed pulse at some point, d_1 distance from the transmitter, one can predict the antenna current waveform, Re $F_s(t)$, or the field at some other distance, E(t´,d), $d = d_1, d_2, \ldots$. Here again the analytic function, E(t´,d) comprises the pulse cycles,

$$\text{Re } E(t´,d) ,$$

and the pulse envelope,

$$\pm |E(t´,d)| .$$

It is also quite possible that the area monitor pulse does not conform to the ideal pulse. In this case also the actual pulse can be digitized and the transform calculated numerically:

$$f(\omega,d_1) = \int_0^T \exp(-j\omega t´) \; \text{Re } F(t´,d_1) \, dt´, \qquad (56)$$

where T is the period of the pulse envelope. The complex source function, $F_s(t)$ can be deduced from distant observations using equation (52).

Therefore, equations (52) through (56) are important for validation of the theory of propagation of the Loran-C pulse.

Let us now consider the relationship between the very special antenna dipole current moment pulse given in Figure 2 and specified by equation (19) at some distance (far field) from the transmitter. Figure 6 illustrates such a field in volts per meter as a function of local time, t', defined by equation (9). This is the far field that would be generated at a distance of 100 km over smooth, homogeneous spherical ground with a conductivity, σ = .005 mhos/m. The intensity is given in absolute units for an antenna current moment that reaches a crest, Figure 2, of 54630 amperes in a one meter antenna at 65 microseconds or 218.5 amperes in a 250 meter antenna uniformly distributed over the length of the vertical structure. There exists small corrections at very short distances for antennas with nonuniform current distribution, especially those that approach $\lambda/4$ wavelengths and it is a comparatively simple matter to introduce most any such current distribution as demonstrated in Reference (15) for a monopole. The top loading of Loran-C antennas also make the problem of source representation somewhat more complex. Such a problem is beyond the scope of this paper and this research. Using the formula:

$$P_r = 1.6(10^{-13})\ \omega^2\ (I_0\ell)^2/\mathcal{Z}_0, = 1.67548(10^{-4})\ \text{watts, radiated power}$$

where $\mathcal{Z}_0$ = 377 ohms, the impedance of free space, and $I_0\ell = 1$.

Then, for P_r = 500,000 watts,

$$\sqrt{\frac{P_r(I_0\ell)}{P_r(1)}} = \sqrt{\frac{500{,}000}{1.67548(10^{-4})}} = 5.463(10^4)\ \text{Ampere-meters} = 94.75\ \text{db.}$$

Table 3 gives numerical values for the cycle zero of the pulse at 100 km. It is necessary to add 2.5 microseconds which has been subtracted out by the radiation mechanism from the antenna and to subtract the cycle number times 10 microseconds to get the secondary phase correction for each cycle. Thus, in the case of the first cycle,

$$9.03 + 2.5 - 10 = 11.53 - 10 = 1.53.$$

For cycle number 1.5,

$$13.82 + 2.5 - 15 = 16.32 - 15 = 1.32.$$

Tables 1 and 2 give the corresponding near fields for 0.1 km and 1 km respectively. A computer oscillogram of the near field at 0.1 km is also given in Figure 8, depicting both the cycles, Re $E(t',d)$ and the envelope $|E(t',d)|$. The third cycle error relative to a continuous wave signal varies between -0.08 μs and 0.11 μs.* It is also evident from Tables 1 through 4 that the distortion is an early time phenomenon. The distortion is not obvious from an oscillogram of the pulse such as depicted in the computer graphs of Figures 6 and 7, d = 100 and 500 km respectively. It is necessary to magnify the detail of the pulse to observe the distortion. That the distortion exists, is evident from the assumed antenna current pulse, the zeroes of which are precisely at 10, 15, 20, 25, ... μs.

The advantages of using a pulse in preference to a CW (continuous wave) signal, as previously pointed out in the introduction, far outweighs the distortion discussed here. This distortion, however, should make us very cautious in our treatment of nonhomogeneous and irregular ground as proposed in Reference (19) as an ultimate prediction scheme. It is also obvious that such errors as discussed above tend to cancel in a time difference coordinate observation. But since a spatial dependence in the error exists, such errors do not cancel exactly.

The effect of nonhomogeneous and irregular ground was illustrated for purposes of this paper by introducing a specially prepared geophysical and geological data base discussed in CRPL; Report 78-9, Reference (20). Thus, a preliminary operation of the computer configuration shown in Figure 3 was accomplished for a propagation path between Searchlight, Nevada and Tecopa, California, a distance of approximately 137 km. The newly acquired topographic data base for Continental United States was employed for this specific propagation path.

---

* It is of special interest to observe that the third cycle error relative to a continuous wave (CW) at 0.1 km, Table 1, is -0.08 μs (microseconds). At 1 km, Table 2, the error is 0.11 μs. At 100 km, Table 3, the error is 0.09 μs. Finally, Table 4, at 500 km, the error is 0.03 μs. Thus, the phase modulation of the pulse over smooth, homogeneous ground appears to be a near field phenomenon.

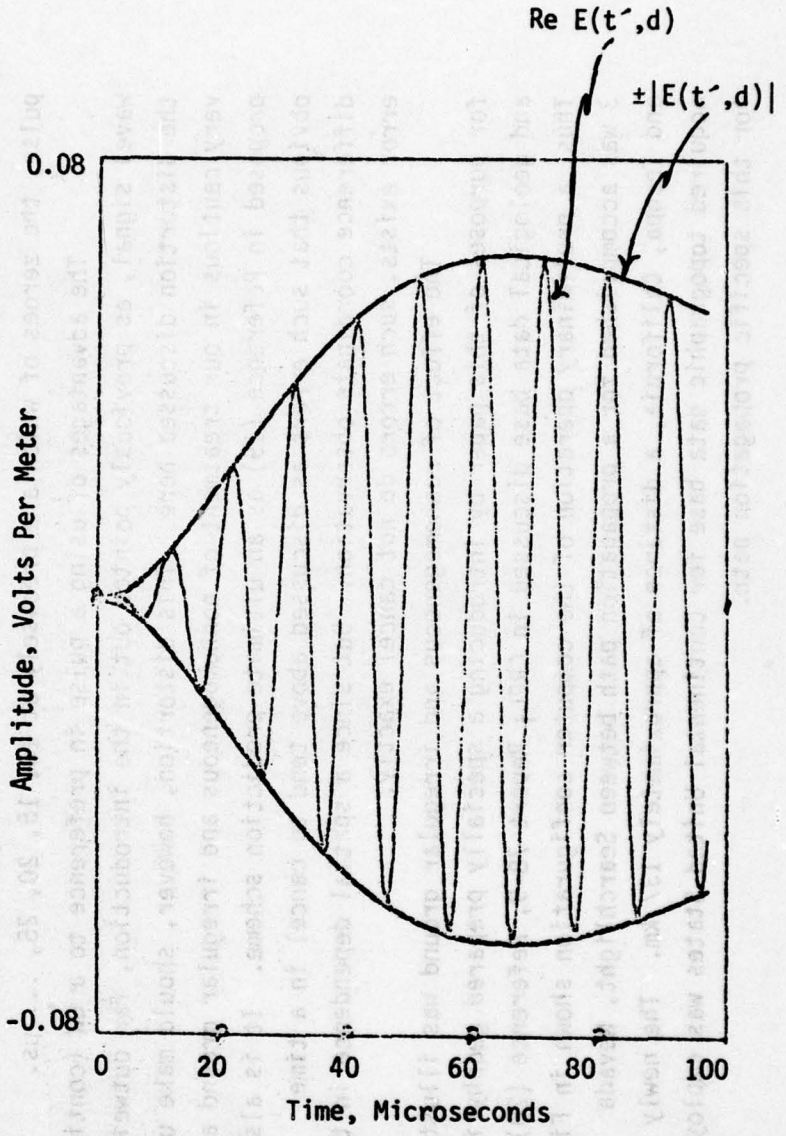

FIGURE 6. THEORETICALLY PROPAGATED LORAN-C PULSE AT A DISTANCE OF 100 KM FROM THE ANTENNA SOURCE CURRENT PULSE GIVEN IN FIGURE 2, ASSUMING THE GROUND TO BE SMOOTH AND HOMOGENEOUS WITH A CONDUCTIVITY, σ = .005 MHOS/M OR GROUND WITH AN IMPEDANCE, |x| = .033.

TABLE 1

ONE TENTH KILOMETER NEAR FIELD CYCLE ZERO AND
SECONDARY PHASE CORRECTION, MICROSECONDS,
FOR VARIOUS ZEROES OF THE CYCLE, Re $E(t',d) = 0$

Cycle Number	Local Time, t', μs of Cycle Zero	Cycle Secondary Phase Correction, t_c, μs	Error Relative to CW Secondary Phase Correction, μs	
1	11.86	4.36	-0.33	
1.5	16.94	4.44	-0.25	t_c (CW) =
2	22.04	4.54	-0.15	4.69
2.5	27.07	4.57	-0.12	
3	32.11	4.61	-0.08	
3.5	37.12	4.62	-0.07	
4	42.15	4.65	-0.04	
4.5	47.16	4.66	-0.03	
5	52.17	4.67	-0.02	
5.5	57.18	4.68	-0.01	
6	62.18	4.68	-0.01	

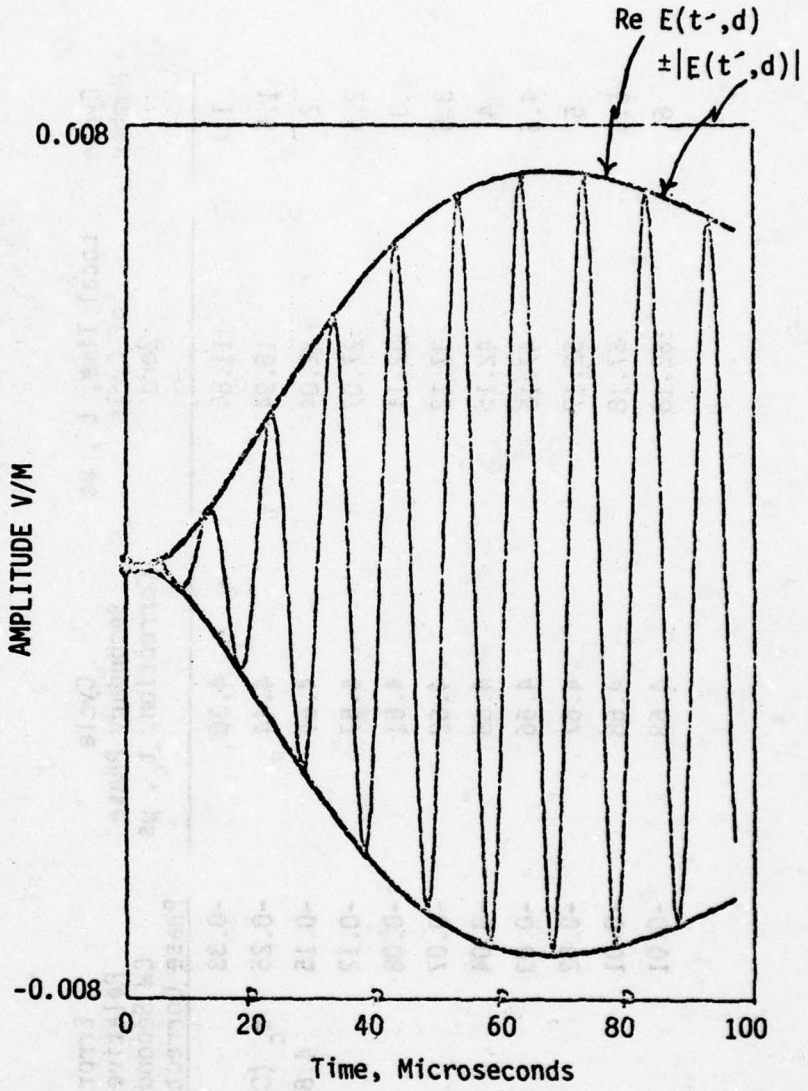

FIGURE 7. THEORETICALLY PROPAGATED LORAN-C PULSE AT A DISTANCE OF 500 KM FROM THE ANTENNA SOURCE CURRENT PULSE GIVEN IN FIGURE 2, ASSUMING THE GROUND TO BE SMOOTH, HOMOGENEOUS WITH A CONDUCTIVITY, σ = .005 MHOS/M OR A GROUND IMPEDANCE, $|x|$ = .033.

TABLE 2

ONE KILOMETER NEAR FIELD CYCLE ZERO AND
SECONDARY PHASE CORRECTION, MICROSECONDS,
FOR VARIOUS ZEROES OF THE CYCLE, Re $E(t',d) = 0$

Cycle Number	Local Time t', μs, of Cycle Zero	Cycle Secondary Phase Correction, t_c, μs	Error Relative to CW Secondary Phase Correction, $t_c - t_c(CW)$, μs	
1	8.94	1.44	0.96	
1.5	13.75	1.25	0.27	
2	18.68	1.18	0.20	
1.5	23.62	1.12	0.14	$t_c(CW) = 0.98$
3	28.59	1.09	0.11	
3.5	33.56	1.06	0.08	
4	38.54	1.04	0.06	
4.5	43.52	1.02	0.04	
5	48.51	1.01	0.03	
5.5	53.50	1.00	0.02	
6	58.49	0.99	0.01	

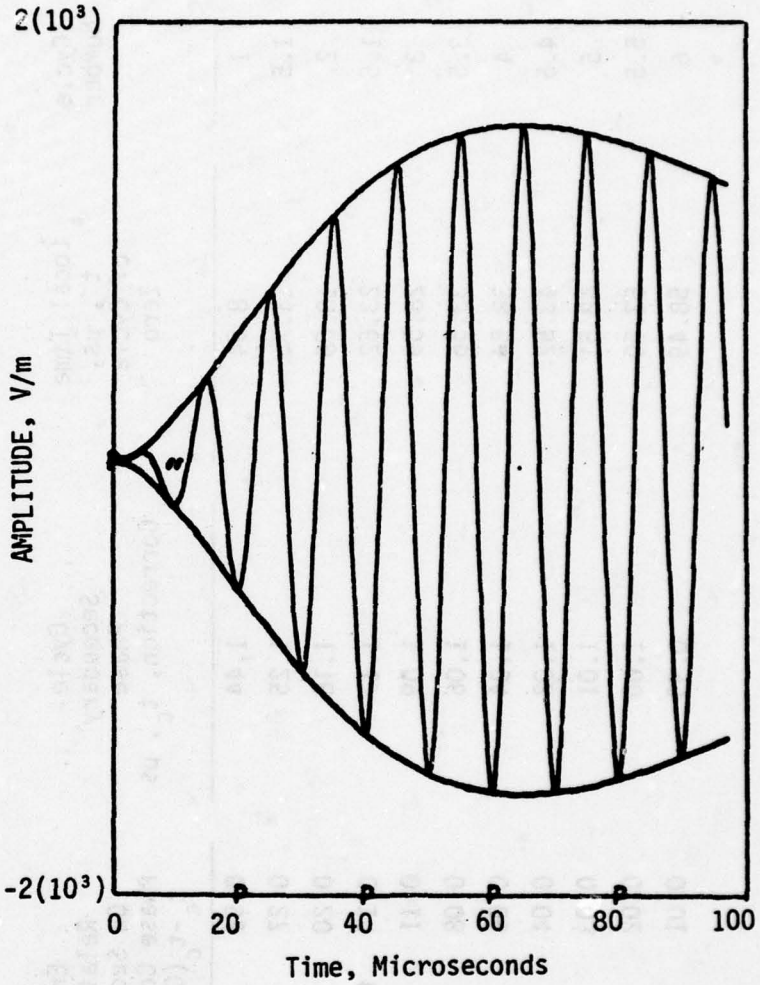

FIGURE 8. THEORETICALLY PROPAGATED LORAN-C PULSE, ILLUSTRATING THE NEAR FIELD AT A DISTANCE OF 0.1 KM FROM THE ANTENNA SOURCE CURRENT PULSE GIVEN IN FIGURE 2. CYCLE ZEROES ARE GIVEN IN TABLE 1.

TABLE 3

ONE HUNDRED KILOMETER FAR FIELD CYCLE ZEROES
AND SECONDARY PHASE CORRECTION, MICROSECONDS,
FOR VARIOUS ZEROES OF THE CYCLE, Re $E(t',d) = 0$

Cycle Number	Local Time, t', μs of Cycle Zero	Cycle Secondary Phase Correction, t_c, μs	Error Relative to CW Secondary Phase Correction, $t_c - t_c(CW)$, μs	
1	9.03	1.53	0.48	
1.5	13.82	1.32	0.27	$t_c(CW) =$ 1.05 μs
2	18.73	1.23	.18	
2.5	23.68	1.18	.13	
3	28.64	1.14	.09	
3.5	33.62	1.12	.07	
4	38.60	1.10	.05	
4.5	43.59	1.09	.04	
5	48.58	1.08	.03	
5.5	53.57	1.07	.02	
6	58.56	1.06	.01	

AD-A077 551 COLORADO RESEARCH AND PREDICTION LAB INC BOULDER F/G 17/7
LORAN-C PULSE TRANSIENT PROPAGATION. PART I. GEOPHYSICAL AND GE--ETC(U)
MAY 79 J R JOHLER , R H DOHERTY , A R COOK DOT-CG-842923-A
UNCLASSIFIED CRPLI-78-9 USCG-D-52-79 NL

2 OF 3
ADA 077551

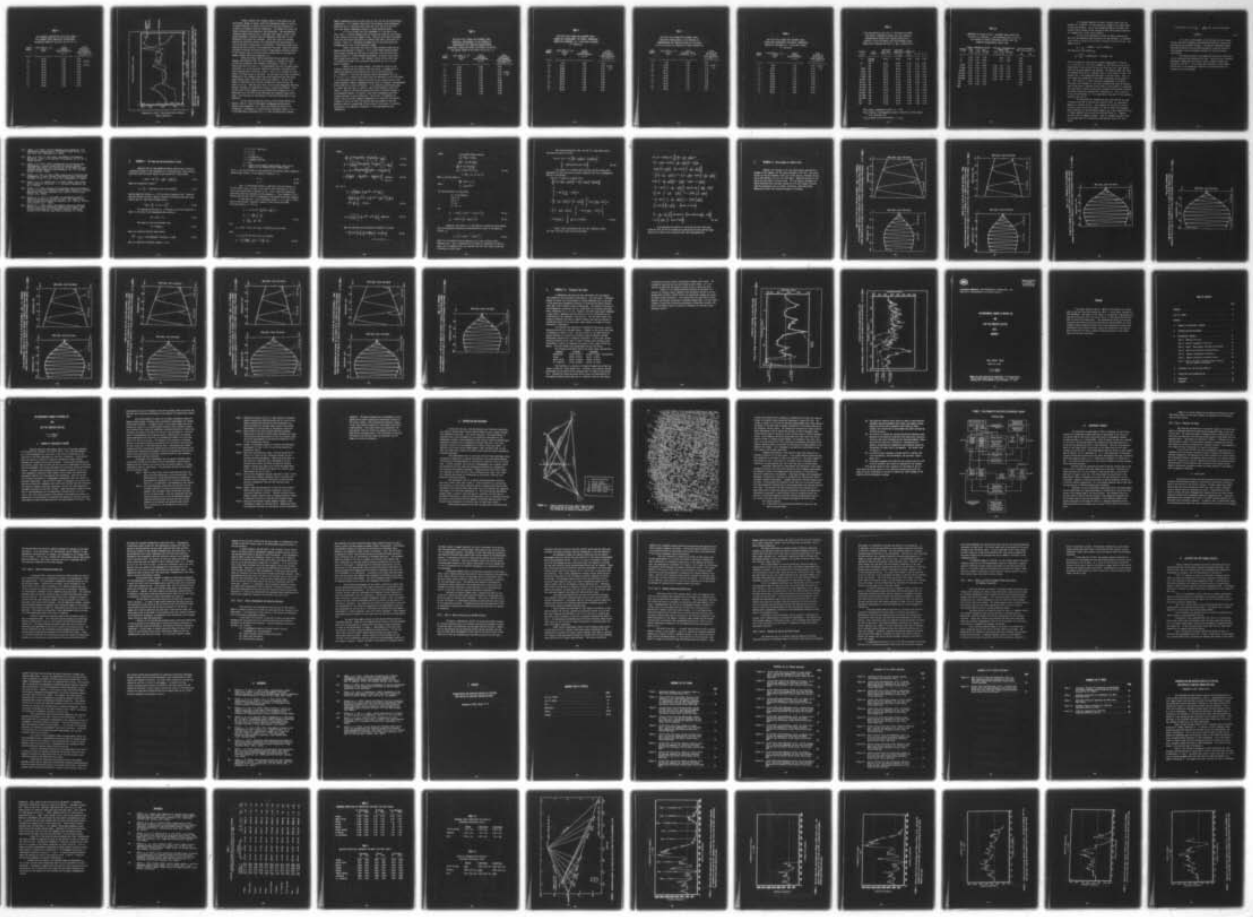

TABLE 4

FIVE HUNDRED KILOMETER FAR FIELD CYCLE ZEROES
AND SECONDARY PHASE CORRECTION, MICROSECONDS,
FOR VARIOUS ZEROES OF THE CYCLE, Re $E(t',d) = 0$

Cycle Number	Local Time, t', μs, of Cycle Zero	Cycle Secondary Phase Correction, t_c, μs	Error Relative to CW Secondary Phase Correction, $t_c - t_c(CW)$, μs	
1	10.66	3.16	0.19	
1.5	15.57	3.07	0.10	$t_c(CW) =$
2	20.54	3.04	0.07	2.97 μs
2.5	25.51	3.01	0.04	
3	30.50	3.00	0.03	
3.5	35.49	2.99	0.02	
4	40.48	2.98	0.01	
4.5	45.48	2.98	0.01	
5	50.47	2.97	0.00	
5.5	55.48	2.97	0.01	
6	60.46	2.96	-0.01	

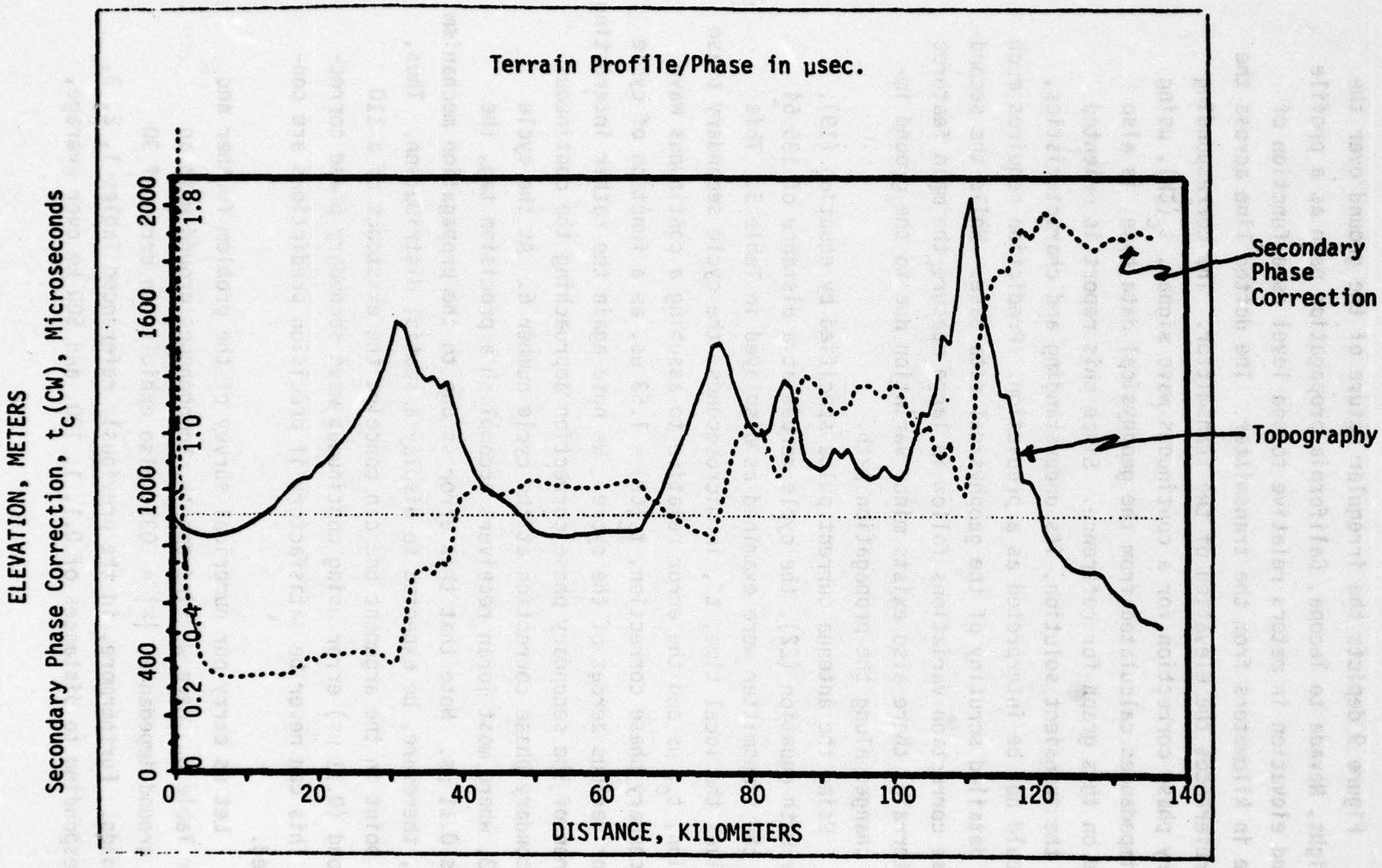

FIGURE 9. GROUND ELEVATION, METERS, ABOVE SEA LEVEL AND THEORETICAL SECONDARY PHASE CORRECTION FOR A 100 kHz CONTINUOUS WAVE SIGNAL, T_C(CW) AS A FUNCTION OF DISTANCE, KILOMETERS, FROM THE TRANSMITTER.

Figure 9 depicts the irregular nature of the ground over the Searchlight, Nevada to Tecopa, California propagation path as a profile of ground elevation in meters relative to sea level as a function of distance in kilometers from the transmitter. The dotted line across the figure references the elevation of the transmitter. The corresponding secondary phase correction for a continuous wave signal, $t_c(CW)$, using ground impedances calculated from the geophysical data base, is also depicted on this graph for reference. Since this report is oriented towards the transient solution, its understanding and characteristics, this should not be interpreted as a prediction. Prediction requires much greater detailed scrutiny of the geophysical data base. While the secondary phase correction variations follow in large measure the main features of the terrain, there also exists minor variation due to the ground impedance changes along the propagation path.

Using the antenna current pulse specified by equation (19), together with equation (22), the cycle zeroes at a distance of 135.64 km from the transmitter were examined as displayed in Table 5. This table gives the local time, t', in microseconds, the cycle secondary phase correction, t_c, μs and the error relative to assuming a continuous wave (CW) secondary phase correction, $t_c(CW) = 1.53$ μs, as a function of cycle number or various zeroes of the cycle. We note again the rather interesting phenomenon of the secondary phase correction approaching the continuous wave secondary phase correction at the cycle number 6. At the cycle number 3, where most loran receivers accomplish a precision tag, the error is 0.11 μs. Note that this error is due to the propagation mechanism and may, therefore, be expected to display a spatial distribution. Thus, at this point in the argument one can conceive the existence of a 110 nanosecond (0.11 μs) error using continuous wave secondary phase corrections! This can never be satisfactory if precision predictions are contemplated.

Let us carry our numerical survey of the problem further and consider Table 6. Here we find smooth, homogeneous ground with an average ground impedance, $|x| = .033$, also exhibits an error of 90 nanoseconds. Furthermore, in the previously referenced Tables 1, 2, 3, 4, corresponding to distances of 0.1, 1, 100, and 500 km over average,

smooth, homogeneous ground, we get errors of -80, 110, 90 and 30 nanoseconds respectively. It is apparent that whilst the irregular and nonhomogeneous ground may have a disturbing effect upon the cycle, the error can also exist over smooth, homogeneous ground in a quite deceptive manner.

It is also evident that this phenomenon is a function of the local time, t', and the problem could be resolved by using the cycle number 6 zero instead of the cycle number 3 zero. But this cycle may be contaminated by sky wave which would cause for greater error than is now under discussion. Hence, it is necessary to sample early at the third cycle and accommodate this error in the prediction scheme.

Tables 7 and 8 give this error at other distances along the propagation path depicted in Figure 9. It is surprisingly constant between the distances selected and this may be fortutious, since the error then tends to cancel in a time difference measurement, at least to the resolution of many loran receivers. This, however, should not be relied upon in a prediction scheme since fortuitous cancellation of error is not a general principle.

Tables 9 and 10 further enhance the numerical survey of the transient solution for the zeroes of the third cycle. A tagged point in time on the envelope using equation (25 a) and an arbitrary value, $C_e = 2.904(10^{-5})$. This sets the envelope tag at approximately 30 μs at d = 0.1 km. It is evident from Table 9 that the envelope to cycle difference, Γ, in microseconds can be readily calculated for the various values of the ground parameters (smooth, homogeneous ground, SHG, or irregular, nonhomogeneous ground (ING) and at various distances. It is noted that the envelope tag, T_c, mimics the cycle tag, t_c, and as a result the envelope to cycle difference, Γ, tends to reflect only weakly the effects of spatial changes in the propagation medium. Of course, a more severe topography would give stronger envelope to cycle differences. Whilst this is suggestive of using a form of receiver automatic compensation for spatially distributed propagation errors, we offer the opinion that any attempt at such compensation should be accomplished in the context of the theory of transient propagation, if any degree of uniqueness is to be guaranteed by such compensation.

TABLE 5

FAR FIELD CYCLE ZEROES AND SECONDARY PHASE CORRECTION, MICROSECONDS, IN THE PRESENCE OF NONHOMOGENEOUS AND IRREGULAR GROUND BETWEEN SEARCHLIGHT, NEVADA AND TECOPA, CALIFORNIA (135.64 km), FOR VARIOUS ZEROES OF THE CYCLE, Re $E(t',d) = 0$

Cycle Number	Local Time, t', μs, of Cycle Zero	Cycle Secondary Phase Correction, t_c, μs	Error Relative to CW Secondary Phase Correction, $t_c - t_c(CW)$, μs	
1	9.56	2.06	0.53	
1.5	14.34	1.84	0.31	
2	19.24	1.74	0.21	$t_c(CW)$=
2.5	24.17	1.67	0.14	1.53
3	29.14	1.64	0.11	
3.5	34.11	1.61	0.08	
4	39.09	1.59	0.06	
4.5	44.07	1.57	0.04	
5	49.06	1.56	0.03	
5.5	54.05	1.55	0.02	
6	59.04	1.54	0.01	

TABLE 6

FAR FIELD CYCLE ZEROES AND SECONDARY PHASE CORRECTION, MICROSECONDS, FOR SMOOTH, HOMOGENEOUS GROUND WITH IMPEDANCE, $|x| = 0.033$ AND A DISTANCE, $d = 135.64$ km

Cycle Number	Local Time, t', μs, of Cycle Zero	Cycle Secondary Phase Correction, t_c, μs	Error Relative to CW Secondary Phase Correction $t_c - t_c(CW)$, μs	
1	9.19	1.69	0.45	
1.5	14.01	1.51	0.27	$t_c(CW) =$
2	18.92	1.42	0.18	1.24
1.5	23.86	1.36	0.12	
3	28.83	1.33	0.09	
3.5	33.81	1.31	0.07	
4	38.79	1.29	0.05	
4.5	43.78	1.28	0.04	
5	48.77	1.27	0.03	
5.5	53.76	1.26	0.02	
6	58.75	1.25	0.01	

TABLE 7

FAR FIELD CYCLE ZEROES AND SECONDARY PHASE CORRECTION, MICROSECONDS, IN THE PRESENCE OF NONHOMOGENEOUS AND IRREGULAR GROUND AT A DISTANCE OF 99.736 km FROM THE SEARCHLIGHT, NEVADA TRANSMITTER

Cycle Number	Local Time, t', μs of Cycle Zero	Cycle Secondary Phase Correction, t_c, μs	Error Relative to CW Secondary Phase Correction $t_c - t_c(CW)$, μs	
1	9.16	1.66	0.55	
1.5	13.92	1.42	0.31	$t_c(CW)$ =
2	18.82	1.32	0.21	1.11
2.5	23.75	1.25	0.14	
3	28.71	1.21	0.10	
3.5	33.68	1.18	0.07	
4	38.66	1.16	0.05	
4.5	43.65	1.15	0.04	
5	48.63	1.13	0.02	
5.5	53.63	1.13	0.02	
6	58.62	1.12	0.01	

TABLE 8

FAR FIELD CYCLE ZEROES AND SECONDARY PHASE CORRECTION, MICROSECONDS, FOR SMOOTH, HOMOGENEOUS GROUND WITH IMPEDANCE $|x| = 0.033$ AND DISTANCE, $d = 99.736$ km

Cycle Number	Local Time, t', μs of Cycle Zero	Cycle Secondary Phase Correction t_c, μs	Error Relative to CW Secondary Phase Correction $t_c - t_c(CW)$, μs
1	9.02	1.52	0.47 $t_c(CW) =$
1.5	13.82	1.32	0.27 1.05
2	18.73	1.23	0.18
2.5	23.67	1.17	0.12
3	28.64	1.14	0.09
3.5	33.62	1.12	0.07
4	38.60	1.10	0.05
4.5	43.59	1.09	0.04
5	48.58	1.08	0.03
5.5	53.57	1.07	0.02
6	58.56	1.05	0.01

TABLE 9

CYCLE AND ENVELOPE LOCAL TIME t′, FOR VARIOUS DISTANCES OVER SMOOTH, HOMOGENEOUS GROUND (SHG) AND IRREGULAR, NONHOMOGENEOUS GROUND (ING) SHOWING DERIVATION OF ENVELOPE TO CYCLE DIFFERENCE (ECD) AND SECONDARY PHASE CORRECTION OF ENVELOPE AND CYCLE, T_c AND t_c RESPECTIVELY

Distance d, km	Type Ground	3rd Cycle Zero Local Time, t′, μs	Envelope Tagged Point In Time, t′, μs	$C_e = 2.904(10^{-5})$ ECD Γ, μs	t_c, μs	T_c, μs
0	Antenna Current	30.00	30.68	0.68	0.00	0.68
0.1	SHG	34.61	29.98	-4.63	4.61	-0.02
1	SHG	31.09	29.33	-1.76	1.09	0.67
2.9921	SHG	30.37	30.48	0.11	0.37	0.48
2.9921	ING	30.53	30.51	-0.02	0.53	0.51
9.9736	SHG	30.48	30.70	0.21	0.48	0.70
9.9736	ING	30.38	30.78	0.40	0.38	0.78
40.8917	SHG	30.73	31.19	0.46	0.73	1.19
40.8917	ING	30.90	31.28	0.40	0.90	1.30
99.7359	SHG	31.14	31.56	0.42	1.14	1.56
99.7359	ING	31.21	31.69	0.48	1.21	1.69
118.6857	SHG	31.24	31.66	0.42	1.24	1.66
118.6857	ING	31.67	32.04	0.39	1.65	2.04
135.6408	SHG	31.33	31.75	0.43	1.33	1.76
135.6408	ING	31.64	32.13	0.49	1.64	2.13
200.	SHG	31.65	32.04	0.39	1.65	2.04
500.	SHG	33.00	33.19	0.19	3.00	3.19

SHG ≙ Smooth, homogeneous ground, $|x| = .033$

ING ≙ Irregular, nonhomogeneous ground as specified in CRPL$_i$ Report 78-9, Reference (20)

ECD ≙ Envelope to Cycle Difference, $\Gamma = T_c - t_c$.

TABLE 10

COMPARISON OF VALUES OF ECD, Γ, SECONDARY PHASE CORRECTIONS FOR CYCLE, t_c, ENVELOPE, T_c, AND CONTINUOUS WAVE, $t_c(CW)$, IN THE PRESENCE OF SMOOTH, HOMOGENEOUS GROUND (SHG), AND IRREGULAR NONHOMOGENEOUS GROUND (ING)

DISTANCE, d, kM	SMOOTH, HOMOGENEOUS GROUND (SHG) |x| = .033			IRREGULAR, NONHOMOGENEOUS GROUND (ING)			100 kHz CONTINUOUS WAVE (CW), $t_c(CW)$, μs	
	ECD, Γ, μs	Cycle t_c, μs	Envelope T_c, μs	ECD Γ, μs	Cycle t_c, μs	Envelope T_c, μs	SHG	ING
0	0.68	0.00	0.68		0.00	0.68	0.00	
0.1	-4.63	4.61	-0.02		4.61	-0.02	4.69	
1	-1.76	1.09	-0.67				0.98	
2.9921	0.11	0.37	0.48	-0.02	0.53	0.51	0.43	0.43
9.9736	0.21	0.48	0.70	0.40	0.38	0.78	0.38	0.28
40.8917	0.46	0.73	1.19	0.40	0.90	1.30	0.63	0.80
99.7359	0.42	1.14	1.56	0.48	1.21	1.69	1.05	1.11
118.6857	0.42	1.24	1.66	0.39	1.67	1.66	1.16	1.52
135.6408	0.42	1.33	1.75	0.49	1.64	2.13	1.24	1.53
200.	0.39	1.65	2.04				1.58	
500.	0.19	3.00	3.19				2.97	
1000.								

It is perhaps important to note in Tables 8 and 9 that the constant $C_e = 2.904(10^{-5})$ can be arbitrarily changed to tag other points on the pulse envelope. But as the propagation medium is changed, the constant should indeed be kept constant so that the envelope dispersion of a tagged point in time can be studied.

It is at first inspection of Table 10 rather perplexing to note that the secondary phase correction for the envelope, T_c, decreases from a value of -0.02 μs at 0.1 km to a value of -0.67 μs at 1 km. Thus, equation (29 a)

$$u_{e_2} - u_{e_1} = 3.003097 - 0.65 = 2.350971 \ \mu s.$$

The velocity of the envelope V_e,

$$V_e = \frac{d_2 - d_1}{u_e} = 3.828205(10^8) = 1.276151c, \ m/s.$$

Thus, if clocks were set using the envelope tagged point in time at $d_1 = 0.1$ km and $d_2 = 1$ km, less 3.003097 μs, the clock set at d_2 would read earlier in time by 0.65 μs than the clock set at d_1, when the two clocks are brought together and compared! The apparent speed with which the envelope traveled was 1.276951c, where c is the speed of light. The paradox lies in the propagation mechanism in the near field. Thus, in this region the attenuation of the higher frequencies by the ground is nil. Thus, there is a linear increase or enhancement in radiation efficiency with frequency at very short distances such that the leading edge of the pulse is enhanced (rises faster as the distance is increased) up to the point at which the electrical constants of the ground attenuate the higher frequencies exponentially, Reference (7). Thus, causality is not violated because $t' > 0$ as specified at the onset of this analysis, equations (19) and (9).

This discussion has assumed that the loran receiver has used an antenna sensitive to the vertical electric field, ξ_r, discussed in Appendix I, equation (18 AI). Loop antennas are also used in Loran-C to replace the vertical whip antenna. In the far field, the secondary phase correction for the horizontal magnetic, H_ϕ, field, equation (19 AI) is almost identical with the vertical electric field, ξ_r. However, the near field is somewhat altered. Thus, for example, the near field for equation (39) can be rewritten using equation (19 AI) for this field,

$$H(s,d)\cdot f_s(s) = z_0^{-1} C\{ \frac{s}{s+\nu} - \frac{s^2}{(s+\nu)^2} \sqrt{\pi\alpha} \exp(s^2\alpha) \operatorname{erfc}(s\sqrt{\alpha}) + \frac{1}{t_0(s+\nu)} \} . \quad (57)$$

It is thus a simple matter to rewrite equation (49) leaving out the last term of equation (49) before performing the integration specified by the inversion integral. The general computation scheme described heretofore has also been developed to study the effects of loop antennas as well as antennas receptive to vertical electric polarization.

The discussion above also assumed the electrical characteristics of the ground were constant with time. These electrical constants may however change with time due to climatic changes, weather and especially rain fall. It is evident that estimates of such changes can be used in the theoretical simulation discussed heretofore to account for any such changes.

4. Conclusions and Recommendations

A full transient propagation computer simulation scheme has been assembled and exercised for a limited number of computations to demonstrate some principles of transient behavior. The authors would recommend computation of additional examples leading to a test of the validity of the theory presented.

It is recommended that an enhanced soil, hydrology and geologic data base be developed in digital form suitable for use in computers for the Western United States, especially in the region of Searchlight, Nevada and Death Valley California.

It is concluded that the computer simulation computations presented in this paper give results of significance to the precision prediction and interpretation of the secondary phase correction and the envelope to cycle difference. The dependence of the envelope to cycle difference upon the spatial dependence of secondary phase correction is weak in most cases and automatic receiver compensation for spatially distributed propagation errors should be employed in the context of theory to guarantee uniqueness, if such compensation is attempted indeed.

It is evident that the spatially distributed propagation parameters can vary with time due to such matters as rain fall and weather conditions affecting the ground electrical characteristics. These effects can be studied numerically with the aid of the analysis developed for this paper.

5. REFERENCES

(1) Hefley, G. (1972), The Development of Loran-C Navigation and Timing, NBS Monograph 129 (Supt. of Doc., U.S. Gov. Print. Off., Washington, D.C. 20402).

(2) U.S. Coast Guard (1974), Loran-C User Handbook, CG-462 (Dept. of Transportation, U.S. Coast Guard, Headquarters, Washington, D.C. 20590).

(3) Johler, J.R. (1959), Propagation of a ground wave pulse around a finite conducting spherical earth from a damped sinusoidal source current, IRE Trans. on Ant. and Prop., AP-7, 1-10.

(4) Johler, J.R. (1962), Propagation of the low frequency radio signal, Proc. IRE, 50, No. 4, 404-427.

(5) Johler, J.R. (1963), The propagation time of a radio pulse, IEEE Trans. on Ant. and Prop., AP-11, Mp/ 6, 661-668.

(6) Johler, J.R. and J.C. Morgenstern (1965), Propagation of the ground wave electromagnetic signal, with particular reference to a pulse of nuclear origin, Proc. IEEE, 53, No. 12, 2043-2053.

(7) Johler, J.R. (1967), Propagation of an electromagnetic pulse from a nuclear burst, IEEE Trans. on Ant. & Prop. AP-15, No. 2, 256-263.

(8) Johler, J.R. and S. Horowitz (1973), Propagation of the Loran-C ground and ionospheric wave pulses, Office of Telecommunications Report 77-20 (Suptd. of Doc., U.S. Gov. Print. Off., Washington, D.C. 20402).

(9) Johler, J.R. and S. Horowitz (1974), Propagation of a loran pulse over irregular, inhomogeneous ground, AGARD-CP-144, No. 28, Conference on FM wave propagation involving irregular surfaces and inhomogeneous media (National Technical Information Service (NTIS), 5285 Post Royal Road, Springfield, Va. 22151.

(10) Johler, J.R., W.J. Kellar, and L.C. Walters (1956), Phase of the low radio-frequency ground wave, NBS Circular 573 (Suptd. of Doc., U.S. Gov. Print. Off., Washington, D.C. 20402).

(11) Norton, K.A. (1937), The propagation of radio waves over the surface of the earth and in the upper atmosphere, Proc. IRE, 25 No. 9, 1203-1236.

(12) Sommerfeld, A. (1909), Über die Ausbreitung der Wellen in der drahtlosen Telegraphie, Ann. Phys., 28, No. 4.

(13) Sommerfeld, A. (1914), Über die Fortpflanzung des Lichtes in dispergierenden Medien, Ann. Phys., 44, No. 10, 172-202.

(14) Brillouin, L. (1914), Über die Fortpflanzung des Lichten in dispergierenden Medien, Ann. Phys., 44, No.10, 203-240.

(15) Johler, J. R. (1971), Loran-A groundwave pulse propagation, Telecommunications Research Report, OT/ITS RR 20 (Suptd. of Doc., U.S. Gov. Print. Off., Washington, D.C. 20402).

(16) Dean, W. N. and D. P. Roth (1976), The AN/BRN-5 Loran Receiver, Navigation, Journal of the Institute of Navigation, Vol. 23, No. 4, Winter, 287-297.

(17) Johler, J. R. (1977), Loran-C propagation error corrections over nonhomogeneous, irregular ground using the internal equation technique, CRPL$_j$ Report 77-9, Contract No. DOT-CG-74629-A (9/15/77) (Colorado Research and Prediction Laboratory, Inc., P.O. Box 1056, Boulder, Colorado 80306).

(18) Johler, J. R. and L. A. Berry (1967), Loran-D phase corrections over inhomogeneous, irregular terrain, ESSA Technical Report IER-59-ITSA 56 (Suptd. of Doc., U.S. Gov. Print. Off., Washington, D.C. 20402).

(19) Burch, L. B., R. H. Doherty and J. R. Johler (1976), Loran calibration by prediction, Navigation, J. of Institute of Navigation, 23, No. 3, 195-200.

(20) Johler, J. R. (1978), Geophysical and geological data base evaluation for Loran-C ground wave propagation medium, CRPL$_j$ Report 78-9 (Colorado Research and Prediction Laboratory, Inc., 1898 So. Flatiron Court, Boulder, Colo., 80301).

(21) Doherty, R. H. and A. R. Cook (1978), An experimental program to measure ECD and test the transient solution, CRPL$_j$ Report 78-10, (Colorado Research and Prediction Laboratory, Inc., 1898 So. Flatiron Court, Boulder, Colo. 80301).

(22) Doherty, R. H. (1974), Spatial and temporal electrical properties derived from LF pulse ground wave propagation measurements, AGARD Conference Proceedings No. 144 (National Technical Information Services (NTIS), 5285 Post Royal Road, Springfield, Va., 22151).

6. APPENDIX I: THE INDUCTION AND ELECTROSTATIC FIELDS

Equation (39) for the Sommerfeld-Norton surface wave represents a rigorous solution to the propagation of a continuous wave from vertically polarized electrical point source on the surface of a plane ground,

$$\xi\ (\omega,d) = j\omega C \left\{ W + \frac{1}{j\omega t_0} + \frac{1}{(j\omega t_0)^2} \right\} , \qquad (1\ AI)$$

where the attenuation function

$$W = \left[1 - j\ \sqrt{\pi\rho_1}\ \exp\ (-\omega^2\rho_1)\ \text{erfc}\ (j\sqrt{\rho_1}) \right] , \qquad (2\ AI)$$

and the numerical distance, $\rho_1 = \omega^2\alpha$ is given by equation (45). Equation (48) was derived from this rigorous formula by convolution with the transform of the U.S. Coast Guard standard pulse,

$$f_s(\omega) = \left[c_1 + j\ (\omega_c + \omega) \right]^{-3} . \qquad (3\ AI)$$

The attenuation function, W, is related to the scalar potential Π which is a solution to the homogeneous wave equation:

$$(\nabla^2 + K_1^2)\ \Pi = 0 . \qquad (4\ AI)$$

The value of W can be calculated from:

$$W = \Pi/(2\Pi_{pri}) , \qquad (5\ AI)$$

where, for vertical electric polarization,

$$\Pi^{(e)} = \Pi_{pri} = I_0 \ell \mu_0 c (4\pi b j\omega D)^{-1} \exp \left[j(\omega t - k_1 d) \right], \qquad (6\ AI)$$

and, in a spherical coordinate system, r, θ, ϕ,

$D = r^2 + b^2 - 2br \cos\theta,$

$b = a + h_1,$

$r = a + h_2,$

$a \simeq 6.36739(10^6)$ m,

$c = 2.997925\ (10^8)$ m/s,

$\Theta = d/a,$

$I_0\ell$ = dipole current moment, Ampere-meters, which can be taken as ±1, to simulate Loran-C phase coding,

and $h_{1,2}$ are the altitudes of the transmitter and receiver above a spherical (earth) datum surface. As the geodesic distance $d \to 0$,

$$W \to 1 , \tag{7 AI}$$

$$\Pi \to \infty . \tag{8 AI}$$

Thus, if the antenna current is specified, and the distance, d, is sufficiently small, so that (2 AI) applies, the significance of (7 AI) lies in the second term of equation (2 AI). This is the term containing the ground electrical constants in the parameter ρ_1. Thus, equation (7 AI) implies that the near field is independent of the ground electrical constants.

In the spherical, polar coordinate system, r, θ, φ, $\frac{\partial}{\partial\phi} = 0$, there exists three TM-waves (tranverse magnetic) that can be calculated from the potential, $\Pi = \Pi^{(e)}$ W:

$$\xi_r = -\,(r \sin\theta)^{-1} \frac{\partial}{\partial\theta}\left[\sin\theta \frac{\partial}{\partial\theta}\Pi\right] ,$$

$$\xi_\theta = r^{-1} \frac{\partial^2}{\partial\theta\partial r}\left[r\,\Pi\right] ,$$

$$H_\phi = \frac{k_1^2}{\mu_0 j\omega} \frac{\partial}{\partial\theta}\left[\Pi\right] . \tag{9 AI}$$

Let,

$$C_s = (4\pi d)^{-1}\ I_0\ell\mu_0 c \exp(j\omega t) = 29.97925 \exp(j\omega t) \text{ Volts.}$$

Then,

$$\Pi = C_s(-jk_1Db)^{-1}Wd \exp(-jk_1D), \text{ Volt-meters,}$$

$$\xi_r = -C_s\left[\frac{\cos\theta}{r\sin\theta} \frac{\partial}{\partial\theta}\Pi + \frac{1}{r} \frac{\partial^2}{\partial\theta^2}\Pi\right] , \tag{10 AI}$$

where,

$$\frac{\partial \Pi}{\partial \theta} = \frac{1}{b}\left[\frac{\exp(-jk_1D)}{D}\right]\left[\frac{br\sin\theta}{D}\right]\left[1+\frac{1}{jk_1D}\right] . \qquad (11\ AI)$$

$$H_\phi = C\left[\frac{k_1^2}{\mu_0 j\omega b}\right]\cdot\left[\frac{\exp(-ik_1D)}{D}\right]\cdot\left[\frac{br\sin\theta}{D}\right]\cdot\left[1+\frac{1}{jk_1D}\right] \qquad (12\ AI)$$

$$E_r = jk_1 C\left[\frac{\exp(-ik_1D)}{D}\right]\left\{\left[\frac{-2\cos\theta}{D} + \frac{3br\sin^2\theta}{D^3}\right] + j\left[\frac{2\cos\theta}{k_1D^2} + \frac{kbr\sin^2\theta}{D^2} + \frac{-3br\sin^2\theta}{k_1D^4}\right]\right\} \text{ Volts/m.} \qquad (13\ AI)$$

(W = 1)

For $W \neq 1$,

$$E_r = C_s\left\{\frac{-\cos\theta}{r\sin\theta}\left[W\frac{\partial}{\partial\theta}\Pi^{(e)} + \Pi^{(e)}\frac{\partial}{\partial\theta}W\right] - \frac{1}{r}\left[\left(\frac{\partial}{\partial\theta}W\right)\left(\frac{\partial}{\partial\theta}\Pi^{(e)}\right) + W\frac{\partial^2}{\partial\theta^2}\Pi^{(e)} + \left(\frac{\partial}{\partial\theta}\Pi^{(e)}\right)\left(\frac{\partial}{\partial\theta}W\right) + \Pi^{(e)}\frac{\partial^2}{\partial\theta^2}W\right]\right\} , \text{ Volts/m.,} \qquad (14\ AI)$$

$$H_\phi = C_s\left[\frac{k_1^2}{\mu_0 j\omega}\right]\left[W\frac{\partial}{\partial\theta}\Pi^{(e)} + \Pi^{(e)}\frac{\partial}{\partial\theta}W\right] \text{ Amperes/m} . \qquad (15\ AI)$$

Now, the residues are calculated and summed in a series:

$$W = \sum_s A_s \exp\left[\beta_s\theta\right] = \sum_s A_s \exp\left[j\mathrm{Im}\beta_s\theta\right]\ \exp\left[\mathrm{Re}\beta_s\theta\right] \qquad (16\ AI)$$

$$s = 0, 1, 2, 3, \ldots ,$$

where,

$$A_s \triangleq \text{normalization function}$$

$$\beta_s = \mathrm{Re}\beta_s + j\,\mathrm{Im}\beta_s ,$$

$$\frac{\partial}{\partial\theta} W = \beta_s \exp\left[\beta_s\theta\right],$$

$$\frac{\partial^2}{\partial\theta^2} W = \beta_s^2 \exp\left[\beta_s\theta\right] ,$$

$$\beta_s = -j\,(k_1 a)^{\frac{1}{3}}\,\alpha^{\frac{2}{3}}\,\tau_s , \qquad (17\ \text{AI})$$

$$\alpha \sim .85 , \quad \tau_0 \sim .7, \quad (s = 0)$$

Thus, τ_s are the roots of

$$\frac{\partial y}{\partial \tau} - 2y^2\tau + 1 = 0$$

where

$$y = -i(k_1 a)^{-\frac{1}{3}}\, x^{-1}$$

For short distances, on the ground,

$D \to d$, the geodesic

$\sin\theta \to \theta$

$\cos\theta \to 1$

$\theta = d/a$

$h_1 = h_2 = 0$

and

$$\xi_r = j\omega C\left[1 + (j\omega t_0)^{-1} + (j\omega t_0)^{-2}\right] W, \qquad (18\ \text{AI})$$

$$H_\phi = j\omega z_0^{-1}\, C\left[1 + (j\omega t_0)^{-1}\right] W. \qquad (19\ \text{AI})$$

Apparently the field, ξ_r in the spherical coordinate system emerges with the attenuation function W as multiplicative factor to the quantity (20 AI), F_i,

$$F_i = \left[1 + (j\omega t_0)^{-1} + (j\omega t_0)^{-2}\right] , \qquad (20\ \text{AI})$$

while it is an additive term in equation (1 AI) due to Norton (1937), Reference (11). This is apparently of no numerical consequence in Norton's paper, but it somewhat alters our equation (42) and (49), which we derived from Norton's surface wave.

Upon rewriting equation (46), for the U.S. Coast Guard pulse, according to equation (18 AI),

$$\xi(s,d)\cdot f_s(s) = b_1 C \left\{ \frac{s}{s+\nu} + \frac{1}{t_0(s+\nu)^3} + \frac{1}{t_0^2 s(s+\nu)^3} \right\} \cdot \left\{ 1 - s\sqrt{\pi\alpha}\, \exp(s^2\alpha)\, \operatorname{erfc}(s\sqrt{\alpha}) \right\} . \qquad (21\ AI)$$

This results in a probably more accurate but more complicated expression for the field than is given in equation (49) in an intermediate form it is as follows:

$$E(t',d) = b_1 \nu C \exp(-\nu t') \frac{1}{2\alpha} \exp(\nu^2\alpha) \cdot \left\{ \left[\left(-\frac{1}{2} + \frac{1}{2t_0\nu} + \frac{1}{2t_0^2\nu^3} \right) t'^2 + \left(\frac{1}{\nu} + \frac{1}{t_0^2\nu^3} \right) t' + \left(\frac{1}{t_0^2\nu^4} \right) \right] \cdot \int_0^{t'} \tau \exp\left[-\left(\frac{\tau}{2\sqrt{\alpha}} - \nu\sqrt{\alpha} \right)^2 \right] d\tau + \left[\left(1 - \frac{1}{t_0\nu} - \frac{1}{t_0^2\nu^2} \right) t' - \left(\frac{1}{\nu} + \frac{1}{t_0^2\nu^3} \right) \right] \cdot \int_0^{t'} \tau^2 \exp\left[-\left(\frac{\tau}{2\sqrt{\alpha}} - \nu\sqrt{\alpha} \right)^2 \right] d\tau + \left[-\frac{1}{2} + \frac{1}{2t_0\nu} + \frac{1}{2t_0^2\nu} \right] \cdot \int_0^{t'} \tau^3 \exp\left[-\left(\frac{\tau}{2\sqrt{\alpha}} - \nu\sqrt{\alpha} \right)^2 \right] d\tau \right\} + b_1 \nu C \left[\frac{1}{t_0^2\nu^3} \right] \cdot \int_0^{t'} \frac{\tau}{2\alpha} \exp\left[-\tau^2/4\alpha \right] d\tau \qquad (22\ AI)$$

Again, after considerable ado, we find, compared to Equation (49), the final form to be the following:

$$E(t',d) = b_1 \nu C \exp(-\nu t') \left\{ \left[\left[-\frac{1}{2}\left(1 - \frac{1}{t_0\nu} - \frac{1}{t_0^2\nu^2}\right)t'^2 \right.\right.\right.$$

$$+ \left(\frac{1}{\nu} + \frac{1}{t_0^2\nu^3} + 4\alpha\nu\sqrt{\alpha} \left\{ 1 - \frac{1}{t_0\nu} - \frac{1}{t_0^2\nu^2} \right\} \right) t' + \left(\frac{1}{t_0^2\nu^4} \right.$$

$$\left.\left.\left. - 4\alpha\nu\sqrt{\alpha} \left\{ \frac{1}{\nu} + \frac{1}{t_0^2\nu^3} \right\} - \left\{ 2\alpha + 8\alpha^3\nu^2 \right\} \left\{ 1 - \frac{1}{t_0\nu} - \frac{1}{t_0^2\nu} \right\} \right) \right]$$

$$+ \left[2 \left(1 - \frac{1}{t_0\nu} - \frac{1}{t_0^2\nu^2} \right) t'^2 + \left(-\frac{1}{\nu} - \frac{1}{t_0^2\nu^3} - 4\alpha\nu\sqrt{\alpha} \left\{ 1 - \frac{1}{t_0\nu} - \frac{1}{t_0^2\nu^2} \right\} \right.\right.$$

$$2\alpha\nu\sqrt{\alpha} \left\{ 1 - \frac{1}{t_0\nu} \frac{1}{t_0^2\nu} \right\} \Big) t' + \left(\frac{-1}{t_0^2\nu^4} + 4\alpha\nu\sqrt{\alpha} \quad 1 + \frac{1}{t_0^2\nu^2} \right\}$$

$$\left.\left. - \left\{ 2\alpha + 8\alpha^3\nu^2 \right\} \left\{ 1 - \frac{1}{t_0\nu} + \frac{1}{t_0^2\nu} \right\} \right) \right] \cdot \exp(\nu^2\alpha) \exp\left[-\left(\frac{t'}{2\sqrt{\alpha}} - \nu\sqrt{\alpha} \right)^2 \right]$$

$$+ \left[\left(-\nu\sqrt{\alpha\nu} \left\{ 1 - \frac{1}{t_0\nu} - \frac{1}{t_0^2\nu} \right\} \right) t'^2 + \left(2\sqrt{\alpha\nu} \left\{ \frac{1}{\nu} \quad \frac{1}{t_0^2\nu^3} \right\} \right.\right.$$

$$+ \left\{ 1 + 8\alpha^2\nu^2 \right\} \left\{ 1 - \frac{1}{t_0\nu} - \frac{1}{t_0^2\nu^2} \right\} \Big) t' + \left(2\sqrt{\alpha\nu} \left\{ \frac{1}{t_0^2\nu^4} \right\} \right.$$

$$\left.\left. - \left\{ 1 + 8\alpha^2\nu^2 \right\} \left\{ \frac{1}{\nu} + \frac{1}{t_0^2\nu^3} \right\} - \left\{ 6\alpha\nu\sqrt{\alpha} + 8\,\alpha^3\nu^3\sqrt{\alpha} \right\} \right.\right.$$

$$\left.\left. \cdot \left\{ 1 - \frac{1}{t_0\nu} - \frac{1}{t_0^2\nu} \right\} \right) \right] \cdot \sqrt{\pi\alpha} \exp(\nu^2\alpha) \left[\operatorname{erfc}(-\nu\sqrt{\alpha}) - \operatorname{erfc}\left(\frac{t'}{2\nu\alpha} - \nu\sqrt{\alpha} \right) \right] \Bigg\}$$

$$+ b_1\nu C \left\{ \frac{1}{t_0^2\nu^4} \left[1 - \exp(-t'^2/4\alpha) \right] \right\} . \qquad \text{(23 AI)}$$

As we approach the transmitter and study the near field both equations (49) and (23 AI) become more accurate and we have derived these equations as special and alternative near field representations.

7. APPENDIX II: OSCILLOGRAMS OF LORAN-C PULSE

Figures 2 AII through 11 AII give oscillograms automatically graphed by the computer for the cases discussed in the text. The cycle, Re $E(t',d)$ and the envelope, $\pm|E(t',d)|$ of the analytic function calculated by the computer, $E(t',d)$, are both shown. Magnified sections of the pulse are also shown in certain cases. The very special distances for which transforms were available turned out to be non-integer distances when the propagation path to Tecopa, California, from Searchlight, Nevada was divided into uniform increments of distance.

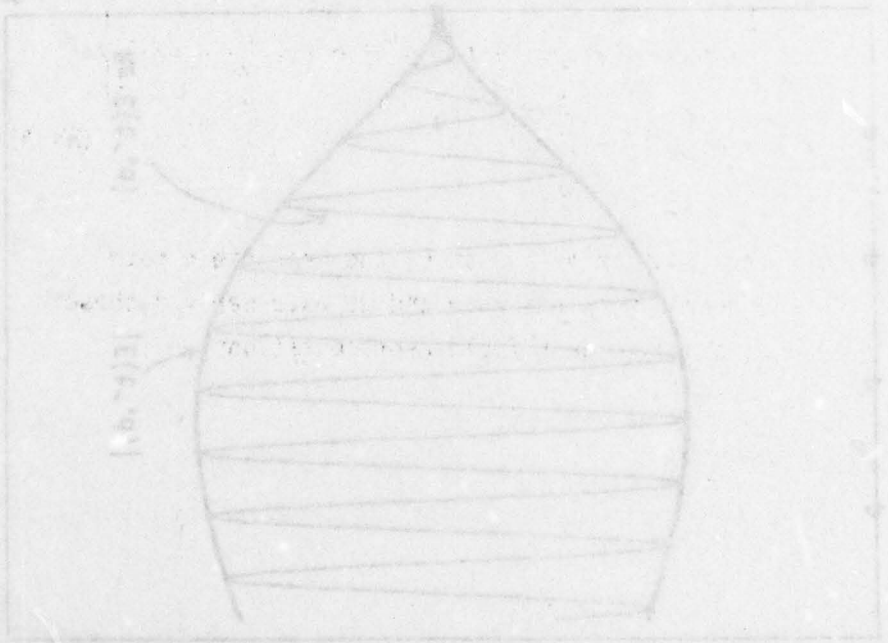

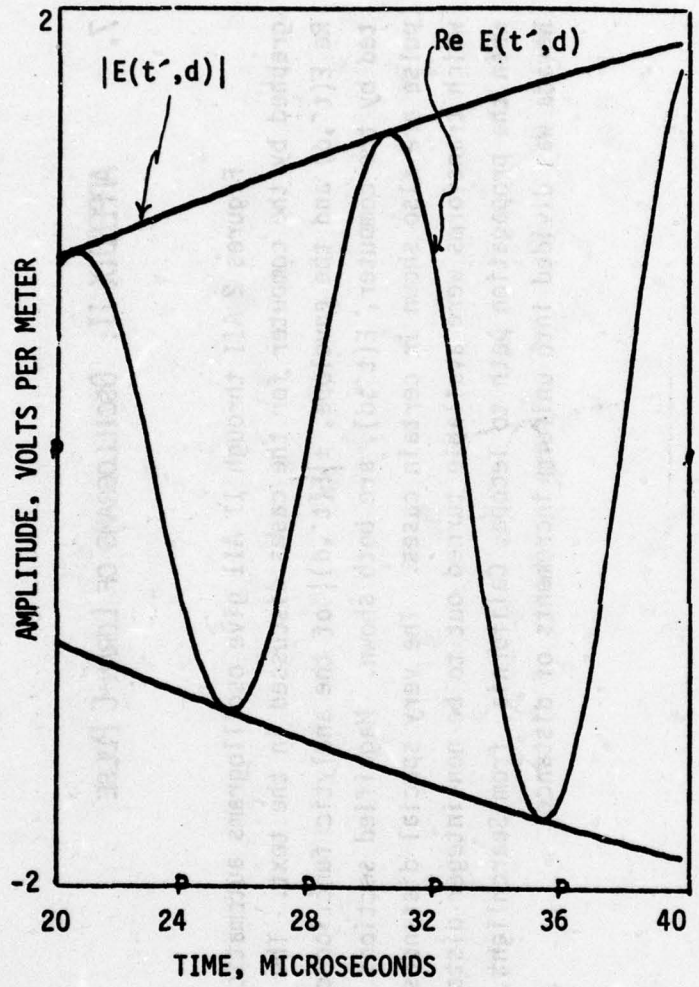

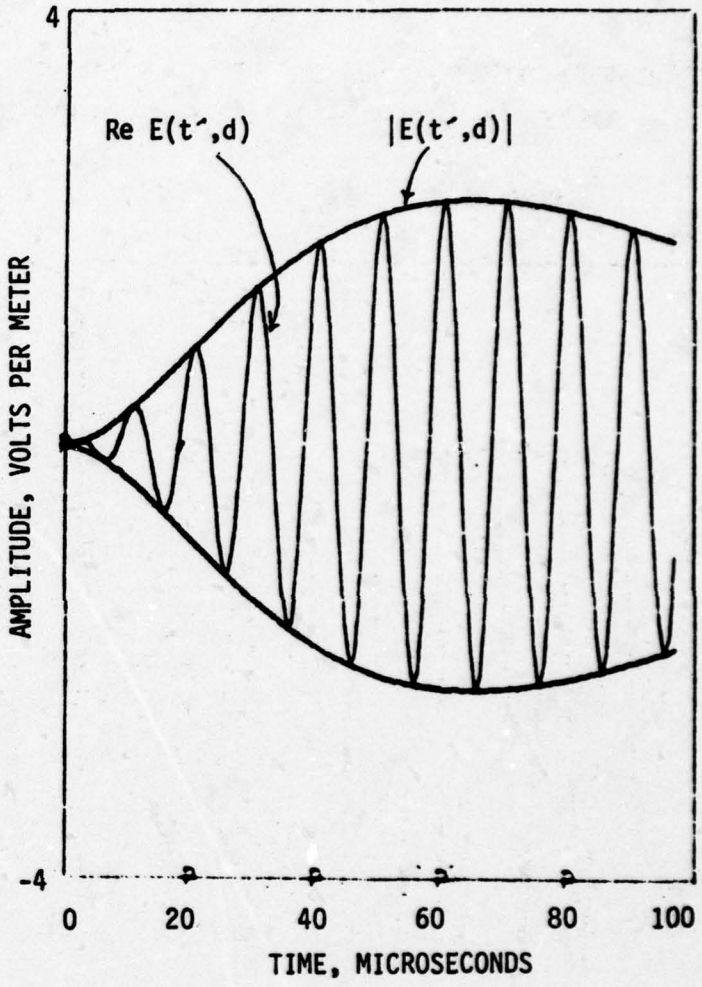

FIGURE 1 A II: THEORETICALLY PROPAGATED LORAN-C PULSE AT A DISTANCE OF 2.9921 KM FROM THE ANTENNA SOURCE CURRENT PULSE GIVEN IN FIGURE 2, ASSUMING THE GROUND TO BE SMOOTH, HOMOGENEOUS WITH AN IMPEDANCE, $|x| = .033$. A MAGNIFIED SECTION OF THE PULSE IS ALSO SHOWN.

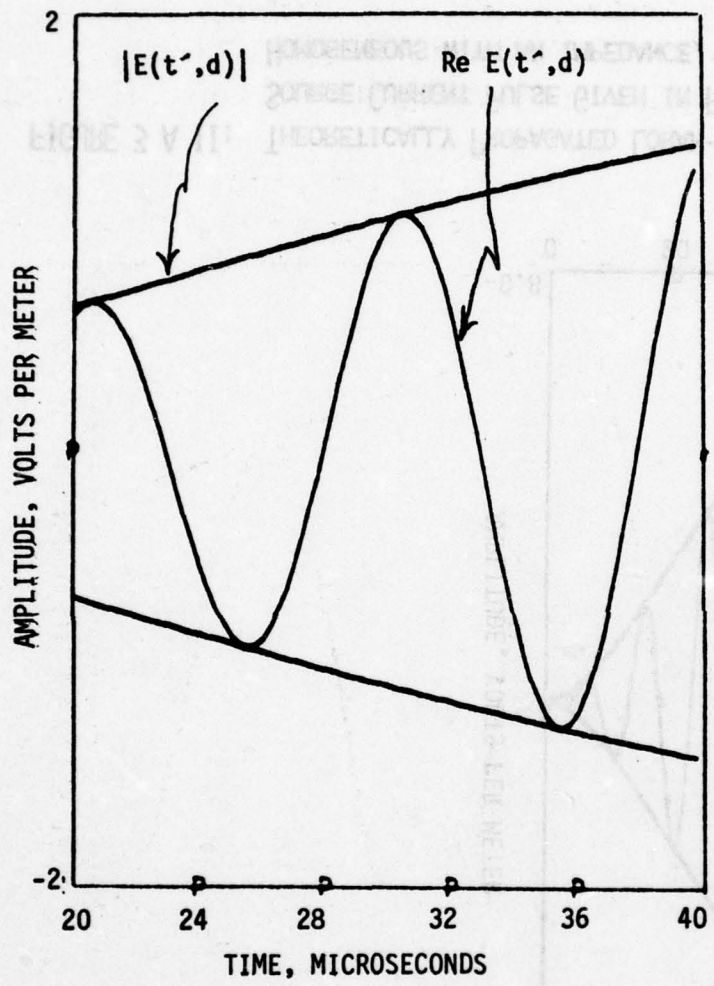

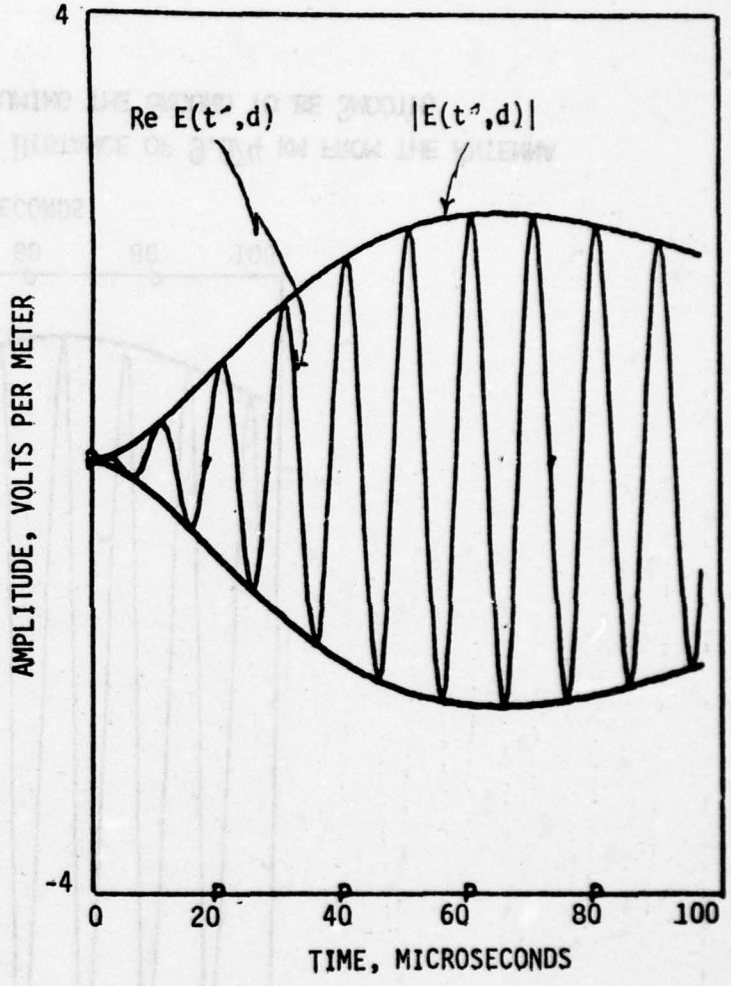

FIGURE 2 A II: THEORETICALLY PROPAGATED LORAN-C PULSE AT A DISTANCE OF 2,9921 KM FROM THE ANTENNA SOURCE CURRENT PULSE GIVEN IN FIGURE 2, IN THE PRESENCE OF THE IRREGULAR AND NONHOMOGENEOUS GROUND MODEL. A MAGNIFIED SECTION OF THE PULSE IS ALSO SHOWN.

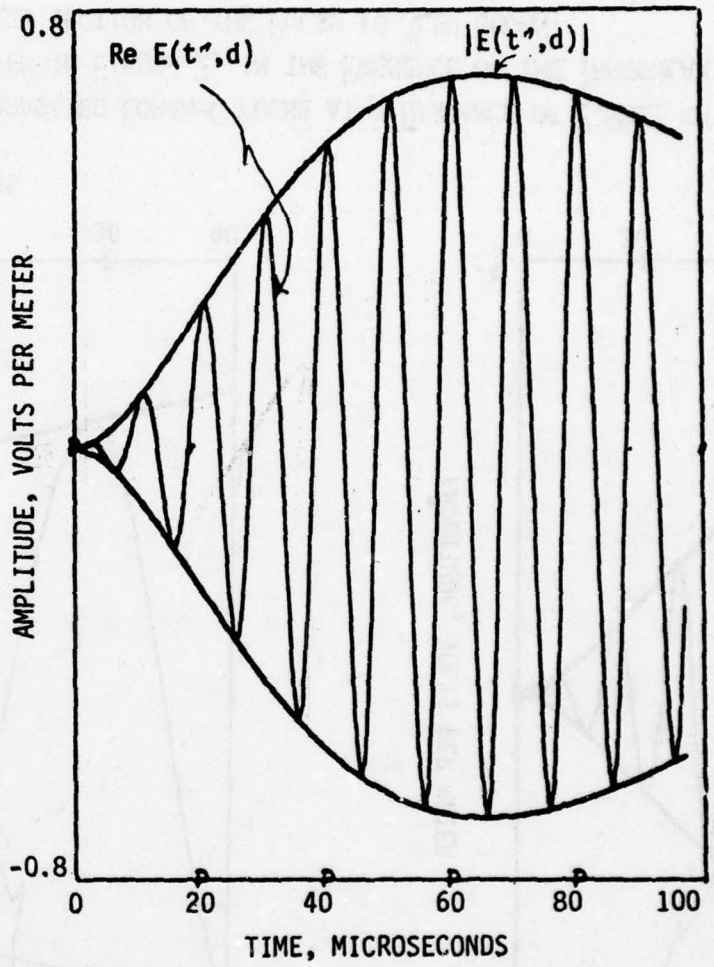

FIGURE 3 A II: THEORETICALLY PROPAGATED LORAN-C PULSE AT A DISTANCE OF 9.974 KM FROM THE ANTENNA SOURCE CURRENT PULSE GIVEN IN FIGURE 2, ASSUMING THE GROUND TO BE SMOOTH, HOMOGENEOUS WITH AN IMPEDANCE, |x| = .033.

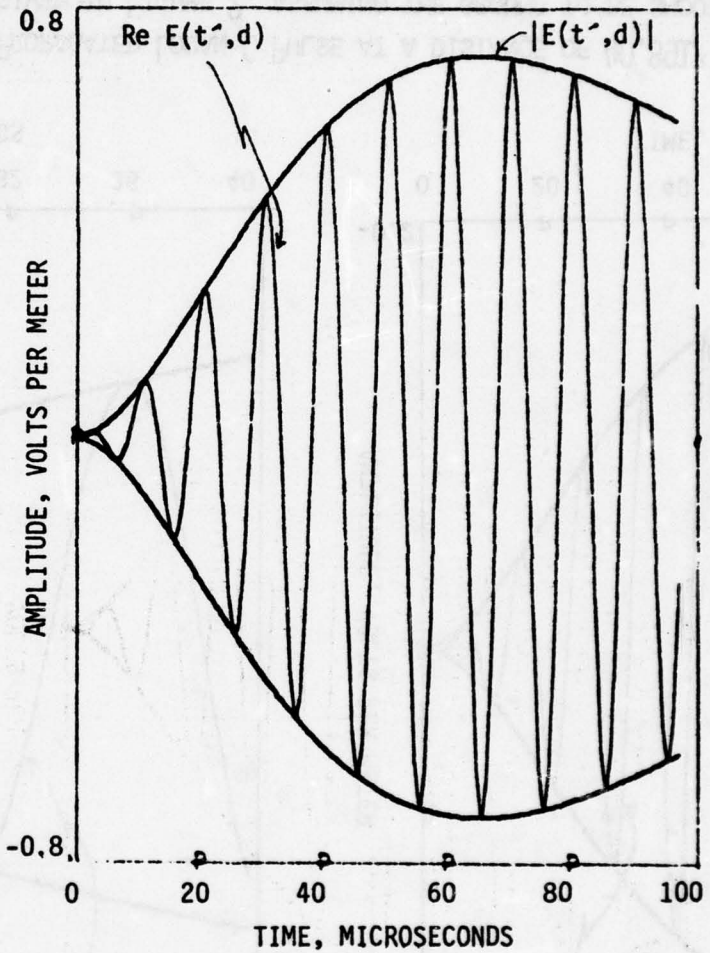

FIGURE 4 A II: THEORETICALLY PROPAGATED LORAN-C PULSE AT A DISTANCE OF 9,974 KM FROM THE ANTENNA SOURCE CURRENT GIVEN IN FIGURE 2, IN THE PRESENCE OF THE IRREGULAR AND NON-HOMOGENEOUS GROUND MODEL.

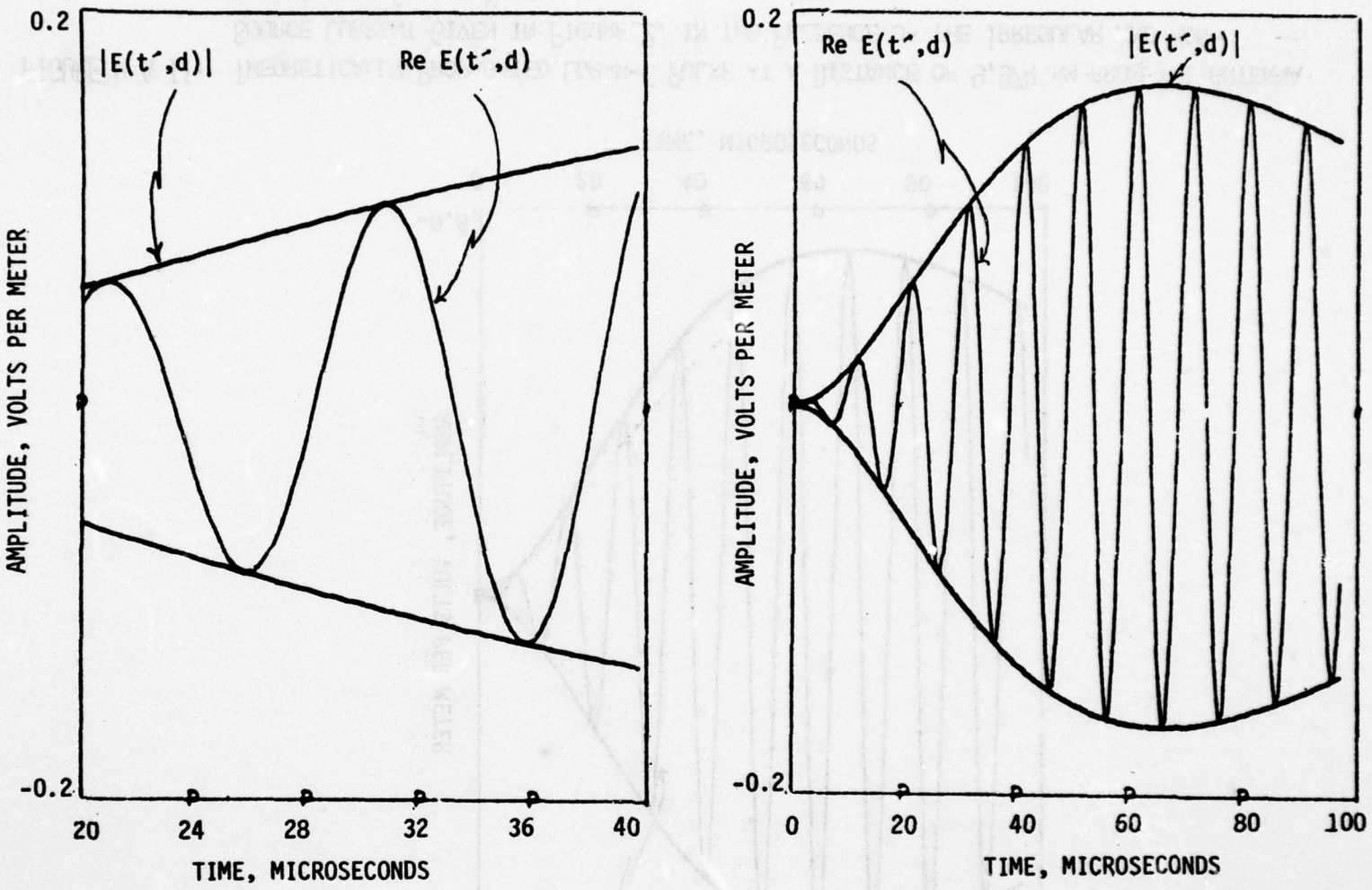

FIGURE 5 A II: THEORETICALLY PROPAGATED LORAN-C PULSE AT A DISTANCE OF 40.8917 KM FROM THE ANTENNA SOURCE CURRENT PULSE GIVEN IN FIGURE 2, ASSUMING THE GROUND TO BE SMOOTH, HOMOGENEOUS WITH AN IMPEDANCE, $|\chi| = .033$. A MAGNIFIED SECTION OF THE PULSE IS ALSO SHOWN.

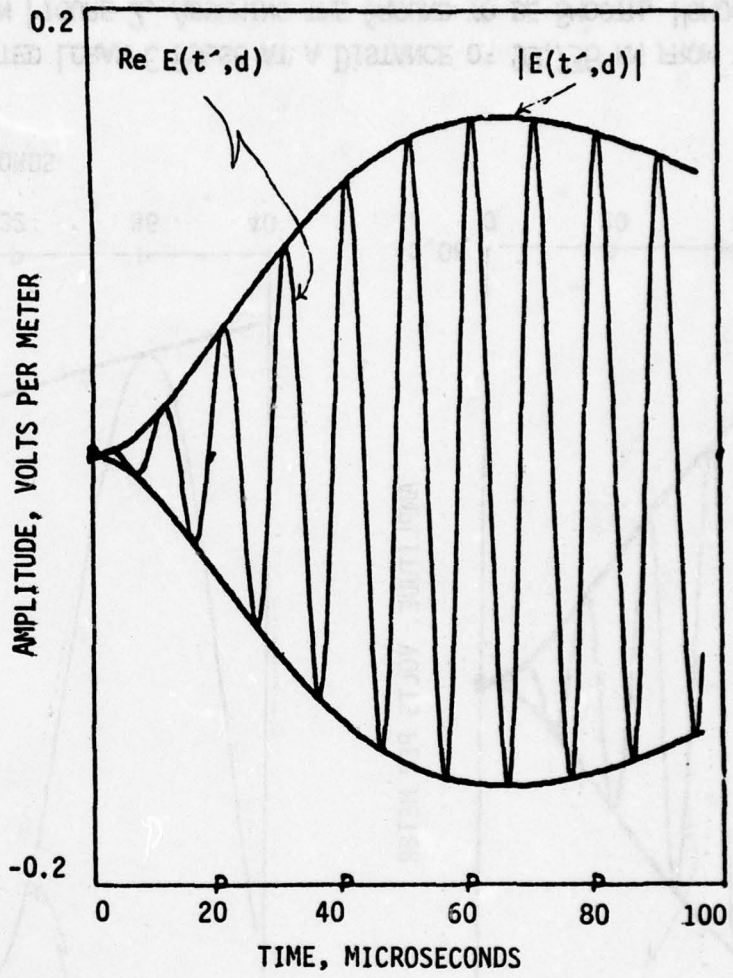

FIGURE 6 A II: THEORETICALLY PROPAGATED LORAN-C PULSE AT A DISTANCE OF 40.892 KM FROM THE ANTENNA SOURCE CURRENT PULSE GIVEN IN FIGURE 2, IN THE PRESENCE OF THE IRREGULAR AND NONHOMOGENEOUS GROUND MODEL.

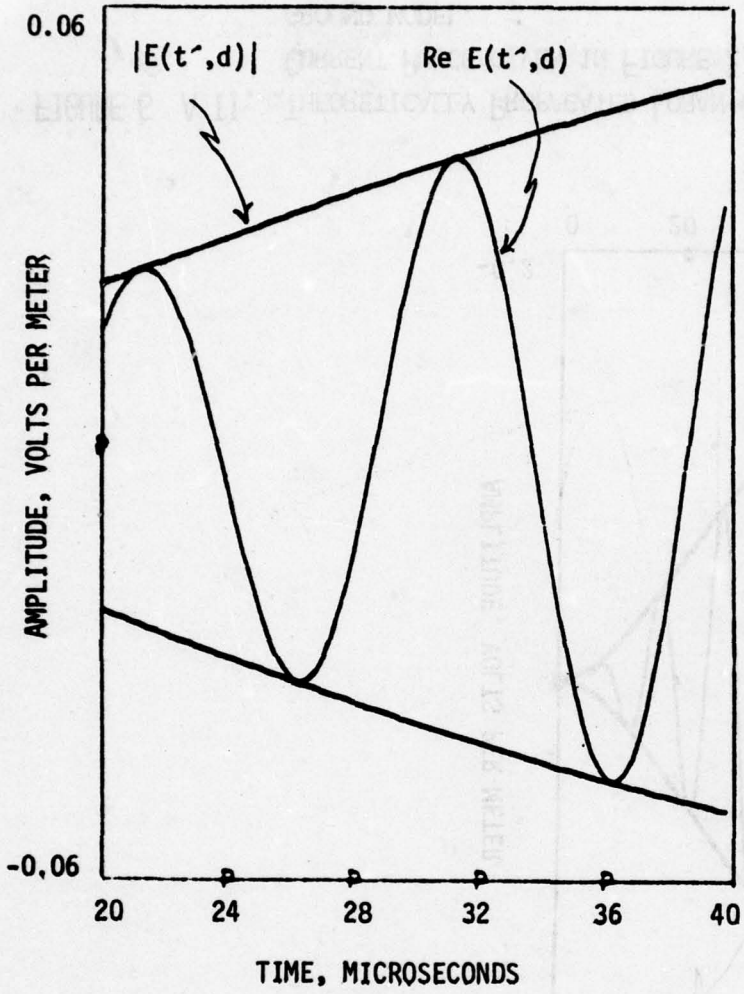

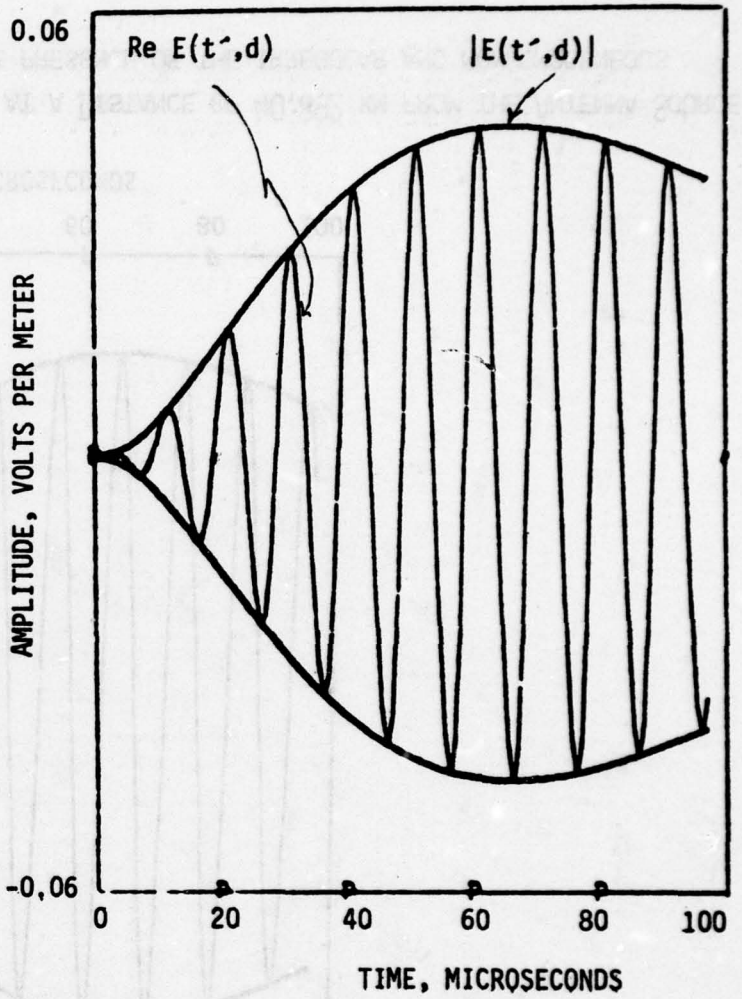

FIGURE 7 A II: THEORETICALLY PROPAGATED LORAN-C PULSE AT A DISTANCE OF 99.736 KM FROM THE ANTENNA SOURCE CURRENT PULSE GIVEN IN FIGURE 2, ASSUMING THE GROUND TO BE SMOOTH, HOMOGENEOUS WITH AN IMPEDANCE, |x| = .033. A MAGNIFIED SECTION OF THE PULSE IS ALSO SHOWN.

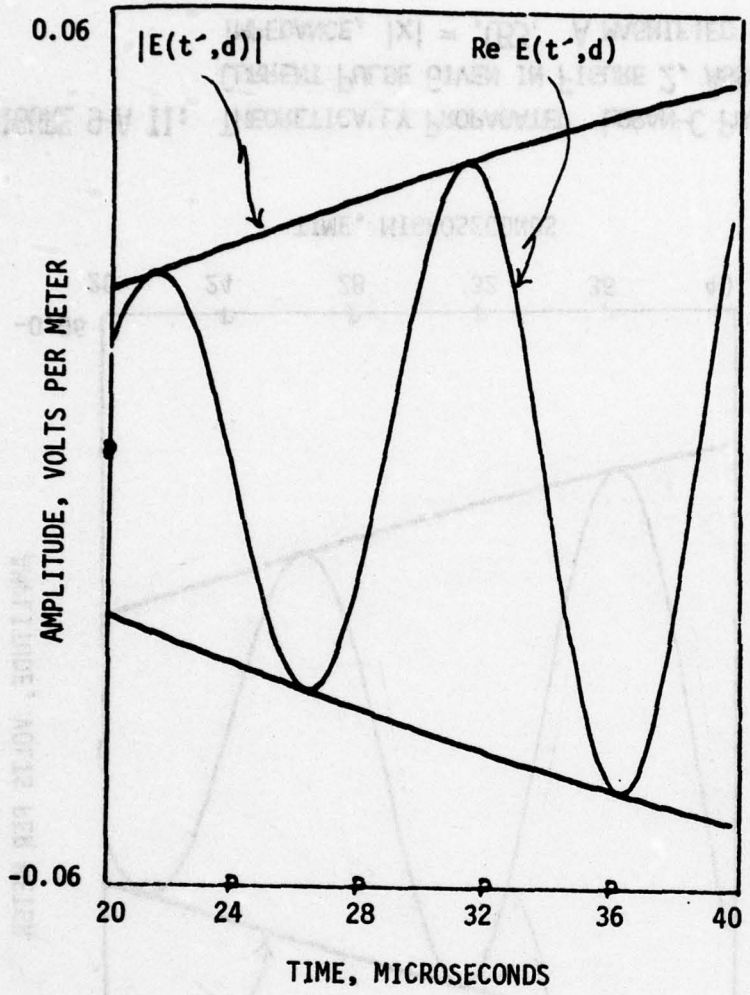

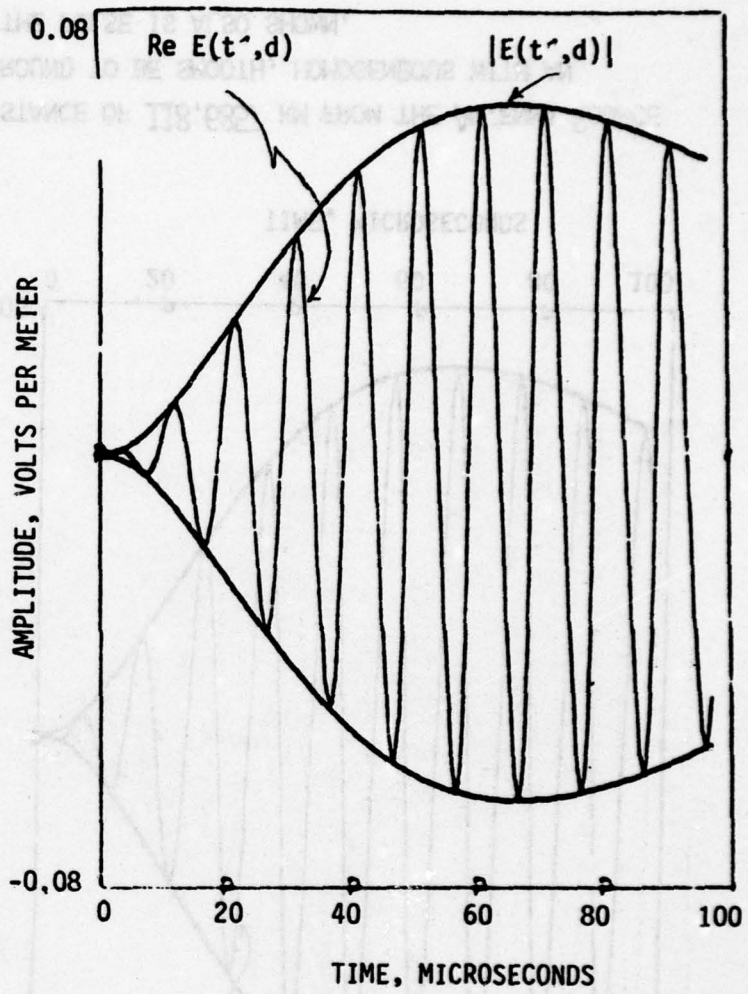

FIGURE 8 A II: THEORETICALLY PROPAGATED LORAN-C PULSE AT A DISTANCE OF 99.736 KM FROM THE ANTENNA SOURCE CURRENT PULSE GIVEN IN FIGURE 2, IN THE PRESENCE OF IRREGULAR AND NONHOMOGENEOUS GROUND MODEL. A MAGNIFIED SECTION OF THE PULSE IS ALSO SHOWN.

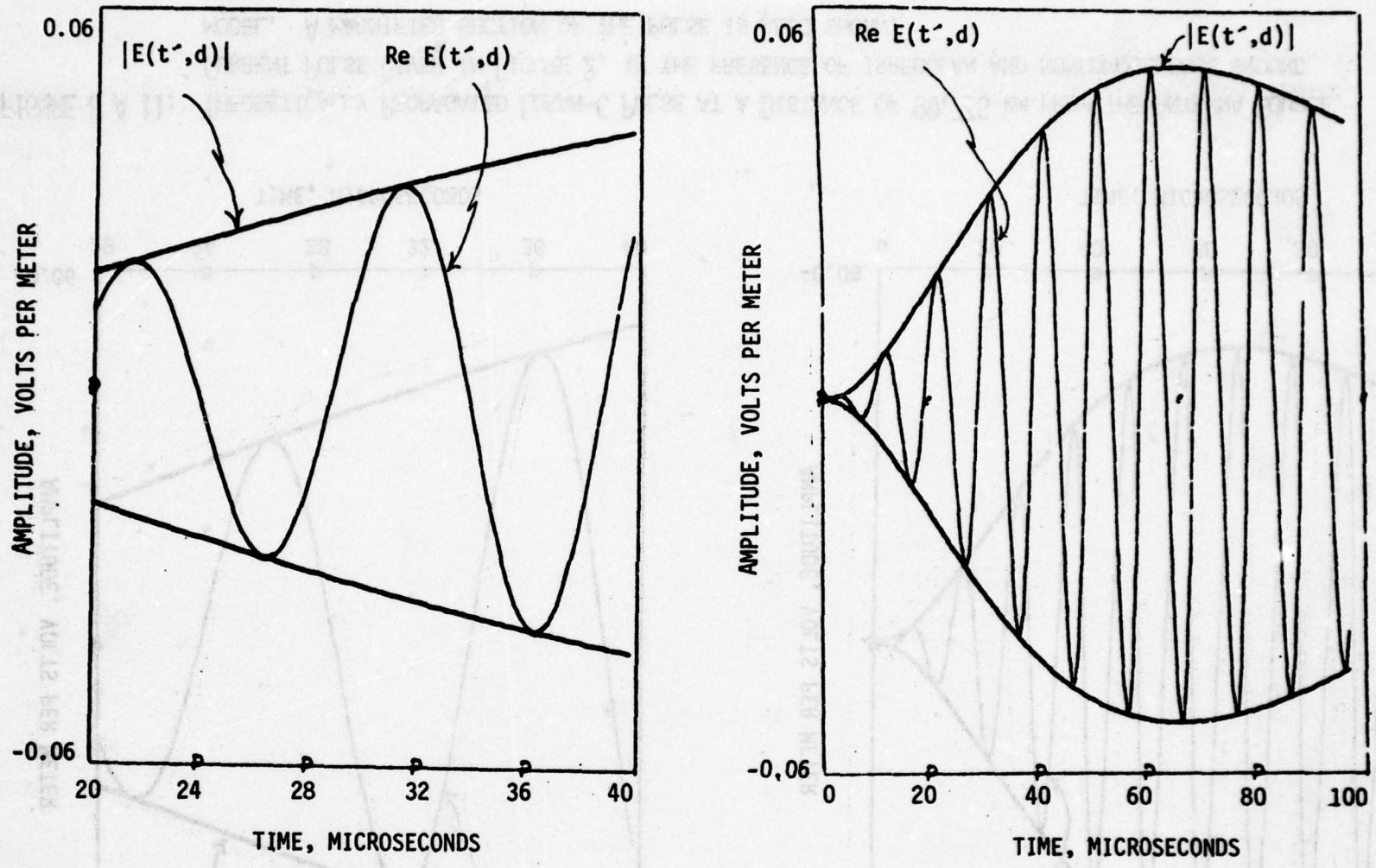

FIGURE 9 A II: THEORETICALLY PROPAGATED LORAN-C PULSE AT A DISTANCE OF 118.6857 KM FROM THE ANTENNA SOURCE CURRENT PULSE GIVEN IN FIGURE 2, ASSUMING THE GROUND TO BE SMOOTH, HOMOGENEOUS WITH AN IMPEDANCE, |x| = .033. A MAGNIFIED SECTION OF THE PULSE IS ALSO SHOWN.

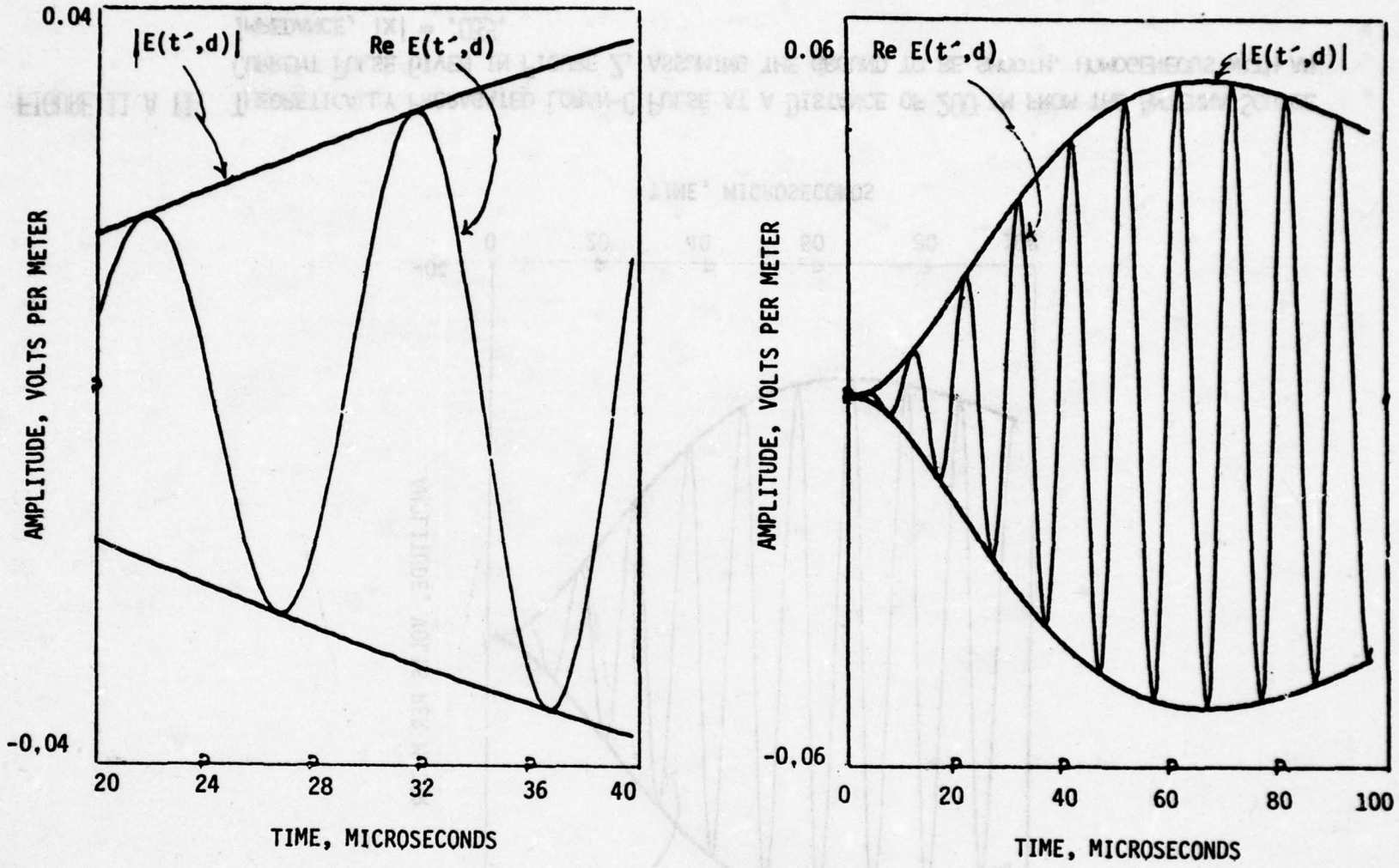

FIGURE 10 A II: THEORETICALLY PROPAGATED LORAN-C PULSE AT A DISTANCE OF 118.686 KM FROM THE ANTENNA SOURCE CURRENT PULSE GIVEN IN FIGURE 2, IN THE PRESENCE OF THE IRREGULAR AND NONHOMOGENEOUS GROUND MODEL. A MAGNIFIED SECTION OF THE PULSE IS ALSO SHOWN.

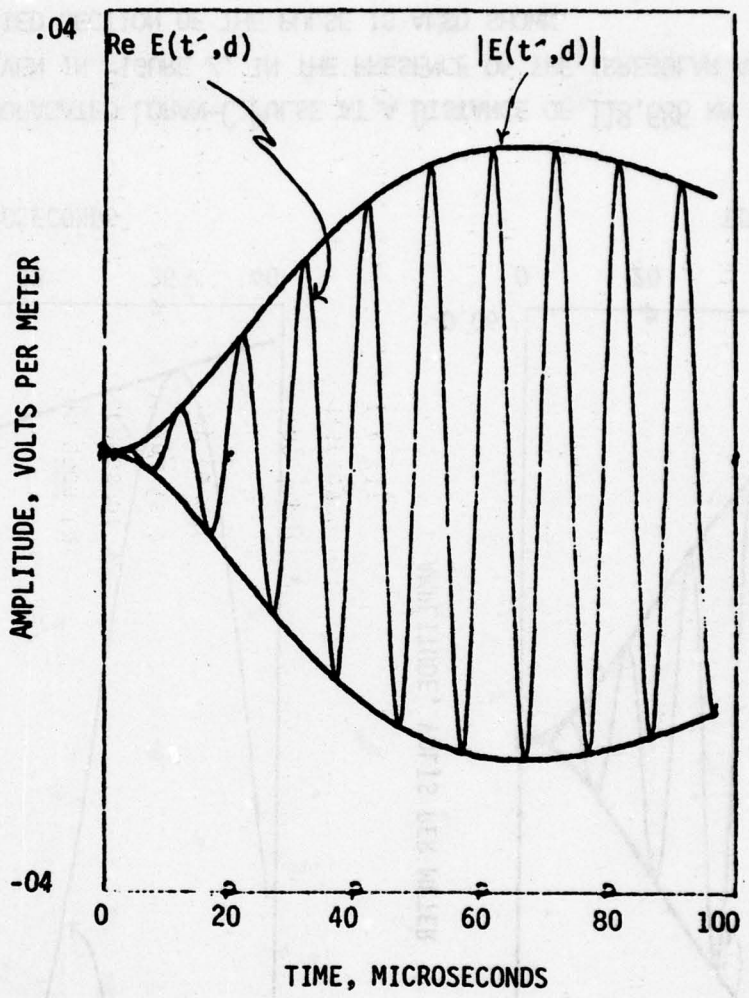

FIGURE 11 A II: THEORETICALLY PROPAGATED LORAN-C PULSE AT A DISTANCE OF 200 KM FROM THE ANTENNA SOURCE CURRENT PULSE GIVEN IN FIGURE 2, ASSUMING THE GROUND TO BE SMOOTH, HOMOGENEOUS WITH AN IMPEDANCE, $|x| = .033$.

8. APPENDIX III: TOPOGRAPHIC DATA BASE

A topographic data base has been introduced into the computation scheme for the continental United States. This data base is important because it enters into the estimates of ground impedance and is also used in the ground wave propagation simulator to establish the phase perturbations due to the irregular nature of the ground. The effects of terrain on wave propagation are obvious and well established in previously published works, References (8, 9, 17, 22). However, the effect upon ground impedance is more subtle, depending upon the nature of the soil overburden and its relationship to the steepness of the terrain. This has been briefly discussed in Reference (20) and is indeed a subject that must be explored in considerable depth for any particular region before an attempt at unique prediction is undertaken.

To illustrate the importance of geophysical data bases, several elevation profiles are displayed herein. A sample of the terrain data base is displayed in Figure 1 A III. The solid lines in the figure displays ground elevation as a function of distance along the geodesic between Searchlight, Nevada and Ft. Cronkhite, California. In this plot, ground elevation relative to sea level is given in meters while distance along the geodesic is given in kilometers and covers a total range of 200 kilometers. This plot extends just beyond Death Valley, California.

The following coordinates define the points under consideration:

Location	Latitude	Longitude	
Searchlight	35°19' 18.18" N	114°48' 17.43"W	(transmitter)
Tecopa	35°49' 4.975"N	116°11' 5.193"W	
Death Valley	36°03' 32.448"N	116°50' 19.467"W	
Ft. Cronkhite	37°50' 29.464"N	122°52' 41.170"W	

The elevation as a function of distance between Searchlight and Tecopa is shown as a short dashed line. Similarly, the elevation between Searchlight and the Death Valley reference point is shown by the dash-dot line. Although the Tecopa and Death Valley points are approximately on the geodetic between Searchlight and Ft. Cronkhite, they are not exactly

so because the terrain differs considerably between these curves. The transmitter datum and the sea level datum are also shown. It is of interest to note that the region of Death Valley is below sea level.

Figure 2 A III depicts elevation relative to sea level as a function of distance along a geodesic from the Master station at Fallon, Nevada 39°33' 06.62"N, 118°49" 56.37"W to Searchlight, Nevada and Tecopa and Death Valley, California. Since these paths are not along a similar geodesic considerable difference is apparent between them. In the Loran-C concept of using time difference measurements to determine location, the path to the Master station is equally as important as the path to the secondary station.

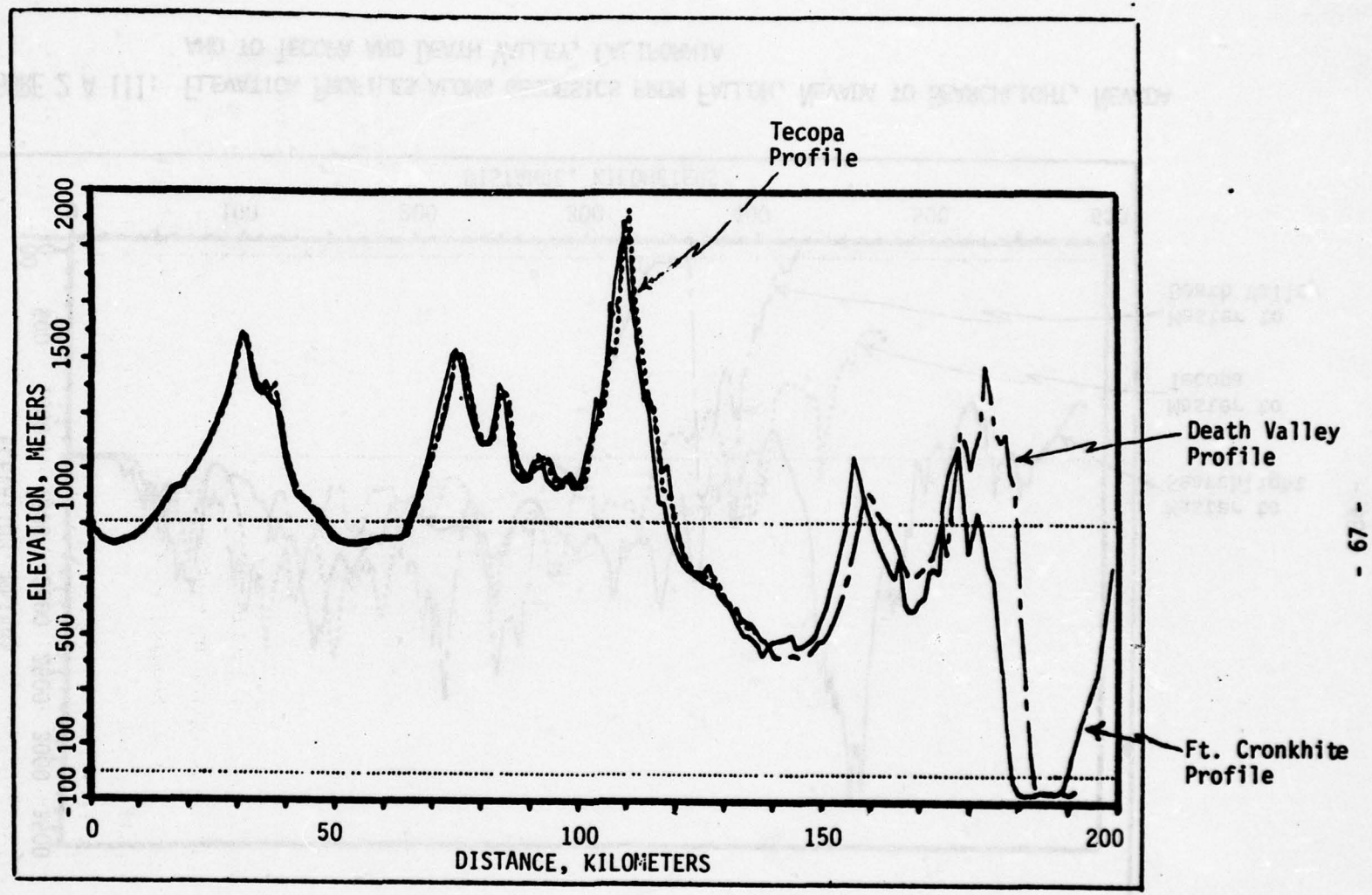

FIGURE 1 A III: ELEVATION PROFILES ALONG GEODESICS FROM SEARCHLIGHT, NEVADA TO TECOPA, DEATH VALLEY AND FT. CRONKHITE, CALIFORNIA.

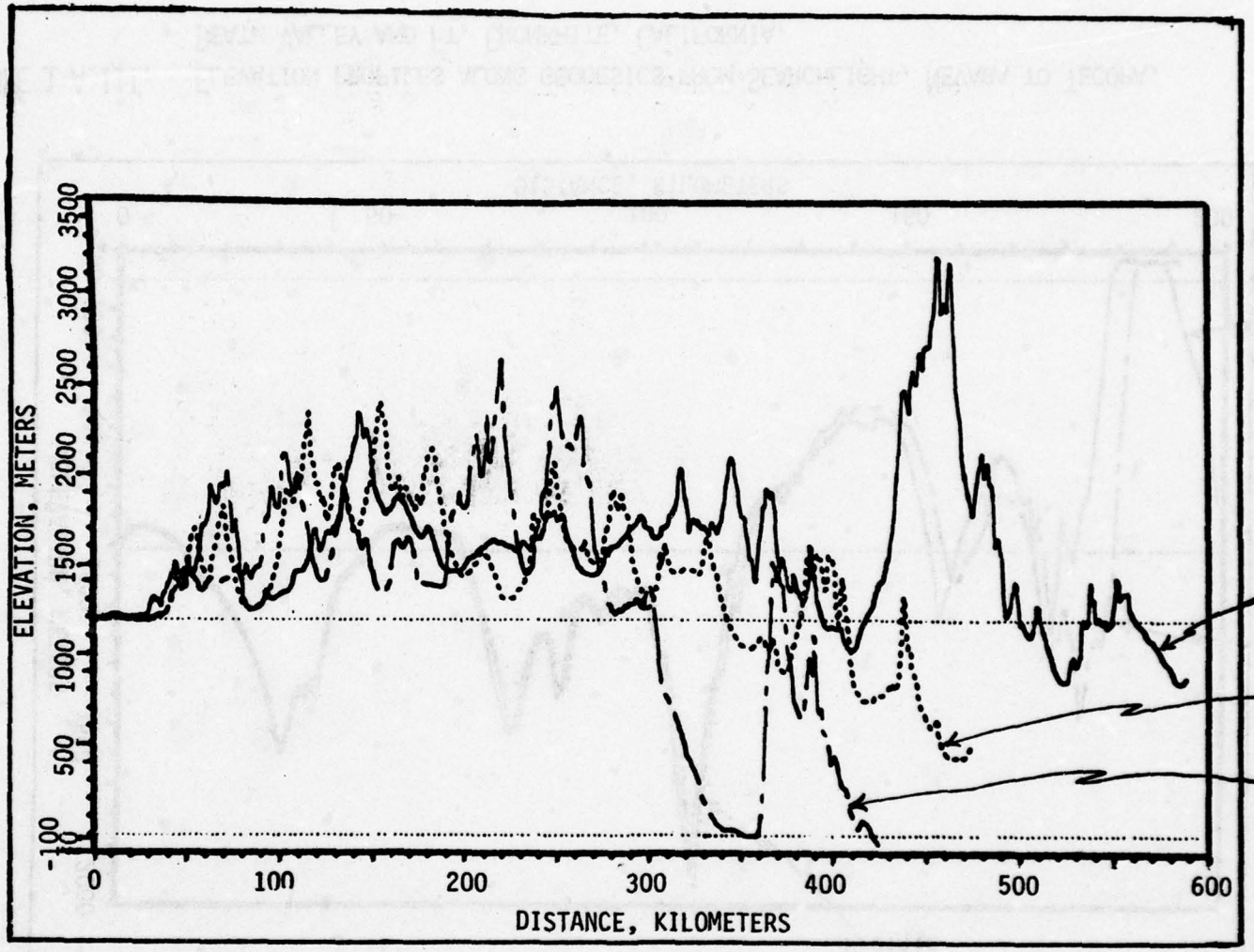

FIGURE 2 A III: ELEVATION PROFILES ALONG GEODESICS FROM FALLON, NEVADA TO SEARCHLIGHT, NEVADA AND TO TECOPA AND DEATH VALLEY, CALIFORNIA

CRPL

1898 SOUTH FLATIRON COURT
BOULDER, COLORADO 80301
P.O. BOX 1056
BOULDER, COLORADO 80306
TELEPHONE: 303/444-1530

COLORADO RESEARCH AND PREDICTION LABORATORY, INC.
SPECIALISTS IN ELECTROMAGNETICS AND COMPUTER SIMULATION

AN EXPERIMENTAL PROGRAM TO MEASURE ECD

AND

TEST THE TRANSIENT SOLUTION

WITH

ADDENDUM

CRPL$_I$ REPORT 78-10

APRIL 15, 1979

R. H. Doherty
A. R. Cook

Report on work sponsored by Department of Transportation, United States Coast Guard, Washington, D.C. 20590 under Contract No. DOT-CG-842923A, dated September 1, 1978

FOREWORD

This paper comprises Task 2: Report on the design of an experiment to test the transient solution for the U. S. Coast Guard, Contract No. DOT-CG-842923A. The intent of this report is to describe a measurement program and to provide a basis for use by the U. S. Coast Guard in establishment of definitive program goals. This experimental design utilizes work previously performed on Coast Guard Contract No. DOT-CG-74629-A to review Integral Equation Computer Program for Loran-C propagation and other work performed on this present contract, namely the evaluation of the Loran-C pulse dispersion for which a computer program simulation of the ground wave pulse has been configured.

TABLE OF CONTENTS

LIST OF FIGURES

ABSTRACT

The essential elements of this combined theoretical experimental program include the following items in the time sequence that would be followed:

(1) Model all baseline and transmitter to monitor paths for terrain and geophysical content of these paths;

(2) Predict with the propagation transient solution the ECDs and phase corrections that should be observed locally and remotely in the vicinity of each transmitter and specifically on the baseline extensions of each transmitter;

(3) Measure both the pulse envelope and the pulse cycle propagation time on the baseline extensions for both the local and all remote signals;

(4) Compare these spatially measured quantities with the predicted values and make adjustments in the modeled paths necessary to establish spatial fiducials for each path. Identify pulse envelope and cycle propagation times with the envelope to cycle difference or ECD and the secondary phase correction;

(5) Utilize this fiducial information as an origin for predicting changes due to temporal variations;

(6) Compare the predicted temporal variations with long period envelope and cycle propagation time measurements made at selected transmitter sites; and

(7) Evaluate the relationship between the temporal envelope propagation time variations and the temporal cycle propagation time.

An addendum to this report outlines a modest program using existing data that could be carried out to demonstrate the feasibility for embarking on the above outlined program. Although existing data is not capable of verifying the ECD portion of the program, the secondary phase correction verification effort is presumed to be the most fundamental aspect of this entire program.

AN EXPERIMENTAL PROGRAM TO MEASURE ECD

AND

TEST THE TRANSIENT SOLUTION

R. H. Doherty
A. R. Cook

I. SUMMARY OF EXPERIMENTAL PROGRAM

Baseline extension measurements (BLE) are an important component of the calibration procedure for Loran-C chains. Thus, such measurements are a chain management tool used both in the initial calibration of the chain and in the later maintenance of the chain calibration. These measurements are used as a criteria to establish transmitter emission delays necessary for reliable service area coverage. In many cases heretofore and, particularly, those cases in which the service area is emphasized as the prime Loran-C environment, calibration procedures are relatively simple and straightforward. In these cases, propagation path impedance estimates can be uniform, atmospheric refractive index effects can be minimal and smooth earth propagation theories are often applied with confidence. When the service area involves land masses or inhomogeneous propagation paths the problem is much more complicated. Thus, the loran signal is propagated over ground that exhibits an electrical impedance that varies with distance from the transmitter and indeed is subject to geology, hydrology, terrain, and other geophysical parameter variations of the earth surface. These applications require extreme care in the determination of the operational characteristics of a loran chain. This care can be ensured in the context of an appropriate theory of propagation of the groundwave to determine the adequacy of baseline extension measurements of phase and amplitude over the leading edge of the pulse. Thus,

both envelope and cycle propagation time (the secondary phase correction and the ECD) can be observed simultaneously and compared with theoretical predictions.

With establishment of Loran-C as a primary navigation system for general purpose usage, stringent chain calibration requirements will become increasingly important. To support the U.S. Coast Guard (USCG) mission to provide for Loran-C as a reliable general purpose radio navigation system, the following effort should be undertaken to provide theoretical context and validation for baseline extension and service area measurements in the presence of nonhomogeneous and irregular ground. Additionally, the problem should demonstrate the feasibility of extending the methods for the treatment of all service area data. The purpose of the program is to develop methods to ameliorate calibration accuracies and to minimize the necessity for data collection in the chain service area. The program tasks should establish precise relationships between baseline extension measurements and service area calibrations and produce criteria and guidelines that could be used for the collection of pertinent calibration data for both secondary phase corrections and ECD variations.

Accordingly, this experimental plan to measure secondary phase corrections and ECDs and to resolve Loran-C measurement inconsistencies between baseline extension and service area calibration methods is hereby submitted to the U.S. Coast Guard. The pertinent features of the program are the following items:

Item 1. Model all West Coast Loran-C chain baseline paths and paths from the transmitters to the area monitors. The modeling should include determination of elevations and geophysical parameters for all points along each path (e.g., see Reference 7 and Addendum to this report).

Item 2. Utilize propagation predictions and solutions to the transient analysis to predict envelope and cycle propagation time (secondary phase corrections and ECDs) for all of these paths. Even the transmitted ECD that would be measured close to the transmitting stations should be predicted from the fact that ECD is held constant at the monitor and something other than 0 ECD is necessary at the transmitter to yield this condition.

Item 3. Document and report to the U.S. Coast Guard all secondary phase correction and ECD predictions for all close in and remote transmitting stations for each transmitter and each area monitor on the West Coast Loran-C chain before measurements of ECD are made on the baseline extensions.

Item 4. Equip a mobile unit with suitably modified equipment appropriate to perform reliable master-secondary and secondary-secondary ECD measurements as well as secondary phase correction measurements on the baseline extensions of all of the transmitting stations.

Item 5. Conduct a measurement program to validate the theoretical development of Items 1 and 2 to verify the predictions produced by Item 2.

Item 6. Reevaluate the modeling of Item 1 and the predictions of Item 2 as a result of any differences between the predictions and the measurements. Modify the path model or the prediction algorithms until measurements and predictions agree within the limits dictated by possible temporal changes that might occur during the measurement period. Use the modified path models for fiducial input requirements for use in Item 7.

Item 7. Utilize the propagation programs described in Item 2 along with potential temporal parameter inputs to predict the possible effect of temporal variations in both envelope and cycle propagation time (ECD and secondary phase correction).

Item 8. Compare long-term measurements of both ECD and secondary phase changes made at selected transmitter sites with variations predicted in Item 7. Wherever possible actual weather changes should be used to compare predicted effects to measured variations in both ECD and secondary phase.

Item 9. Evaluate relationships between temporal changes in ECD and temporal change in secondary phase. Demonstrate these relationships from both the theoretical and the experimental

viewpoint. Thoroughly document how relationships of this nature can be used to improve the operational accuracy of the Loran-C system. Also indicate the necessary changes, if any, that would be required in the present chain operating procedure. This study should also demonstrate the area monitor function relative to temporal variations in both ECD and secondary phase. Also the effect of spatially distributed area monitors should be addressed from the temporal variations standpoint.

II. INTRODUCTION AND BACKGROUND

During the past year, Colorado Research and Prediction Laboratory, Inc. ($CRPL_i$) studied (under Contract DOT-CG-74629-A) Loran-C Signal Propagation Prediction Techniques. This effort resulted in the establishment of improved Loran-C pulse propagation error prediction techniques for nonhomogeneous irregular ground parameters using integral equation methodologies (hereafter referred to as a propagation simulator that uses a full wave transient solution for the propagation of a pulse of most any shape). In addition to this most recent accomplishment, $CRPL_i$ personnel have, in the past, provided various studies and reports concerning the Loran-C propagation prediction problems.

This experimental plan is concerned with utilizing technology unique in prediction capability to address the problem of the relationship between calibration and ECD measurements on the baseline extension versus the service area. In such a program, the effects of nonhomogeneous and irregular ground and the modeling of the radio wave propagation mechanism on a geophysical data base are of paramount importance. Recognizing that the Loran-C signal is a transient or pulse and not a CW or continuous wave signal, this study will evaluate the concept of "Calibration by Prediction" using the full pulse wave transient solution.

The experimental plan is oriented toward measurements from the West Coast Loran-C Chain (See Figure 1). This orientation is used because the existing U.S. Coast Guard transient analysis program under Contract DOT-CG-842923-A involves West Coast chain paths and recent analysis has suggested some anomalies in this chain (Reference 1). Also orienting the measurement program toward a specific chain and specific locations clarifies the experimental descriptions. Actually the experiment could be conducted utilizing any Loran-C chain and possibly the temporal variations would be better illustrated using transmitters in the East Coast or Great Lakes chains.

Relationships between ECD and the secondary phase corrections have

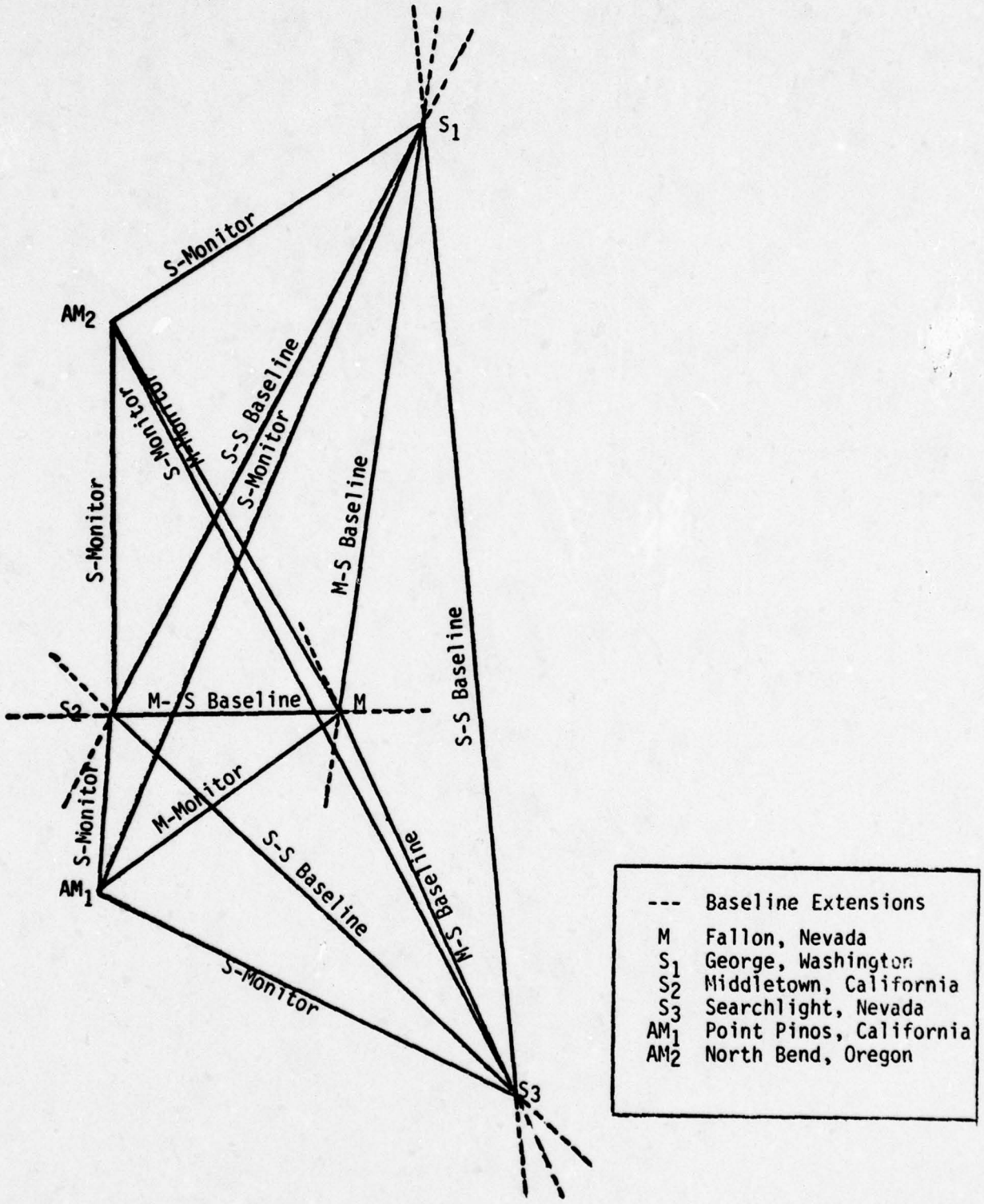

FIGURE 1-A OVERLAY SHOWING WEST COAST LORAN-C BASELINE PATHS AND TRANSMITTER TO MONITOR PATHS. (NOTE: BASELINE EXTENSIONS ARE DENOTED BY DASHED LINES.)

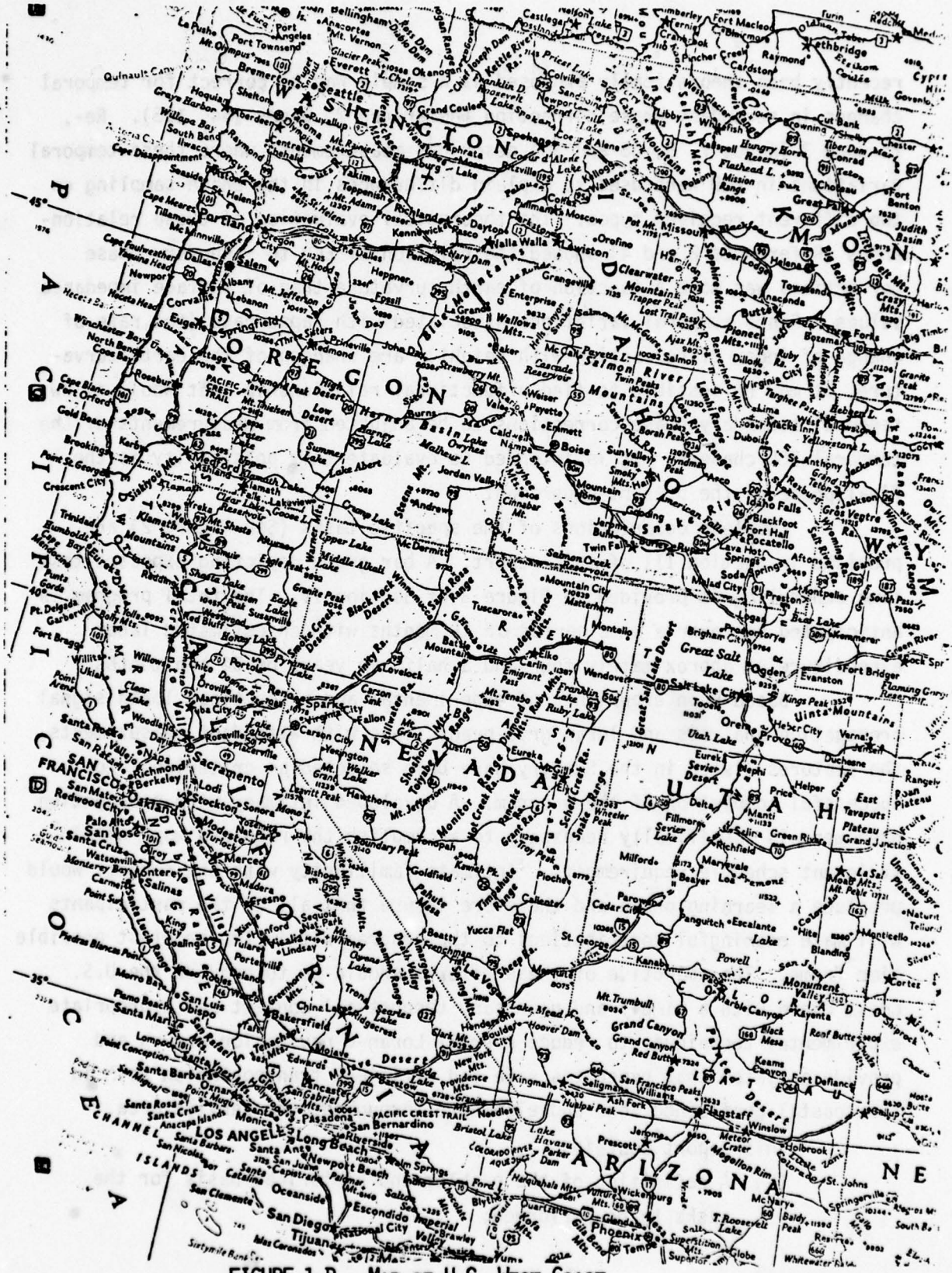

FIGURE 1-B MAP OF U.S. WEST COAST

recently been theoretically proposed as a simple way to correct for temporal changes in secondary phase correction (Reference 2, pages 154, 155). Reference 3 (pages 7, 8, 28 and 30) describes measurements where these temporal variations in ECD were used to explain differences in the phase sampling on two different receiver types. The theoretical evaluation of these relationships (References 2 and 4) showed the relation of ECD to secondary phase corrections was more a function of earth curvature than of surface impedance values. Since temporal variations associated with lapse rate (the rate of change of index of refraction with height) are changes of the earth curvature, it may be possible to find a functional relationship that would allow temporal secondary phase corrections to be adjusted from measurements of the temporal ECD changes. It is intended to evaluate this possibility as the final phase of the present experiment.

Complete descriptions of the specific tasks (See Figure 2) are provided in Section III of this report. A bar graph depicting expected task time scheduling is provided in Figure 3 of Section IV. The total program is anticipated to cover a time period of 18 months with an estimated labor expenditure of approximately four and a half man years or 54 man months.

Based upon experience of experimental and theoretical loran signal propagation analysis and loran grid predictions with attendant measurements, the features listed in the Summary have been selected as criterional to successful completion of the program. A developed intimacy with propagation phenomena is specifically necessary to accomplish the required work within stringent schedule requirements. Intimate familiarity with the subject would preclude a learning phase and therefore insure that all of the participants will make meaningful contributions to the program within the shortest possible time frame. The objective of these efforts should be to provide the U.S. Coast Guard with a timely and necessary theoretical context and appropriate experimental techniques to reduce overall Loran-C navigation errors and provide a system that expedites safe and efficient transportation both in the coastal confluence zone and elsewhere throughout the service area.

This report contains:

(1) A definition of the problem and historical basis for the tasks to be performed;

(2) The technical approach which should be used to relate ECD and secondary phase measurements with spatial and temporal propagation variations and to establish statistically viable criteria for elimination of measurement data while maintaining reliable accuracy;

(3) An outline of a method for correlating ECD and secondary phase measured on the baseline extensions with operational characteristics of the chain including service area measurements, (Note: the baseline extension is defined as a continuation of a geodesic connecting two transmitters and extending beyond the transmitter at either end of the geodesic. See dashed lines in Figure 1);

(4) A definitive work statement relating specific problems with task requirements, task performance, and personnel requirements; and

(5) A program management plan detailing the program structure work flow and personnel that should be committed to the program.

This program should be fully responsive to the needs of the U.S. Coast Guard during the conduct of the experiment by making available the range of Loran-C experience of the entire professional staff engaged in the theoretical and experimental program.

FIGURE 2 FLOW DIAGRAM OF ANTICIPATED EXPERIMENTAL PROGRAM

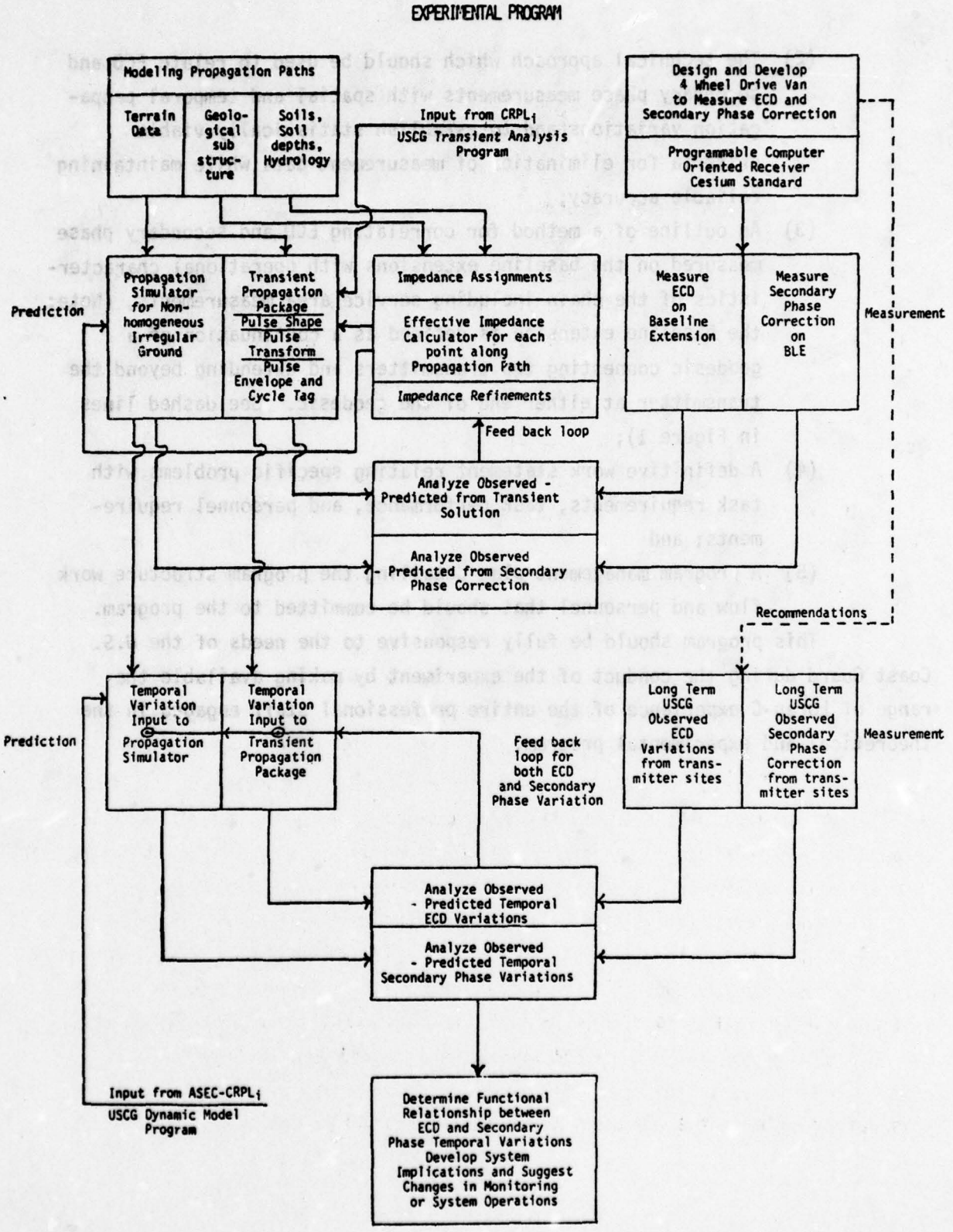

III. EXPERIMENTAL PROGRAM

All references to measurement of ECD or prediction of ECD in this program are interpreted to mean prediction or measurement of 24 points on the leading edge of the Loran-C pulse made using a programmable computer oriented receiver, e.g., Austrom-5000. These 24 points are the zero crossings of the first 6 cycles both positive and negative and the amplitude of the pulse half way between each pair of zero crossings. This will give measurements at four known points on each cycle of the pulse from 0 to 60 microseconds (μs) on the pulse. These measurements would be similar to measurements made by Fehlner, et. al. (Reference 5). R. L. Frank (Reference 6) discussed successive-cycle phase-distortion using these measurements and some preliminary predictions made by Johler, et. al. (Reference 2, Appendix II, Tables A2 to A6). His discussion and analysis is very closely related to ECD and secondary phase correction problems.

By measuring and predicting 24 points along the leading edge of the Loran-C pulse a complete dispersion comparison can be made. Receiver band width characteristics can be included in these predictions as described in Reference 14 (pages 12 and 13). Also from either the predictions or the measurements, ECDs as determined by various receiver manufacturers can be calculated. However, if ECDs were measured by any one technique utilized by a specific receiver manufacturer, it is not readily apparent that an ECD could be predicted for a different manufacturers technique.

Therefore, in this experimental program definition, ECD measurements and ECD predictions will imply measurements or prediction of the 24 specified points on the leading edge of the Loran-C pulse. The secondary phase predictions should relate to the CW solution of the propagation equations and the secondary phase correction measurement is the difference between the signal propagation at the speed of light in a standard atmosphere and the measurement made at the standard zero crossing of third cycle of the Loran-C pulse.

Figure 2 is a block diagram of the proposed experimental program. The various blocks in this block diagram are addressed in the following tasks of this section.

III.1 Task 1: Modeling the Paths

The principal prerequisite to successful conduct of the total program is an adequate modeling of appropriate propagation paths in the chain service area. For these experiments, propagation paths identified by the base lines are expected to provide the maximum amount of meaningful data for expected effort. These paths are depicted in Figure 1. Reference to the figure reveals a total of fourteen paths necessary to adequately describe the system and validate the theoretical transient solution. See Addendum to this report for more information for some of these paths.

To facilitate the efficient use of propagation simulators and in compliance with the concepts presented in CRPL$_i$'s Report 78-9 (Reference 7) entitled "Geophysical and Geological Data Base Evaluation for Loran-C Ground Wave Propagation Medium," propagation path descriptions will include terrain, geological substructure, and soil composition parameters including hydrology. These geophysical data parameters when convoluted with accepted electromagnetic ground wave propagation theory are herein denoted as the geoparametric propagation technique.

A. Terrain Data

In the case of terrain, the data necessary to provide adequate propagation path description requires a resolution to account for relatively gross irregularities of the earth's surface. Previous studies have demonstrated that the natural ground over which the Loran-C signal propagates tends to become inductive (References 8 and 9). Irregularities in the earth's surface and gross inhomogeneities beneath the surface often reflect inductive ground surface impedances along the propagation path. Experience demonstrates that extremely small detail is neither required technically or desirable from an economic viewpoint. In general, gross irregularities appear to be adequately described with a data resolution on the order of one kilometer

spacings (see References 7 and 15). In those special cases of extremely rugged terrain, a resolution of up to 200 meter spacing may be required.

Sources for terrain data are available from CRPL$_i$ computerized Continental United States terrain data base (see Addendum to this report). To presciently determine the necessary data resolution for a particular area requires experienced judgment of potential effects of terrain on the signal propagation. Based upon this experience, the CRPL$_i$ terrain data base appropriate for loran signal analysis has been assembled.

B. Geological Subsurface Structure Data

A second important characteristic of a Loran-C propagation path is contained in the geological subsurface structure. It has long been observed that broadcase frequencies exhibit attenuation rate changes with the geological underlayment that correlates with geologic age. Similarily, there is a strong correlation of Loran-C frequency attenuation rates and phase lags with the age of the geologic subsurface structure.

The purpose of this subtask is to identify and assemble a data base of geological subsurface parameters required to describe the underlayment along all propagation paths relevant to this program. In general, the data will be obtained from geological maps of the service area. To accomplish this work will require significant effort to sift through a vast amount of geological information to obtain a small amount of relevant data. The procedure will be one of development of an expertise that will require judgment and intuition. The learning process is ameliorated when performed in the context of previous and allied propagation data base assembly efforts. We at CRPL$_i$ have begun assembly of these type of bases.

The geological underlayment modeling for the propagation path will be a digitization of data points along the path at intervals comparable to other data. The data density and modeling technique at any point is dictated by expected effects of the area on the signal propagation. For example, areas that exhibit singular discontinuities in geological underlayment are expected to require special modeling techniques for resolution.

Here again, previous experience in similar anomonlies will provide criteria for judgments for initial conductivity assignment and later modeling adjustments. Although this subtask represents a considerable investment of effort, it is expected to provide enormous benefits toward high prediction goals for Loran-C.

C. Soil, Soil Depths, and Hydrology

The final major consideration for characterization of the Loran-C signal propagation path is the overburden or soil parameters. In general, soil tends to decorrelate with the age of bedrock in its formation. Soil thicknesses are quite variable over the surface of the earth and can vary from exposure of the basement rock to depths of several hundred meters.

An electromagnetic ground wave propagating over the earth's surface is influenced by the geoelectrical properties of the soil. Waves entering the ground are exponentially attenuated by the resistivity of the surrounding material. These electrical parameters can vary with the depth or thickness of the soil through which the wave penetrates. Accordingly, for reliable description of soil characteristics indigeneous to geographical areas along propagation paths it is necessary to configure area soil physiographies in layers characterized by appropriate geoelectrical parameters. A predominate consideration in the assignment of geoelectrical parameters to defined soil strata is the area hydrology. Water tables rise and fall, and the corresponding change in moisture content can cause the parameters to vary. These considerations impact the number of strata or geology horizons necessary to adequately describe a geographical region.

Soil data can be retrieved from soil maps and other soil literature available in geology libraries. Other sources may be available in certain government agencies, particularly those of the Department of Agriculture. Here again there is an enormous amount of literature to be sifted to obtain a small amount of relevant and required data. As before, experience in assembling these types of data bases is desirable to economically and efficiently perform this subtask.

The data will be digitized at discrete intervals along the path.

The spacing within the intervals should correspond to spacings of the other data bases. In our experience, soil descriptions can be "sketchy" in some geographical locations and, for example, the assessment of soil depth difficult to obtain. In this case, reliable path descriptions require specialized modeling techniques. Here again experience can play an important part in the successful completion of the total program.

III.2 Task 2: Spatial Propagation Prediction

A secondary phase correction prediction should be made for each of the 14 modeled paths using a propagation simulator for nonhomogeneous irregular ground paths. This geoparametric propagation technique should utilize the following imputs: establish terrain data, initial estimates of conductivity for soils, initial estimates of soil depths and hydrology, and initial estimates of conductivity of substructure of geological formations all convoluted to represent surface impedances along each path. The resulting secondary phase corrections should be used to derive time difference values at every location. The time difference values will of necessity relate to the fact that the time difference numbers at the area monitor are held at a particular value and are held constant. On-site comparisons between computed time difference numbers and measured time difference numbers at the various locations should provide a means for interpreting the validity of the measurement data. They should also determine if more measurements should be made, or if the measurements made at the time are adequate.

An ECD or dispersion prediction should also be made for each of the 14 propagation paths. This prediction should be made using techniques similar to those used in the U.S. Coast Guard transient model program (Reference 15). The actual predictions should yield each zero crossing and each half cycle amplitude for the first 6 cycles of the Loran-C pulse. The initial prediction for the area monitor should be made using the transmitter pulse of known ECD as measured at the transmitting station. (That is, that the third cycle axis crossing will occur at a precisely known point relative to the third cycle crossing derived from the transient solution

utilizing the standard mathematically specified pulse). Subsequently, a prediction should be made for the transmitters assuming the pulse received at the area monitor has the chain specified ECD value and that this pulse conforms to the standard mathematically specified pulse. As was pointed out by M. Dishal (Reference 10), the pulse that would be radiated by the transmitter could not precisely conform to the mathematically specified pulse. An analysis of the error terms discussed by Dishal convoluted with the degree to which a measured pulse, i.e., 4 points per cycle for the first 6 cycles, at both the transmitters and at the area monitors does not conform to the mathematically specified pulse will demonstrate the ability to make predictions and measurements agree. This comparison might influence the final operational recommendations that would result from this experimental program.

The transient model program is capable of predicting propagation for the mathematically defined pulse. It will also be capable of predicting a pulse that would yield the mathematically specified pulse after traversing a described propagation path. Pulse shapes other than the specified pulse could also be predicted using the transient model theory (see Reference 11, for example). However, this would require an additional research effort. Furthermore, predictions using the specified pulse should be utilized fully to determine if predictions of other pulse shapes are required.

The ECD spatial predictions should also be made over the transmitter baselines. In order to make these predictions the pulse used for the transmitter pulse should be the one derived from the prediction assuming the specified pulse and the ECD values assigned for the monitor. A comparison of these predictions for both ends of the baseline paths with measurements made at both ends of the baseline paths will enhance confidence of the prediction techniques, or demonstrate the limitations of the assumptions utilized to make the predictions.

Finally, all of the ECD and secondary phase correction predictions of the 24 points on the leading edge of the pulse should be analyzed to produce ECDs that would be obtained by the different receiver's measuring techniques. In this study, a careful evaluation should be made of the effect on the receivers due to pulses whose pulse shapes are not the mathematically specified pulse shape. If a particular receiver design

appears to be critically affected by the pulse shape, a recommendation may be made to add this receiver type to the measurement program outlined in the next section.

A plan to measure the ECD (that is the 24 points on the leading edge of the pulse) using a programmable computer oriented receiver such as the Austron-5000 should be devised for the Area Monitor. This measurement would be made on only one transmitter signal at a time, and it would be made on the transmitter being visited by the mobile van during the period the van is at that particular transmitter, if possible. It is anticipated that a plan might be worked out using some computer time on the resident Austron-5000. Otherwise, a second Austron-5000 should be provided, if one could be made available for these measurements, so that these measurements would not interfere with the area monitors normal operational program. These measurements would only need to be made a few times per day for one or two days for each transmitter over a total period of approximately three weeks while the mobile van was measuring on the various transmitter baseline extensions. However, if a reasonably simple automated sequential program for making these measurements could be devised, it would be desirable to make these measurements at the area monitors during the entire period when long-term U.S. Coast Guard observed ECD and secondary phase measurements are made at the transmitter locations (see Sections III.5 and III.6).

III.3 Task 3: Spatial Measurements and Required Equipment

This section of the experimental plan provides for the requirements of a mobile research van to make the necessary ECD and secondary phase measurements. Also addressed in this section is the design and implementation of the spatial measurement program.

A four-wheel drive vehicle is required to house the measurement equipment and thus permit access to baseline extensions not otherwise accessible to two-wheel drive vehicles. Principle equipment required for the mobile van includes:

(1) A programmable computer oriented Loran-C receiver programmed for this experiment;
(2) Hewlett Packard Cesium Standard Oscillator;
(3) Heavy duty Alternator;
(4) Extra battery capacity.

The alternator and other electrical power supply capability must be sufficient to operate the measurement equipment without interruption. Accordingly, extra battery capacity is required and facilities for recharging these batteries from commercial power sources is necessary. Also, the van should be equiped to convert from battery operation to commercial power operation with no expected loss or interruption to equipment operation. The equipment should be mounted in the van in a manner to facilitate easy removal and, also, configured in a way that permits storage and operation in the cargo space of a helicopter. Although specific helicopter applications are not spelled out in this experimental plan, previous experiences with mobile van type measurements have demonstrated the potential advantages that may occur if the equipment is so configured. In addition to the above described equipment, the van should have adequate test equipment to determine proper operation for the Loran-C measurements. This test equipment should be sufficient to diagnose problems and to repair most equipment malfunctions.

The design and development of this mobile research van should also include equipment modifications that might be necessary or desirable to best perform the spatial measurements. The functions of the programmable computer oriented receiver should be understood and documented to such a degree to which the measurements could be automotized. Perhaps this program would be better served by a receiver oriented programmable computer, since the computer capabilities and software development may well be crutial to the success of the overall experiment. The techniques for making the measurements along with the determination of the potential automation of the measurements should be well documented for use by the U.S. Coast Guard for making long-term temporal measurements at fixed transmitter sites with similar equipment. These temporal measurements would be needed for the latter parts of the over-all experimental plan.

The actual measurement program for the spatial effects should be thoroughly planned. Primarily this program should consist of making secondary phase and ECD measurements on the baseline extensions of each transmitter as shown by the dotted paths in Figure 1. Measurements of both the close and distant transmitter should be obtained at each location. For the West Coast chain there are actually twelve baseline extensions where these measurements should be made. Careful analysis of the area maps for the vicinity of the transmitting stations would allow the measurement program to be planned in advance. Several locations on each baseline extensions should

be chosen, where it appears possible, to drive a four-wheel drive vehicle. When the measurements are actually made, these would be the starting points for the measurement program. The number of sites that might be occupied on each baseline extension would depend upon insitu progress of the measurement program. A continuous evaluation of measured data during the data collection effort is essential. Also very thorough records are required during the measurement program so that suspect measurements could be repeated and so that all measured data is carefully documented as to location and time of measurement.

Making measurements only on the baseline extensions of the transmitter pairs somewhat minimizes the need for precise location of the measuring point, however the best source of local maps (7½ or 15 minute USGS topographical maps) should be used to locate the van as accurately as possible for each measurement point. All measured data should be preliminarily evaluated by making comparisons with predictions and by using small programmable calculator programs to check the data as it is being measured similar to the after the fact analysis described in Reference 1.

Any major difference between what is measured and what was predicted for a particular path should provide incentive to investigate that particular path or location more thoroughly. This type of flexibility and on-site evaluation in a measurement program can often determine the success of the experimental program. Frequently poorly obtained measurements lead to experimental programs that produce more questions than they are capable of answering.

III.4 Task 4: Spatial Verification and Modification

Following a comprehensive spatial variation measurement program, the initial predictions must be evaluated and prediction parameters should be modified where the predictions did not meet expected accuracy. Comparisons of the measured and the predicted results may be evaluated over the baseline paths where measurements at both ends of the paths allow a unique deduction of both the secondary phase and ECD variations over the path.

Parameters that can be used to correctly predict these baseline paths must also work to predict the paths from the transmitters to the area monitors.

The agreement between the spatial predictions and the spatial measurements can be no better than the stability of the spatial measurements during the measurement period. That is, in order to determine a fiducial value for the propagation over a particular path, the temporal variations that may have occurred during the measurement period must be ignored. Therefore, during the period the baseline extension measurements are being made, careful records should be maintained for all corrections introduced by the area monitors. Also, rather comprehensive weather records should be maintained for that period so that estimates of possible temporal variations can be made. The secondary phase correction and the ECD effects over a particular path should be nearly one order of magnitude greater for the spatial effects than for the temporal effects (Reference 12). Therefore, there should be no problem in deducing a fiducial value for each path that predicts the spatial variations and that can be used as the starting point for predicting temporal variations over that particular path.

The actual measured ECD data for each path should be analyzed using computer simulation techniques equivalent to those used by various receiver manufacturers. Equivalent ECDs for different receiver types will indicate how variable the different manufacturers equipment may be for actual pulse dispersion changes that may occur.

Once allowance has been made for the temporal variations, a comparison between the original propagation prediction defined in III.2 and the actual measured data defined in III.3 will allow one to evaluate how much the original estimates of the soil or geologic conductivities were in error. By simultaneously examining both the ECD and secondary phase correction errors for all 14 paths it should be possible to determine where the major errors were introduced.

After careful simultaneous study of both secondary phase errors and ECD errors for all 14 paths, judiciously chosen adjustments of the conductivity of certain soil types, certain geologic rock types or certain soil depths or hydrology should be made and repredictions of both secondary phase and ECDs for all paths should be made. This process should be

repeated until agreement between predicted and measured data approaches the limit allowed by temporal variations. During this analysis process, particular attention should be attributed to the sensitivity of ECD predictions to the various parameters under consideration.

The final selection of conductivity values for the various subsurface geoparameters will provide the fiducial information necessary as input information for propagation predictives of the temporal variations. Thus, the geoparametric variations will permit a fit to spatially distributed observations which determines the proper conductivity values. The primary benefit of this entire effort will be the validation of secondary phase corrections using the geoparametric parameters and integral equation solutions. The use of the transient solution which includes the integral equation allows a further evaluation of the ECD variations. If the ECD problem is not important, this study will still be very important for establishing the methods for predicting the secondary phase corrections.

III.5 Task 5: Temporal Propagation Predictions

Utilizing results from a dynamic model study, the temporal variations for the secondary phase changes can be evaluated for a selected path that could be monitored for temporal variations. This experimental plan does not include man hours or equipment for monitoring long-term temporal variations. Recommendations for the use of programmable computer oriented receivers such as Austron-5000 receivers at both ends of the path to be monitored for temporal variations would be made. It is anticipated that these measurements could be made over an existing baseline path and could be made by employing the special receivers at two existing transmitter sites. These measurements of the temporal secondary phase changes and ECD changes would be made in accordance with recommendations made as a result of the spatial measurement information and instrumentation design work gained in Section III.3.

The results from the dynamic model study should be used to predict temporal changes in the secondary phase as a function of estimated impedance changes due to weather effects, estimated changes in the surface refractive index and also estimated changes in the lapse rate of the refractive index (that is, change of refractive index with height above the surface). These

changes should be estimated based on the types of terrain the path traverses, i.e., desert conditions, typical farm land conditions, mountainous terrain and/or coastal peneplains.

The above predictions of secondary phase corrections should be extended to an ECD type prediction using a transient propagation solution such as that described in the final report of the transient model U.S. Coast Guard study (reference 15). Here again, predictions should be based upon anticipated changes in surface impedance, the surface refractive index, and the refractive index lapse rate.

All of these temporal variation predictions should be made for long period durations and for the paths where the temporal measurements are scheduled to be made. For these predictions anticipated weather variations for the particular chosen paths should be used for a prediction basis. Based upon the results of previous studies (Reference 13), particular emphasis on the lapse rate predictions should be made if any of the selected paths are subjected to below freezing temperatures for long periods of time.

All of the temporal predictions for the baseline paths over which the measurements would be made must take into account that the system is held constant at the area monitor and not at the transmitter sites. Therefore, the paths from the transmitters to the area monitors must be predicted and these predictions used to remove the effect of the area monitor control as seen over the baselines. The true variations over the baselines can be deduced from measurements made at both ends of the baseline paths. The effects occurring over the paths from the transmitter to the area monitor can be evaluated from the difference between the apparent baseline variations as seen from the measurements and the true baseline variations as deduced from a mathematical treatment of the measurements obtained at both ends of the propagation path.

The effect of the area monitor control process is extremely important to the interpretation of propagation measurements. This subject has been treated somewhat in References 2 and 3, but a thorough understanding of all of the ramifications of this effect is mandatory to make the present experiment successful.

III.6 Task 6: Temporal Validation and Modification

The objective here is to compare measured temporal variations with predictions of an estimated range of variations that might be anticipated.

Here again it is necessary to discuss the effect of an area monitor. It is necessary to see that the effect on the secondary phase and the effect on the ECD is somewhat different. The area monitor maintains a constant secondary phase correction at the area monitor. The value for this correction has been derived from a system calibration involving measurements on a number of points throughout the service area. The transmitted signals are adjusted to keep the area monitor time difference fixed. Therefore, temporal changes over the path from the Secondary transmitter to the area monitor minus the temporal changes over the path from the Master to the area monitor must be removed in order to determine the actual radiation time at the transmitting station. To a much lesser extent a similar condition exists for the ECD, since an assigned ECD number is held for each transmitter at the area monitor. Since ECD values may be held with larger tolerance levels than for the phase values, the ECD changes will be much less frequent. Also, ECD changes will occur separately for the Master or Secondary path, thereby allowing separation of the path changes.

It would be most desirable for a temporal analysis study to be able to isolate secondary phase adjustments and ECD adjustments that are propagation oriented from those that are operator or equipment oriented. Every effort would be made to design the measuring equipment in a manner that would help resolve this issue. This discourse is meant to point out the many ramifications that become important in order to try to interpret propagation measurements or data that supposedly will yeild propagation information.

From measurements made at both ends of a baseline path and the corrections introduced by the area monitor, it should be possible to determine both the ECD and secondary phase variations that occurred over the baseline path and over the paths from the transmitters to the area monitor. These variations should be compared with the predicted variations for each of the paths. The predicted temporal variations for changes in surface impedance and changes in surface refractive index have a different ECD to secondary phase relationship than the predicted variations due to lapse rate changes. Therefore, comparing the measured temporal variations with the predicted temporal variations for these paths should indicate whether the changes were due to surface parameter changes or were due to lapse rate changes.

A comprehensive analysis of all of the measured temporal variation data for all of the monitored paths should allow one to provide a maximum

error level estimated for the particular chain and for the existing operating procedures for that chain. This error model could be provided for all areas served by that particular chain. An error model map of this nature would provide a means for establishing maximum errors that could be expected at any given location in the coverage area due to temporal variations in the propagated signals.

The measured temporal variations for the leading edge of the pulse (commonly referred to as ECD measurements) should be subjected to computer analysis simulating various receiver techniques for deriving ECD from the pulse. If different receiver techniques give different ECD changes, these should be studied to determine if any particular receiver design is apt to have trouble sooner than other receiver designs.

III.7 Task 7: Derive the ECD to Secondary Phase Relationship for Temporal Variations

Utilizing the true variations in secondary phase and ECD that were deduced after removing the effect of the area monitor controlling the chain, an effective mathematical relation should be derived from secondary phase changes relative to ECD changes. This same relationship should be derived theoretically for surface impedances or surface refractive index changes and also for lapse rate changes. The theory suggests that a strong relationship should exist for lapse rate changes but that a less well-defined relationship should exist for surface parameter changes.

The above derived relationship should be used in a computer simulation program designed to allow various receivers to calculate ECD to demonstrate a possible method for receiver compensation for the temporal variation. During this analysis the different ECD derivation techniques should be evaluated independently relative to the potential for utilizing a relationship for deemphasizing temporal variations.

Also, from the observed temporal variations, the present operational techniques used in the Loran-C systems should be evaluated. Recommendations for changes in the present operating techniques may be forthcoming from this study. A complete computer analysis of the temporal variations and the use of spatially distributed area monitors should be a

part of the analysis program. The possible ramification on the overall Loran-C system that would result from holding the ECD constant at each transmitter rather than constant at the area monitor should be thoroughly discussed.

A final analysis of ECD's and secondary phase corrections for both spatially distributed and time distributed measuring locations should be delivered on this project. As a result of this analysis, definitive ratios of errors due to spatial and temporal changes should be defined for both ECD and secondary phase corrections. Recommendations on best methods for minimizing the effects of both of these error sources should be forthcoming from this study.

IV. ESTIMATED TASK TIME SCHEDULE ANALYSIS

Figure 3 depicts the program in terms of individual tasks and the expected effort in man months required to complete each task. The efforts within the tasks include both field experiments and theoretical development as defined in the task descriptions of Section III.

Task 1 is expected to require a significant literature search effort to acquire pertinent data for terrain, geological substructure, soil, and hydrology in appropriate geographical areas. Contributing to the effort expenditure are subtasks to place the data in an appropriate format to permit reliable modeling along the propagation paths. Accordingly, this task is foreseen to require the greatest expenditure of labor among all the tasks.

Task 2 is anticipated to need a mixture of computer programming expertise and novel theoretical development to convolute assembled data bases with developed pulse transient theory for well-founded ECD and secondary phase correction predictions.

Task 3 will require labor for van outfitting and modification and approximately a nine man week on-site effort. The dotted line represents expected U.S. Coast Guard long-term monitoring effort.

Task 4 represents an analysis effort to resolve discrepancies between theoretical and experimental efforts.

The purpose of the proposed efforts for Task 5 is to bring into concert the results from the preceding tasks and those resulting from the U.S. Coast Guard dynamic model study to provide temporal propagation prediction capability. To derive the necessary algorithms requires significant theoretical and computer discipline efforts.

Task 6 is expected to consume several man months of labor in field work and measurement acquisition. Also, a large effort is anticipated for algorithm modification to provide for adequate description of the service

FIGURE 3 EXPECTED TIME TASK SCHEDULE ANALYSIS

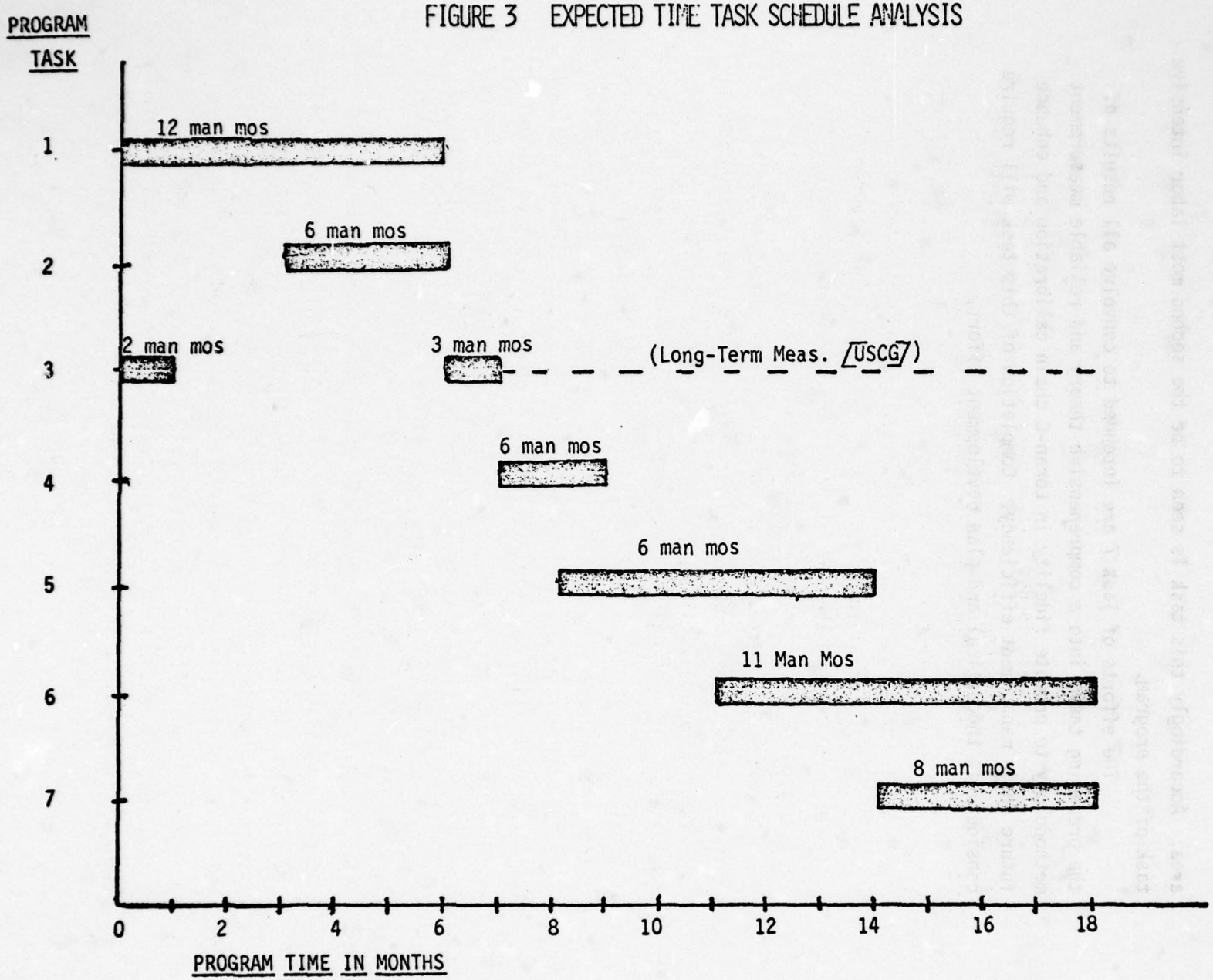

V. CONCLUSIONS AND RECOMMENDATIONS

This program is designed to determine the predictability of Loran-C as an electromagnetic ground wave propagating within geoparametric boundary conditions and under the influence of temporal variations. The experiment should relate the sensitivity of Loran-C spatial variations to surface impedances as derived from soil conductivity, soil depth and hydrology, and geological substructure conductivities. The program should demonstrate and validate the application of Pulse Transient Solutions in loran analyses.

Pursuant to the terms of this contract and in accordance with the attendant statement of work, this report defines an experiment and appropriate ECD measurements to test the pulse transient solution. A transient solution cannot be tested unless the pulse and pulse characteristics are considered. In this experiment, however, the varification of predicted secondary phase corrections are felt to be more significant than the ECD predictions and measurements. An Addendum to this report outlines a modest program using existing data that would emphasize the verification of predicted secondary phase corrections. This preliminary program would lay the foundation for the major program described in this report. Additionally, this preliminary program will serve to aid the Coast Guard in definitivizing goals for the overall program.

This program is intended to resolve questions regarding the extent of geophysical data bases required for high accuracy wave propagation characterization. For example, if the loran signal is relatively insensitive to geophysical conductivities, the prediction problem is ameliorated by rather gross estimates of individual conductivities. In the other extreme, if the loran is very sensitive to small changes in conductivities, prediction problems are increased by requirements to construct adequate geoparametric data bases. In the latter case, several advantages

can be listed that tend to offset the effort required to assemble geophysical data bases. Firstly, the expenditure of effort for data collection is expected to be highest initially and decrease dramatically as the number of geographical areas that are characterized increase. This expectation is based upon the technique's universality wherein geologic underlayment characteristics can be extrapolated to other geographical areas of the earth surface. Secondly, in the event of high correlation between loran signal propagation and geoparametric variation, potentials emerge for other uses of the loran signal. For example, the loran becomes a potential tool for use in geophysical prospecting ventures while still providing high accuracy navigation/positioning capability. Accordingly, difficulty in solving the prediction problem could easily be offset by interest and funding from the geophysical prospecting community. However, an initial investigation of the type outlined in this report is necessary to establish the fundamental question of sensitivity.

This experimental plan should develop suggestions for improved monitoring techniques to be used in Loran-C chain operations. It is anticipated that an assessment of methodologies for reduction of errors due to temporal variations should be forthcomin from this experimental plan. These methodologies should include suggesti s for transfer of technology necessary to incorporate improvements into Loran-C receivers. Evaluation of the possibility of incorporating these improvements into low cost receivers should be discussed.

As a result of the equipment design and measurement portion of this experimental plan, recommendations should be made for equipment modification necessary for purposes of precise monitoring of Loran-C signals anywhere within the service area. Recommendations for automating these precise monitoring functions should also be available.

Finally, a definitive expression of the magnitude of the spatial variations of both the secondary correction and the ECD relative to the temporal variations of these quantities for all possible Loran-C chain conditions should be available from this study.

To provide for timeliness and contunity within the program, periodic letter reports should be provided which delineate program progress and define expected program activity for ensuing time periods. Definitive program reports should be provided on a quarterly basis and the final re-

port should provide proposed methods for enhancing calibration techniques through secondary phase and ECD measurements with considerations of both spatial and temporal variations. The final report should also include the evaluation outlined in Item 9 of the Summary. In addition to this, specific program reports should be provided to the Coast Guard with the predictions outlined in Item 3 above and with the results of the comparison between the predicted and measured ECD and secondary phase on all of the baseline extensions as outlined in Item 6.

VI REFERENCES

(1) Doherty, R. H. and J. R. Johler (1978), Interpretation of West Coast Loran-C spatial errors using programmable calculator analysis techniques, Proceedings of Seventh Annual Technical Symposium, The Wild Goose Association, 4 Townsend Road, Acton, Mass. 01720.

(2) Johler, J. R., R. H. Doherty, and L. B. Burch (1976), Nanosecond precision for Loran-C, OT Technical Memorandum 76-216 (Office of Telecommunications, Institute for Telecommunication Sciences, Boulder, Colorado 80302).

(3) Doherty, R. H. and J. R. Johler (1976), Analysis of ground wave temporal variations in the Loran-C radio navigation system, OT Technical Memorandum 76-222 (Office of Telecommunications, Institute for Telecommunication Sciences, Boulder, Colorado 80302).

(4) Johler, J. R. and S. Horowitz (1974), Propagation of a loran pulse over irregular, inhomogeneous ground, AGARD Conference Proceedings No. 144, 28-1 to 28-13 (North Atlantic Treaty Organization, Advisory Group for Aerospace Research and Development, Paper available from CRPLj, PO Box 1056, Boulder, Colo. 80306).

(5) Fehlner, L. F., et.al. (1976, 1977), Experimental research on the propagation of Loran-C signals, Vol. A Summary report, Vol. B Test operations, Vol. C Measurement systems, Vol. D Data and analysis, JHU/APL TG 1298A, B, C, D. (The Johns Hopkins University, Applied Physics Laboratory, Johns Hopkins Road, Laurel, Maryland 20810).

(6) Frank, R. L. (1977), Successive-cycle phase-distortion effect on Loran-C/D accuracy, Proceedings of the Sixth Annual Convention of the Wild Goose Association (The Wild Goose Association, 4 Townsend Road, Acton, Mass. 01720).

(7) Johler, J. R. (1978), Geophysical and geological data base evaluation for Loran-C ground wave propagation medium, CRPLj Report 78-9, USCG Contract DOT-CG-842923A, (Colorado Research and Prediction Laboratory, Inc., 1898 South Flatiron Court, Boulder, Colo. 80301).

(8) Johler, J. R. (1969), Loran-C/D phase corrections over irregular, inhomogeneous terrain --- Simplified computer methods, ESSA Tech. Report ERL 116-ITS 63 (Suptd of Doc., U.S. Gov. Print. Off., Washington, D.C. 20402).

(9) Johler, J. R. (1971), Loran radio navigation over irregular, inhomogeneous ground with effective ground impedence maps, Telecommunications Research and Engineering Report 22 (U.S. Dept. of Commerce, OT/ITS, 325 Broadway, Boulder, Colo. 80302).

(10) Dishal, M. (1978), Exact drive requirements for Loran-C transmitters, Proceedings of the Seventh Annual Convention of the Wild Goose Association (to be published).

(11) Johler, J.R., and J. C. Morgenstern, (1965), Propagation of the ground wave electromagnetic signal with particular reference to a pulse of nuclear origin, Proc. IEEE 53, No. 12, December.

(12) Doherty, R. H., (1974), Spatial and temporal electrical properties derived from LF pulse ground wave propagation measurements, AGARD Conference Proceedings, No. 144, 30-1 to 30-17 (North Atlantic Treaty Organization, Advisory Group for Aerospace Research and Development, Paper available from CRPLj, P.O. Box 1056, Boulder, Colo. 80306).

(13) Doherty, R. H. and J. R. Johler, (1975), Meteorological influences of Loran-C ground wave propagations, JATP Vol. 37, pp. 1117-1124.

(14) Johler, J. R. and S. Horowitz (1973), Propagation of Loran-C ground and ionospheric wave pulses, OT Report 73-20 (Superintendent of Documents, U.S. Government Printing Office, Washington, D.C. 20402).

(15) Johler, J. R. (1979), Loran-C ground wave secondary phase corrections over nonhomogeneous and irregular ground using transient signal propagation techniques, CRPLj Report 78-12, U.S.C.G. Contract DOT-CG-842923A (Colorado Research and Prediction Laboratory, Inc., 1898 So. Flatiron Court, Boulder, Colo. 80301).

7. ADDENDUM

INTERPRETATION AND PROJECTED ANALYSIS OF EXISTING DATA APPLIED TO BASELINE PROPAGATION PATHS

ADDENDUM TO $CRPL_I$ REPORT 78-10

ADDENDUM TABLE OF CONTENTS

ADDENDUM LIST OF FIGURES

ADDENDUM LIST OF FIGURES CONTINUED

ADDENDUM LIST OF FIGURES CONTINUED

ADDENDUM LIST OF FIGURES CONTINUED

ADDENDUM LIST OF TABLES

INTERPRETATION AND PROJECTED ANALYSIS OF EXISTING DATA APPLIED TO BASELINE PROPAGATION PATHS

ADDENDUM TO CRPL$_i$ REPORT 78-10

This addendum describes further analysis and interpretations similar to those described in References 1, 2 and 3. Interperetations of the G.E. Tempo's worst case path data and stability experiment results beyond the preliminary analysis mentioned in Reference 1 have been delayed until the precise location of the monitored points could be obtained. Table 1 lists the latitude and longitude of these points and the distances to the M, X and Y transmitters. As mentioned in Reference 1 and demonstrated in the analysis of Reference 2, the observed data would have been greatly enhanced if a TD_W reading had been obtained at every location visited. Since such data is not available the present discussions relate only to TD_x and TD_y readings in addition to the TOA_y observations.

Table 2 gives the mean values of the Y secondary phase corrections given by G.E. Tempo, (Reference 4). In addition, M and X secondary phase corrections have been derived from the mean TD_y and TD_x measurements also given in Reference 4. All of the values listed in Table 2 under the G.E. heading are dependent upon the arbitrary fixing of the Tecopa TOA reading to give a secondary phase correction of 1224 nanoseconds. All of the values listed in Table 2 under the CRPL$_i$ heading are based on fixing the value to give a secondary phase correction of 1624 nanoseconds. This value is much closer to the value derived in Reference 5.

Table 3 lists effective impedances to each transmitter for each location using the two sets of data given in Table 2 and techniques described in References 1, 2 and 3. We believe the results listed under CRPL$_i$ in Table 3 are in better agreement with the Coast Guard and NOAA measurements presented in Reference 2. For example, the last 4 entries of Table 5, (Reference

2), all had X paths propagating over the San Joaquin Valley. Also, NOAA ship measurement points 1390, 1411, 1430 and 1716 shown in Figure 1 and Table 8 of Reference 2 had paths propagating over the Valley. The X paths to Friant, Merced, Crows Landing and to a lesser extent Livermore, propagated over the San Joaquin Valley. It would seem reasonable to expect impedances from .0148 to .0288 for these paths, but unreasonably low for impedances from .0043 to .0165 for the paths.

Figure 1 illustrates the geometrical relations between the Loran-C transmitters and the Worst Case Path measurement locations occupied by G.E. Tempo. Figure 2 shows the terrain plot from Searchlight, Nevada to Fort Cronkhite, California, along with the approximate locations and deduced impedance values for the intermediate points along this path. It is interesting to note that the impedance values consistently increase from Tecopa to Friant where the path is very irregular and the values tend to decrease after Friant as the path crosses the San Joaquin Valley. However, the slightly rugged terrain between Crows Landing and Livermore apparently increases the impedance again slightly at Livermore. Figures 3 and 4, terrain plots from Searchlight, Nevada to Death Valley, Calif., and Searchlight, Nevada to Friant, Calif., respectively demonstrate terrain differences from the path in Figure 2 due to the fact that intermediate points were not precisely on the geodesic path between Searchlight and Fort Cronkhite.

A complete analysis over the total path in Figure 2 and the actual intermediate paths to each point similar to the Searchlight to Tecopa analysis given in Reference 5 would demonstrate several factors. One, it would demonstrate the potential advantage of a complete calibration by prediction enterprise. Two, it would demonstrate the sensitivity of the Loran-C changes with slight changes in path geometry. Three, it would tend to verify the deduced impedance values for the Y path and consequently tie down the impedance values for both the M and X paths that are discussed in the next section.

In Figures 5 through 12 the terrain from each point on the Worst Case Path to the Master is plotted. Also given on each figure is the deduced impedance values. As would be expected from looking at Figure 1, the terrain is extremely variable from path to path and only very close to the transmitter is there any similarity at all. The deduced impedance values appear to be

reasonably related to the terrain variations with the exception of the impedances to Death Valley and Darwin. If the impedances are primarily determined by terrain, it would seem that these two impedances should be interchanged. A complete integral equation analysis similar to that indicated in Reference 5 might resolve this question. In a complete prediction analysis the differences in soil and sub soil parameters between the Master to Death Valley and the Master to Darwin paths could be studied closely to determine the reason why the impedance was higher to Darwin than it was to Death Valley.

Figures 13 through 20 show the terrain plots from the X transmitter to each point and also the deduced impedance values for these paths. Again only the portions of the paths close to the transmitter station are similar as would be expected. The impedances for the first three points are no doubt primarily determined by the rough terrain. The specific values for each of these three points may also be somewhat affected by ground conductivities along the paths. The impedance values for the next four points are no doubt primarily influenced by the San Joaquin Valley and the lack of terrain features. The deduced impedance from the X transmitter to Fort Cronkhite is surprisingly high. A study using the integral equation techniques of Reference 5 could help to understand these anomolous points.

In addition to the above analysis a similar analysis is presented for the baseline paths and the near baseline paths to Silver Springs, Nevada, Jean, Nevada, and Arbuckle, California (see Figure 21). The impedances deduced for the X Secondary to the Master (Figure 22) and the Master to Y Secondary (Figure 23) from baseline extension measurements given in Reference 2 was $\Delta_x = .049$ and $\Delta_y = .0423$ respectively. The data given in Table 4 A is the deduced secondary phase corrections for each path to Silver Springs, Jean and Arbuckle. This data was deduced from the distances given in Table 1 and the time difference averages given in Reference 6. Table 4 B gives the effective impedances to each transmitter associated with the secondary phase corrections given in Table 4 A. The three impedances underlined in the table represent the short path impedances for paths shown in Figures 24, 25 and 26 and cannot be independently checked. However, these impedances may be indicative of surface conductivities in the vicinity of the transmitting stations. The paths marked path 1a and b (Figures 27 and 28), path 2a and b (Figures 29 and 30), and path 3a and b (Figures 31 and 32) are nearly

reciprocal. Also, paths 1a and b are close to the Master - X Secondary (Figure 22) and paths 2a and b are close to the Master - Y Secondary (Figure 23). Paths 1a and 1b at .0490 and .0495 agree well with the Δ_x of .049. Paths 3a and b at .0458 and .0450 agree well with each other. Also, path 2b at .0420 agrees well with Δ_y = .0423. However, path 2a at .0476 does not agree well with Δ_y = .0423. Jean, Nevada is very close to the baseline from Master to Searchlight, and the terrain for that path is presented in Figure 23. It can be seen that Jean, Nevada falls at a point on this path directly following the highest terrain on the entire path. From previous integral equation runs, see Reference 5, for example, the maximum impedance values always follow the greater terrain peaks. Therefore it could be anticipated from this terrain plot alone that the impedance from the Master to Jean, Nevada should be higher than that from the Master to Searchlight, Nevada.

Figure 33 is the baseline terrain between the X and Y transmitters. This path is shown in comparison to paths 3a and 3b that is from Y to Arbuckle and from X to Jean. An estimated impedance of .0454 was assigned to this path only as an average of the deduced impedances for paths 3a and 3b. This impedance could be independently determined by making integral equation calculations similar to those given in Reference 5. This impedance could also be independently measured by making X - Y and Y - X baseline extension measurements and analyzing the data as was done for the M - X and M - Y baseline extension measurements as reported in Reference 2.

Ground structure analysis and integral equation computations to all of these stations would demonstrate more fully the potential of Loran-C navigation. Furthermore, computations using the full wave transient analysis algorithm for all of these paths could help the Coast Guard determine the true extent of the envelope to cycle problem over irregular nonhomogeneous terrain.

REFERENCES

(1) Doherty, R. H. (1978), Some comments on a proposed Loran-C signal analysis plan, CRPL$_i$ Report 78-2, U.S.C.G. Contract DOT-CG-78629-A (Colorado Research and Prediction Laboratory, Inc., 1898 South Flatiron Court, Boulder, Colo. 80301).

(2) Doherty, R. H. and J. R. Johler (1978), Interpretation of West Coast Loran-C spatial errors using programmable calculator analysis techniques, Proceedings of the Sixth Annual Technical Symposium, Wild Goose Association, 4 Townsend Road, Acton, Mass., 01720, pp. 227-237.

(3) Johler, J. R., R. H. Doherty and A. R. Cook (1978), Some comments on experimental data collection for West Coast Loran-C Chain, CRPL$_i$ Report 78-2, U.S.C.G. Contract DOT-CG-74629-A (Colorado Research and Prediction Laboratory, Inc., 1898 South Flatiron Court, Boulder, Colo. 80301).

(4) Gambill, B., Jr., and K. Schwartz (1978), Loran-C signal analysis: propagation model evaluation final report, G.E. 78 TMP-51, May, 1978 (General Electric Company - TEMPO, Center for Advanced Studies, Santa Barbara, California).

(5) Johler, J. R. (1979), Loran-C ground wave secondary phase corrections over nonhomogeneous and irregular ground using transient signal propagation techniques, CRPL$_i$ Report 78-12, U.S.C.G. Contract DOT-CG-842923A (Colorado Research and Prediction Laboratory, Inc., 1898 South Flatiron Court, Boulder, Colo. 80301).

(6) Nelson, L. and E. Feniger (1978), Loran-C signal analysis: stability experiment summary status report, G.E. 78 TMP-56, March, 1978, (General Electric Company, TEMPO, Center for Advanced Studies, Santa Barbara, California).

TABLE 1

LOCATIONS, DISTANCE TO TRANSMITTERS AND PREDICTED TDs WITHOUT SECONDARY PHASE CORRECTION FOR POINTS MONITORED BY G.E. TEMPO

	Latitude ϕ Longitude λ	Distance to the Transmitters			TD_s for $\phi_c = 0$		ΔTD_A	ΔTD_B
		D_M	D_X	D_Y				
Tecopa	35 49 5.620 116 11 5.605	475.603	648.833	136.692	28672.55	40836.35	1.94	-1.17
Death Valley	36 03 32.448 116 50 19.467	425.546	584.729	201.449	28625.68	41219.46	2.11	-.72
Darwin	36 19 28.148 117 40 09.796	372.512	506.42	281.736	28540.41	41664.32	.26	-.39
Friant	36 59 38.868 119 42 15.925	293.983	315.708	478.265	28167.01	42582.13	-2.23	.80
Merced	37 11 19.479 120 21 8.260	294.012	258.344	539.777	27975.50	42787.28	-1.66	1.19
Crows Landing	37 25 30.687 121 6 19.127	308.287	193.823	611.500	27712.58	42978.97	-1.63	1.40
Livermore	37 37 26.007 121 46 3.193	333.438	143.550	674.055	27460.91	43103.78	-1.36	2.14
Ft. Cronkhite	37 50 29.464 122 32 41.170	374.589	104.539	746.697	27193.42	43208.86	-.96	2.07
Silver Springs	39 24 16.785 119 14 33.738	38.907	289.757	599.738	28931.55	43838.58	2.31	3.64
Jean	35 46 25.163 115 19 39.089	520.930	7172775	68.997	28751.35	40459.22	.86	-3.26
Arbuckle	39 0 37.708 122 3 20.602	284.525	45.798	672.722	27297.94	43562.85	-1.73	2.56

TABLE 2

SECONDARY CORRECTIONS TO TRANSMITTERS FOR WORST CASE PATH POINTS

	To Y Secondary		To Master		To X Secondary	
	GE	$CRPL_i$	GE	$CRPL_i$	GE	$CRPL_i$
Tecopa	1.224	1.624	2.39	2.79	4.33	4.73
Death Valley	1.829	2.229	2.55	2.95	4.66	5.06
Darwin	2.463	2.863	2.85	3.25	3.11	3.51
Friant	3.960	4.360	3.16	3.56	.93	1.33
Merced	3.475	3.875	2.28	2.68	.62	1.02
Crows Landing	3.406	3.806	2.01	2.41	.38	.78
Livermore	4.178	4.578	2.04	2.44	.68	1.08
Ft. Cronkhite	4.080	4.480	2.01	2.41	1.05	1.45

TABLE 3

CALCULATED EFFECTIVE IMPEDANCES FOR WORST CASE PATH POINTS

	Y Secondary		Master		X Secondary	
	GE	$CRPL_i$	GE	$CRPL_i$	GE	$CRPL_i$
Tecopa	.0344	.0468	.0258	.0317	.0419	.0468
Death Valley	.0413	.0506	.0318	.0382	.0504	.0554
Darwin	.0446	.0516	.0415	.0483	.0349	.0407
Friant	.0484	.0537	.0542	.0591	.0105	.0183
Merced	.0378	.0433	.0394	.0473	.0069	.0158
Crows Landing	.0323	.0376	.0324	.0404	.0043	.0148
Livermore	.0385	.0433	.0306	.0382	.0165	.0288
Ft. Cronkhite	.0331	.0378	.0267	.0337	.0342	.0482

TABLE 4 A

SECONDARY PHASE CORRECTIONS FOR STABILITY
EXPERIMENT MONITORING POINTS

	Master	X Secondary	Y Secondary
Silver Springs	.45 μ sec.	2.76 μ sec.	4.09 μ sec.
Arbuckle	2.70 μ sec.	.97 μ sec.	5.26 μ sec.
Jean	4.09 μ sec.	4.95 μ sec.	.83 μ sec.

TABLE 4 B

EFFECTIVE IMPEDANCES FOR STABILITY
EXPERIMENT MONITORING POINTS

	Master	X Secondary	Y Secondary
Silver Springs	.0215	.0495 (path 1b)	.0420 (path 2b)
Arbuckle	.0490 (path 1a)	.0459	.0458 (path 3a)
Jean	.0476 (path 2a)	.0450 (path 3b)	.0329

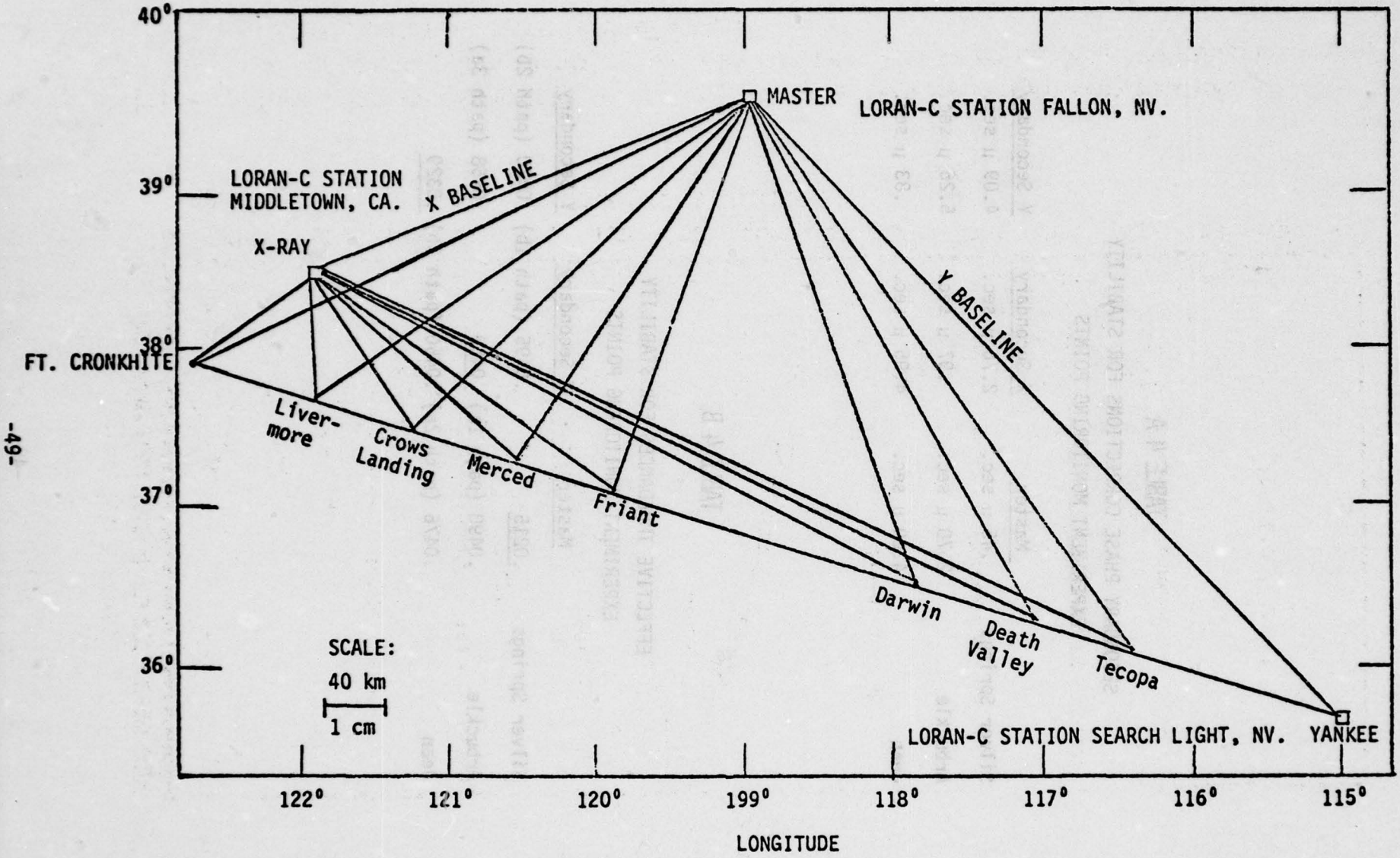

FIGURE 1. APPROXIMATE GEOMETRY FOR TRANSMITTER PATHS TO WORST CASE PATH MEASUREMENT SITES.

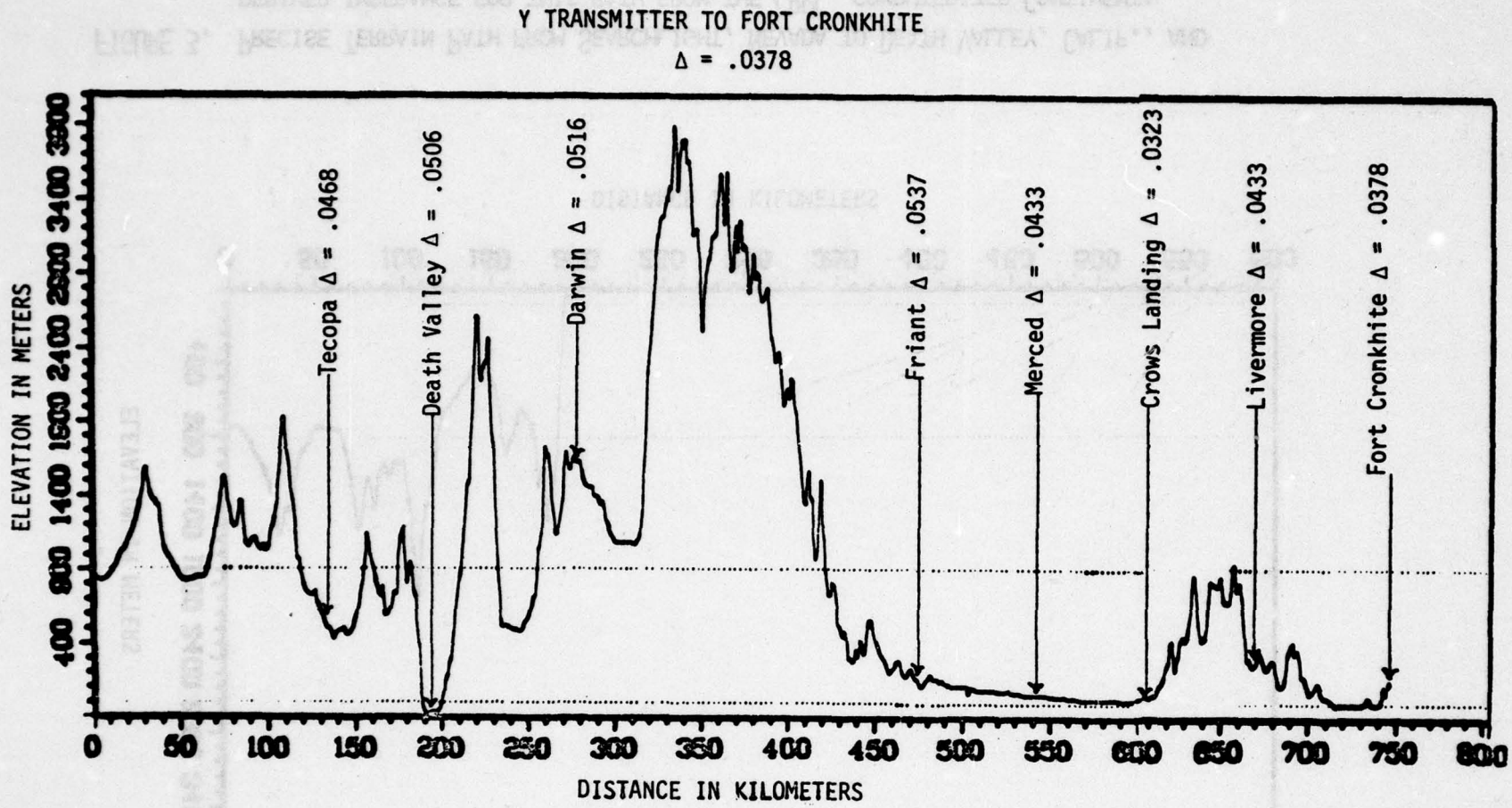

FIGURE 2. TERRAIN PATH FROM SEARCHLIGHT, NEV. TO FORT CRONKHITE, CALIF. WITH APPROXIMATE LOCATIONS OF INTERMEDIATE POINTS AND DERIVED IMPEDANCES FOR THESE POINTS FROM THE $CRPL_I$ COMPUTERIZED CONTINENTAL UNITED STATES TERRAIN DATA BASE.

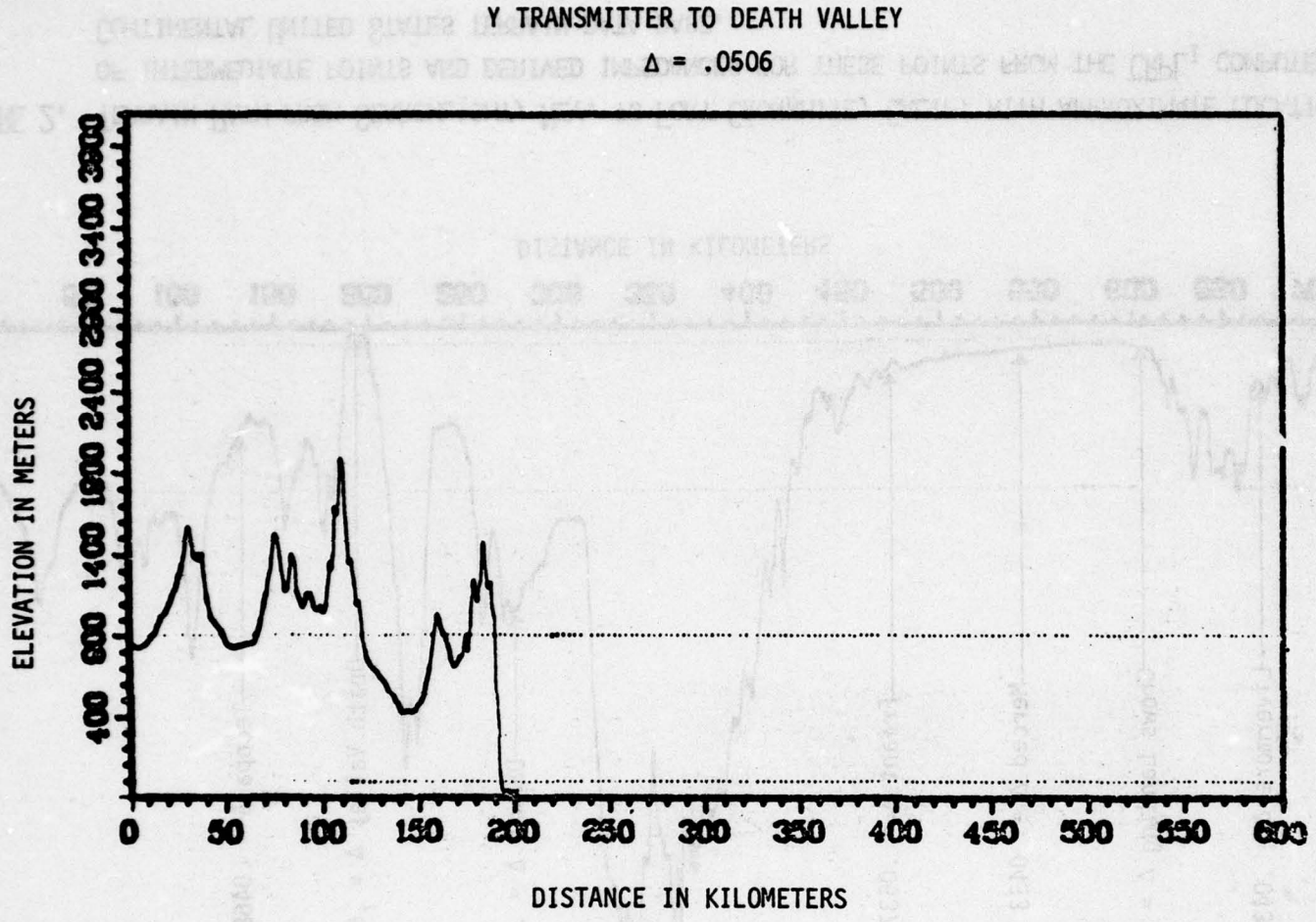

FIGURE 3. PRECISE TERRAIN PATH FROM SEARCHLIGHT, NEVADA TO DEATH VALLEY, CALIF., AND DERIVED IMPEDANCE FOR THIS PATH FROM THE CRPL$_I$ COMPUTERIZED CONTINENTAL UNITED STATES TERRAIN DATA BASE.

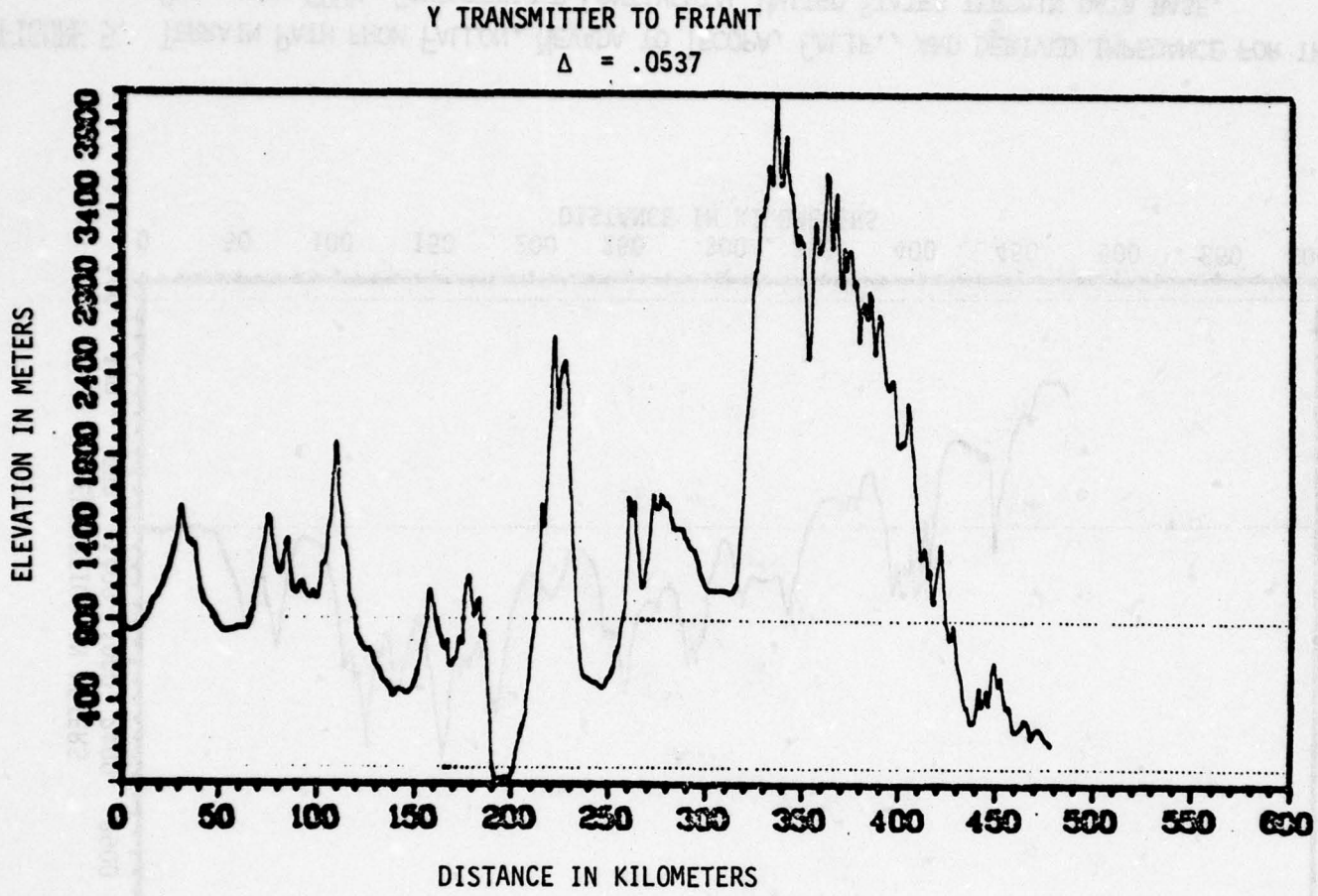

FIGURE 4. PRECISE TERRAIN PATH FROM SEARCHLIGHT, NEVADA TO FRIANT, CALIF., AND DERIVED IMPEDANCE FOR THIS PATH FROM $CRPL_I$ COMPUTERIZED CONTINENTAL UNITED STATES TERRAIN DATA BASE.

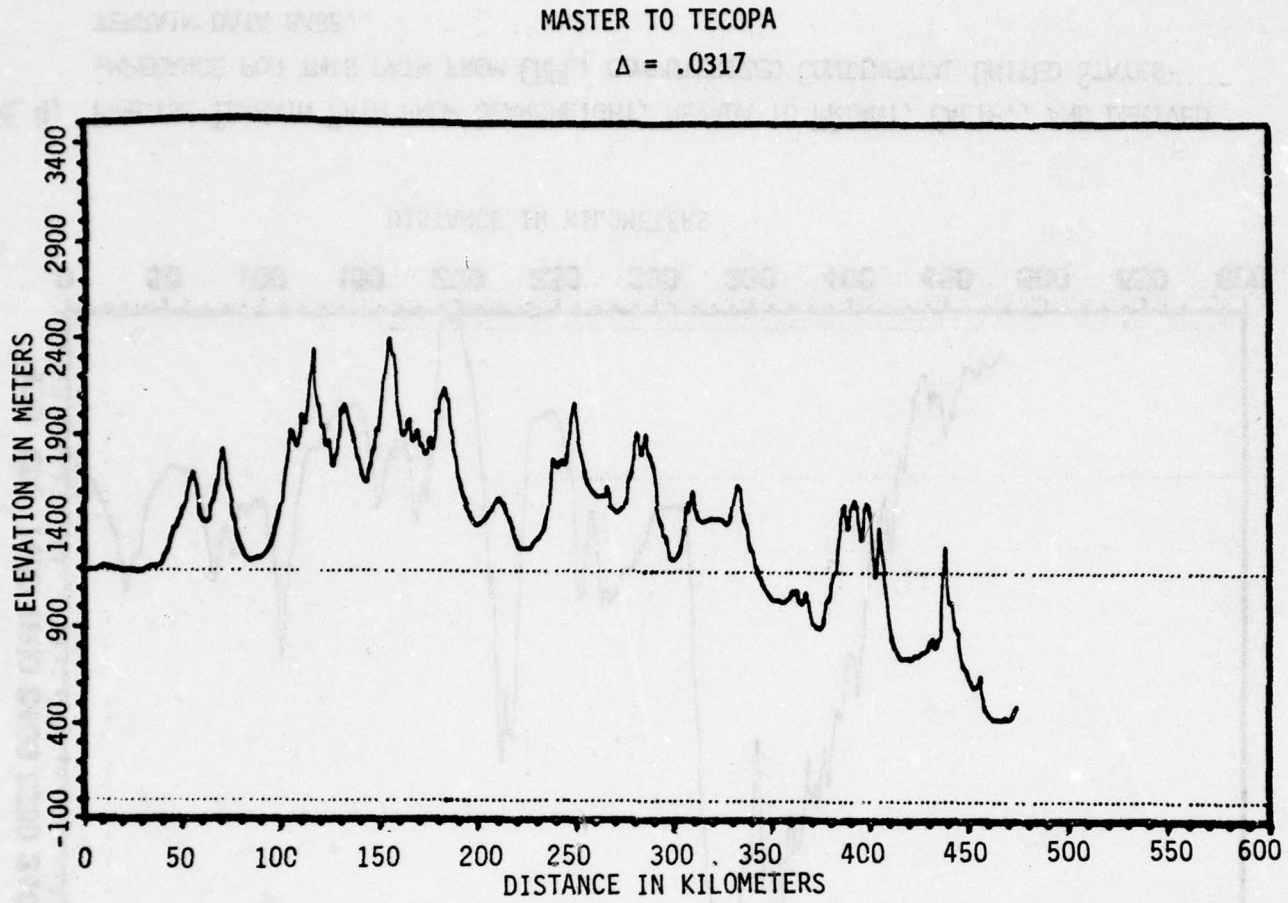

FIGURE 5. TERRAIN PATH FROM FALLON, NEVADA TO TECOPA, CALIF., AND DERIVED IMPEDANCE FOR THIS PATH FROM CRPL$_I$ COMPUTERIZED CONTINENTAL UNITED STATES TERRAIN DATA BASE.

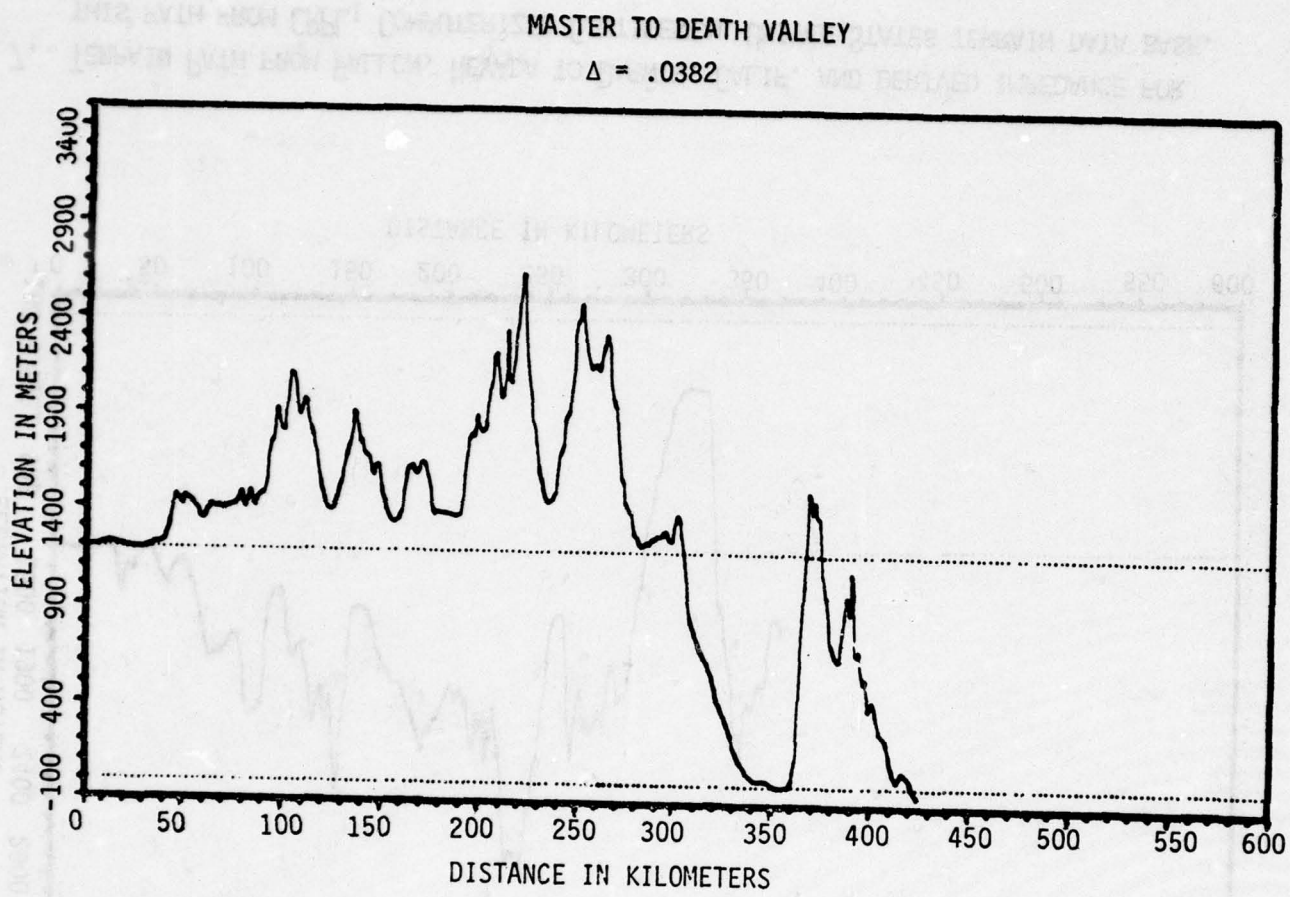

FIGURE 6. TERRAIN PATH FROM FALLON, NEVADA TO DEATH VALLEY, CALIF. AND DERIVED IMPEDANCE FOR THIS PATH FROM CRPL$_I$ COMPUTERIZED CONTINENTAL UNITED STATES TERRAIN DATA BASE.

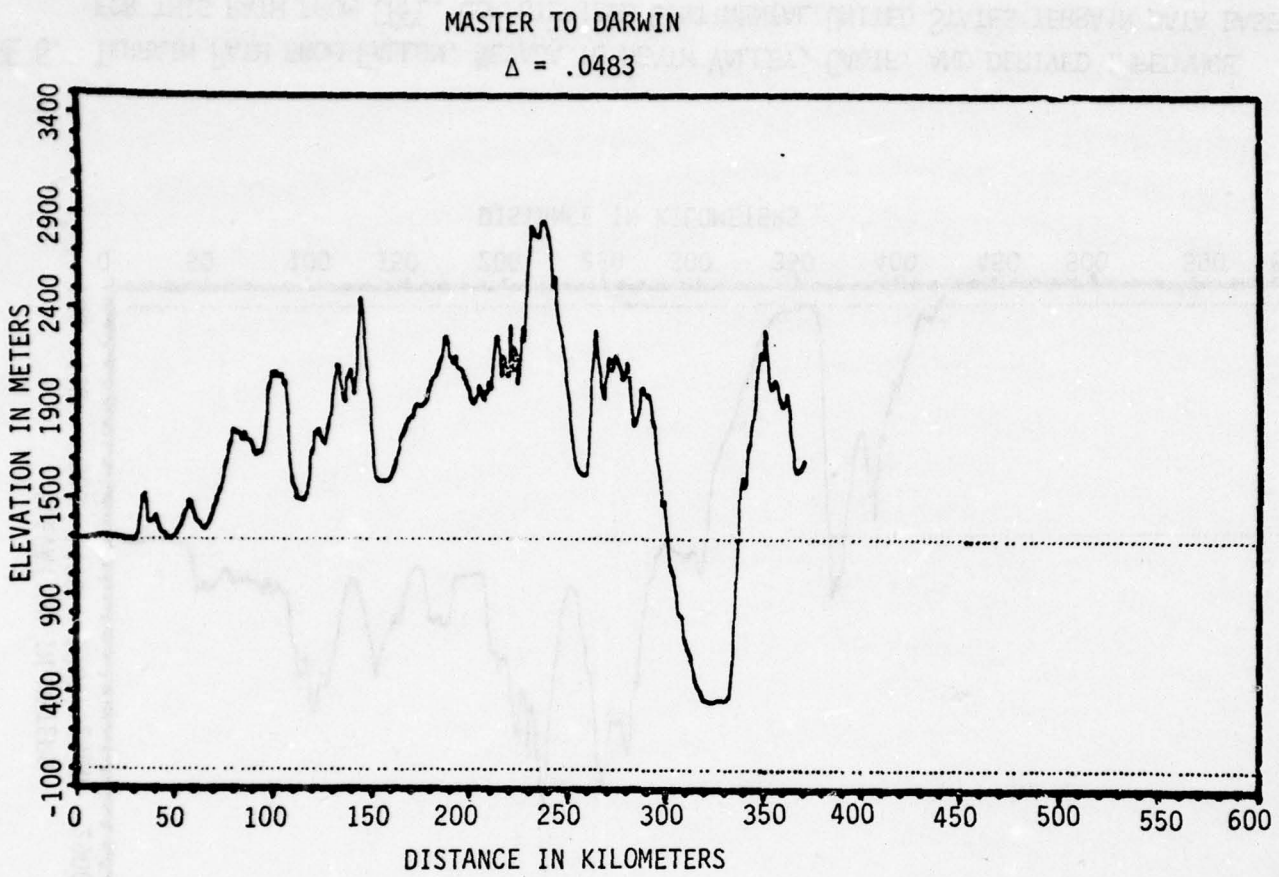

FIGURE 7. TERRAIN PATH FROM FALLON, NEVADA TO DARWIN, CALIF. AND DERIVED IMPEDANCE FOR THIS PATH FROM CRPL$_I$ COMPUTERIZED CONTINENTAL UNITED STATES TERRAIN DATA BASE.

AD-A077 551 COLORADO RESEARCH AND PREDICTION LAB INC BOULDER F/G 17/7
LORAN-C PULSE TRANSIENT PROPAGATION. PART I. GEOPHYSICAL AND GE--ETC(U)
MAY 79 J R JOHLER , R H DOHERTY , A R COOK DOT-CG-842923-A
UNCLASSIFIED CRPLI-78-9 USCG-D-52-79 NL

3 OF 3
ADA 077551

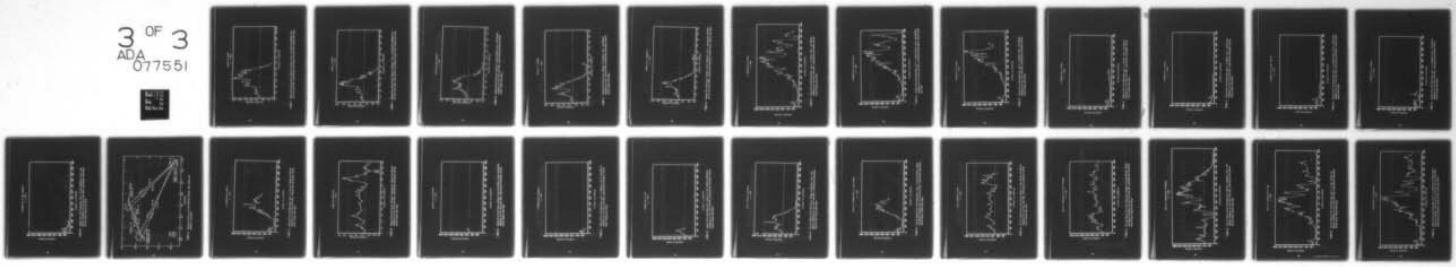

END
DATE FILMED
1-80
DDC

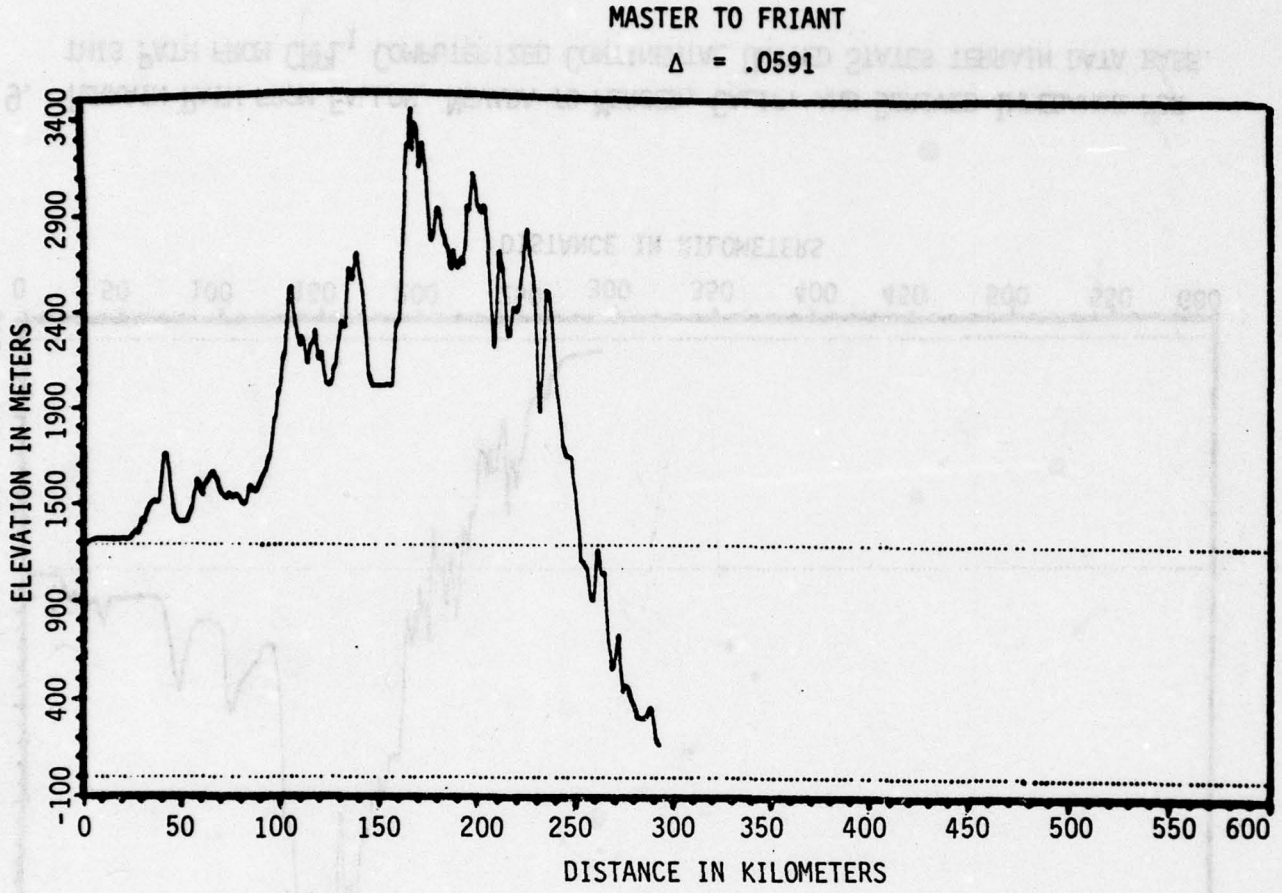

FIGURE 8. TERRAIN PATH FROM FALLON, NEVADA TO FRIANT, CALIF. AND DERIVED IMPEDANCE FOR THIS PATH FROM CRPL$_I$ COMPUTERIZED CONTINENTAL UNITED STATES TERRAIN DATA BASE.

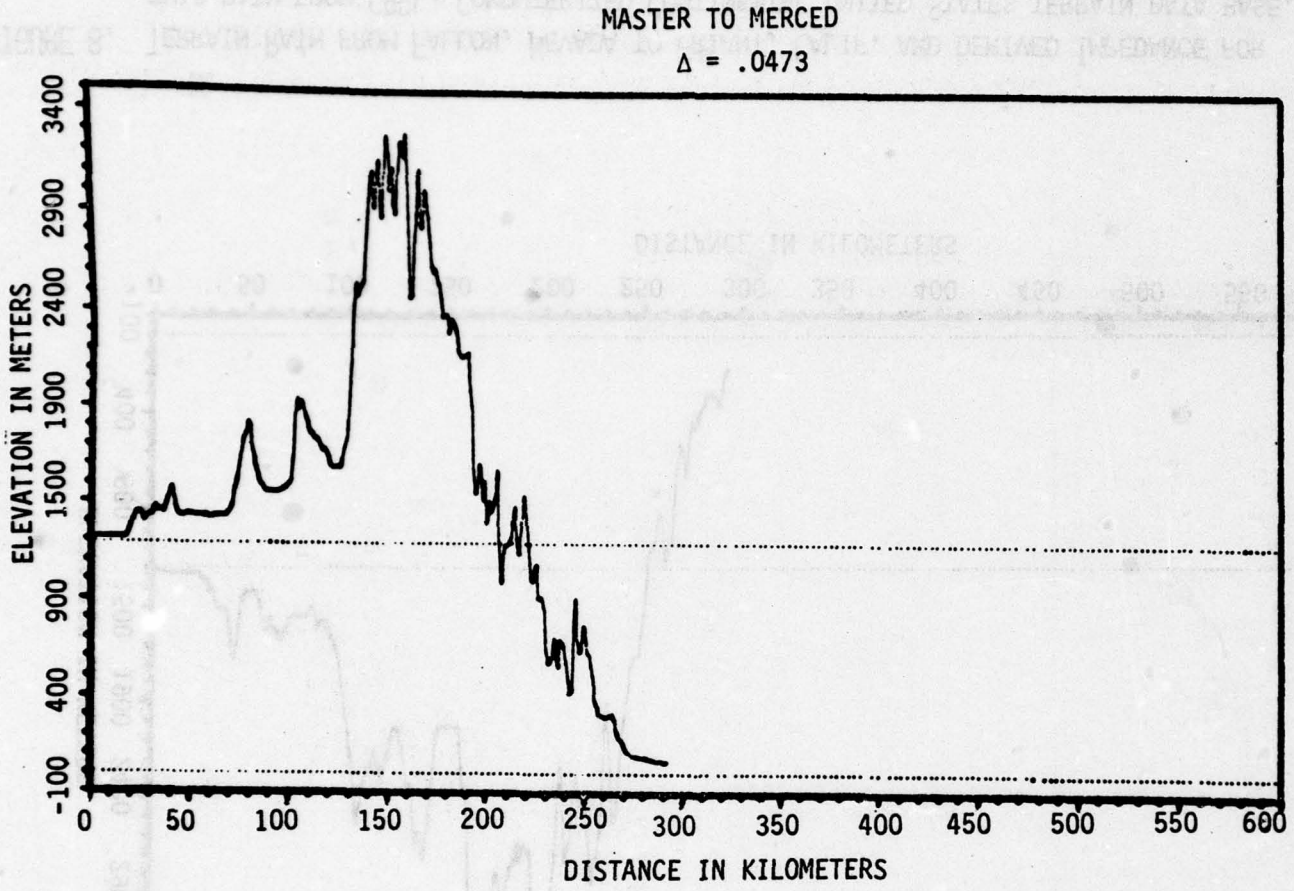

FIGURE 9. TERRAIN PATH FROM FALLON, NEVADA TO MERCED, CALIF. AND DERIVED IMPEDANCE FOR THIS PATH FROM $CRPL_I$ COMPUTERIZED CONTINENTAL UNITED STATES TERRAIN DATA BASE.

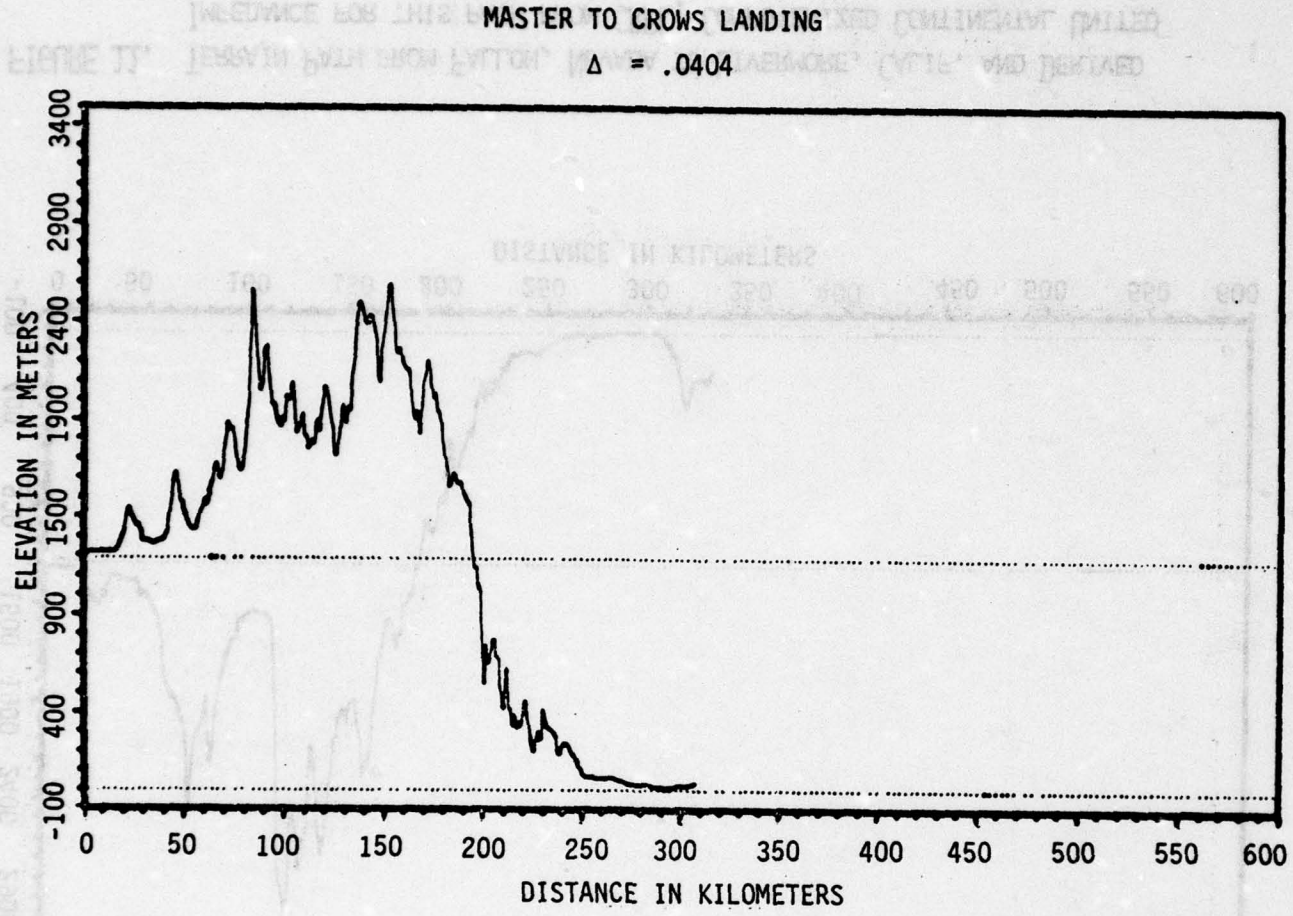

FIGURE 10. TERRAIN PATH FROM FALLON, NEVADA TO CROWS LANDING, CALIF. AND DERIVED IMPEDANCE FOR THIS PATH FROM $CRPL_I$ COMPUTERIZED CONTINENTAL UNITED STATES TERRAIN DATA BASE.

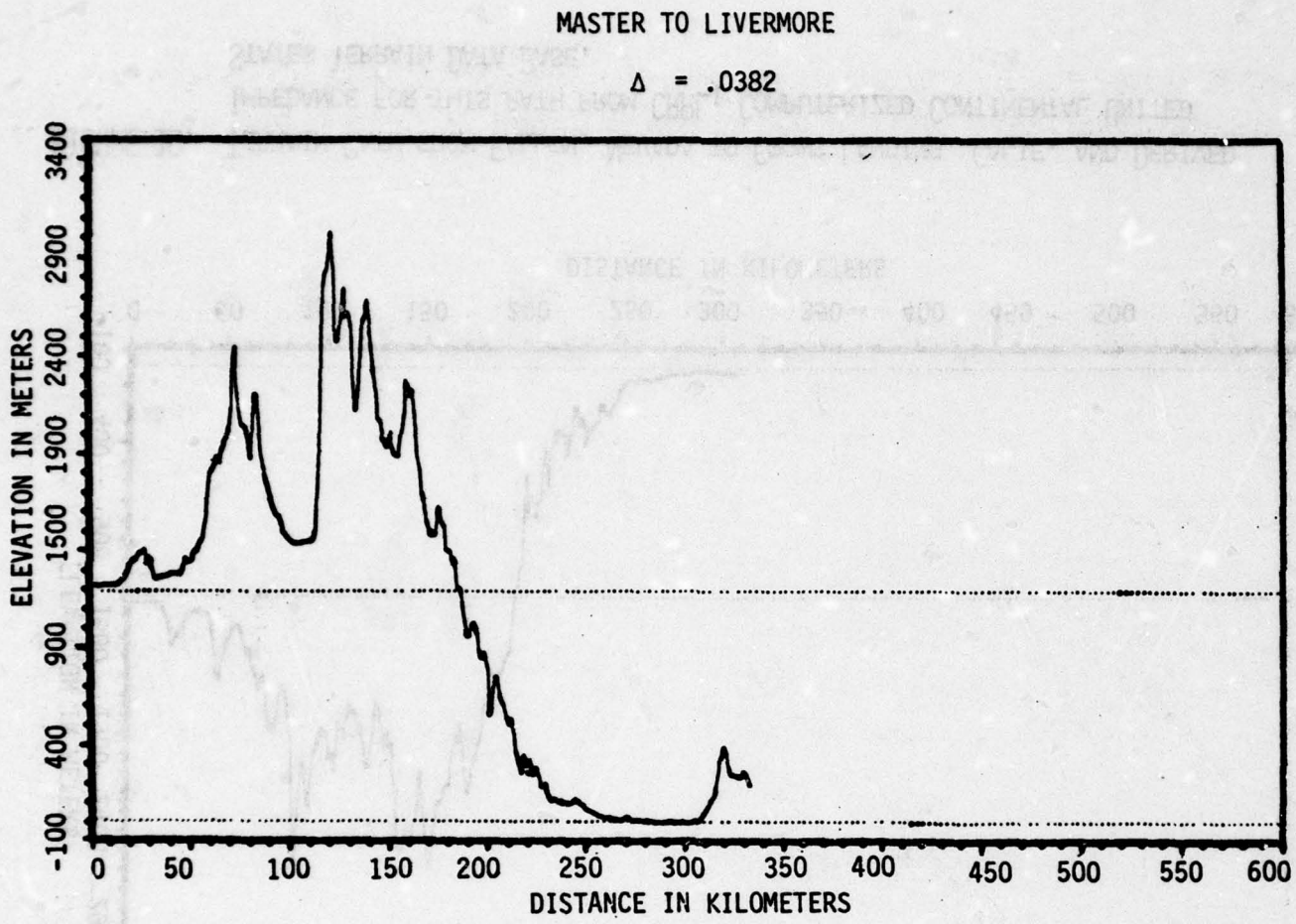

FIGURE 11. TERRAIN PATH FROM FALLON, NEVADA TO LIVERMORE, CALIF. AND DERIVED IMPEDANCE FOR THIS PATH FROM CRPL$_I$ COMPUTERIZED CONTINENTAL UNITED STATES TERRAIN DATA BASE.

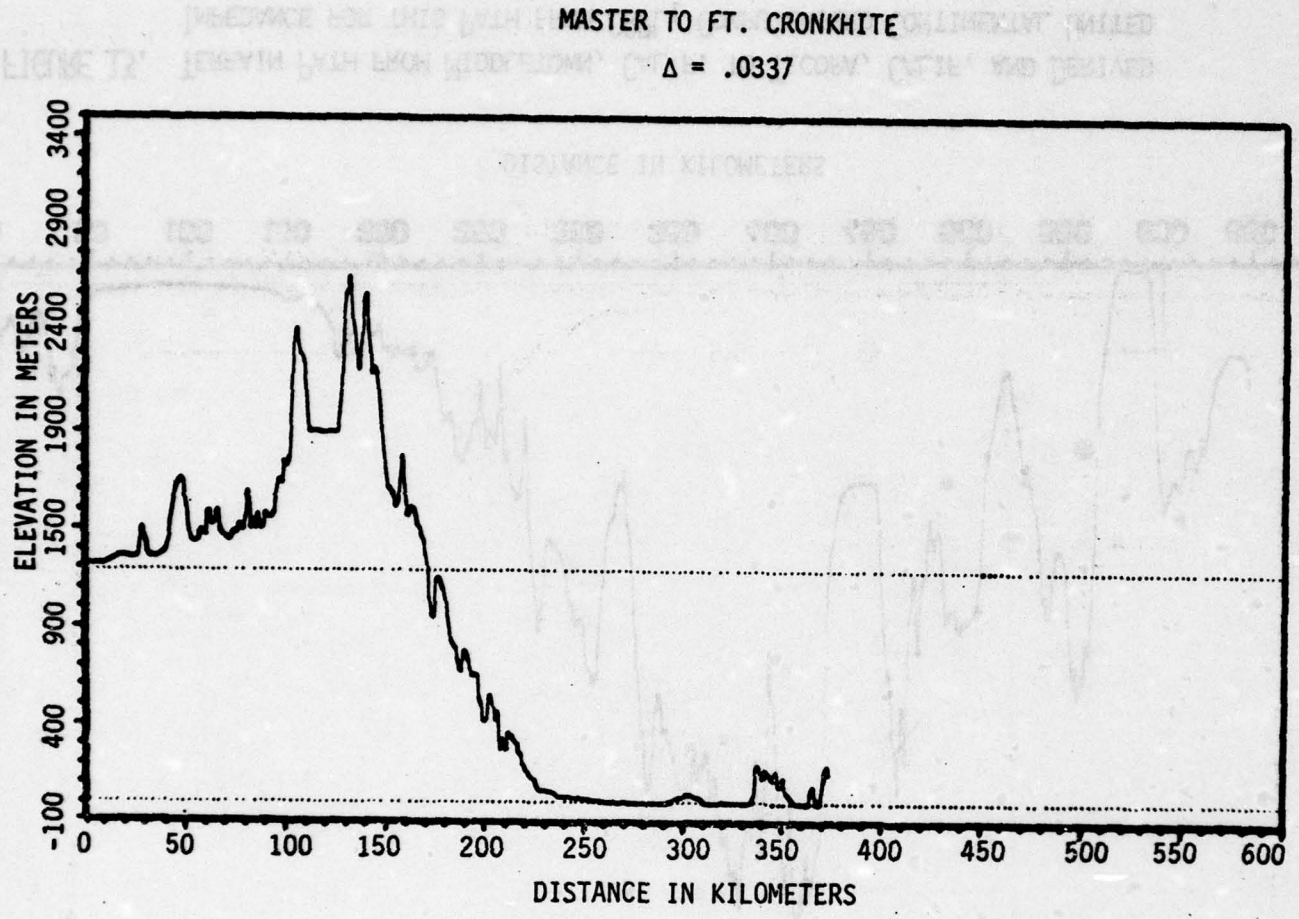

FIGURE 12. TERRAIN PATH FROM FALLON, NEVADA TO FORT CRONKHITE, CALIF., AND DERIVED IMPEDANCE FOR THIS PATH FROM CRPL$_I$ COMPUTERIZED CONTINENTAL UNITED STATES TERRAIN DATA BASE.

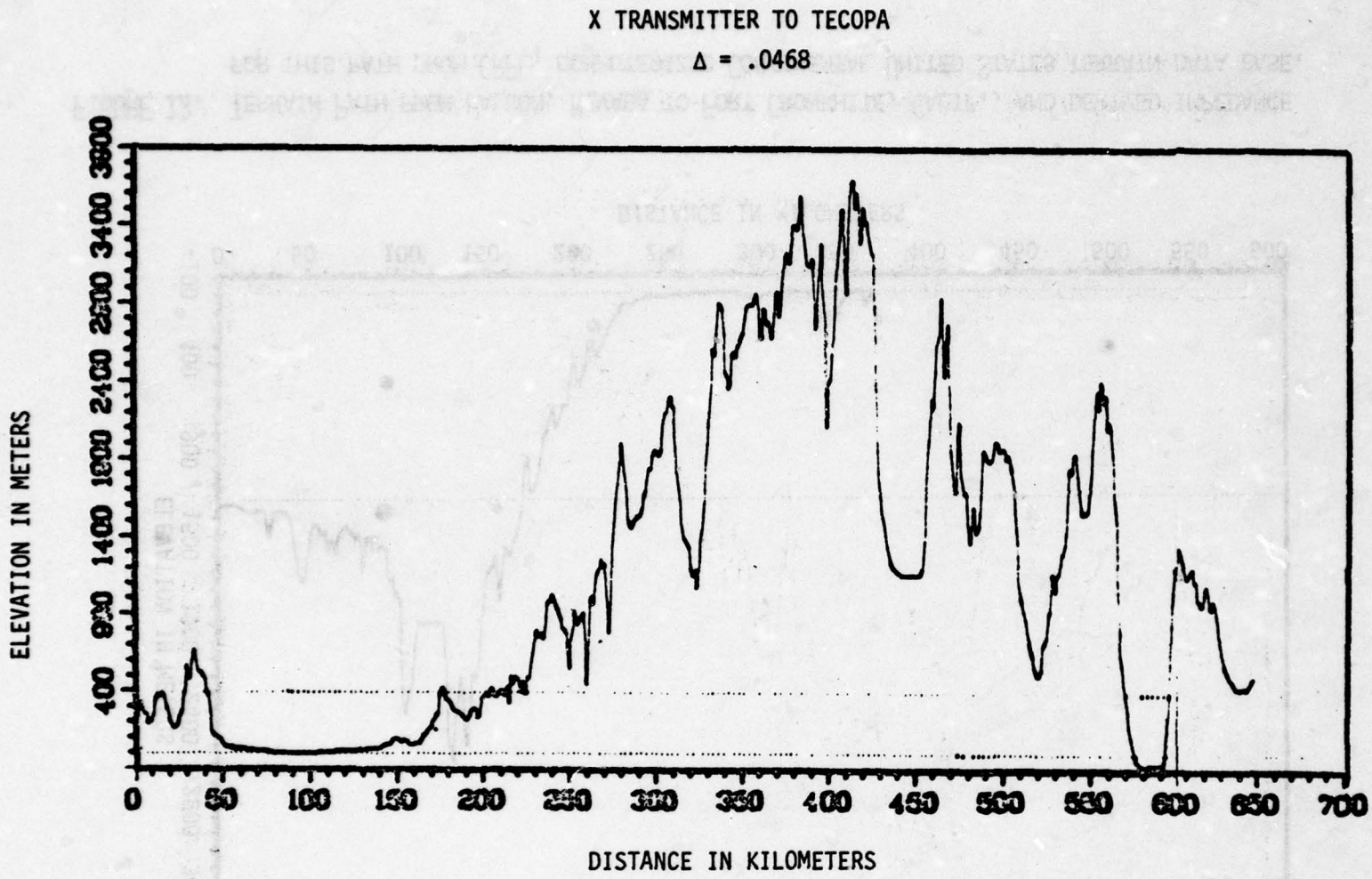

FIGURE 13. TERRAIN PATH FROM MIDDLETOWN, CALIF. TO TECOPA, CALIF. AND DERIVED IMPEDANCE FOR THIS PATH FROM $CRPL_I$ COMPUTERIZED CONTINENTAL UNITED STATES TERRAIN DATA BASE.

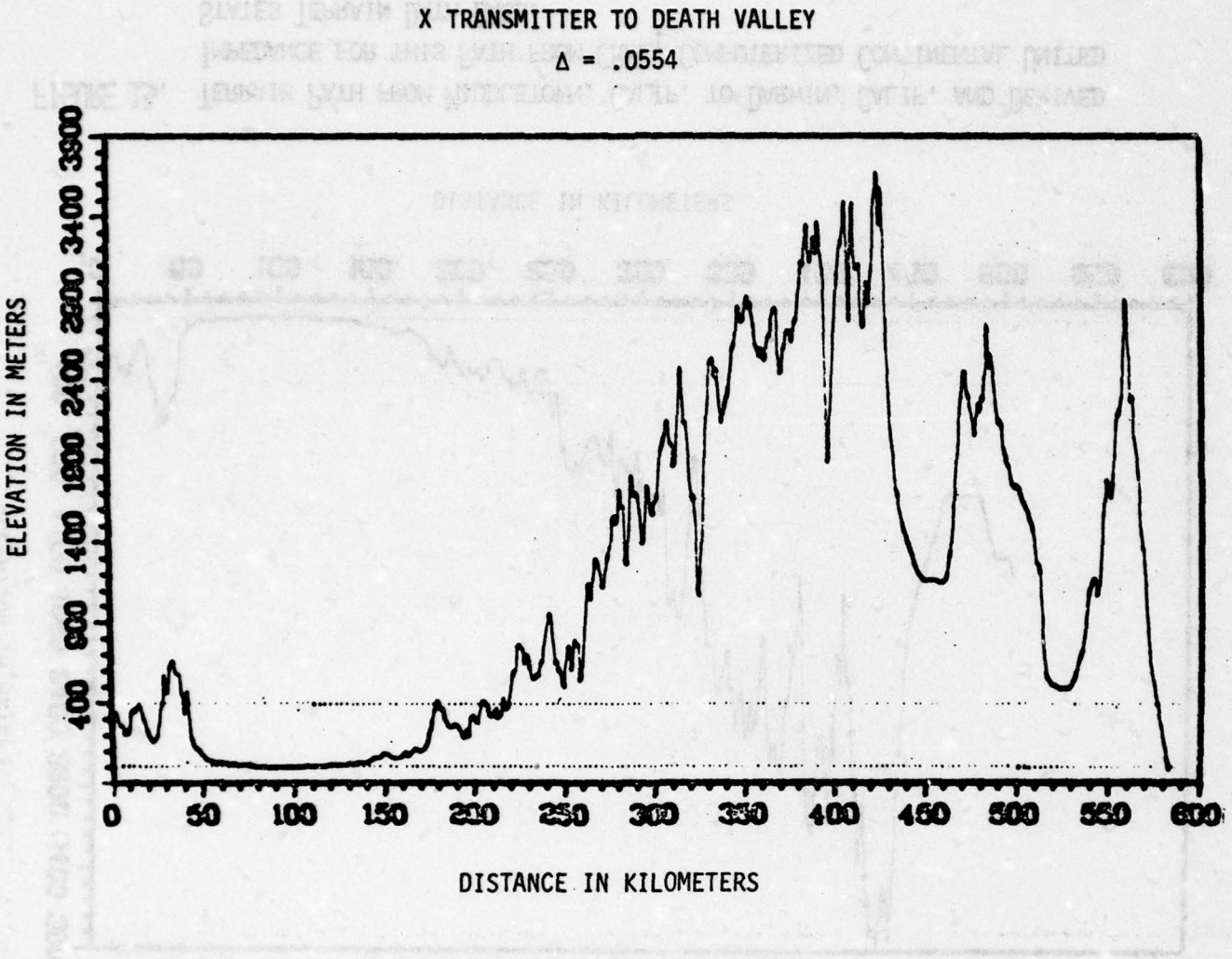

FIGURE 14. TERRAIN PATH FROM MIDDLETOWN, CALIF. TO DEATH VALLEY, CALIF. AND DERIVED IMPEDANCE FOR THIS PATH FROM $CRPL_I$ COMPUTERIZED CONTINENTAL UNITED STATES DATA BASE.

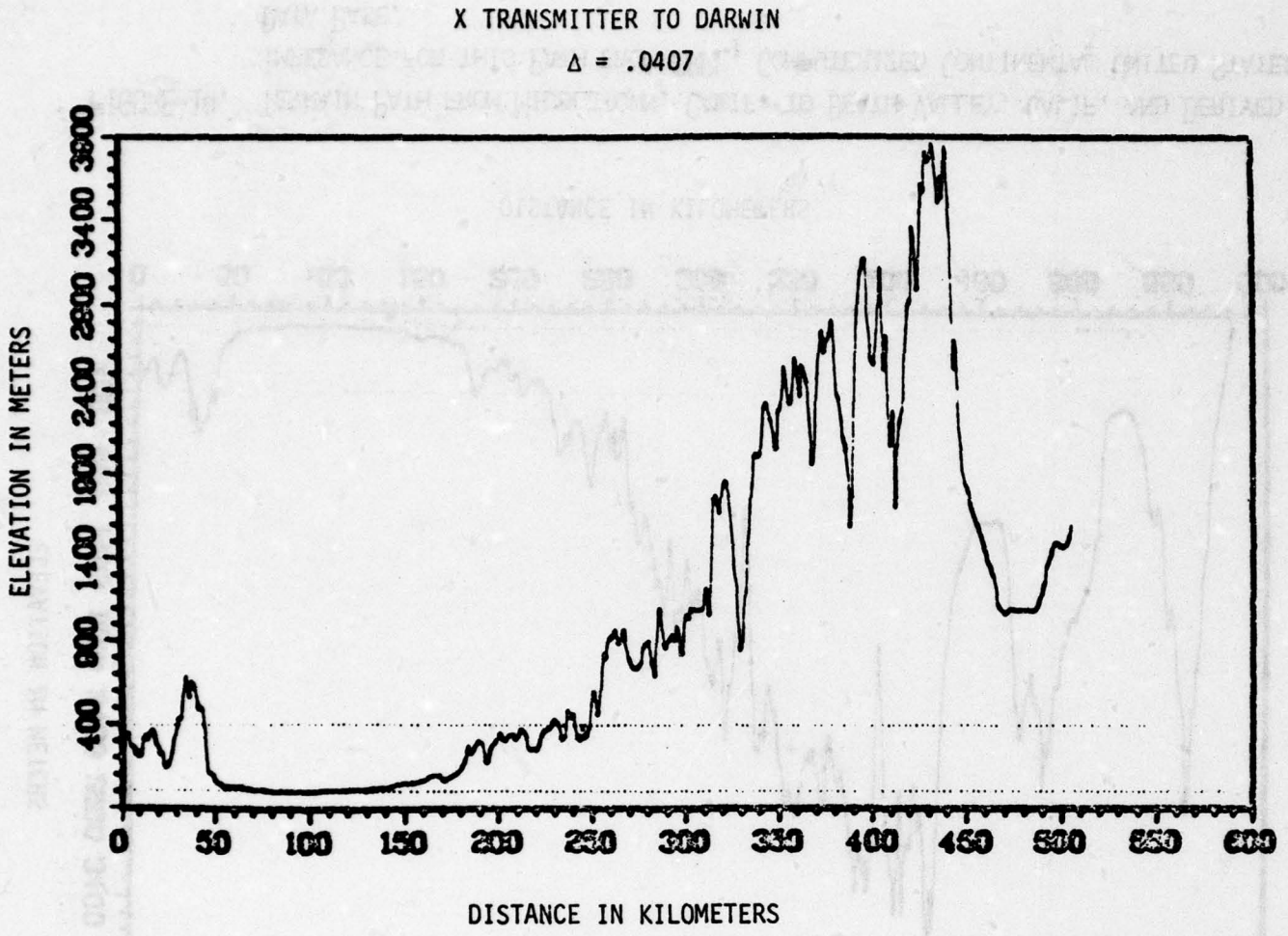

FIGURE 15. TERRAIN PATH FROM MIDDLETOWN, CALIF. TO DARWIN, CALIF. AND DERIVED IMPEDANCE FOR THIS PATH FROM CRPL$_I$ COMPUTERIZED CONTINENTAL UNITED STATES TERRAIN DATA BASE.

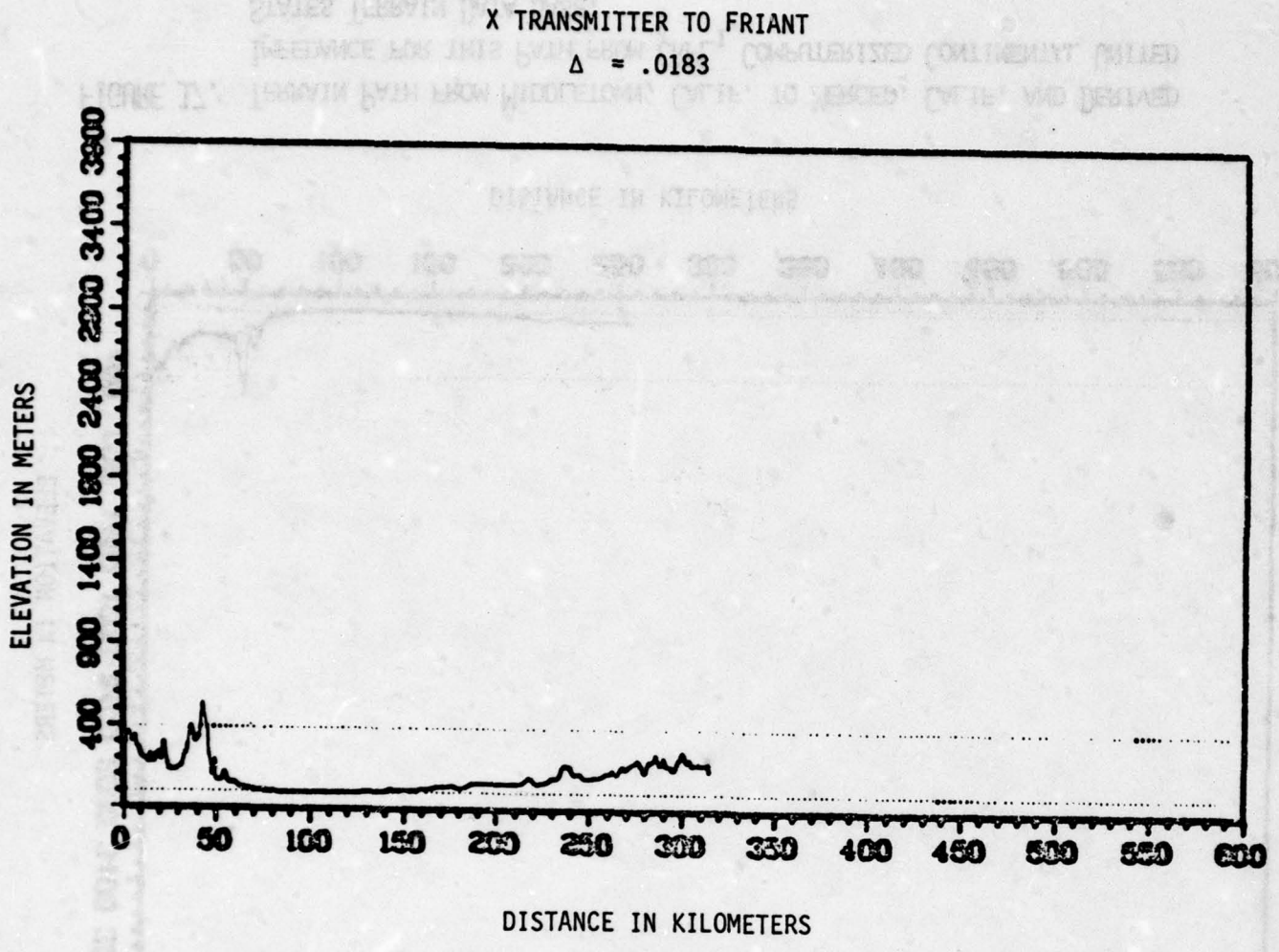

FIGURE 16. TERRAIN PATH FROM MIDDLETOWN, CALIF. TO FRIANT, CALIF. AND DERIVED IMPEDANCE FOR THIS PATH FROM $CRPL_I$ COMPUTERIZED CONTINENTAL UNITED STATES TERRAIN DATA BASE.

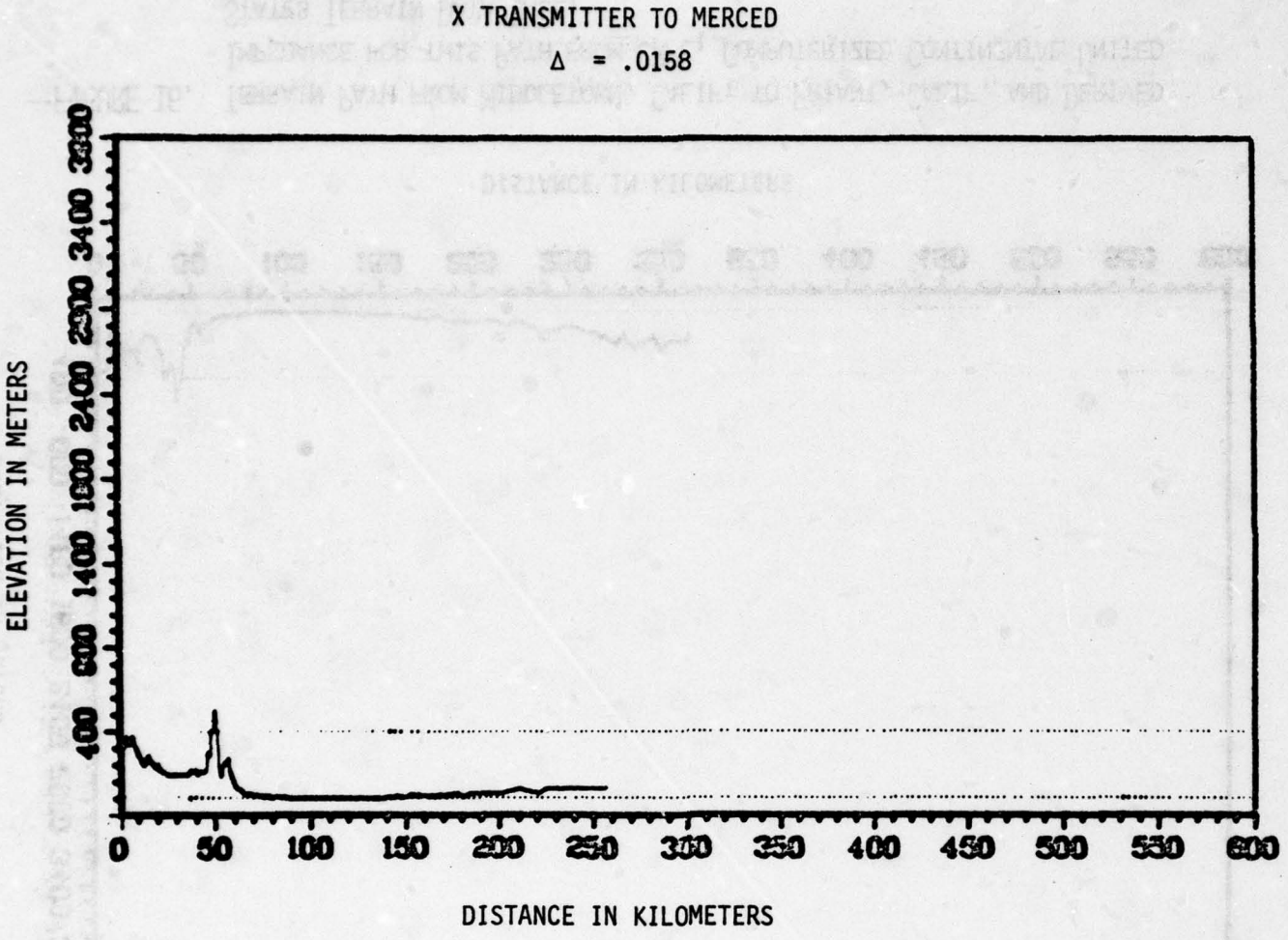

FIGURE 17. TERRAIN PATH FROM MIDDLETOWN, CALIF. TO MERCED, CALIF. AND DERIVED IMPEDANCE FOR THIS PATH FROM $CRPL_I$ COMPUTERIZED CONTINENTAL UNITED STATES TERRAIN DATA BASE.

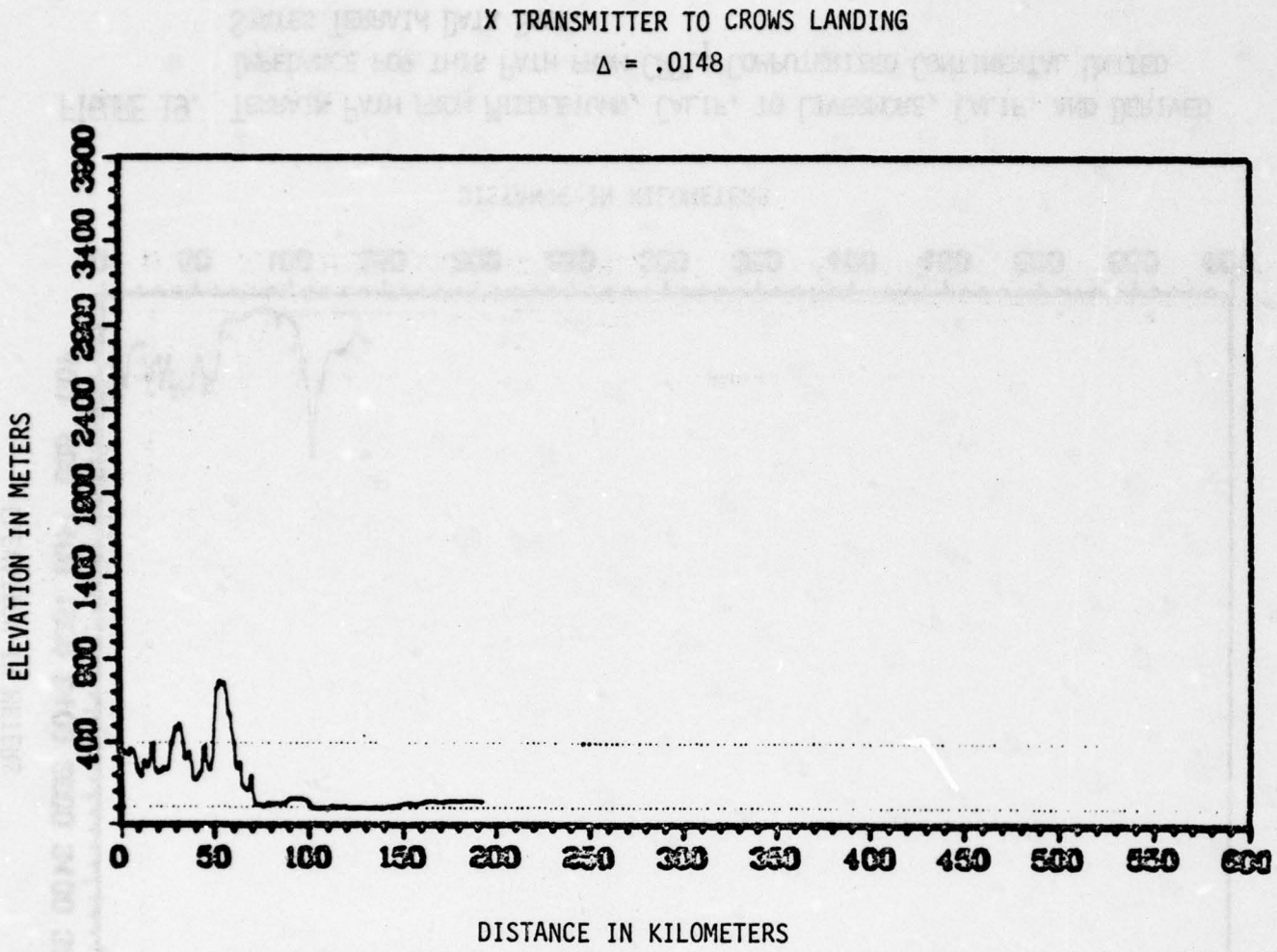

FIGURE 18. TERRAIN PATH FROM MIDDLETOWN, CALIF. TO CROWS LANDING, CALIF. AND DERIVED IMPEDANCE FOR THIS PATH FROM $CRPL_I$ COMPUTERIZED CONTINENTAL UNITED STATES TERRAIN DATA BASE.

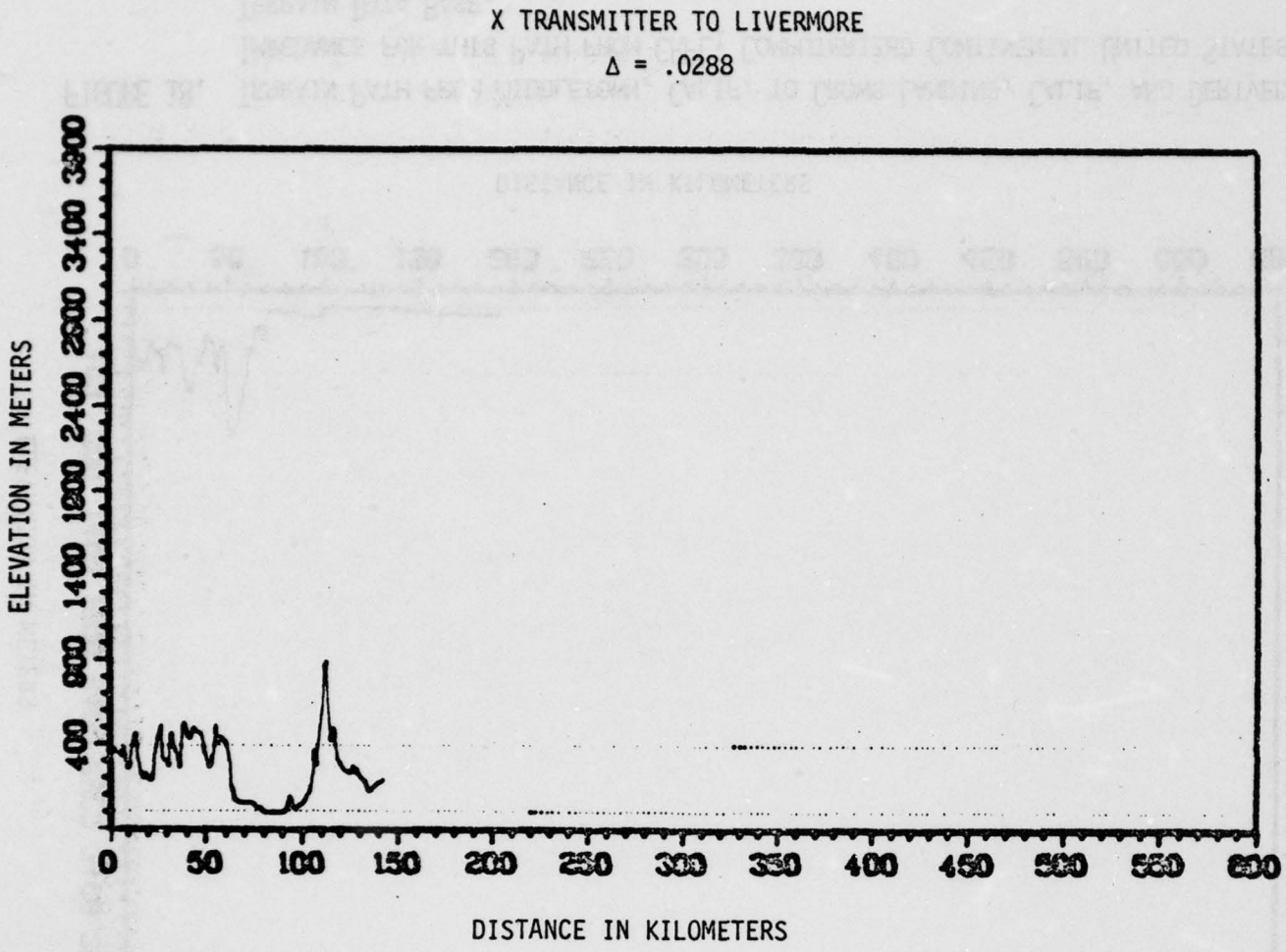

FIGURE 19. TERRAIN PATH FROM MIDDLETOWN, CALIF. TO LIVERMORE, CALIF. AND DERIVED IMPEDANCE FOR THIS PATH FROM $CRPL_I$ COMPUTERIZED CONTINENTAL UNITED STATES TERRAIN DATA BASE.

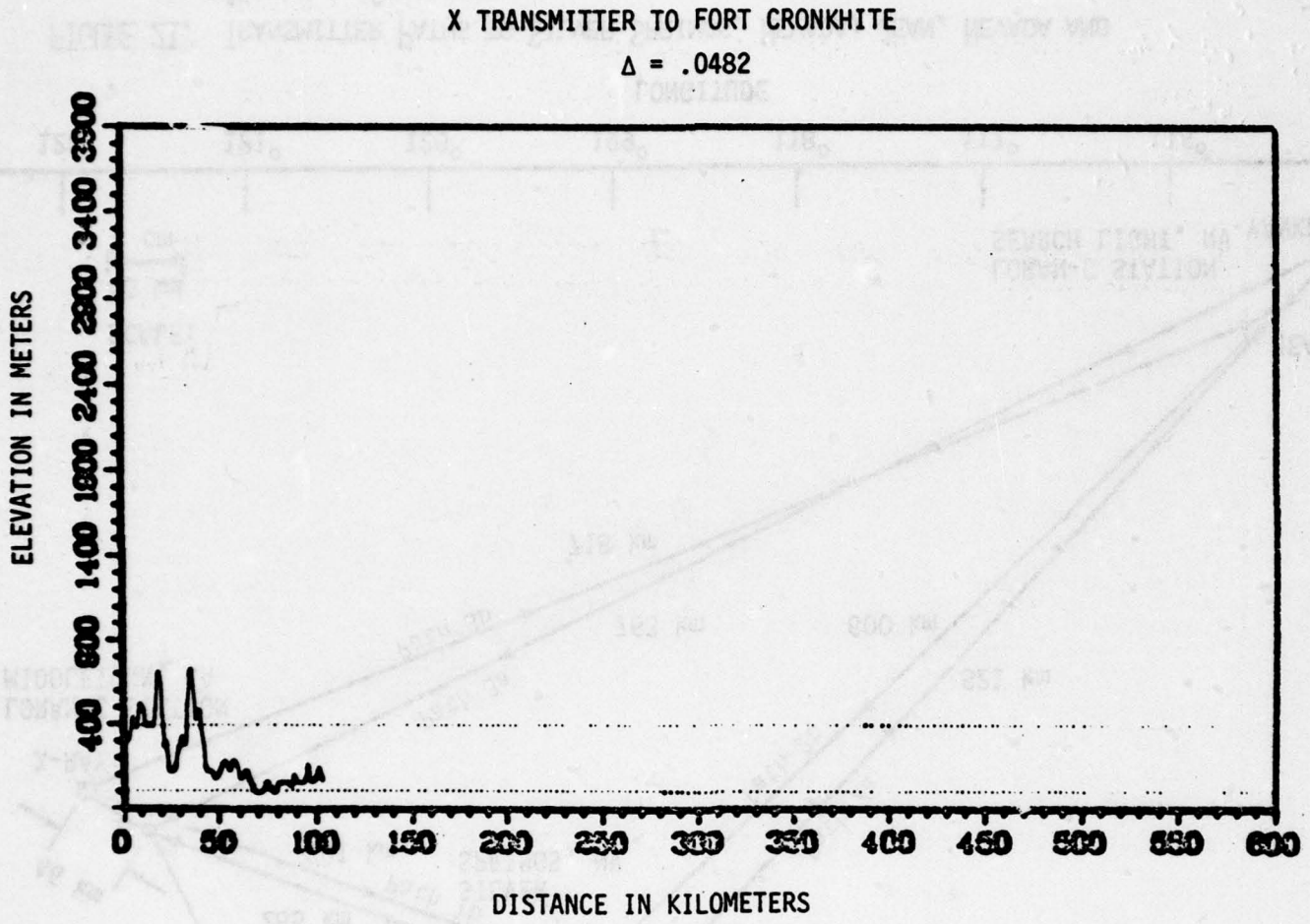

FIGURE 20. TERRAIN PATH FROM MIDDLETOWN, CALIF. TO FORT CRONKHITE, CALIF. AND DERIVED IMPEDANCE FOR THIS PATH FROM $CRPL_I$ COMPUTERIZED CONTINENTAL UNITED STATES TERRAIN DATA BASE.

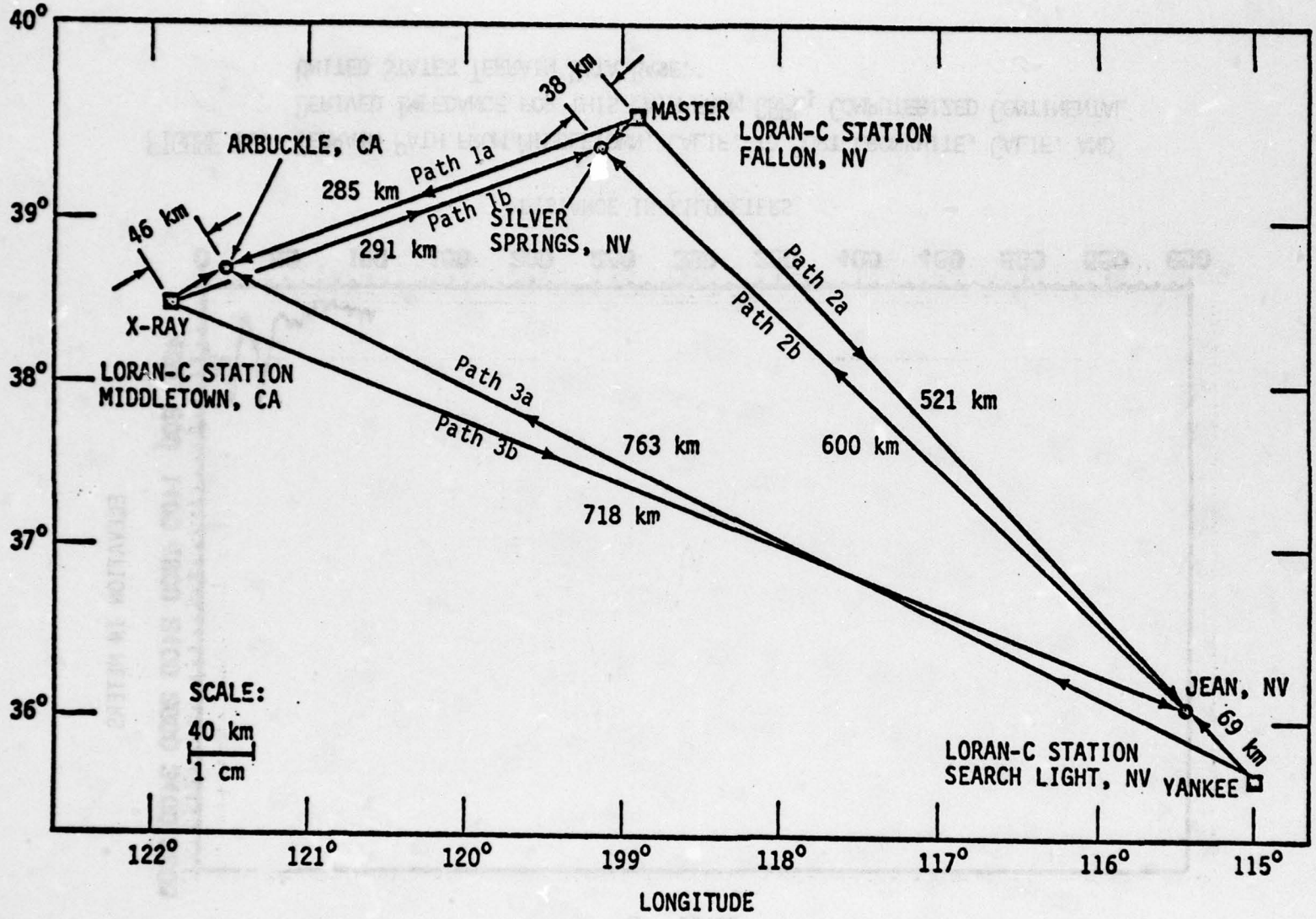

FIGURE 21. TRANSMITTER PATHS TO SILVER SPRINGS, NEVADA; JEAN, NEVADA AND ARBUCKLE, CALIFORNIA.

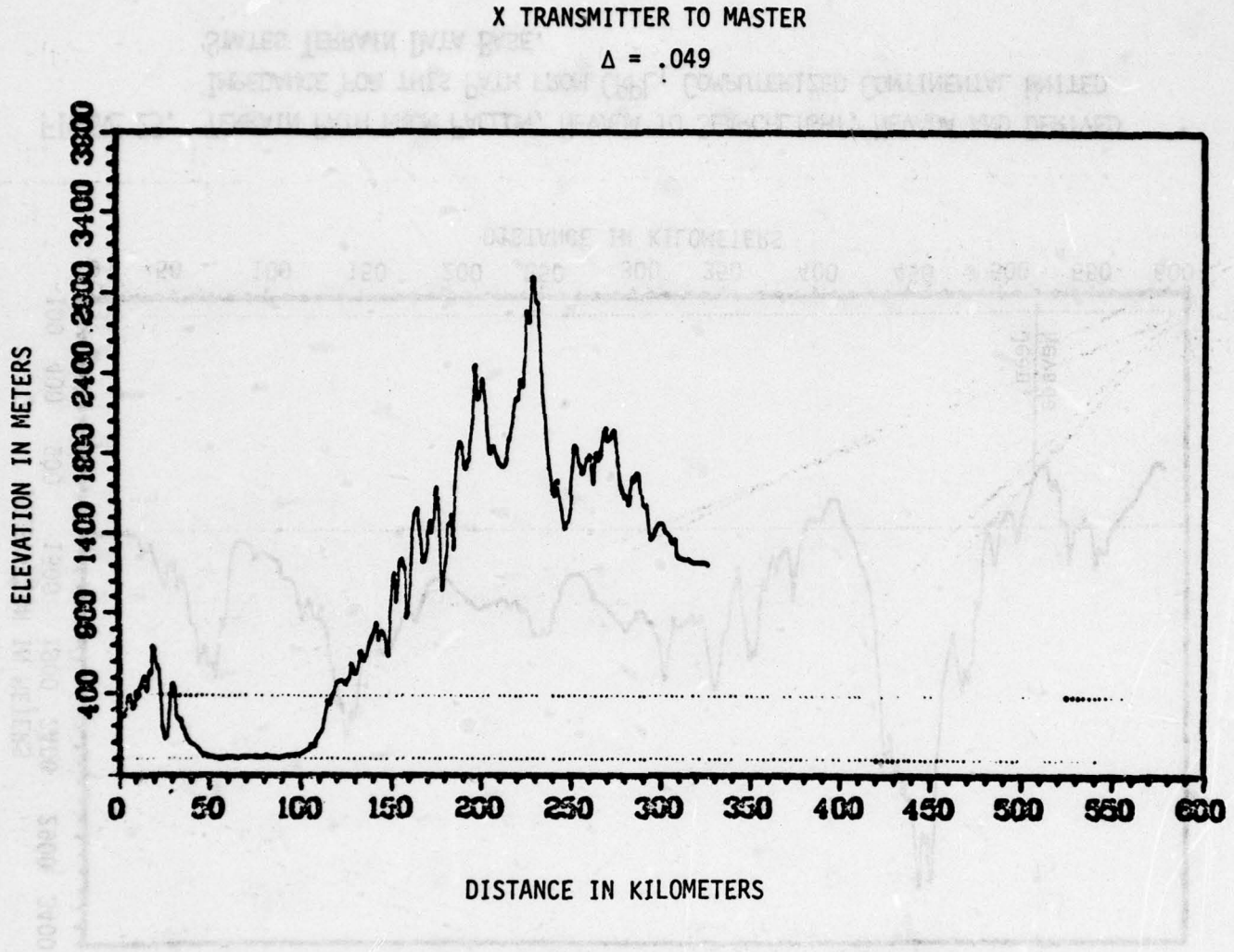

FIGURE 22. TERRAIN PATH FROM MIDDLETOWN, CALIF. TO FALLON, NEVADA AND DERIVED IMPEDANCE FOR THIS PATH FROM $CRPL_I$ COMPUTERIZED CONTINENTAL UNITED STATES TERRAIN DATA BASE.

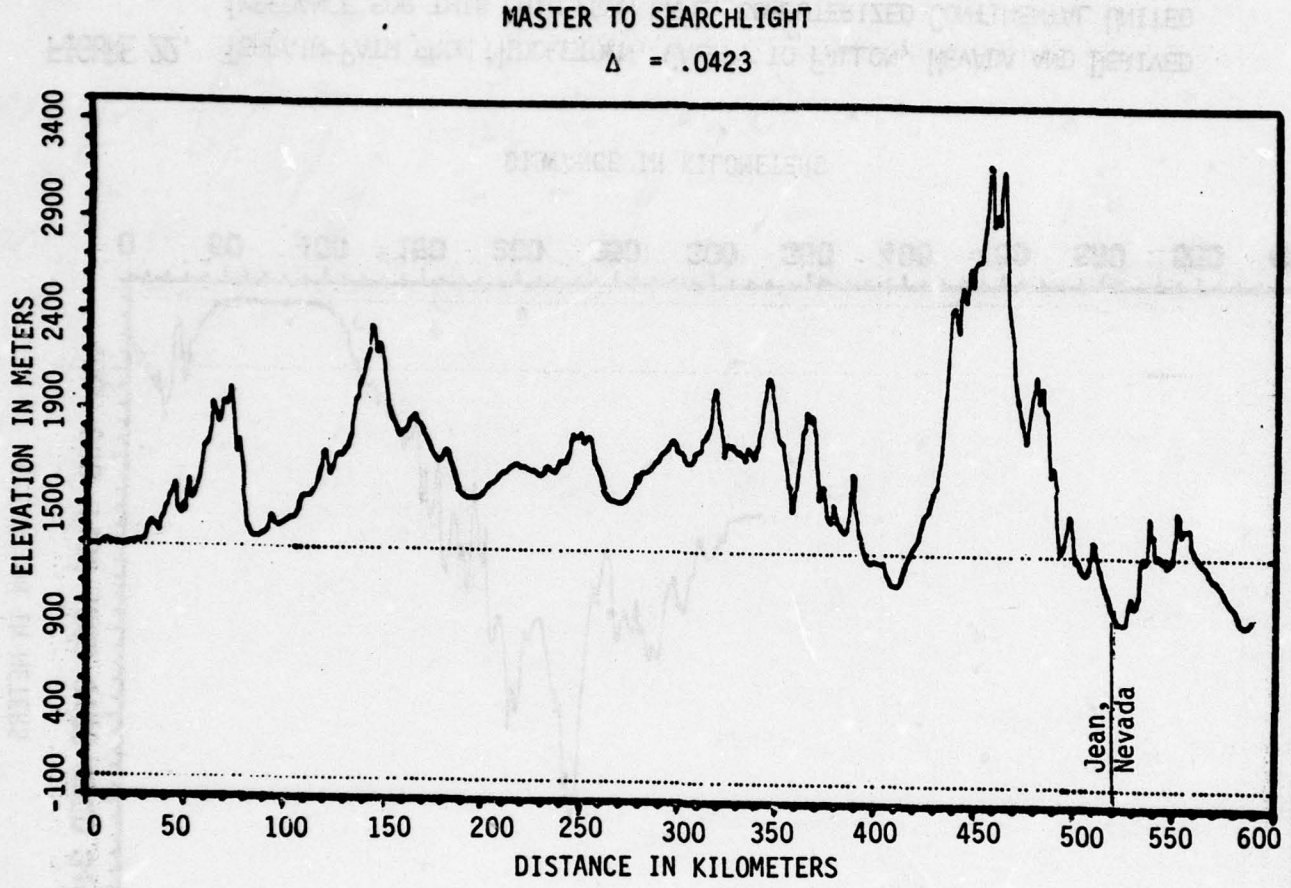

FIGURE 23. TERRAIN PATH FROM FALLON, NEVADA TO SEARCHLIGHT, NEVADA AND DERIVED IMPEDANCE FOR THIS PATH FROM CRPL$_I$ COMPUTERIZED CONTINENTAL UNITED STATES TERRAIN DATA BASE.

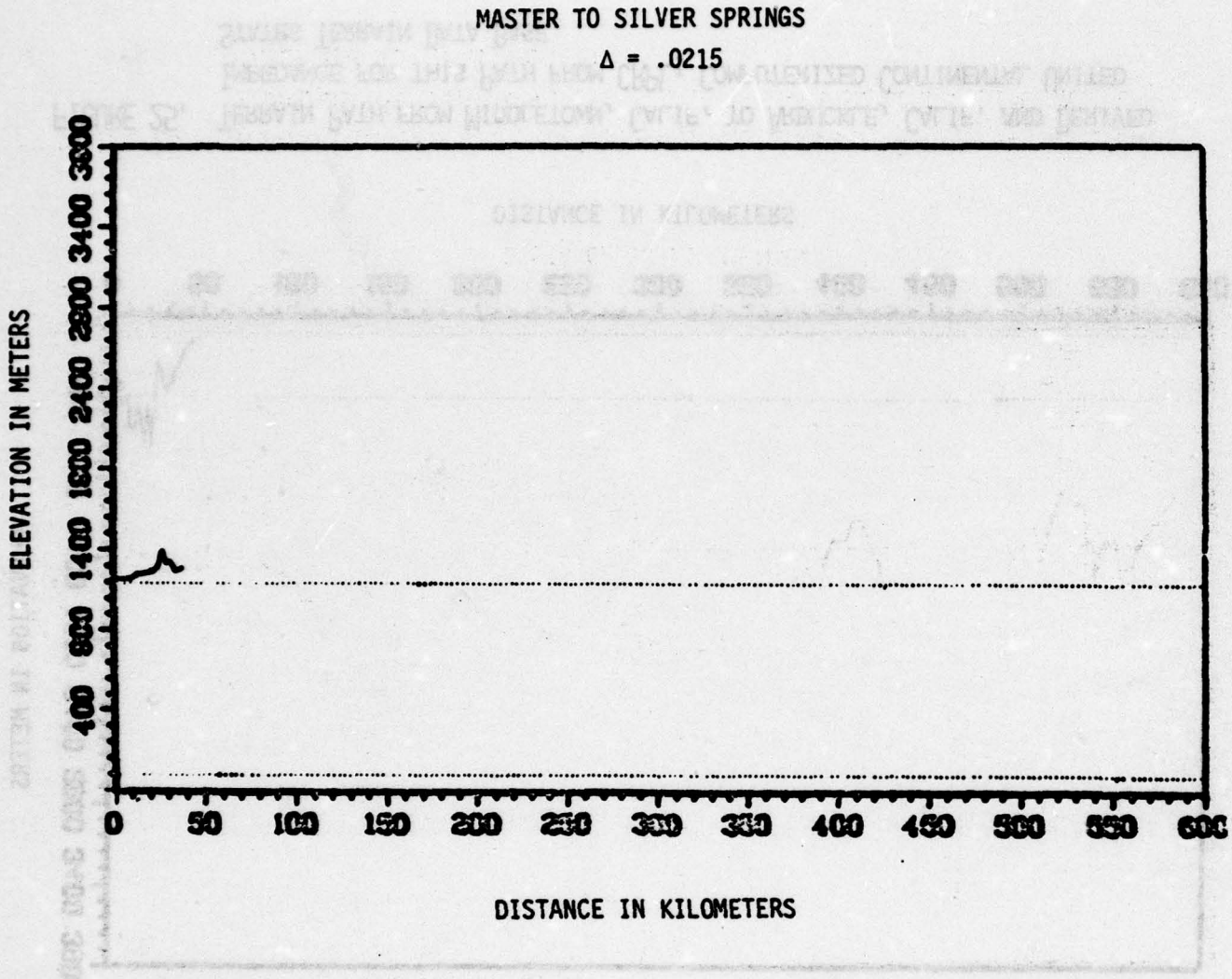

FIGURE 24. TERRAIN PATH FROM FALLON, NEVADA TO SILVER SPRINGS, NEVADA AND DERIVED IMPEDANCE FOR THIS PATH FROM CRPL$_I$ COMPUTERIZED CONTINENTAL UNITED STATES TERRAIN DATA BASE.

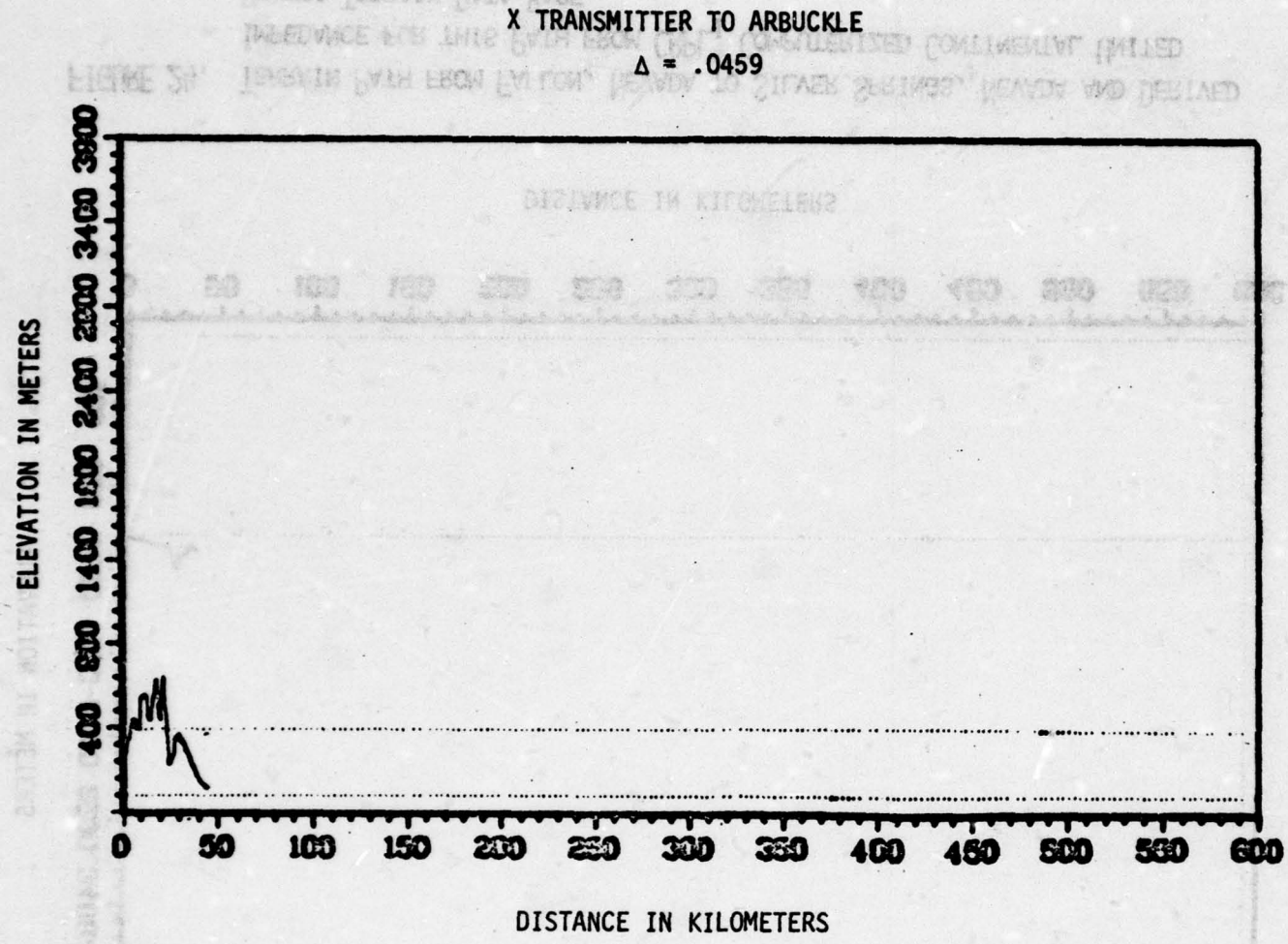

FIGURE 25. TERRAIN PATH FROM MIDDLETOWN, CALIF. TO ARBUCKLE, CALIF. AND DERIVED IMPEDANCE FOR THIS PATH FROM CRPL$_I$ COMPUTERIZED CONTINENTAL UNITED STATES TERRAIN DATA BASE.

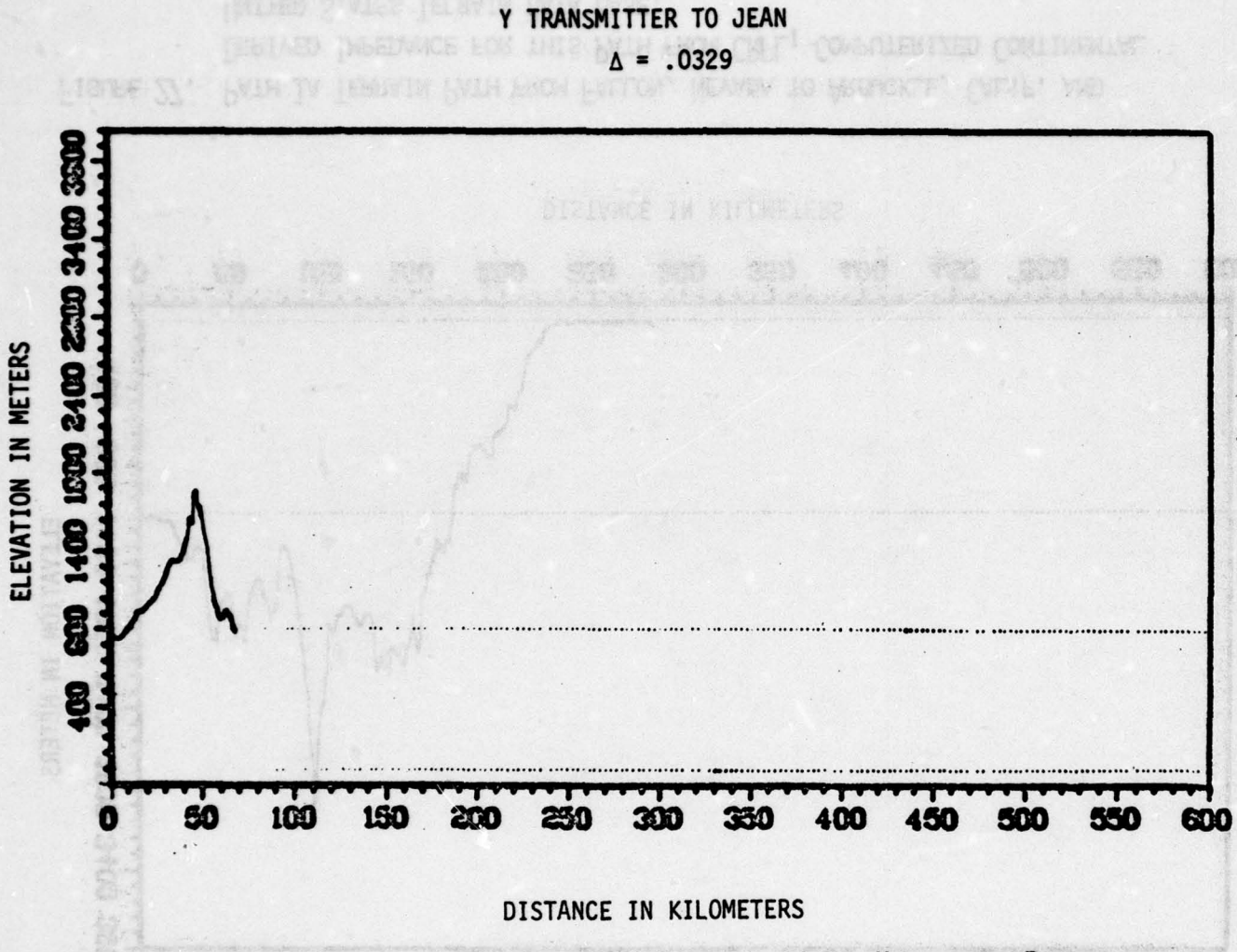

FIGURE 26. TERRAIN PATH FROM SEARCHLIGHT, NEVADA TO JEAN, NEVADA AND DERIVED IMPEDANCE FOR THIS PATH FROM $CRPL_I$ COMPUTERIZED CONTINENTAL UNITED STATES TERRAIN DATA BASE.

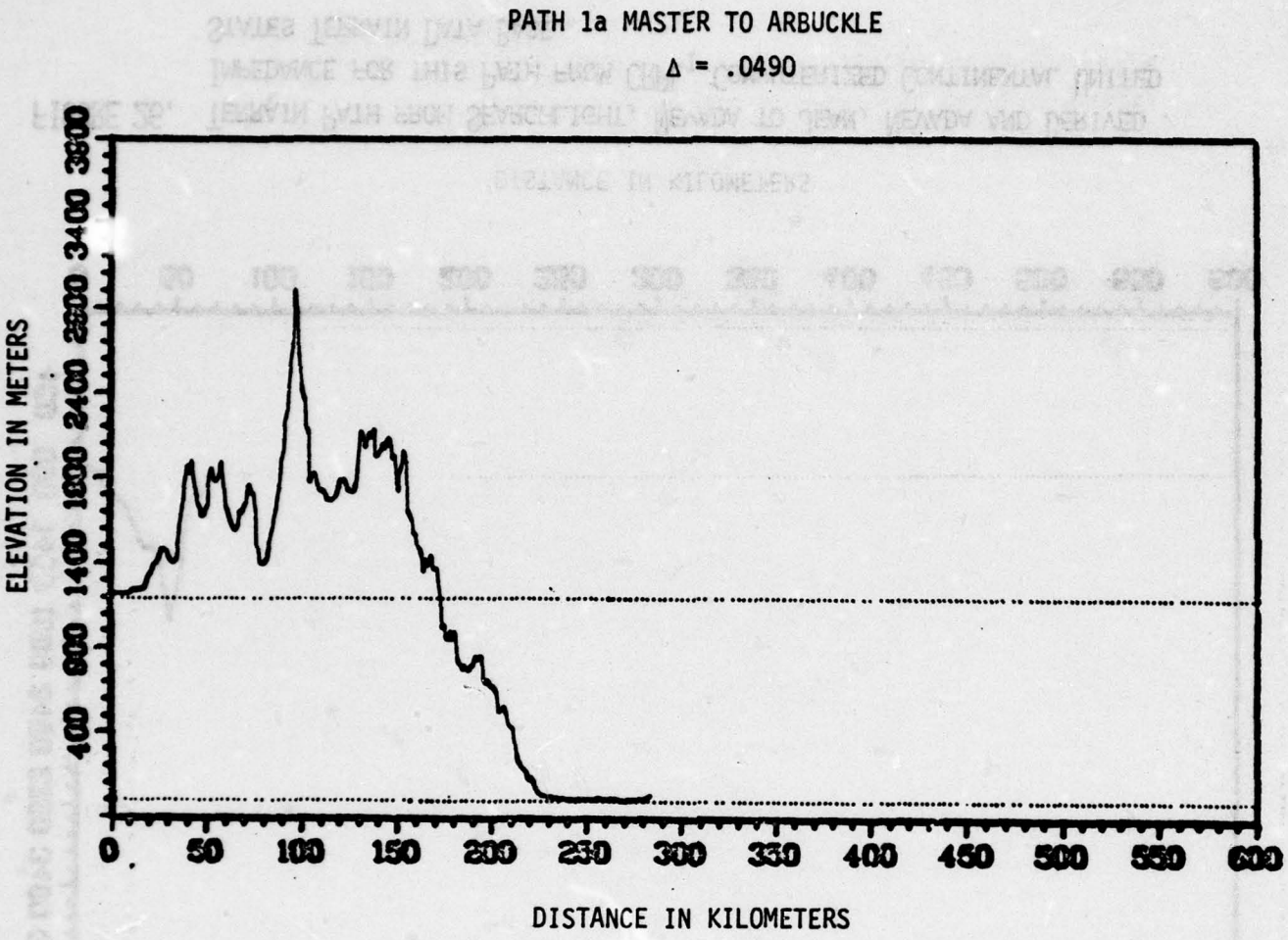

FIGURE 27. PATH 1A TERRAIN PATH FROM FALLON, NEVADA TO ARBUCKLE, CALIF. AND DERIVED IMPEDANCE FOR THIS PATH FROM CRPL$_I$ COMPUTERIZED CONTINENTAL UNITED STATES TERRAIN DATA BASE.

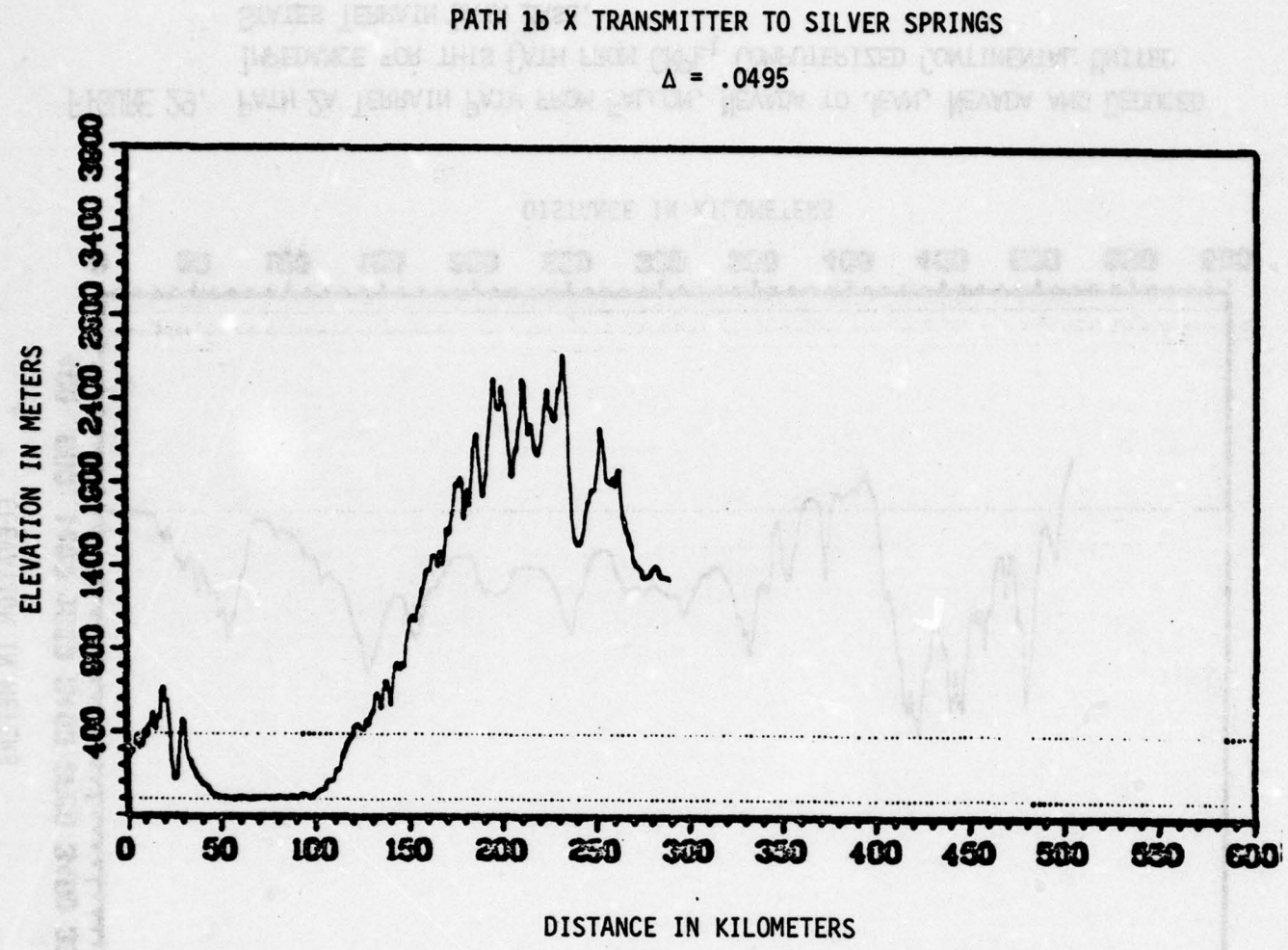

FIGURE 28. PATH 1B TERRAIN PATH FROM MIDDLETOWN, CALIF. TO SILVER SPRINGS, NEVADA AND DEDUCED IMPEDANCE FOR THIS PATH FROM CRPL$_I$ COMPUTERIZED CONTINENTAL UNITED STATES TERRAIN DATA BASE.

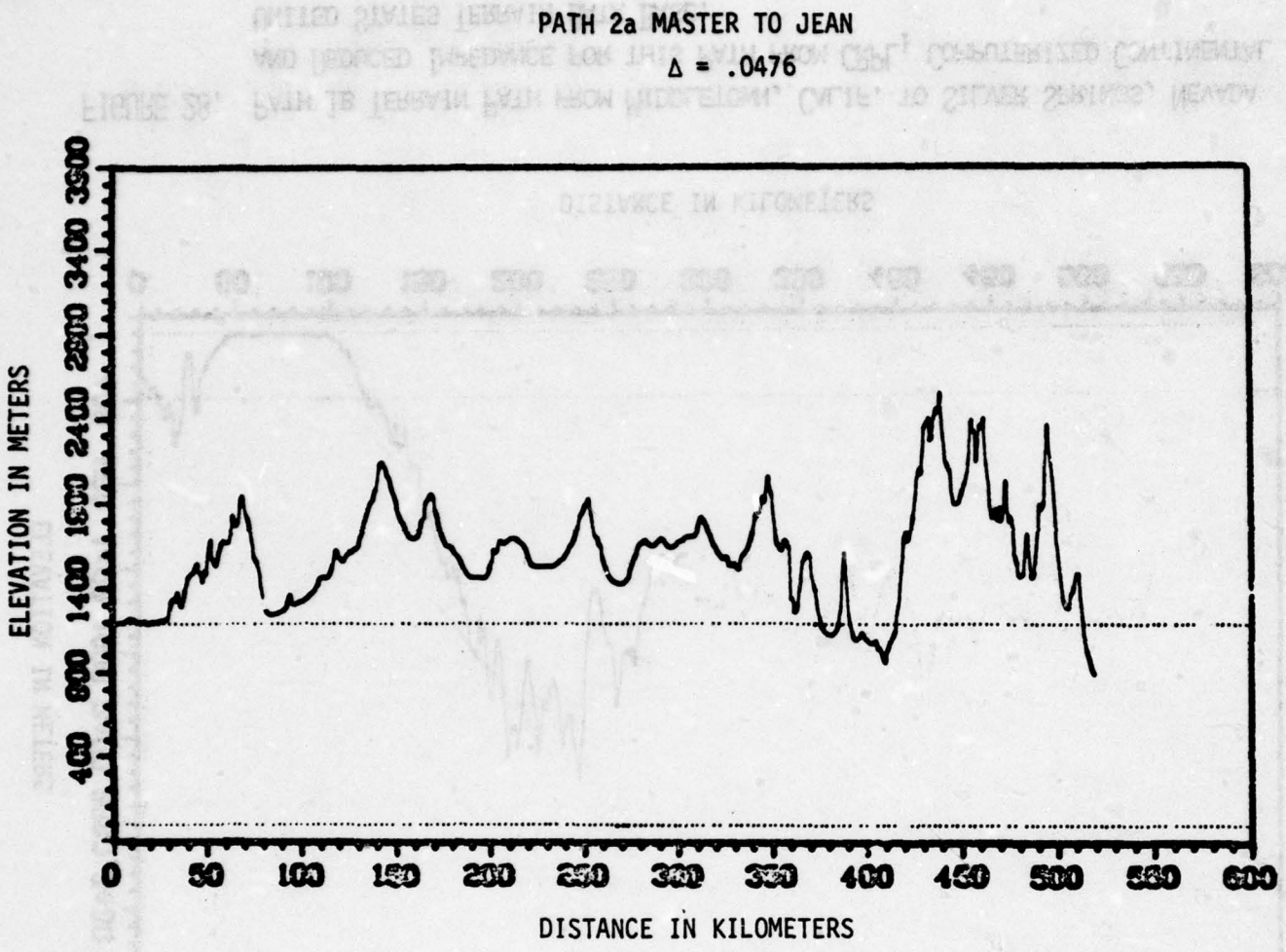

FIGURE 29. PATH 2A TERRAIN PATH FROM FALLON, NEVADA TO JEAN, NEVADA AND DEDUCED IMPEDANCE FOR THIS PATH FROM $CRPL_1$ COMPUTERIZED CONTINENTAL UNITED STATES TERRAIN DATA BASE.

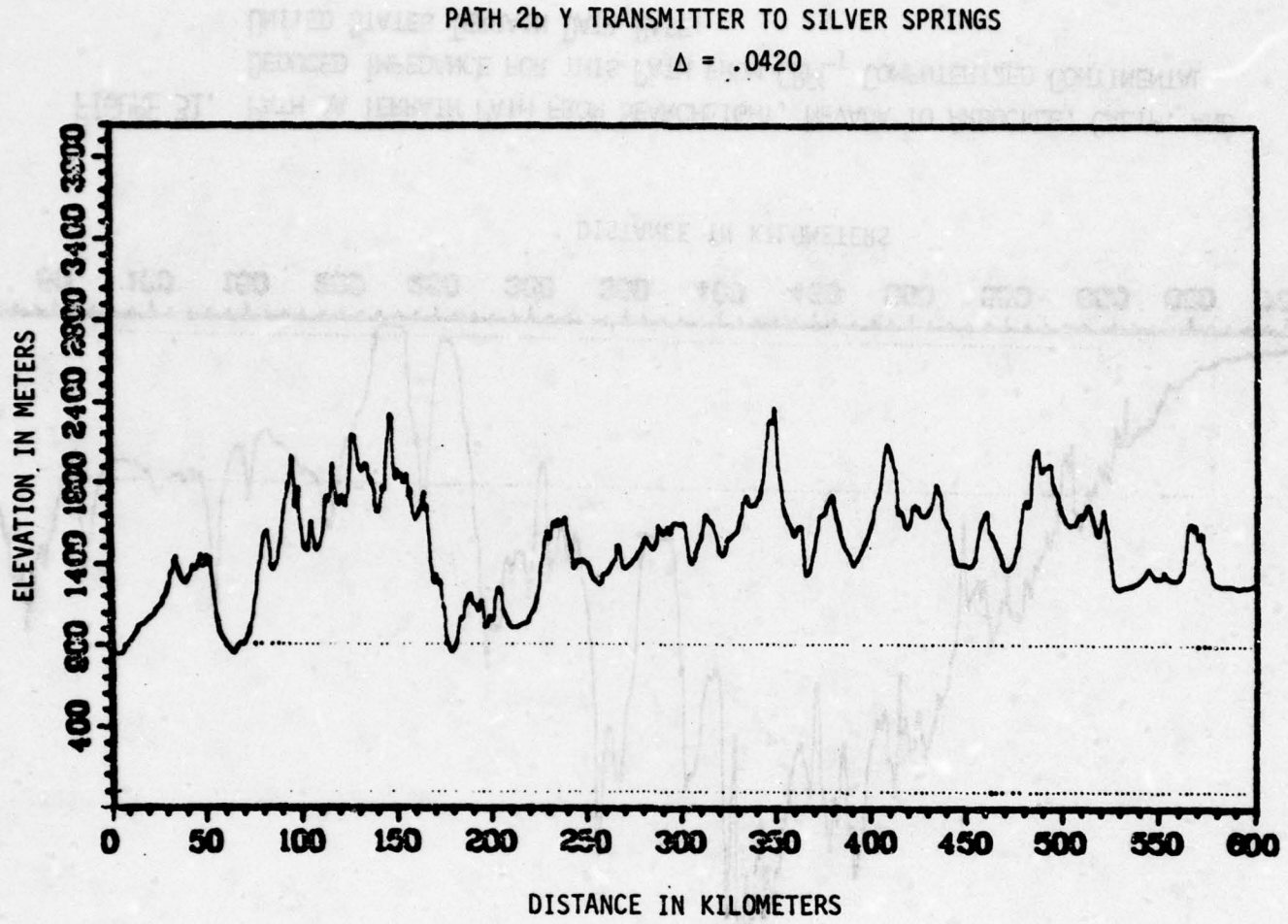

FIGURE 30. PATH 2B TERRAIN PATH FROM SEARCHLIGHT, NEVADA TO SILVER SPRINGS, NEVADA AND DEDUCED IMPEDANCE FOR THIS PATH FROM CRPL$_I$ COMPUTERIZED CONTINENTAL UNITED STATES TERRAIN DATA BASE.

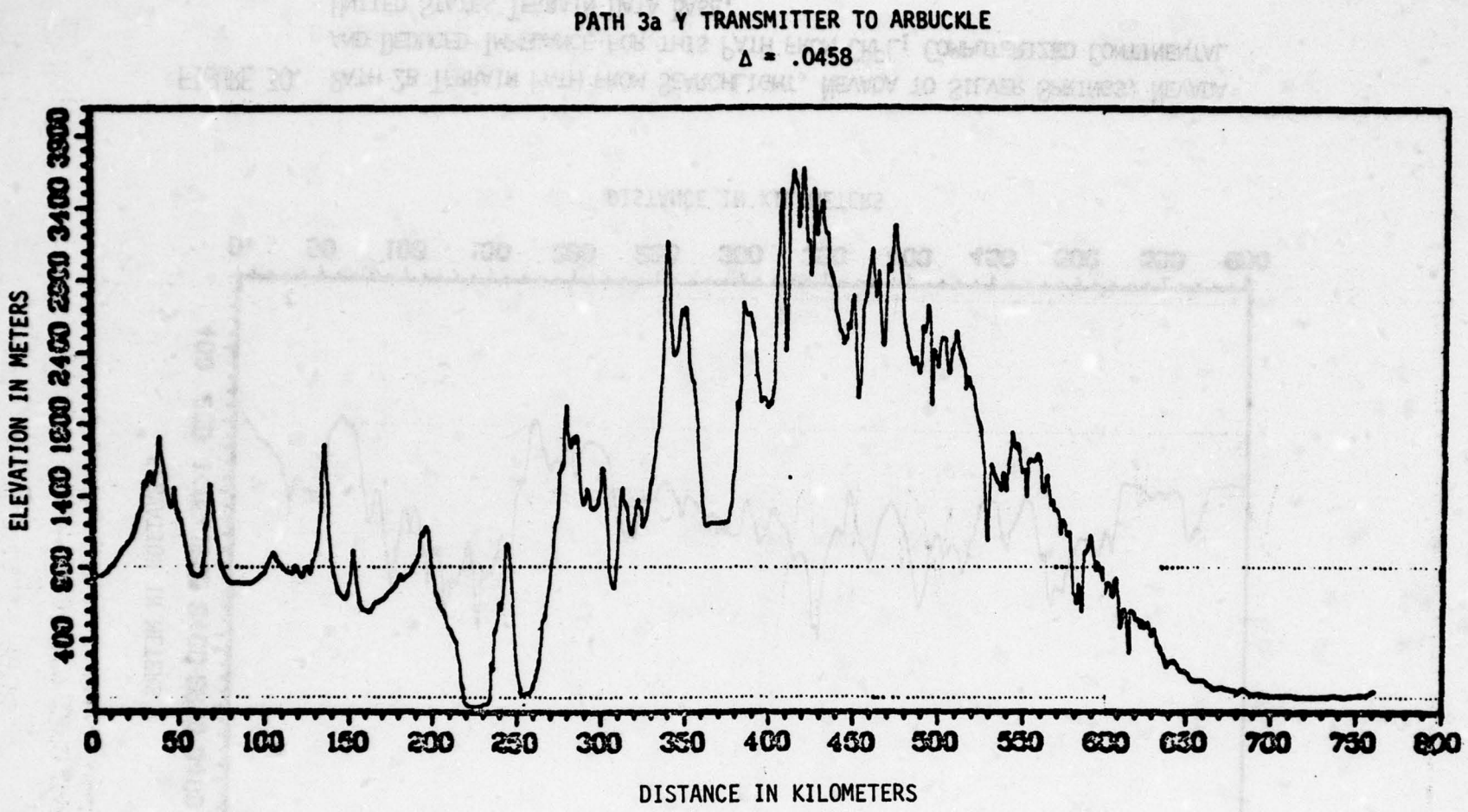

FIGURE 31. PATH 3A TERRAIN PATH FROM SEARCHLIGHT, NEVADA TO ARBUCKLE, CALIF. AND DEDUCED IMPEDANCE FOR THIS PATH FROM $CRPL_I$ COMPUTERIZED CONTINENTAL UNITED STATES TERRAIN DATA BASE.

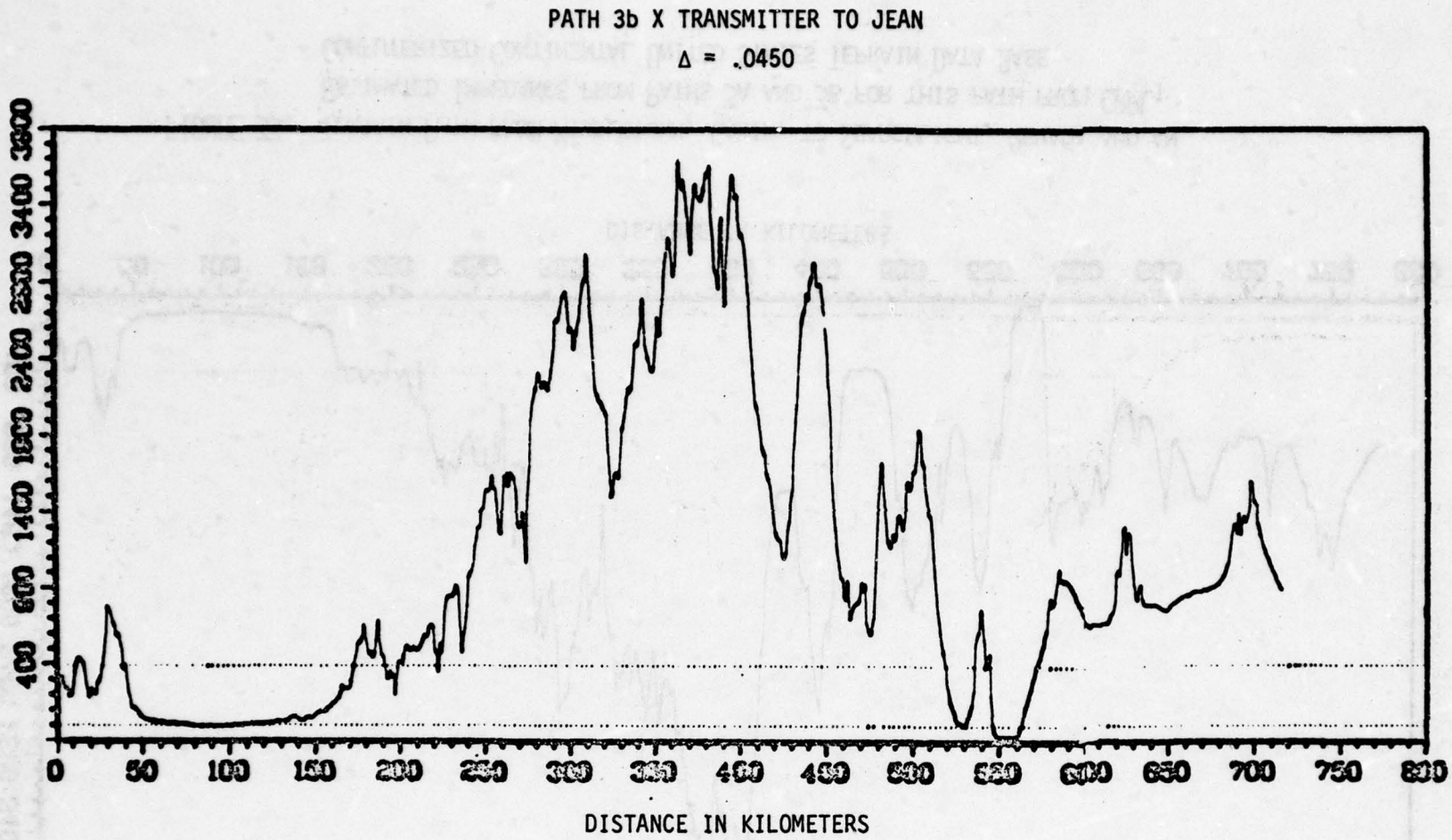

FIGURE 32. PATH 3B TERRAIN PATH FROM MIDDLETOWN, CALIF. TO JEAN, NEVADA AND DEDUCED IMPEDANCE FOR THIS PATH FROM CRPL$_I$ COMPUTERIZED CONTINENTAL UNITED STATES TERRAIN DATA BASE.

*U.S. GOVERNMENT PRINTING OFFICE: 1979 632-629/156 1-3

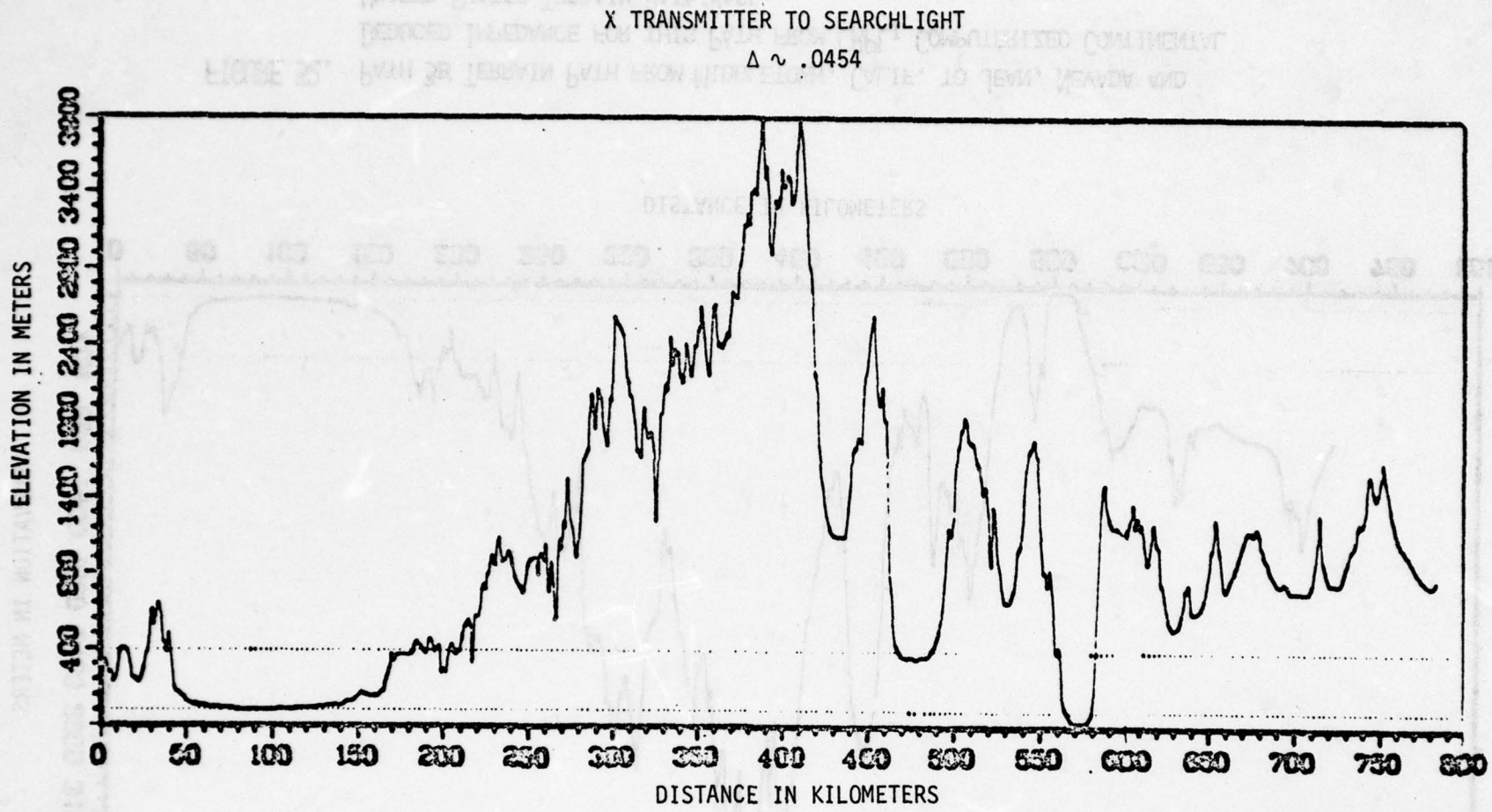

FIGURE 33. TERRAIN PATH FROM MIDDLETOWN, CALIF. TO SEARCHLIGHT, NEVADA AND AN ESTIMATED IMPEDANCE FROM PATHS 3A AND 3B FOR THIS PATH FROM CRPL$_I$ COMPUTERIZED CONTINENTAL UNITED STATES TERRAIN DATA BASE.